Assessing sensory and parasympathetic contributions to airway hyperreactivity using optogenetic activation and multicolor labeling of airway neurons

By

Alexandra Bowman Pincus

A DISSERTATION

Presented to the Neuroscience Department
and the Oregon Health & Science University
School of Medicine
in partial fulfillment of the requirements for the degree of

Doctor of Philosophy

April 2021

School of Medicine
Oregon Health & Science University

CERTIFICATE OF APPROVAL

This is to certify that the PhD dissertation of

Alexandra Bowman Pincus

has been approved

David B. Jacoby, M.D.

Mentor/Advisor: David Jacoby, MD

Committee Chair: Vivek Unni, MD, PhD

Member: Allison Fryer, PhD

Member: Kelly Monk, PhD

Member: George Giraud, MD, PhD

Member: David Lewinsohn, MD, PhD

TABLE OF CONTENTS

Acknowledgements

First thanks go to my PI and mentor, Dr. David (Obi Wan) Jacoby.
Who despite the constantly increasing demands on his time over the past few years never failed to meet with me weekly, to think deeply about my projects, to read many terrible drafts of my writing, to come running whenever a experiments worked, and to administer comforting doses of chai, cheese, and ice cream when they didn't. Thank you for teaching me how to think like a scientist, and for being incredibly nice about it.
You're my favorite jedi master. I hope you're kvelling.

To Dr. Allison Fryer: Thank you for always leaving your office door open. You helped make me into a better scientist: pushing me to strive for excellence in all my presentations, sitting down with me to discuss outlines and figures and control groups and big ideas, and asking all the pharmacology questions in lab meetings. Thank you for being my guide to the ins and outs of the graduate system, and thank you for the words of encouragement when I did something well.

Next thanks to my lab team: Matt, Jane, Brenda, Becky, Emily, Katie, Quinn, Gina, Nicole, Jess, Aubrey, Lauren, Chris, Jeff, Madeline, Shay, Clare, and Meredith.
You taught me how to actually do all the crazy experiments I came up with, you didn't mind me running to your offices and desks with questions at odd hours, you came with me to get chocolate croissants and chai when things got rough (these things are very important), and you used up many hours and many more neurons thinking about my experiments and how to do them better and my results and what they might mean. Thank you for the lab meetings, the presentation practices, the birthday treats and the farmer's market lunches. Thanks for making the lab my home for so many years. I'll be popping back in to hang out over the next two years, just you wait and see :)

To my DAC committee: Vivek, Kelly and George. Thank you for helping to guide me on this journey. I deeply appreciate your time, your insightful questions, your excellent career advice, and how it always feels like you're rooting for me to succeed. Thank you for playing such an important role in my scientific mentorship team.

To my friends and fellow students: I could not do this without you. Thank god you exist and you like hanging out with me sometimes, or I would be totally doomed.

Many, many people at OHSU helped make this research possible, whether by collaborating, exchanging ideas, sharing expertise or reagents, or just leaving their door open so I could come by and talk if I needed to. This non-exhaustive list of superstars includes Sweta Adhikary and John Williams, Sam Huang and Hiroyuki Nakai, Stefanie Kaech-Petrie, Brian Jenkins, Crystal Shaw, Paul Barnes, Dan

Marks, Leslie Wakefield, Chris Harrington, Matthew Pomaville and Kevin Wright, Doug Zeppenfield and Larry Trussel, and Marvin Bentley.

Thank you to Dawen Cai, Stephen Liberles, Rachael Brust, Alexander Chesler, Nima Ghitani, and Ikuo Tooyama for generosity with their time, expertise, and protocols. I am fortunate to have such collaborative experts working in this field.

To my family:
I love you all so much, and I couldn't have gotten through this without you. Mom: thank you for the endless support, the daily pep talks, the Starbucks coffees ordered from your phone for pick up at my corner shop, and for being mad at all the right people on my behalf. Derek and Sam, thanks for living through this with me, and sending care packages and liking texts and telling me you're proud. Mom and Dad, thank you for always listening when my conversations dove deep into science, for sending me ideas for cool journal articles to present, and for showing up front and center at my presentations and conferences and telling me you thought they were awesome. You are the best <3

Dissertation Funding:
NRSA F30 HL145906, Pulmonary T32 HL083808, MSTP T32 GM109835,
Tartar Trust Fellowship

Publications

Manuscripts:

Pincus, A.B., Fryer, A.D., & Jacoby, D.B. (2021). Mini Review: Neural mechanisms of airway hyperresponsiveness. *Neuroscience Letters*. https://doi.org/10.1016/j.neulet.2021.135795

Pincus, A. B., Adhikary, S., Lebold, K. M., Fryer, A. D., & Jacoby, D. B. (2020). Optogenetic control of airway cholinergic neurons in vivo. *American Journal of Respiratory Cell and Molecular Biology*, *62*(4), 423–429. https://doi.org/10.1165/rcmb.2019-0378MA

Drake, M. G., Lebold, K. M., Roth-Carter, Q. R., **Pincus, A. B.**, Blum, E. D., Proskocil, B. J., Jacoby, D. B., Fryer, A. D., & Nie, Z. (2018). Eosinophil and airway nerve interactions in asthma. *Journal of Leukocyte Biology*, *104*(1). https://doi.org/10.1002/JLB.3MR1117-426R

Abstracts:

Pincus, A., Fryer, A., & Jacoby, D. (2019). Optogenetic activation of mouse airway parasympathetic neurons to provoke bronchoconstriction. *European Respiratory Journal*, *54*(suppl 63), PA5214. https://doi.org/10.1183/13993003.congress-2019.pa5214

Pincus, A.. and Drake, M. G. (2019). Quantitative 3D confocal microscopy illuminates eosinophil-nerve interactions in airways, *International Eosinophil Society (IES) Conference*

Pincus, A., Fryer, A. D., & Jacoby, D. B. (2019). Optogenetic activation of parasympathetic neurons causes bronchoconstriction, *American Physician Scientist Association Conference*

Pincus, A., Fryer, A., Jacoby, D., & Lebold, K. (2018). Maternal allergen exposure increases offspring sensory airway innervation and airway hyperreactivity in mice. *European Respiratory Journal*, *52*(suppl 62), PA1380. https://doi.org/10.1183/13993003.congress-2018.pa1380

Pincus, A., Drake, M., Fryer, A., Lee, N., Lee, J., Jacoby, D., & Lebold, K. (2017). Regulation of tracheal parasympathetic nerve ganglia development by eosinophils. *European Respiratory Journal*, *50*(suppl 61), OA4851. https://doi.org/10.1183/1393003.congress-2017.oa4851

Pincus, A., Lee, N., Lee, J., Fryer, A., Jacoby, D., & Lebold, K. (2017). Eosinophils regulate airway parasympathetic nerve ganglion structure, *International Eosinophil Society Conference*

Abstract

Asthma is a highly prevalent airway disease characterized by inflammation, structural remodeling of the airways and airway hyperreactivity. Despite recent advances, asthma treatment remains inadequate for many patients, because the underlying pathology of asthma remains to be fully understood. One characteristic feature of asthma, airway hyperreactivity, is defined as increased bronchoconstriction in response to inhaled agonists, and is mediated by airway nerves. Studies have shown increases in sensory innervation of the epithelium and changes to parasympathetic nerve function in human asthma and animal models of asthma. It is my hypothesis that structural changes to the sensory and parasympathetic nervous systems contribute to airway hyperreactivity associated with asthma. These changes can include increased nerve density, abnormal ganglia architecture, or alterations in neurotransmitter content and receptor expression. The complexity of the sensory and autonomic nervous systems makes it difficult to identify a role for specific nerves in airway hyperreactivity. Therefore, in this dissertation I describe the development of novel tools to depolarize specific nerve populations and image individual nerves in the airways to better understand the changes to sensory and parasympathetic nerves in airway hyperreactivity. I investigate the physiological changes occurring in airway sensory and parasympathetic nerves in two mouse models of allergic asthma: one defined by acute antigen treatment, the other by lifelong airway eosinophilia. My data demonstrate that these tools can be used successfully to identify the role of unique subsets of nerves in airway hyperreactivity. I use a combination of optogenetics and imaging to demonstrate that differences in eosinophil localization and nerve interactions leads to parasympathetic nerve hyperreactivity in an acute antigen challenge asthma mouse model but not in a mouse model of chronic airway hyperreactivity and eosinophilia. Overall, my dissertation: 1) demonstrates a successful protocol for optogenetic activation of airway nerves, both parasympathetic and sensory, 2) uses optogenetics to show differences between different mouse models of eosinophilic asthma in the mechanism of hyperreactivity, 3) assesses eosinophil localization around airway nerves to explain hyperreactivity differences, 4) optimizes tools for multicolor labeling and nerve tracing that can be used to image airway nerves and their connections, and 5) develops a PANbow genetic construct with utility for multicolor labeling of autonomic nerves, which will be used to improve analysis of parasympathetic nerve subpopulations in the future.

Chapter 1: Introduction

A. Airway Structure

a. Anatomy of airways

Mammalian airways are a system of hollow passageways, lined with mucosal epithelial tissue and arranged with a single trunk that branches into smaller and smaller arms (Figure 1.1). Extrapulmonary airways include the mouth and nose, which are entryways for airflow and are responsible for filtering large and medium-sized particulate matter via the epiglottis and nasal hair cells, respectively. Air then flows through the trachea and bifurcates at the carina, where flow splits into right and left primary bronchi. This is where the extrapulmonary component of the airways ends and the intrapulmonary region (passageways surrounded by lung parenchyma) begins. Primary bronchi enter lungs, where they branch three more times. After this fourth branch the airways become terminal bronchi. Up to this point, airways are labeled conducting airways, as they are conduits for air flow without substantial gas exchange. Here, epithelium of the airways changes and flattens, and the average proximity of airway branches to blood vessels increases. The end of the conducting airways marks the start of the respiratory zone, which comprises respiratory bronchioles, alveolar ducts and alveolar sacs. In humans, the respiratory zone contains nineteen generations of branches, ending in a mesh of air pockets, or alveoli, surrounded by single epithelial cells in direct contact with capillary endothelial cells. More detailed descriptions of these all structures follow.

i. Nasal Airway

Nasal airways include the area from the nostrils through the nasal passages and into the trachea. The major functions of the nasal airway are 1) to adjust temperature and partial pressure of water in inspired air, and 2) to filter out large and medium sized particles. About half of total resistance to respiratory airflow is achieved by the ostium internum within the nasal airway, an area which restricts and bends airflow. This part of the airway is lined with pseudostratified columnar ciliated epithelium and contains a large number of mucus-secreting goblet cells (Widdicombe, 1981). Mucins are a class of glycoproteins that, along with water, are the main component of mucus. Mucus protects airway epithelium from desiccation and build-up of noxious substances. Particles, such as air pollutants and droplets containing airborne infections, are cleared from the airway through mucociliary transport. Nasal glands, located below the epithelium, line nasal airway and produce additional mucus for secretion. Nasal glands are innervated by secretomotor parasympathetic nerves through the pterygopalatine ganglion (Lundy & McNary, 2019).

ii. Trachea

The trachea is a single hollow tube lined with pseudostratified columnar ciliated epithelium and supported by rings of cartilage (Watson & Brinkman, 1964). The trachealis muscle runs from anterior to posterior along the dorsal trachea, and postganglionic parasympathetic cell bodies arranged in ganglia are embedded outside of this muscle between rings of cartilage. Goblet cells are present in epithelium, and are more prevalent in the trachea than distal airway (Widdicombe, 1981).

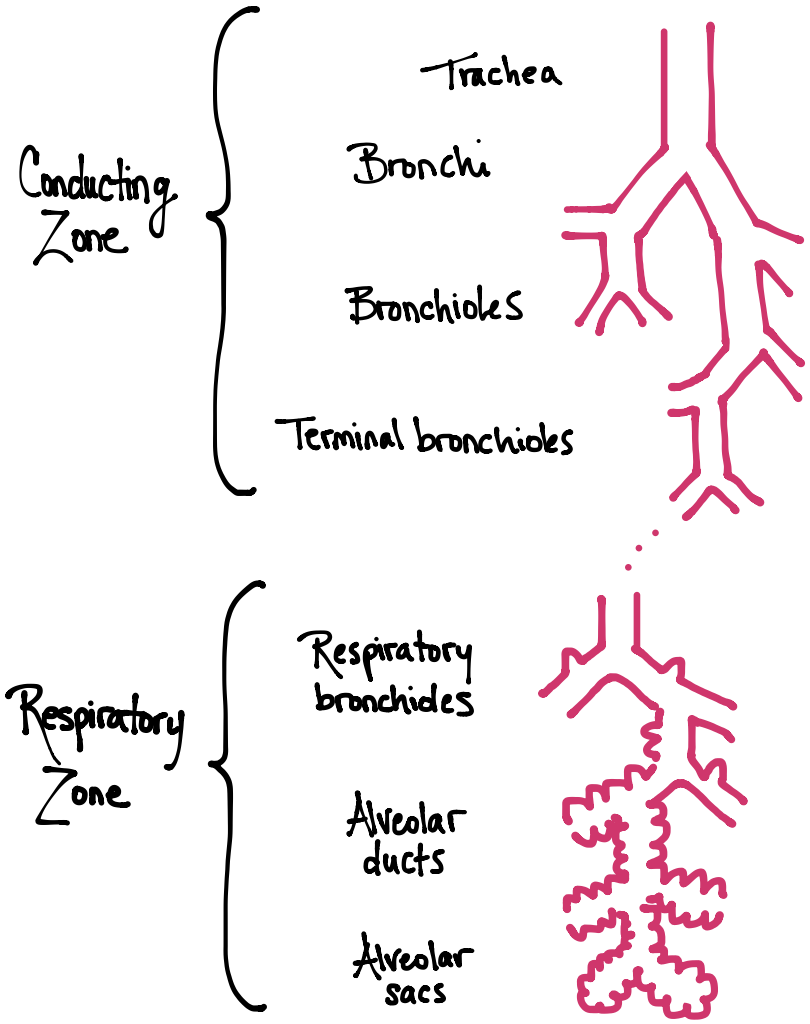

Figure 1.1. Anatomy of the airways. Air flows in through the mouth or nose, down through the conducting airways including the trachea, bronchi, and bronchioles, and into the respiratory zone, including the respiratory bronchioles, alveolar ducts, and alveolar sacs, where gas exchange occurs. Figure adapted from Rynko 2013.

Submucosal glands are found only in cartilage-containing airways, located between mucosa and cartilage rings. About 6000 of these glands are found in adult human tracheas, with 30,000 more in bronchi and other conducting airways. Respiratory airways notably lack these glands (Widdicombe, 1981). In healthy airways submucosal glands are responsible for the vast majority of mucus secretion, secreting mucus that is less viscous than that of goblet cells. Submucosal glands are regulated by both sympathetic and parasympathetic innervation (Nadel and Davis, 1980).

iii. Bronchi and bronchioles

Bronchi and bronchioles are surrounded by circular bands of smooth muscle that contract airways. Bronchi also have circular bands of cartilage, like the trachea, whereas bronchioles lack cartilage rings. Pseudostratified columnar ciliated epithelium contains a variety of specialized cells that are active in asthma. Goblet cells are non-ciliated cells that synthesize and secrete glycoproteins, and exhibit hyperplasia in asthma and chronic bronchitis. Recent studies have shown abundant mucus in lower airways in asthma arising from both goblet cell hyperplasia as well as from other, developmentally distinct mucus-producing ciliated cells (Vieira Braga *et al.*, 2019). Pulmonary neuroendocrine cells are rare airway epithelial cells with increased prevalence in asthmatic airways. These cells release neurotransmitters to promote immune responses: gamma aminobutyric acid release from these cells induces goblet cell hyperplasia, while the release of calcitonin gene-related peptide stimulates group 2 innate lymphoid cells (ILC2s) (Sui *et al.*, 2018).

iv. Alveoli

Alveoli are the site of gas exchange in the airways. Adult human lungs have 300 million alveoli on average, each a small bubble of lumen about 0.3mm in diameter surrounded by a single layer of flattened epithelial cells in close proximity to capillary endothelium (West, 1974). The large surface area to volume ratio of alveoli allows for maximally efficient gas exchange, and a layer of surfactant secreted by type II epithelial cells helps keep alveoli from collapsing despite the lack of cartilaginous structures.

b. Blood supply in the lungs

Because of the unique role of lungs in oxygenating blood, two separate circulatory systems exist within this organ. Bronchial circulation is a high pressure vascular system, originating from the aorta, that supplies oxygenated blood to the trachea, bronchi, and structural airway tissues. In contrast, pulmonary circulation is a low pressure system of deoxygenated blood pumped directly from the right ventricle into pulmonary arteries, and from there into an extensive meshwork of capillaries surrounding alveoli. Within these alveolar/capillary networks, blood is oxygenated and relieved of carbon dioxide by gases diffusing along their concentration gradients. Newly oxygenated blood then flows through pulmonary veins into the left ventricle, where it is pumped through the aorta to the rest of the body. The earliest known publication correctly describing this system is *Commentary on Anatomy in Avicenna's Canon,* written by Ibn al-Nafis in 1242.

c. Anatomical differences between human and non-human airways

Mouse lungs differ from that of humans in a number of ways. While human lungs have two lobes on the left side and three lobes on the right, mouse lungs have a single left lobe and four lobes branching off the right primary bronchi. Both humans and mice possess five lung lobes in total. Distribution of glands also differs in mice compared to humans. As previously described, human airways have goblet cells and submucosal glands located throughout the trachea and cartilaginous airways. Mouse airways have submucosal glands limited to the very proximal portion of their trachea, in close proximity to the larynx. Because of this, mucus in mouse lungs derives mainly from goblet cells. Mice also have a more sparse distribution of smooth muscle, greater chest wall compliance, and fewer generations of airway branches than humans (Whimster, 1986, Choi *et al.*, 2000, Widdicombe *et al.*, 2001).

B. Airway Nerves

Airway nerves are a critical component of airway architecture, function, and pathology. The studies in this dissertation focus on two broad categories of airway nerves, sensory and parasympathetic, however other nerve types will be reviewed in this introduction for context. Sensory neurons innervate airway epithelium, detect stimuli, and send signals centrally to the brainstem. Brainstem neurons activate parasympathetic nerves, which release acetylcholine onto smooth muscle M_3 muscarinic receptors to cause bronchoconstriction. Altogether this is known as the reflex bronchoconstriction pathway (Karczewski and Widdicombe, 1969) (Figure 1.2).

a. Afferent sensory nerves

i. Anatomy

Airway sensory nerves are pseudounipolar Aδ and C fibers that travel in the vagus to supply airway epithelium, submucosa, and smooth muscle (Figure 1.3). Afferents supplying the trachea arise from cell bodies in the jugular ganglia and are derived from neural crest cells, whereas sensory nerves from lungs and distal airways arise from cell bodies in nodose ganglia and are derived from epibranchial placodes (Baker and Schlosser, 2005). A few airway sensory nerve cell bodies are located in dorsal root ganglia in the thoracic region of the spinal cord (Kummer *et al.*, 1992). Sensory nerve endings are dispersed through the trachea and primary bronchi epithelial layer, with increased density of nerve endings around airway branch points, in the proximal trachea, and on the dorsal aspect of the airways (Scott *et al.*, 2013). Sparrow provides beautiful mapping of sensory innervation in airways (Weichselbaum *et al.*, 1996, Sparrow *et al.*, 1999, Lamb and Sparrow, 2002). Nerve endings in the airway may terminate in or around the airway epithelium or within the trachealis muscle (Canning and Spina, 2009). Of all the nerve fibers running through the vagus, 80% of them are sensory nerves, a highly varied and diverse population with high neuroplasticity and important roles in physiology and disease.

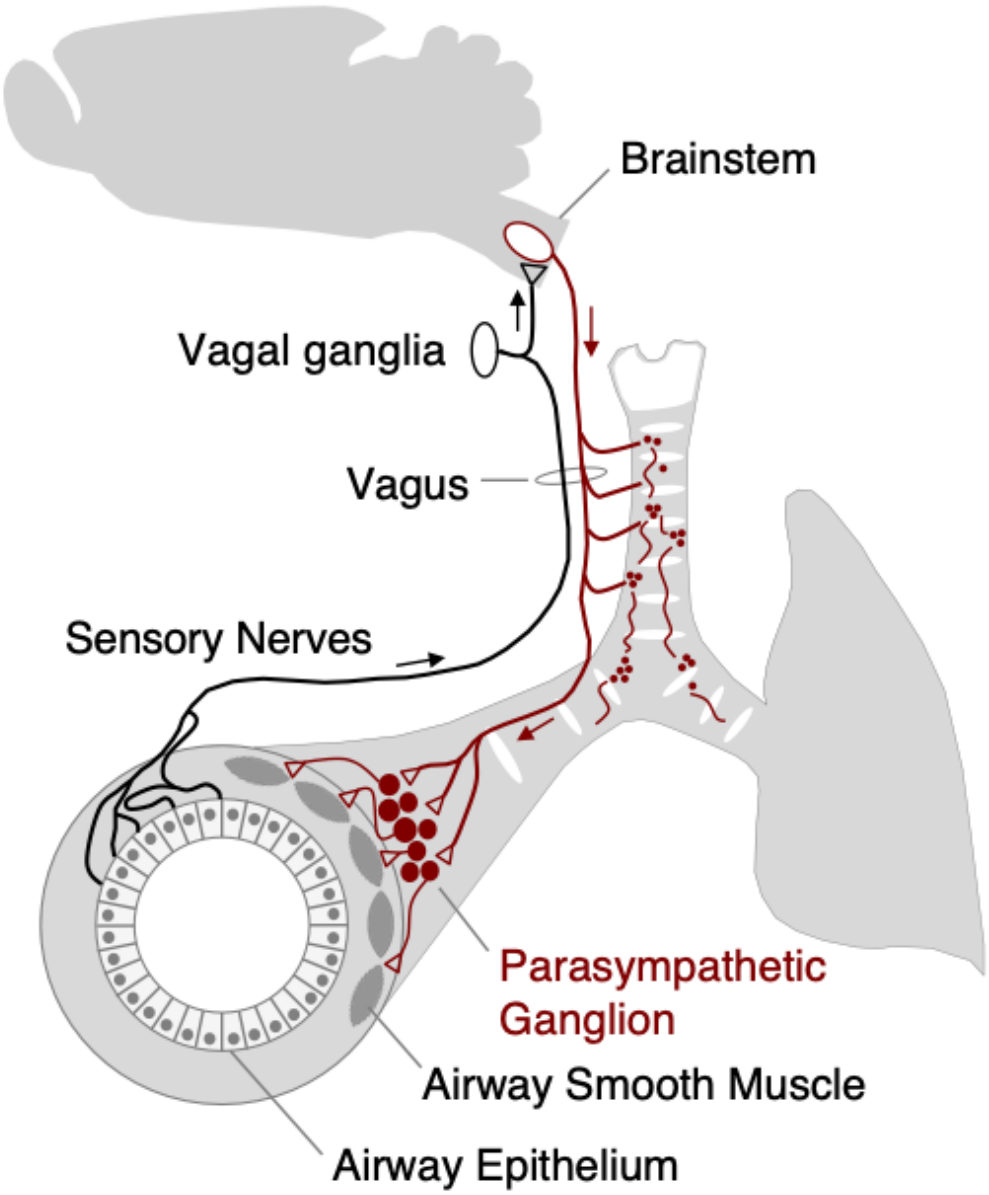

Figure 1.2. Nerves of the airways. In reflex bronchoconstriction, sensory neurons detect stimuli and send signals centrally to the brainstem. These brainstem neurons form a pathway to activate parasympathetic nerves, which release acetylcholine onto smooth muscle muscarinic receptors and cause bronchoconstriction.

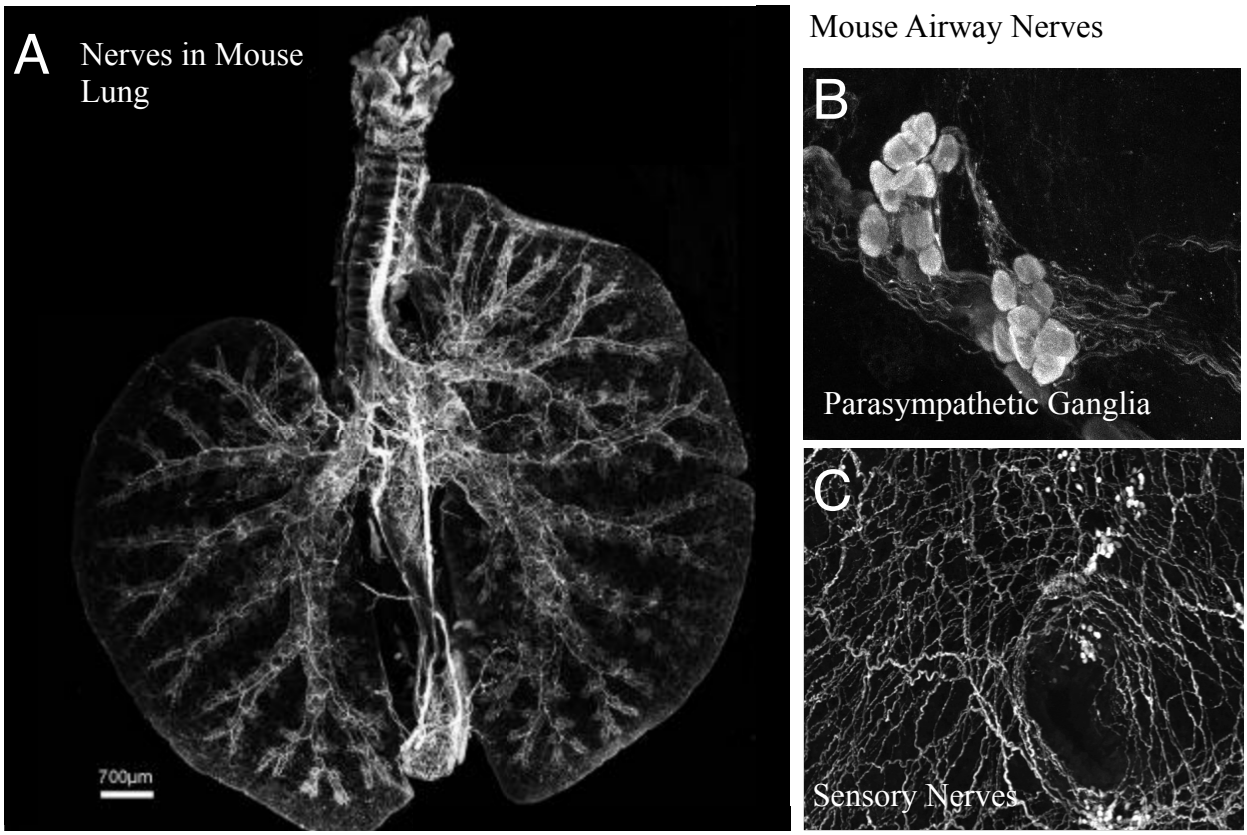

Figure 1.3. Airway innervation in the mouse. (A) Optically-cleared whole mouse lung labeled with pan-neuronal marker PGP9.5 (white), showing nerves in the trachea (top), esophagus (bottom middle), and branching through the airways. (B) Parasympathetic ganglion located within the trachea. (C) Sensory nerve endings within the mouse lung surrounding an airway (black oval). Reprinted with permission from Scott *et al.*, 2014 (A) and Scott 2012 (C).

ii. Development of sensory nerves

Airway sensory neurons have two distinct developmental origins. Neurons in the jugular ganglia are primarily derived from neural crest cells, which are multipotent cells that form on the lateral border of the neural tube in the earliest stages of embryonic development. Cells in the dorsal root ganglia are similarly derived. By contrast, most neurons in the nodose ganglia, which comprises the vast majority of airway sensory neurons, are derived from epibranchial placode cells (Baker and Schlosser, 2005). As animals develop, neurotrophic factors are responsible for stimulating nerve growth, and then for maintaining nerves as animals mature. Nodose ganglia neurons rely on bone marrow derived neurotrophic factor (BDNF), both for development and for adaptive growth in adulthood, whereas jugular ganglia neurons rely on nerve growth factor (NGF). A small group of vagal neurons respond to both (Nassenstein *et al.*, 2010), which is important when considering potential mechanisms for increased innervation in airway diseases.

iii. Subtypes of sensory nerves

Airway sensory neurons have been classified by electrophysiological properties into three different categories. These are 1) slowly adapting stretch receptors (SARs), 2) rapidly adapting stretch receptors (RARs), and 3) C-fibers. The first two of these are Aδ fibers, with myelinated axons larger in diameter than C fibers (Adrian, 1933, Knowlton and Larrabee, 1946, Paintal, 1955). SAR nerve endings are located in the trachealis muscle, and exhibit sustained firing in response to lung inflation. By contrast, RARs innervate airway epithelium, exhibit burst firing during inhalation, and are stimulated by inhaled irritants. C-fibers also terminate within the airway epithelium. They are chemoreceptors, activating in response to a wide variety of chemical stimulants, including capsaicin, bradykinin, histamine (Riccio *et al.*, 1996, Kajekar *et al.*, 1999), adenosine, serotonin, methacholine, nicotine (see Table 1.1), and hyperosmolality, although not all receptors are activated by all agents. They are thought to be the primary activators of centrally-mediated reflex bronchoconstriction, and may also directly activate airway parasympathetic ganglia as part of a separate autonomic axon reflex (Undem and Carr, 2002).

Stepping beyond these functional categories, a recently published atlas of vagal sensory neurons defined 24 different nerve subtypes within nodose and jugular ganglia using single-cell RNA sequencing and transcriptomic analysis (Kupari *et al.*, 2019). Nodose/jugular ganglia from C57BL/6 mice were flow sorted into single cells, and populations of sensory nerves were separated from glia, endothelial cells, and contaminating superior cervical ganglion neurons by using known markers *Vglut2*, *Tubb3*, *Snap25*, and *Uchl1*. The resulting atlas includes the complete transcriptional profiles of eighteen transcriptionally distinct subtypes of sensory nerves within nodose ganglia, including several subtypes of pulmonary chemosensors that express a variety of receptors and may be uniquely primed to sense inflammatory signaling (Figure 1.4). A principal finding of this study is that labeling neurons as *TRPV1-expressing* or *Htr3a-expressing* oversimplifies transcriptional neuronal categories, as receptors and neuropeptides are expressed by multiple functional groups of neurons within ganglia.

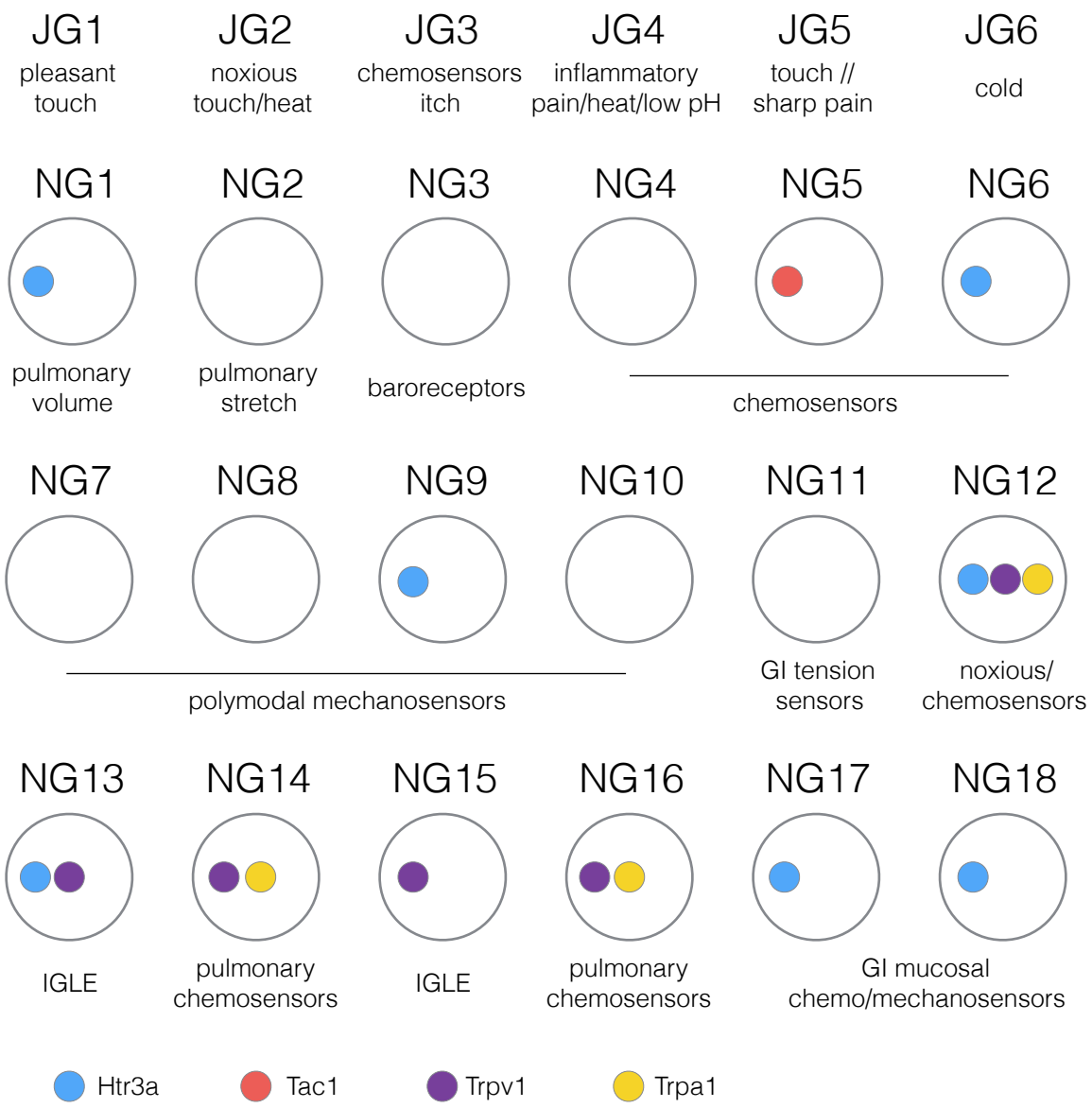

Figure 1.4. Subtypes of sensory nerves defined by transcriptome analysis and single cell RNA sequencing. Sensory nerves that project to the airway are primarily located in nodose ganglia (NG), and 18 subtypes of nodose neurons were described in this study. Htr3a = serotonin receptor 3a. Tac1 = tachykinin 1. Trpv1 = transient receptor potential vanilloid 1. Trpa1 = transient receptor potential ankyrin 1. Figure adapted from Kupari *et al.*, 2019.

This represents a significant step forward for the field: in the past, studies have used a single receptor to identify a subset of nerves that may play a role in airway hyperreactivity.

iv. Sensory nerve receptors and neurotransmitters

Sensory nerves in the airways involved in reflex bronchoconstriction express a variety of receptors which may lead to nerve activation.

Table 1.1. Receptors on airway sensory nerves leading to nerve activation

Receptor	Description	References
$5HT_3$	Ionotropic receptors. Bind serotonin (5HT). Expressed on a subset of nodose, but not jugular vagal afferents. Activation leads to reflex bronchoconstriction. Endogenous release of 5HT from mast cells or platelets enhances bronchoconstriction in allergic inflammation.	(Chuaychoo *et al.*, 2005, Dürk *et al.*, 2013, Mendez-Enriquez *et al.*, 2021)
nACh	Ionotropic receptors. Bind acetylcholine, nicotine. One mechanism by which inhalation of cigarette smoke induces bronchoconstriction.	(Lee *et al.*, 2018)
TRPV1	Ionotropic receptors. Bind capsaicin. Found on C fibers and some Aδ fibers after antigen challenge. Activation contributes to airway inflammation and remodeling.	(Lieu *et al.*, 2012, Choi *et al.*, 2018)
A1	Metabotropic receptors. Bind adenosine. Adenosine may lead to bronchoconstriction and dyspnea when administered therapeutically.	(Hong *et al.*, 1998)
$P2X_3$	Ionotropic receptors. Bind ATP. Important for cough and pain regulation. Selective antagonists may be used to treat idiopathic chronic cough.	(Abdulqawi *et al.*, 2015, Morice *et al.*, 2019)

b. Efferent autonomic nerves: Parasympathetic

i. Anatomy

Parasympathetic nerves form the downstream part of reflex bronchoconstriction after sensory nerves. Preganglionic parasympathetic cell bodies are located in the brainstem, primarily in the nucleus ambiguous of the medulla oblongata. Axons from preganglionic neurons run caudally within vagus nerves. Vagus nerves loop around either the aorta (left side) or the subclavicular artery (right side) giving rise to the recurrent laryngeal nerve before continuing caudally to supply the trachea, lung, heart, and gastrointestinal systems. Preganglionic nerves leave the vagus to enter the trachea and main

bronchi and synapse onto postganglionic cell bodies embedded within the tracheal walls. Much of the classic anatomical work done to characterize these nerves was handicapped by use of tissue sectioning, which does not allow for an accurate overall understanding of the complexity of neural architecture. Baker *et al* (1986) provided what is perhaps the most complete image of airway parasympathetic nerve anatomy using whole mount staining of acetylcholinesterase activity in ferret tracheas (Figure 1.5) (Baker *et al.*, 1986). The organized structure they describe features 1) bilateral nerve trunks running longitudinally between the trachealis muscle and the edge of the cartilaginous rings, 2) a superficial meshwork of parasympathetic nerves covering the trachealis muscle and submucosal glands, 3) a deep nerve meshwork surrounding smooth muscle cells and submucosal acini and ducts, 4) medium to large clusters of large round parasympathetic cell bodies (10-38 cell bodies per ganglia), averaging 34 um in diameter with a prominent nucleus and a small axon "stalk" located along the bilateral trunks, and 5) smaller, more elongated cells bodies (24 um diameter) without stalks, yet still with a prominent nucleus, located in smaller clusters (1-4 cell bodies) within the superficial meshwork. They called larger cell bodies type I parasympathetic cells and smaller cell bodies type II.

ii. Subtypes of parasympathetic nerves

Early studies in cats and ferrets described two types of parasympathetic nerves based on size and depolarization patterns. Baker *et al* (1986) described ferret type I and type II cells. Using horseradish peroxidase labeling of individual neurons and a camera lucida, they characterized the morphology of type I parasympathetic neurons, describing 4-8 processes emerging from each cell body: one central process that was much larger and always (n=7 neurons) left the ganglia and entered the longitudinal trunk, and occasionally smaller processes dividing from the larger axon. The larger process was reported to extend for 1-2mm before entering the superficial muscle plexus where it ended in varicosities around smooth muscle. Mitchell *et al* (1987) described similar populations of large and small cells in cats, and characterized them using electrophysiology. Large cells fired with an inspiratory rhythm, displayed post-spike after-hyperpolarization, and had cell bodies located in tracheal smooth muscle. Axons of these large cells projected up to 6mm from the cell bodies and had numerous varicosities over the last 5mm. Small cells fired with an expiratory rhythm and had no significant post-spike after-hyperpolarization. Their cell bodies were located in the posterolateral tracheal adventitia near the intercartilaginous spaces. Axons of these small cells projected towards the nerve plexus around mucosal glands, but axon terminations were not definitively determined (Mitchell *et al.*, 1987).

iii. Neurotransmitters

The primary neurotransmitter released by parasympathetic nerves is acetylcholine. Acetylcholine is synthesized by the enzyme choline acetyltransferase, which transfers an acetyl group from coenzyme A to choline (Nachmansohn and Machado, 1943, Feldberg and Mann, 1946). It is stored in vesicles and released from nerve terminals under resting conditions and in response to stimulation (Birks and Macintosh, 1957). Once in the synapse, it is broken down and hydrolyzed to choline by

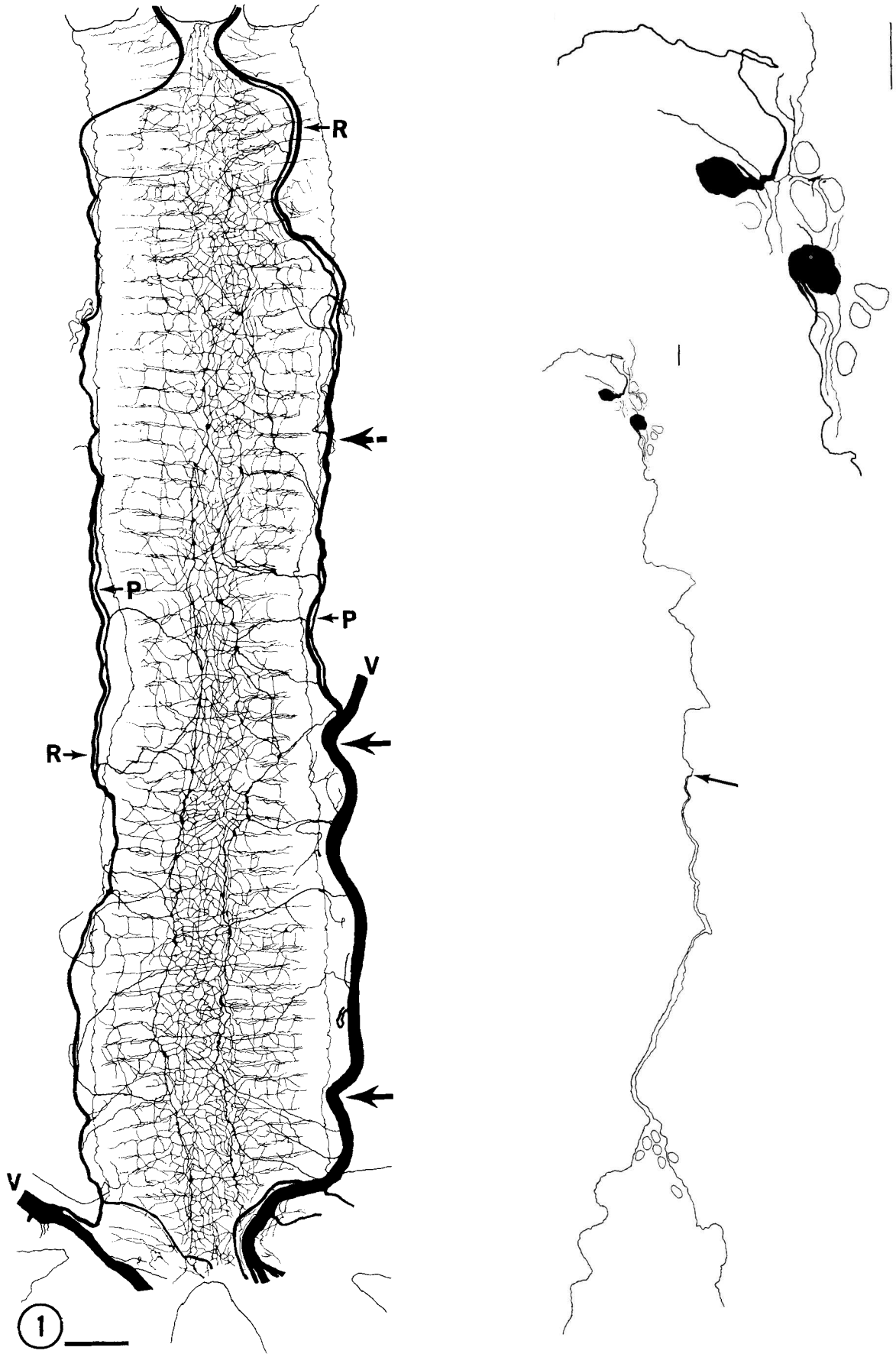

Figure 1.5. Anatomy of parasympathetic nerves in the trachea. Reprinted from Baker *et al.*, 1986.

acetylcholinesterase. This process can be blocked by acetylcholinesterase inhibitors, including physostigmine, which prolong the duration of acetylcholine in the synaptic cleft and increase downstream effects of parasympathetic nerve stimulation.

Acetylcholine is released by preganglionic parasympathetic neurons onto nicotinic receptors on postganglionic neurons. These ion channels rapidly depolarize postganglionic nerves, which then release acetylcholine onto postjunctional muscarinic receptors. In the lungs, bronchoconstriction is mediated by M_3 muscarinic receptors on airway smooth muscle. Parasympathetic nerves via release of acetylcholine maintain airway tone and mediate bronchoconstriction.

Additional neurotransmitters have also been identified in parasympathetic ganglia. Substance P has been identified in some postganglionic neurons through immunohistochemical labeling (Dey *et al.*, 1988, 1991, 1996, Scott *et al.*, 2014). Substance P expression appears to increase in postganglionic parasympathetic nerves in models of asthma, indicating the expression of this neuropeptide in the parasympathetic population may play a role in airway disease (Wu *et al.*, 2003). Neuronal nitric oxide synthase (nNOS) has been reported in ferrets and humans (Dey *et al.*, 1996, Fischer *et al.*, 1996), and tyrosine hydroxylase (TH) has been seen in human airway intrinsic ganglia after lung transplant (Springall *et al.*, 1990). Other neuropeptides, such as vasoactive intestinal peptide and neuropeptide Y, have also been identified in rodent and human parasympathetic ganglia (Dey *et al.*, 1996, Fischer *et al.*, 1996, Richardson *et al.*, 2003). These data together suggest an abundant transcriptional heterogeneity in postganglionic parasympathetic neurons in the airways that remains to be fully defined.

iv. Electrophysiological properties

Parasympathetic neurons with two distinct types of firing properties have been described, most thoroughly in guinea pigs (Myers *et al.*, 1990). Tonic neurons, representing about one third of all postganglionic parasympathetic neurons, respond throughout a given current step with sustained, repetitive action potentials. Phasic neurons, representing the remaining two thirds, respond with initial bursts of action potentials at the beginning of the current step but then accommodate rapidly. Both groups of neurons have similar resting membrane potentials (-44mV) and after-hyperpolarization periods (60-200ms) (Baker, 1986). Later findings in mice showed similar properties: after-hyperpolarization periods of 30-80ms, resting membrane potentials of around -50mV, and two distinct firing types (Weigand and Myers, 2010). Observations of heterogeneous electrical properties (Coburn and Kalia, 1986, Kajekar *et al.*, 2001) and evidence of postganglionic parasympathetic neurons synapsing onto each other (Coburn and Kalia, 1986) have led to the theory that postganglionic parasympathetic airway neurons are capable of integrating and modulating signals from preganglionic nerves (Burnstock G, 1987, Myers and Undem, 1991, Kajekar *et al.*, 2001).

v. Axonal reflex

The axonal reflex defines the ability of C-fibers to activate postganglionic parasympathetic neurons directly through release of neuropeptides such as substance P, calcitonin gene-related peptide, and neurokinin A within the trachea. Activation leads to the same effects as centrally-mediated parasympathetic activation: bronchoconstriction, mucus secretion, and recruitment of inflammatory cells (Canning and Spina, 2009). The axonal reflex was identified in guinea pigs and rats (Undem *et al.*, 1990). However, it does not seem to contribute substantially to bronchospasm in human airways (Barnes, 2001), possibly due to decreased density of afferent nerve terminals in humans as compared to other species.

c. Efferent autonomic nerves: Sympathetic

Sympathetic nerves are present in the airways. Their cell bodies are located primarily in the stellate ganglia, and their axons run alongside those of sensory dorsal root axons to synapse onto parasympathetic ganglia and bronchial vasculature. Sympathetic nerves do not significantly affect airway tone in humans (Canning and Fischer, 2001). However, parasympathetic preganglionic neurons in the brainstem are regulated by sympathetic nerves from the locus coeruleus (Haxhiu *et al.*, 2003), and expression of alpha 2A adrenergic receptors on these preganglionic neurons may play a role in airway disease (Wilson *et al.*, 2007).

d. Efferent autonomic nerves: Bronchodilatory

Acetylcholinergic parasympathetic nerves provide dominant control of airway tone. Another class of efferent nerves modulates this tone, and the effects of these nerves can be seen once the adrenergic and cholinergic effects are blocked (Irvin *et al.*, 1980). In the past, this population has been called non-adrenergic non-cholinergic (NANC) nerves, although they are now more commonly classified by the neuropeptides and neuromodulators they release. These nerves arise from the myenteric plexus of the esophagus and project ventrally to the trachealis muscle (Canning and Undem, 1993, Balentova *et al.*, 2013). Bronchodilatory nerves promote airway relaxation through release of nitric oxide and vasoactive intestinal peptide. Of these, nitric oxide is the more potent bronchodilator in humans (Ward *et al.*, 1993).

e. Central nervous system nerves

Between the afferent sensory and the efferent parasympathetic nerves lie connections of the central nervous system (Figure 1.6). Studies in ferrets suggest that sensory neurons release glutamate onto AMPA receptors to activate central neurons, and that blocking this activation prevents reflex tracheal bronchoconstriction (Haxhiu *et al.*, 2000). Anterograde tracing studies have mapped projections of nodose neurons to second order neurons in the nucleus of the solitary tract in the medulla, while jugular neurons project primarily to the medullary paratrigeminal nucleus (McGovern, Davis-Poynter, *et al.*, 2015, McGovern, Driessen, *et al.*, 2015). The nucleus of the solitary tract is the central station for termination of sensory afferents originating in the lungs (Kubin *et al.*, 2006). Although the

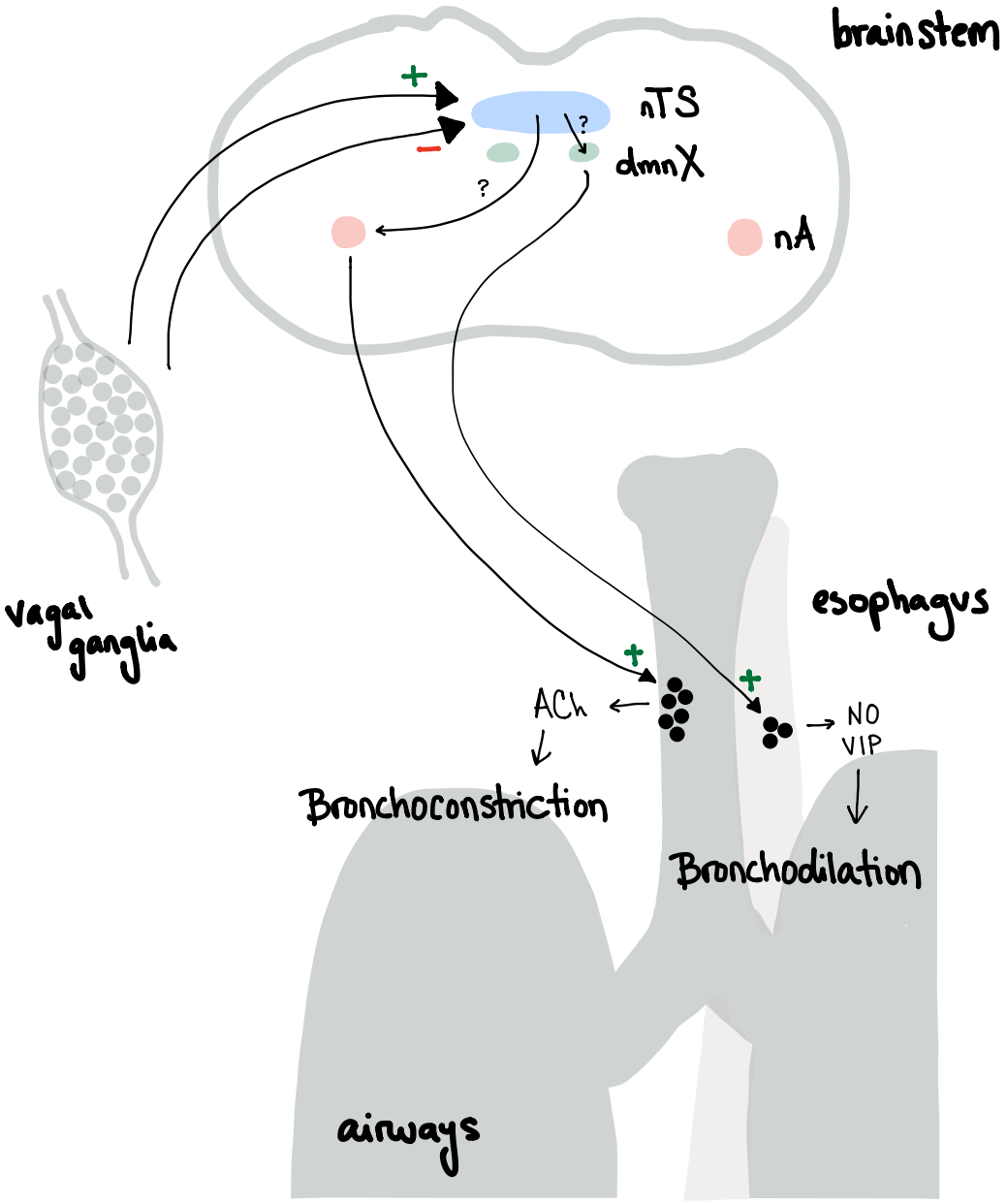

Figure 1.6. Central nervous system nerves connect sensory and parasympathetic nerves in reflex bronchoconstiction and sensory nerve mediated bronchodilation. Sensory nerves project to the nucleus of the solitary tract (nTS), and from there nerves eventually project (along an uncertain pathway) to preganglioinic parasympathetic nerves in the nucleus ambiguous (nA) or dorsal motor nucleus of the vagus (dmnX). Preganglionic neurons project to postganglionic neurons in trachea, which release acetylcholine (ACh) to cause bronchoconstriction, or in esophagus, which release nitric oxide (NO) or vasoactive peptide (VIP) to cause bronchodilation. Figure adapted from Mazzone and Canning, 2002.

pathways have not been fully mapped, these connections eventually reach the nucleus ambiguous and dorsal vagal nucleus, where cell bodies of airway-related preganglionic parasympathetic neurons reside. Neurons in the brainstem integrate signals from airway sensory neurons and deliver them to preganglionic parasympathetic neurons that control airway tone. Preganglionic parasympathetic nerves are regulated by many other brain regions, including sympathetic nerves from the locus coeruleus (Hadziefendic and Haxhiu, 1999).

C. Eosinophils

Eosinophils are granulocytic white blood cells, which represent 1-3% of all circulating leukocytes. They function as a primary defense against parasitic helminth infections and play a key role in atopic diseases including asthma (Weller and Spencer, 2017). Eosinophilia is generally believed to be harmful in the setting of diseases like asthma. This logic is supported by the beneficial effects of eosinophil-depleting drugs, such as mepolizumab, which is an antibody that binds and inhibits interleukin 5 and reduces asthma exacerbations in populations with severe eosinophilic asthma refractory to other treatments (Ortega *et al.*, 2014).

a. Discovery

Eosinophils were first discovered in 1879 by Paul Ehrlich, a celebrated immunologist who advocated for the humoral theory of acquired immunity. Dr. Ehrlich identified eosinophils in histological samples by the distinctive pink cytoplasm and multi-lobed nucleus. Eosinophils have since been identified in many species of mammals, fish, birds, and reptiles, although the morphology of their nuclei and granules varies between species. It is estimated that eosinophils have existed for at least 350 million years, based on identification by electron microscopy in Coelacanths, a rare species of extant fish that first appeared in the fossil record 350 million years ago (Jarial, 2005).

b. Morphology

Eosinophils are so named because their cytoplasmic granules react strongly with the acidic aniline dye "eosin Y," and appear bright pink under light microscopy. Their size ranges from 12–15μm in humans and 9–12μm in mice. Their nuclei are polymorphic, appearing multilobed in humans and ring-like in mice. The mammalian ancestor that would eventually evolve into present-day laboratory mice (*Mus musculus*) and humans (*Homo sapiens*) diverged 100 million years ago. Their eosinophils have also diverged over that time. As a result there are some differences between mouse and human eosinophils, such as the shape of their nuclei and the expression of certain surface ligands, but these are vastly outweighed by the similarities (Lee *et al.*, 2012), notably their conserved roles in modulating innate and adaptive immune responses, maintaining tissue and metabolic homeostasis, and inducing remodeling and fibrosis under pathological conditions (Lee *et al.*, 2010).

c. Granulocyte proteins

Within the cytoplasm of eosinophils are an abundance of membrane enclosed granules, which contain four cationic proteins: major basic protein, eosinophil cationic protein, eosinophil-derived neurotoxin, and eosinophil peroxidase (Gleich *et al.*, 1974, Weller and Spencer, 2017). When eosinophils become activated by signaling on their cell surface receptors, they degranulate, releasing their granule proteins into the local environment. Major basic protein performs a key role mediating eosinophil-induced airway hyperreactivity by antagonizing M_2 muscarinic receptors on airway parasympathetic neurons (Evans *et al.*, 1997). Antibodies against eosinophil major basic protein prevent antigen-induced M_2 receptor dysfunction and airway hyperreactivity in guinea pigs.

D. Asthma

a. Definition of asthma

Asthma is a respiratory condition characterized by episodes of limited airflow and respiratory symptoms such as coughing, wheezing, and shortness of breath. It is estimated to affect nearly 400 million people worldwide, and the incidence is rising, particularly in developing nations (Vos *et al.*, 2017). Pathologically, asthma is characterized by airway inflammation, structural remodeling of the airways, and airway hyperreactivity. Asthma is a highly heterogeneous disease, and diagnosis depends on an assessment of the pattern of symptoms and patient response to treatment.

b. Asthma subtyping

i. Clinical Phenotypes

Asthma may be broken down by clinical phenotypes (Wenzel, 2012, Papi *et al.*, 2017), based on onset and triggers:

a. Childhood-onset allergic asthma: this is the most common asthma phenotype. Onset occurs in childhood, and it is more common in people who also have atopic dermatitis, atopic rhinitis, or food allergies. It is also genetically linked, with odds ratios between 2 and 4 reported for children who have a parent with the disease. Patients often present with coughing and wheezing following respiratory infection. The probability of this asthma persisting to adulthood increases with smoking, female sex, and early exposure to viral infections and household allergens.
b. Exercise-induced asthma: excessive bronchoconstriction in response to intense aerobic exertion. May be worsened by cold or immersion in water (as in swimming pools). This subtype does not have an associated inflammatory response.
c. Aspirin-induced asthma: symptoms of respiratory distress brought on specifically by aspirin (acetylsalicylic acid). Aspirin blocks cyclo-oxygenase (COX) and shifts the phospholipase A2 pathway away from prostaglandins and towards cysteinyl leukotriene, which leads to increased bronchoconstriction and mucus production, to which these patients may be particularly susceptible (Hamad *et al.*, 2004).

d. Cough-variant asthma: cough with airway hyperreactivity in adults. This is uncommon, as cough in adults is more often associated with gastro-esophageal reflux, post-nasal drip, or upper airway dysfunction.
e. Occupational asthma: asthma induced by occupational exposure to allergens or irritants. This is estimated to account for 5-20% of adult onset asthma.
f. Late-onset asthma: onset of asthma after 12 years of age. May be associated with smoking or obesity, and atopic or non-atopic disease.

Although they may be descriptive in a clinical setting, these phenotypes do not sufficiently categorize the pathological mechanisms or even best treatment options for individuals with disease. For that, asthma endotypes are more useful.

ii. Asthma endotypes

An endotype is a subtype of a condition defined by a distinct pathological mechanism. A wide variety of asthma endotypes have been proposed, which combine clinical phenotypes of asthma with molecular biomarkers and treatment response. One commonly referenced endotype is Th2 dominant (or "Type 2 high") asthma (Lötvall *et al.*, 2011, Agache, 2019). This endotype is defined as asthma driven by Th2 cells and cytokines, including IL-5, and characterized by the presence of eosinophils. It is generally true that patients with this endotype typically begin experiencing asthma symptoms in childhood and are sensitized to allergens that trigger exacerbations (Lötvall *et al.*, 2011). However, within this endotype there remains a huge degree of variability in regards to disease phenotype, severity, and response to treatment (Agache, 2019). This indicates a gap: both a gap in understanding the physiology of asthma (and whether this endotype really defines a unified pathological mechanism) and a practice gap in treating patients with severe eosinophilic asthma.

c. Characteristics of asthma

Three characteristic features of asthma are airway inflammation, structural remodeling, and airway hyperreactivity. Airway inflammation refers to the influx of immune cells into the airways. In Th2 dominant allergic asthma, the most common asthma endotype, the dominant immune cell is the eosinophil. Other common infiltrating cells are Th2 T-cells and mast cells. Immunoglobulin E (IgE) and cytokines IL-4, IL-5, and IL-13 are essential mediators of the immune response in Th2 dominant asthma. Structural remodeling refers to changes to the airway structure seen in asthma, and includes smooth muscle hypertrophy, goblet cell hyperplasia, sub-basement membrane fibrosis, and narrowing of the airway lumen. The last characteristic feature is airway hyperreactivity, which is mediated by airway nerves, and defined as increased bronchoconstriction in response to an inhaled agonist. Airway hyperreactivity will be discussed in depth later in this introduction.

d. Anti-eosinophil therapies in asthma

No treatment options cure asthma completely. Current treatments for asthma include β2 adrenergic receptor agonists, muscarinic receptor antagonists (both of which reverse bronchoconstriction), and

inhaled steroids (which reduce inflammation). More recently developed treatments for asthma include biologics that target the underlying mechanisms of asthma inflammation. These are summarized in Table 1.2.

Table 1.2. Antibodies for the treatment of asthma

Treatment	Target	Description	References
Omalizumab	IgE	Reduces exacerbations and improves lung function. Recommended add-on for patients on inhaled steroids and long-acting β2 adrenergic receptor antagonists who remain symptomatic.	(Busse *et al.*, 2011, Hanania *et al.*, 2011, Garcia *et al.*, 2013)
Mepolizumab	IL-5	Reduces exacerbations, reduces steroid use, and improves symptoms in patients with severe asthma refractory to other treatments. Reduces blood and sputum eosinophils. Most benefit for patients with high peripheral eosinophils.	(Nair *et al.*, 2009, Pavord *et al.*, 2012, Bel *et al.*, 2014, Ortega *et al.*, 2014, 2016)
Reszilumab	IL-5	Reduces exacerbations, decreases sputum eosinophils, improves lung function (modestly) in patients with high eosinophils.	(Castro *et al.*, 2011, 2015, Corren *et al.*, 2016)
Benralizumab	IL-5R	Reduces exacerbations and reduces steroid use in patients with severe eosinophilic asthma. Reduces blood, sputum, and submucosal eosinophils.	(Laviolette *et al.*, 2013, Bleecker *et al.*, 2016, FitzGerald *et al.*, 2016, Nair *et al.*, 2017)
Lebrikizumab	IL-13	Improves lung function (modestly) in patients with periostin high phenotypes.	(Corren *et al.*, 2011, Hanania *et al.*, 2015, 2016)
Dupulimab	IL-4αR	Monoclonal antibody, blocks IL-4 and IL-13 signaling. Reduces exacerbations and improves lung function.	(Wenzel *et al.*, 2016)

E. Animal models of allergic asthma

a. Animal models of disease

Animal models are useful tools for investigating aspects of disease that would be challenging to fully examine in humans. Hau conceptualizes five categories of animal models of disease (Hau, 2008):

1. Induced (experimental) models: healthy animals in which the disease to be studied is induced, as in the asthma model using house dust mite sensitization and challenge (Cates *et al.*, 2004)

2. Spontaneous (genetic, mutant) models: natural conditions that arise in non-human species that reveal parallel mechanisms of disease. Not commonly used in asthma, since mice do not typically experience spontaneous allergic airway disease (Kips *et al.*, 2003)
3. Genetically modified models: models in which a disease state is induced through genetic modification, as in the IL-5tg mouse (Lee *et al.*, 1997) and IL-5/Eotaxin-2tg (Ochkur *et al.*, 2007) mouse models of asthma.
4. Negative models: models in which an element, such as a protein, receptor, or cell type, thought to be essential to the disease is removed, as in the eosinophil knock-out (PHIL) mouse (Lee *et al.*, 2004)
5. Orphan models: diseases in animals that have no correlate in humans, yet allow us to study conserved biological pathways and mechanisms. Not applicable to asthma.

b. Modeling allergic asthma

No single model will recapitulate the entirety of the human experience. Mouse modeling has some limitations for evaluating the natural etiology of disease, since mice are not known to be naturally afflicted with asthma. Cats have been diagnosed with allergic asthma acquired from exposure to such allergens as dust from cat litter, pollens, and mold. Respiratory allergies and asthma are also common in horses, who may be diagnosed with Inflammatory Airway Disease (IAD) (which has a predominantly eosinophilic inflammatory response) or heaves (a similar phenotype with a neutrophilic inflammatory response). For allergic asthma, mouse models have sought to recapitulate specific aspects of the disease, including inflammatory phenotype and airway hyperreactivity, either through environmental exposures or enhancement of inflammatory drivers.

i. Antigen sensitization and challenge model

Antigen sensitization and challenge is used to model late-onset eosinophilic asthma endotypes in a variety of animal species. Commonly used antigens include ovalbumin and house dust mite (HDM). Proteins from house dust mite, or *dermatophagiodes pteronyssinus*, are highly allergenic, and the majority of patients with allergic eosinophilic asthma are sensitized to house dust mite, which makes it more clinically relevant than ovalbumin (Voorhorst *et al.*, 1967, Woodcock *et al.*, 2003). This model calls for a short period of exposure to high concentrations of antigen (timing and dosage varies in different laboratories, but 2-3 days of exposure is common), followed some time later by further exposure to low doses of the antigen and subsequent animal experiments/harvest. The initial sensitization phase activates Type 2 helper T cells and upregulates production of IgG1 and IgE, while the subsequent challenge phase induces a robust inflammatory response from the prepared cells (Yu *et al.*, 1999, Cates *et al.*, 2004). House dust mite sensitization and challenge in wildtype mice induces airway eosinophilia, type 2 cytokine production (including IL-4, IL-5, and IL-13), epithelial cell hyperplasia, mucus cell metaplasia, and airway hyperreactivity (Cates *et al.*, 2004, Gregory *et al.*, 2009, Jones *et al.*, 2017).

ii. Airway IL-5 transgenic model

Mice overexpressing the cytokine IL-5 in the airways are used to model endotypes of chronic hypereosinophilic and early-onset eosinophilic asthma. These mice were created by pronuclear injection of a genetic construct containing IL-5 driven by an airway epithelium specific promoter, CC10 (Lee *et al.*, 1997). IL-5 induces recruitment of eosinophils to the tissue in which it is expressed, and increases eosinophil production in the bone marrow and survival in the airways. It has been shown by this group and others (Drake *et al.*, 2018) that these mice, without any additional environmental exposures, display many characteristics of allergic asthma, including chronic lung pathology and airway hyperreactivity.

iii. Eosinophil knock-out mouse

Mice lacking eosinophils were developed in order to investigate the necessity of eosinophils for pathological remodeling and airway hyperreactivity in asthma disease models. PHIL mice were developed in the James Lee laboratory (Lee *et al.*, 2004), by expressing a transgene of diphtheria toxin A under an eosinophil-specific promoter (EPO). This causes eosinophils to die upon maturation. They showed that these mice do not develop airway hyperreactivity after antigen sensitization and challenge, demonstrating the fundamental and necessary role of eosinophils in airway hyperreactivity in those models.

F. Neural mechanisms underlying airway hyperreactivity

Airway hyperreactivity (also called "hyperresponsiveness," both terms used interchangeably in the literature. In this dissertation I will use hyperreactivity) is defined as increased constriction of airways in response to an inhaled agonist (Hargreave *et al.*, 1986), is characteristic of asthma, and is often accompanied by other exaggerated airway responses including cough, mucus production, and increased microvascular leakage. Airway hyperreactivity is seen in many animal models of asthma and asthma exacerbation, including virus infection, antigen sensitization and challenge, exposure to ozone or to organophosphate pesticides, and obesity. In all these animal models airway hyperreactivity is mediated, in whole or part, by changes in neural control of the airways.

Neural changes underlying hyperreactivity could include changes in 1) afferent (sensory) nerves, 2) neurons within the central nervous system, or 3) efferent nerves, including parasympathetic cholinergic nerves and nitrergic bronchodilatory nerves. Reflex bronchoconstriction is initiated when an external chemical or mechanical stimulus depolarizes sensory nerves, which signal through the central nervous system to activate efferent parasympathetic nerves, which in turn release acetylcholine onto airway smooth muscle to cause contraction. The following sections are a detailed discussion of how each of these airway nerve pathways contributes to airway hyperreactivity.

a. Afferent sensory Nerves

i. Electrophysiological sensitivity

The physiological role of sensory neurons is to respond to chemical and mechanical stimuli in the lungs, such as pulmonary stretch or inhaled irritants. The sensitivity of these nerves increases in many disease models. For example, antigen exposure in sensitized animals alters the intrinsic, electrophysiological properties of nodose ganglion neurons. Ovalbumin-exposed guinea pig nodose neurons react to antigen with increased resting membrane potential, making it easier for these nerves to fire (Undem and Weinreich, 1993).

ii. Increased innervation

Airway sensory nerve morphology also changes in response to long-term antigen challenge and resulting long-term inflammation. The long term effect of inflammation on increased sensory nerve density and airway hyperreactivity has been shown in humans and animal models of asthma (Drake *et al.*, 2018). Bronchoscopic biopsies of human airways from patients with severe eosinophilic asthma and non-asthmatic controls were labeled with antibodies against PGP9.5, a general marker for peripheral nerves, and whole mount tissues were optically cleared and imaged in three dimensions. Computer modeling and quantification of airway nerves revealed increased epithelial nerve length and branching in patients with moderate to severe asthma (Figure 1.7), suggesting that sensory nerve overgrowth may be a mechanism underlying airway hyperreactivity. Experiments in transgenic mice that express IL-5 in airway epithelium, causing airway eosinophilia, revealed similar increases in sensory innervation, although these changes were not seen in *wild*type mice exposed acutely to house dust mite.

iii. Maternal and prenatal exposures

Prenatal factors may also contribute to developmental changes favoring hyperreactivity. To study this (Lebold *et al.*, 2020), female transgenic mice that overexpress IL-5 were bred with wildtype males, and gave birth to offspring both with and without increased airway IL-5. Genetically wild-type offspring of this cross had markedly increased sensory innervation and airway hyperreactivity. The amniotic fluid surrounding the wildtype fetuses had high levels of IL-5, resulting in fetal eosinophilia. Fetal exposure to IL-5 permanently altered neural supply to the lung, as these wildtype offspring exhibited hyperinnervation and hyperreactivity into adulthood, even though neither IL-5 nor eosinophilia were present after birth. The central role of fetal eosinophils in airway hyperinnervation was seen in subsequent experiments where IL-5 transgenic mice were crossed with mice congenitally devoid of eosinophils. In these studies, IL-5 was still elevated in the amniotic fluid but the fetuses could not develop eosinophilia, and they did not develop hyperinnervation or hyperreactivity as adult mice.

iv. Neuropeptide expression and regulation

Increases in expression of neuropeptides, including substance P, occur in the setting of allergic inflammation and may also drive airway hyperreactivity. Increase in the percentage of epithelial nerves

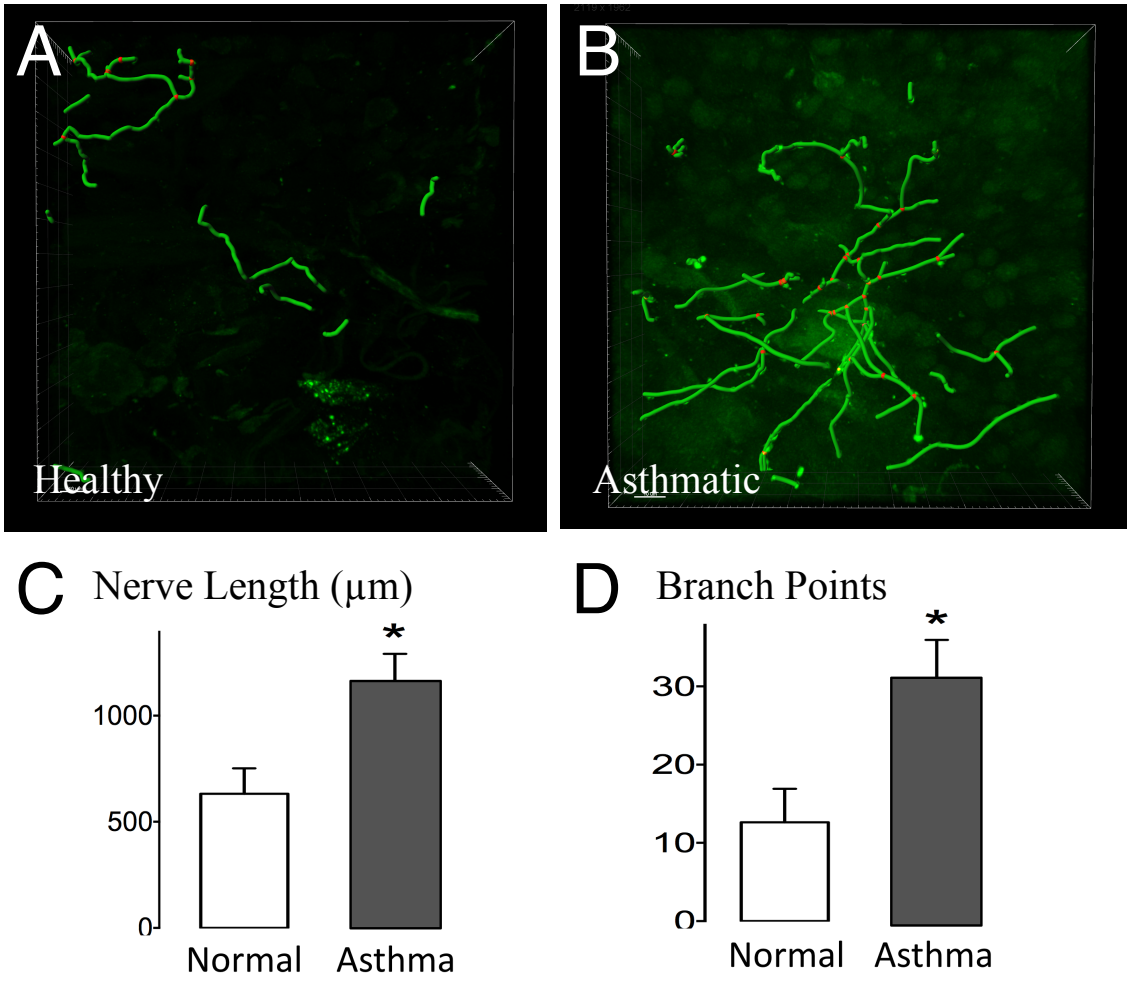

Figure 1.7. Human airway sensory nerves. (A-B) Computer model of nerves within epithelium of human bronchial biopsies from healthy patients (A) and patients with asthma (B), with nerve model in green and nerve branch points marked with a red dot (Imaris software). (C-D) Quantification of nerve length and branch points, showing increases in patients with asthma. *$p < 0.05$. Reprinted with permission from Drake *et al.*, 2018.

expressing substance P has been seen in biopsies from humans with eosinophilic asthma (Drake *et al.*, 2018). Substance P containing nerve endings are located most densely in the epithelium of the ventral aspect of the airways and do not tend to cluster around airway branch points (Scott *et al.*, 2013). This sets them apart from the majority of sensory nerve endings and suggests they may serve a distinct role in control of airways. Peptidergic sensory nerves have long been studied in the context of airway hyperreactivity. Antigen challenge increases mRNA and protein expression of substance P, calcitonin gene related peptide, and neurokinin A in sensory nerves 24 hours after exposure (Fischer *et al.*, 1996). Changes in neuropeptide expression are partly due to *de novo* expression in neurons that did not previously produce tachykinins, and does not merely reflect increased production in existing peptidergic neurons (Undem *et al.*, 1999). Furthermore, neurons in the nodose and jugular ganglia that newly express tachykinins in response to antigen challenge are larger in diameter than peptidergic neurons in naive animals (>20μm), suggesting they belong to distinct subset of neurons (Dinh *et al.*, 2005), potentially the rapidly adapting stretch receptors (Myers *et al.*, 2002).

Decreased breakdown of substance P is a separate, complementary mechanism leading to airway hyperreactivity. Neutral endopeptidase is the primary enzyme responsible for cleaving substance P in the airway. Antigen challenge (Samarasinghe *et al.*, 2010), virus infection (Dusser *et al.*, 1985, Jacoby *et al.*, 1985), cigarette smoke (Dusser *et al.*, 1989), and exposure to some toxic chemicals (Sheppard *et al.*, 1988), all cause airway hyperreactivity to substance P by decreasing neutral endopeptidase activity in airway epithelium. Conversely, neutral endopeptidase is increased in airway epithelium of asthma patients on long term steroids, and the resulting increased breakdown of substance P may contribute to the beneficial effects of steroid treatment (Sont *et al.*, 1997).

v. Subtypes

Subtypes of sensory nerves that contribute to airway hyperreactivity continue to be identified. MgprC11 is known for its role mediating itch in dermal dorsal root ganglia neurons, and was recently identified on jugular airway neurons. The study argued that MgprC11 defines a novel subgroup of sensory nerves that drive cholinergic bronchoconstriction and airway hyperreactivity (Han *et al.*, 2018). This may be true, but it is becoming increasingly clear that single receptors do not often define the most important nerve subpopulations for understanding disease. Patients with asthma have increased sensitivity to TRPV1 receptor agonists (Belvisi *et al.*, 2016), and TRPV1 knockdown attenuates airway hyperreactivity in mice (Choi *et al.*, 2018). However, agonists to the TRPA1 receptor, often found on the same nerves as TRPV1 receptors, are inhibitors of bronchoconstriction in two different animal models of allergic asthma (Marsh *et al.*, 2020). The single-cell RNA sequencing study by Kupari et al. defined subgroups of airway nerves in nodose and jugular ganglia by primary component analysis, and found most receptors span multiple groups, including receptors TRPV1 and TRPA1 (Kupari *et al.*, 2019). This may help explain contradictory findings in the literature, and demonstrates the pitfalls of categorizing cellular subtypes by one receptor only. It also highlights the

potential benefits of a well-defined transcriptional atlas and phylogeny to understand sensory nerve contributions to airway hyperreactivity.

G. Central Nervous System

Neuroplasticity in the nucleus of the solitary tract, nucleus ambiguous, and other regions likely plays a role in airway hyperreactivity, a process known as central sensitization (Bonham *et al.*, 2006). Central neuroplasticity may be mediated through synaptic properties, intrinsic properties of the neuron, or both, and would allow neurons to modulate their output when integrating signals from so many different sources: afferent sensory fibers, higher brain regions, local networks, and circulating neuromodulators.

i. Nucleus of the Solitary Tract (NTS)

Several studies have examined the changes to NTS neuron excitation in asthma and inflammation. Neurons of the NTS have increased firing activity after antigen exposure in rats (Spaziano *et al.*, 2015) and in monkeys after extended exposure to antigen (Chen *et al.*, 2001). A study of secondhand smoke exposure in young guinea pigs found an increase in evoked excitatory postsynaptic currents onto second order neurons in the NTS, which was reversed by blocking NK1 receptors, implicating a role for endogenous substance P (Sekizawa *et al.*, 2008). A different study performed in rhesus monkeys found decreased expression of histamine H3 receptors in NTS neurons may also contribute to increased central nervous system hyperreactivity. Histamine H3 receptors modulate the release of other neurotransmitters and have wide-ranging effects on synaptic transmission, and these receptors were found to be downregulated in young rhesus monkeys exposed over months to inhaled antigens and ozone (Sekizawa *et al.*, 2010).

ii. Airway-related preganglionic parasympathetic neurons

Neurons in the NTS project, directly or indirectly, onto airway-related vagal preganglionic neurons in the nucleus ambiguus, and to a lesser extent in the dorsal vagal nucleus (Hadziefendic and Haxhiu, 1999). These parasympathetic preganglionic neurons are regulated by extensive networks of neurons in the brainstem, including sympathetic regulation from the locus coeruleus (Haxhiu *et al.*, 2003). Central nervous system hyperreactivity may have important clinical implications for secondhand smoke exposure, early life allergen exposure, and potentially understanding nocturnal asthma (Haxhiu *et al.*, 2006).

a. Parasympathetic Nerves

Preganglionic parasympathetic nerve cell bodies reside in the brainstem, and travel in the vagus to synapse with postganglionic parasympathetic nerve cells. Postganglionic cell bodies are located in clusters, called ganglia, within the walls of the trachea and bronchi. Postganglionic nerves supply smooth muscle and airway mucus glands, control airway tone, and mediate bronchoconstriction via release of acetylcholine onto M_3 muscarinic receptors (Roffel *et al.*, 1990, Fisher *et al.*, 2004).

i. M_2 muscarinic receptors

Acetylcholine release is normally limited by inhibitory M_2 muscarinic receptors on postganglionic parasympathetic nerves (Fryer and Maclagan, 1984). These neuronal M_2 receptors are dysfunctional in patients with asthma (Ayala and Ahmed, 1989, Minette *et al.*, 1989), and are also dysfunctional in every animal model of airway hyperreactivity tested, including antigen challenge, virus infection, exposure to ozone, exposure to organophosphate pesticides, and obesity (Fryer and Jacoby, 1991, Fryer and Wills-Karp, 1991, Schultheis *et al.*, 1994, Adamko *et al.*, 1999, Yost *et al.*, 1999, Proskocil *et al.*, 2008, 2015, Nie *et al.*, 2014). In all these models, loss of neuronal M_2 muscarinic receptor function eliminates the negative feedback control they normally provide and significantly increases acetylcholine release and vagally mediated bronchoconstriction. Mechanisms leading to decreased M_2 function vary among these models, underscoring the heterogeneity of pathways involved in airway hyperreactivity.

ii. Antigen challenge

In antigen challenge models, animals are sensitized to an antigen, such as ovalbumin or house dust mite, then challenged with inhalation of the same antigen, resulting in eosinophilic inflammation and airway hyperreactivity. Antigen induced hyperreactivity is blocked by severing the vagus nerves or administering atropine, demonstrating the central role of reflex bronchoconstriction (Michoud *et al.*, 1976, McCaig, 1987, Costello *et al.*, 1999, McAlexander *et al.*, 2015). M_2 muscarinic receptors are dysfunctional in antigen challenged animals (Fryer and Wills-Karp, 1991). Loss of M_2 function requires eosinophils (Elbon *et al.*, 1995), and eosinophil major basic protein (Evans *et al.*, 1997), the principal pre-formed protein in eosinophil granules. Eosinophil major basic protein is an endogenous antagonist for M_2 muscarinic receptors, as demonstrated in radioligand binding studies (Jacoby *et al.*, 1993). *In vivo*, M_2 dysfunction is reversed acutely by agents, including heparin, that bind major basic protein (Fryer and Jacoby, 1992), while antibodies against eosinophil major basic protein prevent antigen-induced M_2 receptor dysfunction and airway hyperreactivity in guinea pigs (Evans *et al.*, 1997). Thus, in antigen challenged guinea pigs, acute airway hyperreactivity is mediated by loss of M_2 receptor function due to the presence of an endogenous antagonist, eosinophil major basic protein.

In both antigen challenged animals and humans with fatal asthma, more eosinophils are associated with airway nerves than are found anywhere else in the airway (Costello *et al.*, 1997) (Figure 1.8). Airway nerves release eotaxin, which actively recruits eosinophils by binding to eosinophil CCR3 receptors (Fryer *et al.*, 2006). Eosinophil adhesion to neurons is associated with degranulation and release of eosinophil major basic protein, which binds to M_2 receptors, increasing acetylcholine release and bronchoconstriction (Sawatzky *et al.*, 2002).

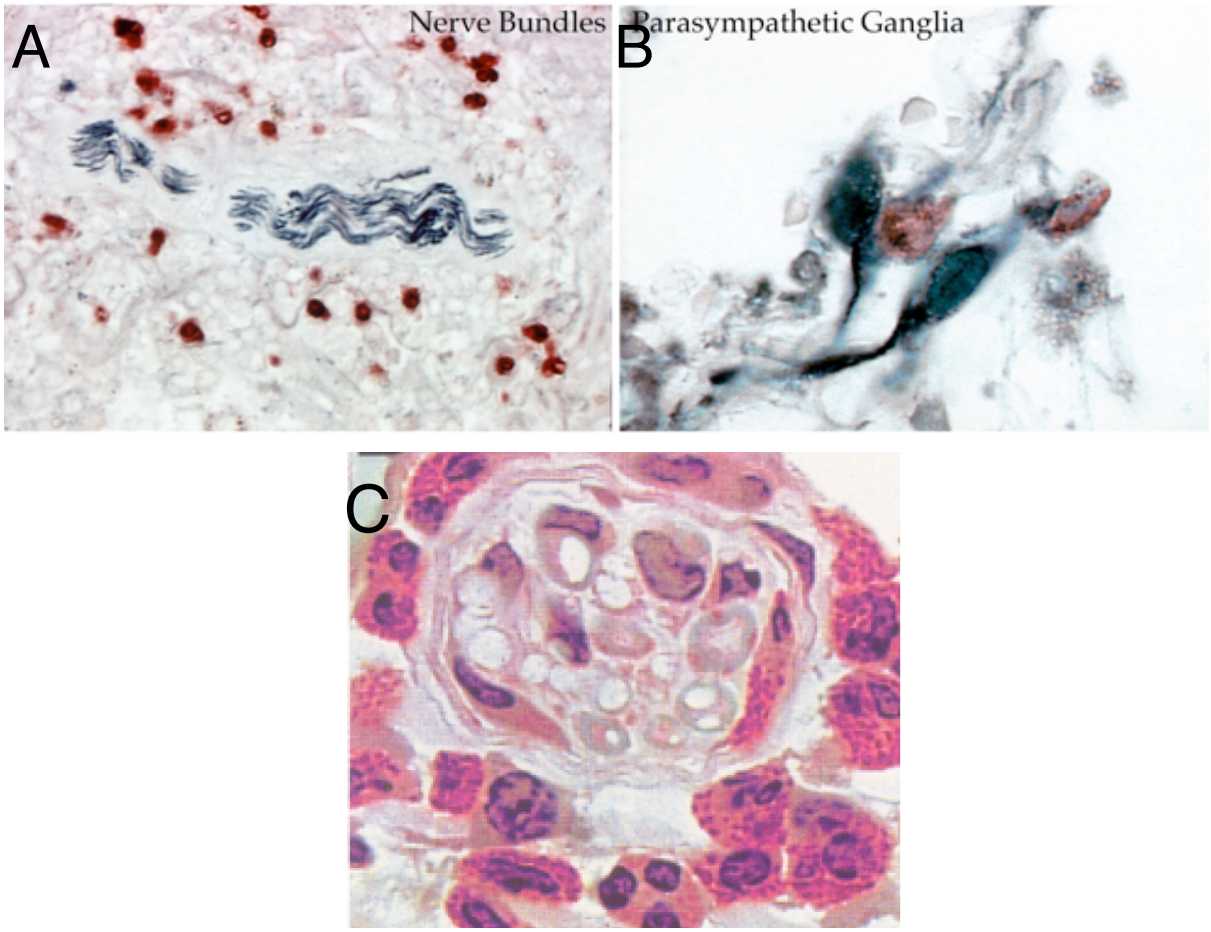

Figure 1.8. Nerve-eosinophil interactions, showing eosinophils closely associate with airway nerves in asthma. (A-B) Airways of patients who died from fatal asthma, showing eosinophils (major basic protein antibody, pink) localizing around nerve bundles (PGP9.5 antibody, black) (A) and a parasympathetic ganglion (B). (C) Guinea pig airway stained with hematoxylin and eosin. Cross section of nerve bundle center, eosinophils in pink. Reprinted with permission from Costello *et al.*, 1997.

iii. Viral infection

In addition to eosinophil mediated receptor blockade, other mechanisms can also impair M_2 receptor control of acetylcholine release. Viral infection is a frequent cause of asthma exacerbations (Johnston *et al.*, 1995, 2005, Atmar *et al.*, 1998). In the setting of viral infection, M_2 receptor dysfunction is due to both a direct, leukocyte-independent effect on M_2 function and an indirect, leukocyte-dependent effect (Fryer and Jacoby, 1991, Fryer *et al.*, 1994). Macrophage activation may be particularly important in virus-induced M_2 receptor dysfunction (Lee *et al.*, 2004), an effect that likely involves production of both TNF-α and IL-1β, and may be due to decreased expression of M_2 receptors on parasympathetic neurons (Rynko *et al.*, 2014).

iv. Ozone and Organophosphate pesticides

Environmental pollutants such as ozone and organophosphate pesticides are associated with asthma prevalence and contribute to exacerbations. Ozone induces airway hyperreactivity and M_2 dysfunction through release of eosinophil major basic protein (Schultheis *et al.*, 1994, Yost *et al.*, 1999) and also through release of reactive oxygen species from airway epithelium, and activation of the mitogen activated protein kinase pathway (Verhein *et al.*, 2013). Organophosphate pesticides, including chlorpyrifos and parathion, also cause airway hyperreactivity by decreasing neuronal M_2 receptor function (Fryer *et al.*, 2004). Organophosphates at exposure levels below those required to inhibit acetylcholinesterase potentiate airway hyperreactivity by driving lung macrophages to release TNF-α (Nie *et al.*, 2009, Proskocil *et al.*, 2013) which may decrease M_2 expression similar to viral infection (Lee *et al.*, 2004, Rynko *et al.*, 2014). Obesity induced airway hyperreactivity appears to have a unique mechanism that involves an interaction between increased insulin (released in insulin resistant obesity) and M_2 muscarinic receptors (Nie *et al.*, 2014).

In all these models, loss of M_2 receptor function and increased acetylcholine release is a common endpoint, arrived at via different inflammatory mechanisms, often involving either eosinophils or macrophages. Notably, however, mechanisms for M_2 dysfunction converge on eosinophils if animals are sensitized to an antigen before exposure to a subsequent environmental insult. In antigen-sensitized animals, airway eosinophils can be activated by viral infection, ozone inhalation, or exposure to pesticides, all causing release of major basic protein and blockade of M_2 receptors (Schultheis *et al.*, 1994, Adamko *et al.*, 1999, Yost *et al.*, 1999, Proskocil *et al.*, 2008, 2015).

v. Role of neurotrophic factors

In addition to these acute functional changes in the control of acetylcholine release, there is also evidence for increased cholinergic innervation in chronic inflammatory asthma. Studies of human bronchial biopsies demonstrated increased cholinergic fibers in asthmatic subjects (Dragunas *et al.*, 2020), and this was associated with increased brain-derived neurotrophic factor and its principal receptor, TrkB. Likewise, airway hyperreactivity after antigen challenge is attenuated in mice lacking TrkB receptors (Britt *et al.*, 2019). Early exposure to antigen in mice (postnatal days 5-20) leads to

increased innervation of smooth muscle mediated by neurotrophin-4 and TrkB signaling (Aven *et al.*, 2014). Thus, early or chronic exposure to antigens increases cholinergic input to smooth muscle and contributes to airway hyperreactivity.

b. Nitrergic and peptidergic bronchodilatory nerves

Bronchodilation is mediated by neuropeptides, such as vasoactive intestinal peptide (VIP), and by nitric oxide. VIP and other related peptides promote relaxation in human bronchi (Palmer *et al.*, 1986), and expression of VIP may be reduced in patients with asthma (Ollerenshaw *et al.*, 1989). However, while blocking endogenous VIP potentiates nerve-mediated bronchoconstriction in guinea pigs (Belvisi *et al.*, 1993), it does not in human airways (Ward *et al.*, 1993).

In human airways, the principal bronchodilatory mediator is nitric oxide, which is produced by nerves, airway epithelium, and endothelial cells (Ricciardolo, 2003). Nitrergic nerves arise from the myenteric plexus of the esophagus and project ventrally to the trachealis muscle (Canning and Undem, 1993). Blocking nitric oxide production potentiates nerve-mediated contraction in human airways (Ward *et al.*, 1993), and potentiates airway hyperreactivity in patients with mild asthma to the same degree as inhaled antigen (Ricciardolo *et al.*, 2001). Antigen sensitization and challenge decreases nitric oxide mediated bronchodilation (Ko and Lai, 1988, Aizawa *et al.*, 1997, Miura *et al.*, 1997). This is due at least in part to increased arginase (Meurs *et al.*, 2002), which breaks down L-arginine, the substrate for nitric oxide synthase, and decreases nitric oxide production. Arginase isozymes are increased in patients with asthma (North *et al.*, 2009). Administration of L-arginine and other substrates for nitric oxide production after antigen challenge leads to recovery of airway relaxation in guinea pigs (Maarsingh *et al.*, 2006).

H. Methods of airway nerve activation

Prior to the studies described in this dissertation, three methods existed for activation of airway nerves and assessment of airway hyperreactivity. The first was pharmacological activation of nerves using an agonist such as methacholine or serotonin. Neither of these drugs have receptors exclusively located on nerves, thus the bronchoconstriction response measured as a result of their administration is a combination of reflex bronchoconstriction effects with direct smooth muscle activation, potentially with indirect activation of other tissues. The second and third methods are more nerve specific: vagal nerve stimulation and electrical field stimulation. However, each of these methods has its own limitations, as will be described below, and neither has the capacity to target only specific subsets of nerves within the vagus for investigation.

a. Vagal nerve stimulation

Electrical stimulation of the vagus nerve *in vivo* allowed early investigators to assess the composition of the vagus (a combination of parasympathetic, sensory, and in some cases sympathetic fibers) across a

variety of species, including dogs (Woolcock *et al.*, 1967, Dixon *et al.*, 1980), rabbits (Karczewski and Widdicombe, 1969), and cats (Nandiwada *et al.*, 1983). Vagotomy (cutting the vagus bilaterally in between the vagal ganglia and the airways), in combination with electrical stimulation of the vagus, continues to allow investigators to measure the effects of nerve stimulation on the airways in larger animals, including guinea pigs (Gordon *et al.*, 1984, Buels *et al.*, 2012) and rats (Nie *et al.*, 2014). However, this technique is very difficult in small animals such as mice, and not often used. In humans, chronic vagus nerve stimulation has variable effects, and has been seen to cause deterioration of lung function in patients with obstructive lung disease (Lötvall *et al.*, 1994), although acute stimulation has shown some recent promise in treating acute asthma exacerbations (Miner *et al.*, 2012, Steyn *et al.*, 2013).

b. Electrical field stimulation

Airway nerves are also studied *in vitro*, by removing the trachea (and occasionally the esophagus as well) from an animal, suspending it from a pressure sensor, and applying an electrical field to activate any patent nerves in the tissue and measure airway contraction. Electrical field stimulation induces both contracting and relaxing effects, due to simultaneous stimulation of cholinergic, capsaicin sensitive, adrenergic, and non-adrenergic non-cholinergic neurons (Undem *et al.*, 1989), although varying stimulus parameters gives some degree of selectivity to which nerves are activated (Ellis and Undem, 1990, Myers and Undem, 1991). A significant downside of this method is that airways are removed from the animal, and severing the vagus nerve is inherent to the process. Unlike vagal nerve stimulation and electrical field stimulation, optogenetics presents a method for airway nerve activation that could target specific subsets of genetically distinct airway nerves with great precision. Chapter 3 of this dissertation describes the development of a method for optogenetic activation of airway parasympathetic neurons, and Chapter 4 describes the expansion of that method to study models of airway hyperreactivity.

I. Summary and Hypothesis

Airway hyperreactivity is a fundamental characteristic of asthma that clearly requires an intact nervous system. Studies have shown increases in sensory innervation of the epithelium in human asthma and changes to parasympathetic nerve function in human asthma and animal models of asthma. However, the separate contributions of sensory and parasympathetic nerves to asthma remain to be fully understood. It is my hypothesis that structural and pharmacological changes to sensory and autonomic nervous systems contribute to airway hyperreactivity associated with asthma. These changes can include increased nerve density, abnormal ganglia architecture, and alterations in neurotransmitter content and receptor expression. However, the complexity of the sensory and autonomic nerves makes it difficult to identify a role for specific nerves in airway hyperreactivity. Here, I developed novel tools to image individual nerves and depolarize specific populations, and tested whether these tools could be used to identify the role of unique nerve subsets in airway hyperreactivity associated with asthma. I

developed a method for optogenetic activation of airway nerves to test the results of activating specific nerve subtypes, beginning with cholinergic parasympathetic neurons (Chapter 3). I expanded this method to activate sensory nerves in the airways, and used both techniques to investigate the differences between activation of specific nerve subsets in mouse models of acute and chronic eosinophilic asthma (Chapter 4). I tested the hypothesis that differences in eosinophil localization and nerve interactions would lead to sensory nerve hyperreactivity in the chronic model and parasympathetic nerve hyperreactivity in the acute model. Finally, I developed a technique for AAV9-based multicolor labeling and simultaneous immunolabeling of airway postganglionic parasympathetic nerves and used it to test the hypothesis that a subgroup of these neurons project to other neurons within the ganglia (Chapter 5A). I also worked to develop a Brainbow-like mouse line for sustainable multicolor labeling of airway neurons (Chapter 5B).

Chapter 2. Methods

Choice of animals versus humans

Rationale for mice as an animal model of allergic asthma

Mice were the chosen model to study allergic asthma in these experiments due to the: 1) robustness of our antigen challenge protocol to establish airway hyperreactivity, 2) availability of genetically manipulated animals (*e.g*. IL-5 knock-in, channelrhodopsin knock-in), 3) availability of protocols, reagents, and equipment (*e.g.* mouse ventilator, antibodies), and 4) minimization of the cost and resource burden as compared to larger mammals. C57BL/6 were used over other strains because the transgenic animals necessary for optogenetics experiments (CHAT-Cre #028861 and #031661 and CH2-EYFP #024109) as well as the transgenic model of chronic airway hyperreactivity (IL5tg mice) were both available on this background. It is worth noting that BALB/c have a greater immunological response to antigen treatment, with higher levels of IL-5, IL-13 and IgE after antigen exposure, but it would have been time prohibitive to backcross all the necessary mouse lines onto this background. Mice, unlike humans, horses, and cats, do not naturally develop asthma. The mouse models used in these studies therefore recapitulate only certain aspects and symptoms of human asthma, specifically hypereosinophilia and airway hyperreactivity. Sensory hyperinnervation has been previously reported to occur in both human and mouse airways in the context of airway hyperreactivity, but whether there are similar changes in parasympathetic innervation is currently unknown.

Mouse Models

Mice

Mice were housed in temperature controlled pathogen-free facilities with light dark cycles of 12 hours each and regular (weekly to biweekly) cage changes. Mouse experimental protocols were approved by the Institutional Animal Care and Use Committee at Oregon Health & Science University.

Table 2.1 Summary of Mouse lines (with stock no. from the Jackson Laboratory, if applicable)

Mouse	Citation/Stock no.	Description
IL-5tg (NJ1726)	(Lee *et al.*, 1997)	Express IL-5 driven by the CC10 promoter, specific to airway epithelium. Lung-specific expression of IL-5, upregulation of eosinophil production, and increased recruitment of eosinophils to airways. Display histologic changes consistent with asthma, including goblet cell hyperplasia and epithelial hypertrophy. Develop splenomegaly as side effect of abundant eosinophil production (Figure 2.1)
PHIL	(Lee *et al.*, 2004)	Express diphtheria toxin A (DTA) under transgenic eosinophil peroxidase (EPO) promoter. Newly differentiated eosinophils in bone marrow activate EPO promoter, expressing cytocidal DTA and leading to eosinophil cell death. Mice therefore lack eosinophils but contain all other hematopoietic cells. PHIL mice exposed to acute antigen sensitization and challenge have reduced airway hyperreactivity compared to WT animals. Side effects of eosinophil loss include thinner, patchy fur and decreased breeding productivity.
CHAT-Cre	#028861 and #031661	Expression of Cre protein driven by endogenous choline acetyltransferase promoter. Expresses flox-stopped genes in parasympathetic neurons. Bred with CH2 and HALO mice to express light-sensitive channels in parasympathetic neurons (Figure 2.2)
Advillin-iCre	(Lau *et al.*, 2011) #032027	Expression of Cre protein driven by advillin promoter and dependent on tamoxifen activation. Expresses flox-stopped genes in sensory nerves.
TAC1-Cre	#021877	Expression of Cre protein driven by tachykinin1 promoter. Expresses flox-stopped genes in substance P and neurokinin A expressing cells, including a subgroup of airway sensory neurons.
CH2	#024109	Flox-stopped channelrhodopsin 2-EYFP fusion gene in Rosa26 locus.

		Channelrhodopsin 2 is a light-activatable cation channel. Illumination of cells expressing channelrhodopsin 2 with blue light leads to reversible nerve depolarization and firing.
HALO	(Madisen *et al.*, 2012) #014539	Flox-stopped halorhodopsin-EYFP fusion gene in Rosa26 locus. Halorhodopsin is a light-activatable chloride channel. Illumination of cells expressing halorhodopsin with yellow-red light leads to reversible inhibition of neuron firing.
SYN1-Cre	(Zhu *et al.*, 2001) #003966	Expression of Cre protein driven by rat synapsin1 promoter. Often used as a pan-neuronal promoter to drive expression of flox-stopped genes.
Ai9 tdTomato	#007909	Flox-stopped CAG-driven red fluorescent protein inserted into the Gt(ROSA)26Sor locus.
THY1-YFP	(Feng *et al.*, 2000) #003709	Expression of yellow fluorescent protein driven by the thymus cell antigen 1 promoter. Expresses at high levels in motor and sensory neurons, as well as subsets of CNS neurons.
eoCre	(Doyle *et al.*, 2013)	Expression of Cre recombinase is driven by the endogenous eosinophil peroxidase promoter on mouse chromosome 11. Crossing with a floxed GFP mouse line leads to expression specifically in eosinophils.
WT	#000664	C57BL/6 mice purchased from Jackson Laboratory

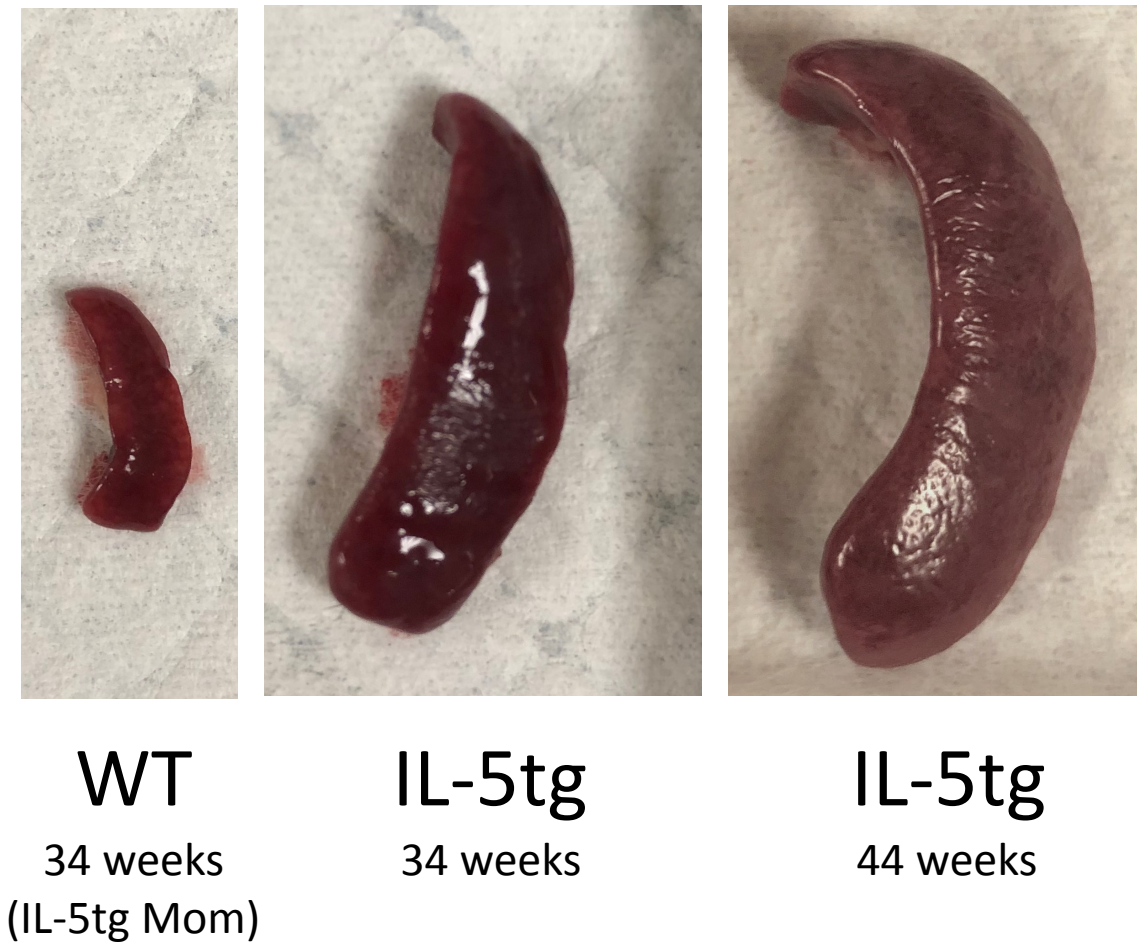

Figure 2.1. Splenomegaly in IL-5tg mice. Spleens of older IL-5tg mice are easily palpable in the left abdomen. Extra care must be taken during intraperitoneal (i.p.) injections not to accidentally perforate this organ - for this reason it is recommended that anesthesia and other i.p. injections be performed on the animal's right side.

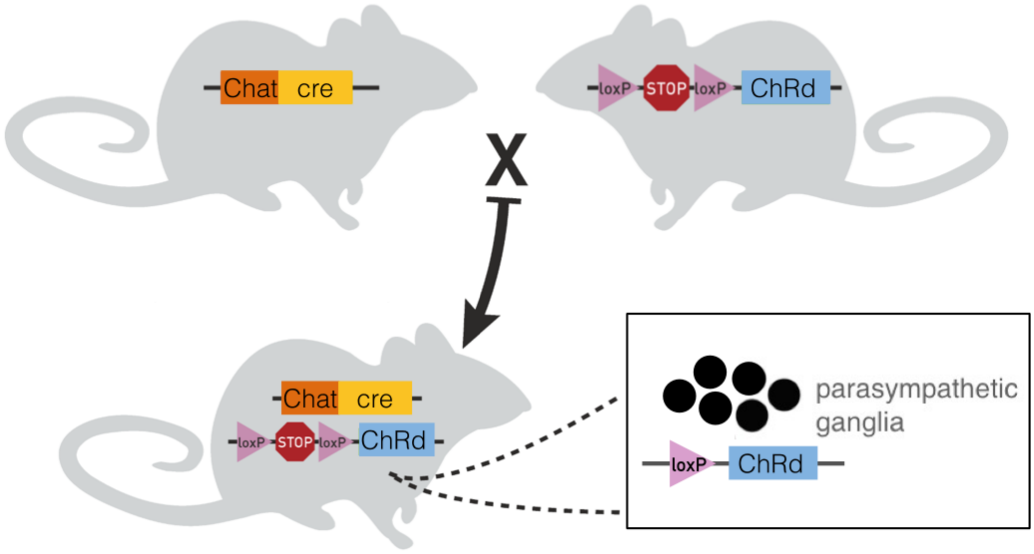

Figure 2.2. Diagram showing the result of breeding choline acetyltransferase Cre (CHAT-Cre) mice with a channelrhodopsin line. Breeding CHAT-Cre mice to mice with a flox-stopped channelrhodopsin 2-EYFP fusion gene results in deletion of the stop codon in cells expressing choline acetyltransferase, and expression of fluorescent, light-sensitive channels in parasympathetic neurons.

Genotyping from Mouse Ear Samples

Equipment:

- Isoflurane chamber
- Forceps
- Scissors
- 96 well Veriti Thermal Cycler (Applied Biosystems)
- Gel electrophoresis chamber

Reagents:

- Alkaline lysis buffer, pH 12
    - 50mL ddH_2O
    - 125µL 10N NaOH
    - 20µL 0.5M EDTA
- Neutralization solution, pH 5
    - 50mL ddH_2O
    - 325 mg Tris-HCl
- Econotaq
- Agarose
- DNA ladder
- QIAquick gel extraction kit

Retrieving Mouse DNA

1. Anesthetize mice in isofluorane chamber with 2L/min O_2
2. Using forceps and scissors, clip small ear sample - about the size of a sesame seed
3. Add 75µL lysis buffer to sample
4. Put tube with ear and lysis buffer in Thermal Cycler - Hotshot program
    a. Step 1 - 95^{0}C - 30 min - Alkaline lysis boil
    b. Step 2 - 4^{0}C - hold - cooling
5. Add 75µL neutralization solution
6. Store at -20^{0}C until ready to genotype

PCR amplification

1. Calculate amounts needed for Reaction mix: # samples + 3 controls + 10%
   Ex. 24 samples + 3 controls + 3 extra = 30 reactions total to prepare

Ex. Solution	**Amount per sample**	**# reactions**	**Total**
EconoTaq	12.5 µL	30	375 µL
Primer 1	1 µL	30	30 µL
Primer 2	1 µL	30	30 µL

Primer 3	1 µL	30	30 µL
Primer 4 (or sub H_2O)	1 µL	30	30 µL
RNAse free H_2O	7.5 µL	30	225 µL
Total Reaction mix	24 µL	30	720 µL

2. Add 24µL of Reaction mix and 1µL of extracted DNA to each tube
3. Prepare 1 positive control (DNA from mouse with gene), 1 negative control (DNA from mouse without gene), and 1 H_2O (no DNA) control
4. Place tubes in Thermal Cycler. Select appropriate program and run.
    a. Reaction temperatures and duration for annealing vary for each gene, so separate programs have been saved into the machine. Each program cycles 35 times. PCR denaturation occurs at 95^0C for 30 seconds, and extension at 72^0C for 1 minute. Annealing temperature/duration is: IL-5tg, 56.5^0C for 1 minute, PHIL 53^0C for 1 minute, CHAT, CH2, and TAC1 65^0C for 15 seconds, Advillin 60^0C for 15 seconds.

Table 2.2. Genotyping Primers

Mouse	**Forward**	**Reverse**
IL-5tg	CAG TGC TTG ACT TTA AAG AGG	TGG CAG TGG CCC AGA CAC AGC
PHIL	AAG TAT GAT GGG GGT GTT TC	GAG CGG GTT TTC ATT ATC TAC
CHAT	CAA AAG CGC TCT GAA GTT CCT	CAG GGT TAG TAG GGG CTG AC
CHAT-neo	TTC ACT GCA TTC TAG TTG TGG T	GAT AGG GGA GCA GCA ACA AG
Advillin	ACC CCG ACT TTG TGA TGT TTC	CTG CCT GTC CCT GAA CAT G
CH2	ACA TGG TCC TGC TGG AGT TC	GGC ATT AAA GCA GCG TAT CC
TAC1	TGG TGG CTG GAC CAA TGT	GCA TAT TTG GCT TTT ACT CTG G
HALO	ATA TCC TGC TGG TGG AGT GG	GCC ACG ATA TCC AGG AAA GA
SYN1	CTC AGC GCT GCC TCA GTC T	GCA TCG ACC GGT AAT GCA
eoCre (2 sets)	CTG CTG AAC CTG AGG ATG TGA GG	GGG TGG ACA GTT GGG AGG TG
	GAA GAA AGA AAC CAT CAC AGG ACC TC	GGG TGA GGA TGA GTG TGG CTA AG

Gel Electrophoresis and Extraction

1. Plan gel layout: one well per sample, plus one well (at least) for DNA ladder on each row. Determine whether you'll use a large or small gel, depending on number of samples.
2. Large gel: Make 2% agarose using 4 grams of agarose plus 200 mL TAE. Small gel: 1.2 grams of agarose plus 60 mL TAE.
    a. Heat to dissolve using microwave. Let cool in chemical hood. Once it's cool enough to hold, add 20 µL SybrSafe DNA stain, 6 for small gel (or 2/0.6 µL ethidium bromide). Swirl to mix.
    b. Pour agarose into gel container. Make sure it isn't leaking. Add comb for wells.
        i. If something happens, like the gel is leaking or breaks or you get a lot of bubbles, you wait for it to harden and re-melt the agarose in the beaker. Any impurities in the agarose (say from dropping the gel on the floor before re-melting it) result in images with lots of little dots and squiggles in them, which is not ideal.
    c. Add 10 µL of sample and 2.5 µL loading dye to each sample well. Add 4 µL of DNA ladder to central well (ex. TrackIt 100bp ladder - up to 2000 bp, or Ultra low bp ladder - up to 300bp).
    d. Run sample at ~100 volts until the color line is ~2/3rds of the way down.
    e. Image gel on UV light table.

3. *Gel Extraction*: Using a clean razor blade, and making sure not to expose your skin to UV rays, position gel of UV light table and cut out band of DNA for purification. Try not to get too much extra agarose, but don't miss any DNA either.
4. Use QIAquick gel extraction kit. Weigh the gel slice in a colorless tube. Add 3 volumes Buffer QG to 1 volume gel (100 mg gel ~100 µl). The maximum amount of gel per spin column is 400 mg. For >2% agarose gels, add 6 volumes Buffer QG.
5. Incubate at 50°C for 10 min (or until the gel slice has completely dissolved). Vortex the tube every 2–3 min to help dissolve gel. After the gel slice has dissolved completely, check that the color of the mixture is yellow (similar to Buffer QG without dissolved agarose). If the color of the mixture is orange or violet, add 10 µl 3 M sodium acetate, pH 5.0, and mix. The mixture turns yellow.
6. Add 1 gel volume isopropanol to the sample and mix.
7. Place a QIAquick spin column in a provided 2 mL collection tube or into a vacuum manifold. To bind DNA, apply the sample to the QIAquick column and centrifuge for
   1 min or apply vacuum to the manifold until all the samples have passed through the column. Discard flow-through and place the QIAquick column back into the same tube. For sample volumes >800 µl, load and spin/apply vacuum again.
8. If DNA will subsequently be used for sequencing, in vitro transcription, or microinjection, add 500 µl Buffer QG to the QIAquick column and centrifuge for 1 min or apply vacuum. Discard flow-through and place the QIAquick column back into the same tube.
9. To wash, add 750 µl Buffer PE to QIAquick column and centrifuge for 1 min or apply vacuum. Discard flow-through and place the QIAquick column back into the same tube. **Note:** If the DNA will be used

for salt-sensitive applications (*e.g.*, sequencing, blunt- ended ligation), let the column stand 2–5 min after addition of Buffer PE.

10. Centrifuge the QIAquick column in the provided 2 mL collection tube for 1 min to remove residual wash buffer.
11. Place QIAquick column into a clean 1.5 mL microcentrifuge tube.
12. To elute DNA, add 50 µl Buffer EB (10 mM Tris·Cl, pH 8.5) or water to the center of the QIAquick membrane and centrifuge the column for 1 min. For increased DNA concentration, add 30 µl Buffer EB to the center of the QIAquick membrane, let the column stand for 1 min, and then centrifuge for 1 min. After the addition of Buffer EB to the QIAquick membrane, increasing the incubation time to up to 4 min can increase the yield of purified DNA.

Sensitization and challenge with House Dust Mite (HDM)

Equipment:

- Isoflurane chamber
- 200 μL pipette
- 200 μL pipette tips
- Rack for eppendorf tubes

Reagents:

- House dust mite (Greer Laboratories XPB82D3A2.5)
    - Aliquoted into tubes of 50 μL or 100 μL of 4 mg/mL in PBS and stored at -20^{0}C.
    - Sensitization: Dilute 1:2 for 2 mg/mL final concentration
    - Challenge: Dilute 1:4 for 1 mg/mL final concentration
- PBS

1. Select mice for treatment. (Figure 2.3) All mice in one cage should be treated with either house dust mite (HDM) or saline (PBS). Groups should be matched for age and sex.
2. Label mouse cage with treatment group and date of each treatment after it is given.
3. Place eppendorf tubes with PBS and HDM in tube rack. Treat PBS group before HDM group.
4. Anesthetize mice in isoflurane chamber using 2 L/min oxygen and 5% isoflurane. Breathing rates for mice will drop once anesthesia sets in - once they are breathing at about 120 BPM turn isoflurane down to 2.5%.
5. With left hand, pick up mouse by the neck scruff and turn it so that the ventral side is exposed and the rostral side is raised above the caudal. With right hand, pull up 25 μL of PBS/HDM from eppendorf, then slowly pipette into mouse nostril.
    a. Aim for one nostril - if both are covered in liquid the mouse cannot breath in.
    b. Sometimes tilting the mouse to one side helps, so the nostril being given treatment is slightly raised.
    c. Liquid should all be taken up in one or two breaths for PBS, sometimes more for HDM (especially during the challenge phase).
    d. Mice under the appropriate level of anesthesia breath in treatment more easily. Not enough anesthesia and they will snort it out. Too much anesthesia (deep, gasping breaths) and they will breath through their mouth and not take up the treatment.
    e. If mice start to wake up before they've taken up all the treatment, put them back in the chamber and wait for their breathing to slow again.
6. Return individual mice to cage once treatment is complete.

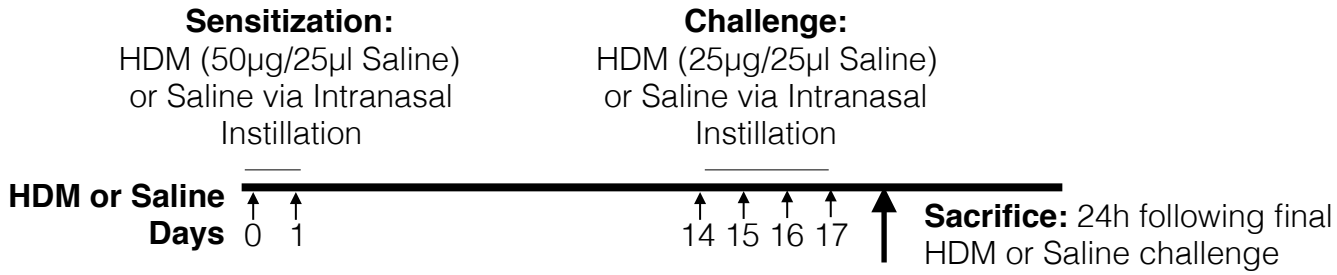

Figure 2.3. Timeline of House Dust Mite (HDM) sensitization and challenge. Mice of any genotype are acutely exposed to the common household allergen, house dust mite, in a regimented sensitization and challenge paradigm. Mice are anesthetized with isofluorane prior to each dose, and a 200 μL pipette is used to carefully inject each dose into the left nostril while the mouse in anesthetized. Dose for sensitization is 50 μg in 25 μL PBS. Dose for challenge is 25 μg in 25 μL PBS.

Tamoxifen treatment

Equipment:

- Isoflurane chamber
- Weight scale
- 1 mL syringe
- 26 gauge needle
- EtOH wipes

Reagents:

- Tamoxifen (Sigma #T5648)
- Corn oil

1. Make tamoxifen solution at a concentration of 20 mg/mL in corn oil. Measure out tamoxifen into light-proof container with wide bottom. Add corn oil. Shake O/N at 37^0C.
2. The following day, bring all equipment plus tamoxifen solution to mouse room. Anesthetize mice and weigh on scale. Administer tamoxifen solution by i.p. injection (weight (g) x 5 = # μL, for 100 mg/kg)
3. Administer same dose of tamoxifen to each anesthetized mice on the following days, for 5 days of treatment total. Store tamoxifen at 4^0C in the dark so it does not degrade.
4. Wait at least 3 weeks following final tamoxifen injection to insure sufficient production of channelrhodopsin in Advillin-CH2 mice. A quick test of blue light on the hindpaw can verify that sufficient sensory production of CH2 has been achieved.

In vivo Measurements of Airway Physiology

Ventilator calibration

Equipment:

- Ventilator (Figure 2.4)
- Pneumonitor attached to tubing with syringe and separate tubing with plug (for attachment to female joint of three-way stopcock)
- 30 mL syringe attached to tubing with plug
- Heating pad
- Heat lamp

Protocol:

1. Turn on oxygen tank, ventilator, ADInstruments power supply, heating pad (set at 42^{0}C - press START), computer, and heat lamp.
2. Log into computer and pull up template for ventilator. Save as a new file with name of mouse (*e.g.* M2019-001).
3. Calibrate airway pressure:
    a. Turn stopcock to shut off any flow from ventilator to pressure transducer
    b. In LabChart, set airway pressure to zero:
        i. Airway Pressure -> BP Amp -> Zero -> OK
    c. Now calibrate using pneumonitor. Attach plug side to open end of stopcock by pressure transducer. In Lab Chart: Airway Pressure -> Unit Conversion -> "Off" -> OK
    d. Press "Start" in LabChart. Push/pull syringe attached to pneumonitor until liquid level on both sides is even (should be at 0 but sometimes it's a little off if the liquid is low). Look at voltage reading of Airway Pressure in LabChart when pneumonitor is even and write down (*e.g.* 0cm = ? mV)
        i. Usually somewhere between -0.5 and 0.5mV
    e. Push syringe until there are 8 cm of difference between two liquid levels (so if levels were even at 0 cm then push until one side is 4 cm and one is -4cm). Look at voltage reading of Airway Pressure in LabChart and write down (*e.g.* 8cm = ? mV) (usually around 70mV)
    f. In LabChart click "Stop." Go to Airway Pressure -> Unit Conversion -> in *Calibrate* section type in the values for 0 cm and 8 cm from above -> OK
    g. Click "Start." Push syringe until there are 4 cm of difference between two liquid levels (2cm on one side and -2cm on the other). Verify that LabChart Airway Pressure reads 4cm (if it reads between 3.98 and 4.02 cm I call it good.)
    h. Repeat as needed until pressure is accurately calibrated. Remove pneumonitor and turn stockcock to resume airflow from ventilator to pressure transducer.
4. Calibrate airway flow:
    a. Turn stopcock to shut off any flow from ventilator to flow monitor.
    b. In LabChart, set airway flow to zero:
        i. AirwayFlow -> Spirometer -> Zero -> OK

c. Now calibrate using 30 mL syringe. Make sure syringe is pulled back to 25 mL. Attach plug to open end of stopcock by flow monitor.
d. Press "Start" in LabChart. Slowly push 5 mL of air through syringe, watching readout on LabChart to make sure there are no spikes. (If air is pushed too fast, it will exceed the measurement ability of the flow monitor and will show up as a spike.) Push "Stop" in LabChart.
    i. Airway flow readout should look very similar to the drawing by the Little Prince of the snake that has swallowed an elephant (de Saint-Exupery, 1943).
e. In LabChart, place cursor at time point of airway flow where you started to push air through the syringe, then drag until time point where you stopped to highlight the area that indicates 5 mL of flow. Go to Airway Flow -> Spirometry Flow -> Calibrate -> type in 0.005L injected volume -> OK
f. Repeat as needed until flow is accurately calibrated. Remove syringe and turn stockcock to resume airflow from ventilator to flow monitor.

5. Place PEEP tube in water cylinder about 0.5cm below surface.
6. Press "Start" in LabChart. Make sure airway pressure reading is zero. Attach "Frank the mouse" (a fake mouse - actually a 30 mL syringe sealed tight and attached to a plug) to the ventilator. PEEP cylinder should begin bubbling and pressure reading in LabChart should oscillate at a mean of 2cm. (Adjust PEEP tube up and down to achieve 2 cm if necessary.) Flip left switch on ventilator to ON. Let run for a few seconds, then switch on right switch to perform a few inspiratory pauses. Look at all LabChart readouts to make sure everything is working properly.
    a. Leaks in the expiratory tube will show up as a lack of plateau during inspiratory pauses
    b. Leaks in the inspiratory tubing may make airway pressure peaks jagged
7. If tidal volume readout is dipping below 0 mL: Airway Flow Corrected -> Arithmetic -> change equation to get baseline of 0 mL (usually +/- 0.0001)
8. Verify that Tidal Volume is 200 µL. It is very rare that this gets thrown off, but sometimes accidents happen. If it isn't at 200 µL, make slight adjustments to the silver knob where the oxygen enters the ventilator until 200 µL is achieved.
9. Verify that the deep inhalation cylinder (on the ground, 25 mL cylinder filled with water) is full and tubing is close to the bottom.
10. If you will be delivering nebulized drugs to the animal, clean out the nebulizer by pipetting 10 µL of PBS onto the silver screen and dabbing with a kimwipe. Then pipette 100 µL of dH_2O onto the silver screen, turn on the nebulizer, and let it all run through. Open up the plug on the side of the nebulizer and roll a filament of kimwipe to push through to clean out the inner chamber.

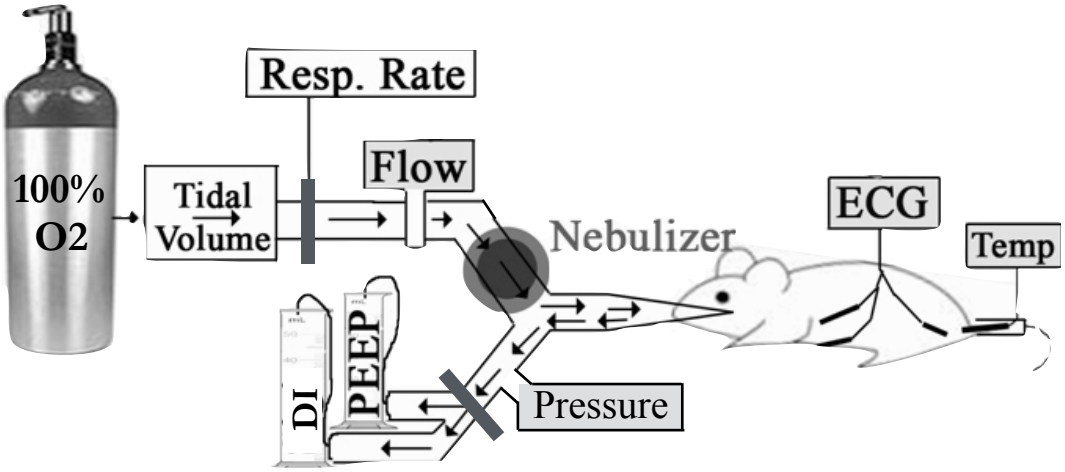

Figure 2.4. Diagram of mouse ventilator and calibration apparatuses. Ventilator system consists of a spirometer to measure air flow (ML141, AD Instruments), a pressure transducer (measures principle outcome measure, mouse airway pressure), metering valves (inspiratory time 175ms, expiratory time 300ms), two expiratory water columns for positive end expiratory pressure (PEEP) (2 cm H2O) and deep inhalation (DI, 25 cm H2O), in-line nebulizer (AeroNeb) to deliver serotonin, and LabChart Pro acquisition software. Delivered air is 100% O2. Needle electrodes connected to an electrocardiogram measure heart rate and rhythm. A retail thermometer measures body temperature. Adapted from Scott 2012.

Anesthesia and surgical preparation

Equipment:

- Mouse ventilator
- Heating pad
- Heat lamp
- Scissors
- Graefe forceps (2)
- Size 15 scalpel
- Microscissors
- Bull clamps
- Curved hemostatic forceps (2)
- Gauze dampened with PBS
- EKG needle electrodes
- Rectal thermometer

Optional: for maximum exposure of sensory nerve cell bodies

- Short Fixators (Fine Science Tools No. 18200-01)
- Blunt Retractors, 1mm wide (Fine Science Tools No. 18200-09)
- Elastomer, 2m roll (Fine Science Tools No. 18200-07)
- 1 Tall and 2 Short magnetic fixators (Fine Science Tools No. 18200-01 and 02)
- Small magnetic base plate (Fine Science Tools No. 18200-03)
- Micromanipulator

Reagents:

- Ketamine/xylazine (1 mL ketamine, 100 μL xylazine into 8.9 mL PBS)
- Succinylcholine (10mg/mL)
- PBS

To ventilate mouse for serotonin dose response/optogenetics experiments:

1. Anesthetize mouse with 100 mg/kg i.p. ketamine and 10 mg/kg i.p. Xylazine
2. Once mouse stops moving, place on heating pad and under heat lamp. Wait for breathing to slow, and for mouse to not reaction to soft hindpaw pinch.
3. Make a midline neck incision with scissors, extending 1 cm caudally from the base of the neck over the thorax
4. Carefully separate the submandibular glands
5. Use forceps to rip in half the body of both sternohyoid muscles to expose the trachea
6. Inset a 21-gauge catheter into the cricothyroid membrane to the level of the second cartilage ring and retract the needle. Insert end of catheter into mouse ventilator and turn on to initiate ventilation. Press start in LabChart program.
7. Place gauze dampened with PBS over exposed trachea. Gauze should be left on at all times when not performing surgery or light exposure, in order to reduce desiccation of trachea over time.
8. Inject succinylcholine (0.05 mg in 0.05 mL i.p.) to eliminate respiratory effort.

9. Insert EKG needle electrodes and rectal thermometer

To surgically expose the trachea for parasympathetic/sensory activation:

10. Use bull clamps to clip submandibular glands away from trachea
11. Retract soft tissue and muscle (may need to extend skin cut more caudally) to expose the sternum to the level of the first two ribs
12. Grip sternum in left hand to the left of midline with long Graefe forceps. Using 15 scalpel in right hand, slice muscle and bone (not all the way through) on either side of the sternum and across the midline where the second pair of ribs articulate. Using microscissors with right hand, cut through remaining muscle and bone where cuts were made, removing this section of sternum without lacerating any major blood vessels.
13. If the thymus is visible, a 2-mm section from the proximal end may be removed to allow a clear light path to the trachea.
14. Using curved hemostatic forceps, grip the sternomastoid muscle on each side and pull laterally and caudally. Lock clamps and position such that trachea and vagus nerves are maximally exposed. Dab any blood with damp gauze to clear the path for light (Figure 2.5).

To surgically expose the vagus and nodose ganglia: (unpublished protocol courtesy of Rachael Brust from the Stephen Liberles lab)

15. Position one retractor to pull down the sternomastoid muscle (if exposing the mouse's left vagus nerve, pull the muscle down and somewhat to your right).
16. Position a second retractor to slightly pull the trachea to your left.
17. Bluntly dissect to expose carotid and vagus.
18. Reposition retractor 2 so that it is very slightly pulling the carotid and vagus to your left.
19. Follow the vagus up to the digastric muscle and use forceps to carefully open some of the delicate connective tissue in this area, revealing the bottom on the nodose ganglion. You may position a third retractor to pull the digastric muscle up a bit.
20. Use a micromanipulator to position your fiberoptic such that it is just above the vagus (but not touching), targeting the vagus just as it is leaving the ganglion.

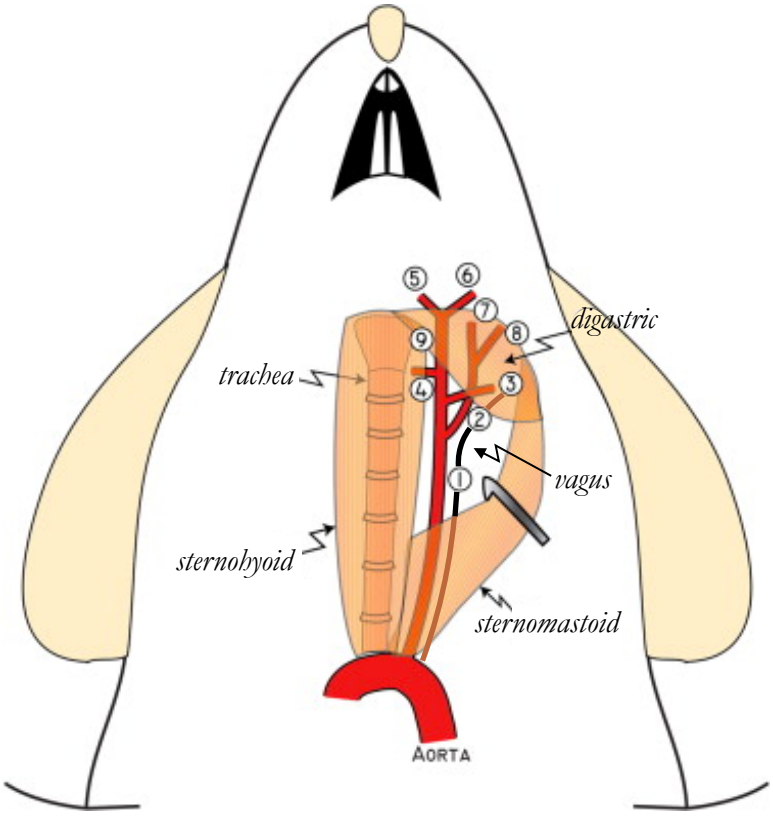

Figure 2.5. Diagram showing retraction of sternomastoid muscle and digastric muscle to expose vagus. (1) common carotid artery, (2) internal carotid artery, (3) occipital artery, (4) superior thyroid artery, (5) lingual artery, (6) auricular branch, (7) terminal internal carotid artery, (8) pterygopalatine artery, (9) external carotid artery. Muscles and vagus nerve labeled in italics. Adapted from Santillan *et al.*, 2014.

Measurements of pulmonary inflation pressure and serotonin response

(start after performing "Anesthesia and surgical preparation" as described above)

Equipment:

- Mouse ventilator
- Digital clock with seconds visible

Reagents:

- PBS
- Serotonin (5HT) at doses of 10mM, 30mM, and 100mM

Note: for some experiments you may need additional reagents, such as physostigmine, guanethidine, or atropine on hand. The timing and dosage of these drugs, when used, is described thoroughly in chapters 3 and 4.

1. Double check that airway pressure and EKG readouts appear normal. Airway pressure should be between 7-10cm H_2O at baseline (lower for an untreated mouse, higher for mice after house dust mite treatment or physostigmine). Heart rate should be between 200 and 400 beats per minute for an untreated mouse.
2. Perform a repeated sequence of maneuvers with the mouse ventilator, first with no nebulized solution, then with PBS, then repeat with 10, 30, and 100mM doses of 5HT in sequence. When the seconds hand of the digital clock reads:
    a. 40 seconds - 2 deep inhalations to open any collapsed airways
    b. 50 seconds - 6 inspiratory pauses
    c. 58 seconds - pipette solution onto nebulizer
    d. 0 seconds - turn on nebulizer. Type dosage (i.e "neb on," "pbs," "10") into LabChart and hit enter. Wait 60 seconds.
    e. 0 seconds (again) - 6 inspiratory pauses
3. Repeat 40 seconds later

Optogenetic activation of airway neurons

(start after performing "Anesthesia and surgical preparation" as described above)
See Chapter 3 for development of this method

Equipment:

- Mouse ventilator
- 454 nm light-emitting diode (LED) (Prizmatix)
- Optic fiber with 500um core diameter
- Collimator (1cm diameter, 0.63 NA)
- Master-8 system pulse stimulator (A.M.P.I.)

Reagents:

- Physostigmine (0.1 mg/mL in 0.1% EtOH, 0.5mg/kg i.p.)
- Guanethidine (2.5 mg/mL, 5mg/kg i.p.)
- Indomethacin (0.4 mg/mL in 0.3% DMSO, 2mg/kg i.p.)
- L-NAME (7.5 mg/mL, 30mg/kg i.p.)
- Atropine (1 mg/mL, 3 mg/kg i.p.)

1. Remove gauze covering from trachea. Position LED Collimator such that the light is as close to the trachea as possible, centered midway between the larynx and carina (Figure 3.2).
2. Type "light" into LabChart comments. Hit start on Master-8 pulse stimulator. Simultaneously hit enter so that comment lines up with start of light.
3. Type "end light" into LabChart comments. Hit enter when light pulses end.

Note: Master-8 should be pre-programmed with frequency (aka "interval"), pulse width, and pulse number as required for experiments.

Experiment	**Interval (ms)**	**Pulse Width (ms)**	**Pulse number**
Parasympathetic activation	50	5	600
Sensory Activation	20	5	1500

4. Analyze peak pressure change by measuring maximal peak achieved during 30 seconds of light and subtract peak pressure from 10 seconds before light.

Statistical Analysis

Airway pressure response to serotonin

Change in airway peak pressure over response to PBS was calculated for each mouse at serotonin doses of 10, 30, and 100mM. Two-way ANOVA with Sidak's test for multiple comparisons was used to calculate overall differences between groups, as well as differences between groups at individual doses. P values <0.05 were considered significant.

Airway pressure response to light

The airway peak pressure response of groups of animals (saline treated, HDM treated, wildtype, and IL-5tg) were compared using one-way ANOVA. "Light" and "Light after Atropine" responses were analyzed separately. P values <0.05 were considered significant.

Inflammation

Bronchoalveolar Lavage and Blood Collection

Overview: collect mouse blood and bronchoalveolar lavage (BAL) fluid. (Usually performed in conjunction with *Harvesting Mouse Tissues*.) Count total white blood cells (WBCs) and assess proportion of lymphocytes, macrophages (BAL only), eosinophils, neutrophils, and monocytes (blood only).

Equipment:

- Scissors
- Graefe Forceps (2)
- 1 mL syringe
- 1.5 mL eppendorf tubes
- Ice
- 1 mL syringe with 0.02 mL heparin
- Microscissors
- Cannula for mouse trachea
- Glass slide

Reagents:

- Sterile PBS

Bronchoalveolar lavage (BAL)

1. In an anesthetized mouse: use scissors and forceps to expose trachea, using scissors for the dermis and forceps to pull away glands and muscles.
2. Using the microscissors, make a small incision perpendicular to the length of the trachea in the cricohyoid membrane. Insert the cannula into the trachea.
    a. This part is the most difficult. Unless you already had the mouse cannulated for ventilation experiments, in which case skip to step 3!
3. Using the 1 mL syringe (no heparin) draw up 0.5 mL of PBS, insert syringe into cannula, and gently push PBS into mouse lungs. Once syringe has been emptied, draw back slowly. You should see some frothy solution entering the syringe. Draw back to about 0.5 mL and deposit fluid in 1.5 mL eppendorf tube on ice. (Very little fluid is recovered from the first 0.5 mL)
4. Repeat step 3 twice more, each time pushing 0.5 mL into lungs and then drawing slowly back out and depositing fluid in the same eppendorf tube. More liquid should be recovered each time.

Blood

5. Using scissors, open mouse abdomen from navel to posterior end of sternum.
6. Using forceps, pull intestines to the mouse's right (surgeon's left as mouse lies supine) to expose the inferior vena cava.
7. Insert needle of 1 mL syringe with heparin into IVC just posterior to the branch point of the left kidney.

8. Pull back on syringe to be sure of placement - blood should begin to fill the syringe with minimal resistance. If there is no blood move the needle up and down fractionally, continuing to apply gentle pulling pressure on syringe.
9. Once in the vein, gently draw up blood, occasionally allowing the vein to refill if needed. 0.3 to 0.5 mL of blood should be recovered.
    a. If blood is drawn to fast or if a clot obstructs the syringe and then is suddenly dislodged by forceful pulling, the blood cells may shear as they cross the needle to enter the syringe, leading to hemolysis and interfering with later analysis.
10. Store blood in eppendorf tube on ice. Smear 5 µL on slide for blood counts or use for other analysis.

Bronchoalveolar Lavage WBC Counts and Differentials

Equipment:

- Centrifuge (for eppendorf tubes)
- Centrifuge (for slides)
- Metal slide holders - Figure 2.6A
- Funnel Filters
- Coplin jars
- Slide holder for coplin jars - Figure 2.6B
- Two beakers (500 mL)
- Drying rack for slides

Reagents:

- Wright stain

Counting White Blood Cells in Bronchoalveolar lavage (BAL)

11. Centrifuge BAL at 300 x g for 10 min, then take off supernatant and resuspend the pellet in 100 µL PBS
12. Cytospin:
    a. pre-label BAL slides
    b. Prepare slides in metal slide holder with disposable filter
    c. Pipette 90 µL into funnel and spin
    d. Fix slide in methanol to prepare for WBC differential (see "Wright stain" below)
13. Keep last 10 µL in tube on ice.
14. When all samples are ready, take ice bucket with tubes to microscope. Load 10 µL of sample (may dilute 1:10 for HDM and samples with many WBCs) into Hemocytometer. Average number of cells in big squares = $x10^4$ cells/mL
    a. There may be red blood cells (smaller, donut-shaped) and epithelial cells (big and hairy) in the sample. Don't count these! Only count the white blood cells.

Wright Stain for BAL

1. Fill coplin jar with -20^{0}C methanol. Fix slides in methanol for 10 min. (This can be done days/weeks ahead of time)
2. Work with up to 8 slides at a time (1 on each end with back of slide facing side of jar, 3 pairs of back to back slides in the middle). Fill a coplin jar with Wright stain. Insert slides into slide holder. Fill two beakers with dH_2O. Lay out holder for drying slides.
3. This happens FAST so be ready and have a clock/timer with seconds in easy view.
    a. Insert slides into Wright stain for 12 seconds
    b. Remove from Wright stain and dunk in 1st beaker. Dip 5 times up and down.
    c. Remove from 1st beaker and dunk in second. Wait 30 seconds.
4. Wipe backside of slides with kimwipe and set in drying rack

A

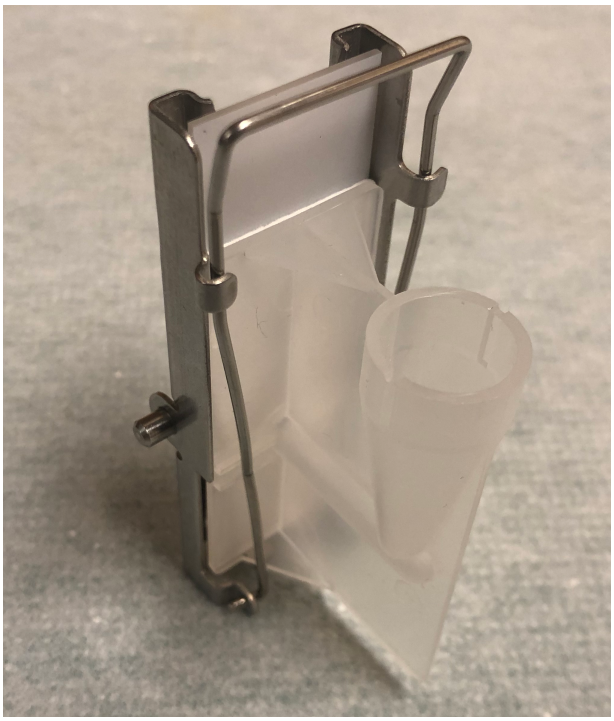

B

Figure 2.6. Equipment for bronchoalveolar lavage (BAL) WBC counts and differentials. (A) Metal slide holder with slide and funnel attached. (B) Slide holder with slides and coplin jar.

Statistical Analysis

Total number of white blood cells for saline vs. HDM and wild type vs. IL-5tg were compared using two tailed Student's t-tests. Total numbers of eosinophils, neutrophils, lymphocytes, and macrophages between the groups were compared using two tailed Student's t-tests. P values <0.05 were considered significant.

Imaging Nerves

Harvesting Mouse Tissues

Purpose: to collect mouse trachea, lungs, dorsal root ganglia (DRGs), and nodose/jugular ganglia blood for later use in Immunohistochemistry

Equipment:

- 1 mL syringe with needle
- 10 mL syringe with 25 gauge needle
- Disposable blue chuck
- Microscissors
- Razor blade
- Scissors
- Forceps (2)
- 10 mL glass jar filled halfway with Zamboni's fixative
- 1 mL pipette and pipette tips
- Petri dish
- Dissecting scope
- Very fine forceps (2)

Reagents:

- Pentobarbital (1:10 dilution; 39mg/mL)
- PBS
- EtOH spritzer
- Ice

Perfusion

1. Assemble equipment and mice. Fill 1 mL syringe with pentobarbital (250 µL for 25g mouse) (or, if you need really rapid anesthesia, 400 µL) and fill 10 mL syringe with 10 mL of PBS.
2. Scruff mouse: pick up tail near bum with left hand. Place mouse on top of cage horizontal to bars such that it has something to grab with its hands. Take right hand, using thumb on one side and curled fingers on the other, and moving somewhat from tail to head squish mouse against cage bars and grab. When you're done you should have the neck and back firmly scruffed in right hand. Still holding tail with left, lift mouse up and turn hand over so mouse belly is visible. Tuck tail into pinky of right hand so left is free to grab syringe.
3. Administer pentobarbital: using left hand, insert needle into mouse's lower left (normal) or right (IL-5tg mice, so you don't hit their giant spleens) abdomen, inserting just below the skin. Push.
4. Don't put mouse back in cage with other mice. Put in weigh boat or empty cage. Wait until mouse stops moving, then move to chuck. Check for sufficient anesthesia with strong toe pinch. If you see agonal breathing you have waited too long.

5. Spritz belly and neck of anesthetized mouse with EtOH to damp down fur and help prevent fur from getting in all the tissues you're collecting.
6. Using forceps in left hand, pinch midline skin of abdomen about ⅔ rds of the way between diaphragm and urinary meatus. Using scissors in right hand, cut hole through skin and muscle until viscera are visible, then extend midline excision anteriorly to diaphragm.
7. Cut horizontally from midline incision to the mouse's left to expose descending colon. Use forceps to move descending colon and other intestines to the mouse's right so that the spleen, left kidney, and inferior vena cava (IVC) become visible. Cut the IVC.
8. Move quickly now because the mouse is bleeding out. Hold the white nub of sternum just below the diaphragm with forceps and lift so the whole diaphragm becomes visible, moving liver out of the way with closed scissors if necessary. Cut into ribcage and diaphragm, first nicking each side to collapse (but not cut!) the lungs, then moving around rib cage to cut diaphragm away, going from each side to meet in the middle.
9. Cut anteriorly along ribcage on each side, cutting towards mouse's armpits. Keep hold of sternum nub with forceps and lift as you go. Stop when you have a clear shot of the right ventricle of the heart.
10. Keep forceps in left hand. Grab 10 mL PBS syringe with right hand. Aim needle in right ventricle - aim just above the right coronary artery, and don't push in too far or you'll puncture all the way through. Slowly start to push PBS through heart. You should see blood emptying from abdomen. Eventually this liquid should turn clear and the hands/feet/liver should noticeably pale. In a perfect perfusion on a mouse that was not previously ventilated the lungs should be white. (Ventilation damages the lungs, so they never clear completely and will still look pink and speckely).
11. Once all 10 mL have been administered remove the heart to prevent re-perfusion

Collecting Trachea, Lungs, Head and Spine

12. Once perfusion is done, expose the **trachea**. Neck area should be spritzed with EtOH if it wasn't already. Cut through skin of neck (one vertical and two horizontal incisions), pull apart submandibular glands (horizontally), grab and rip apart (vertically) each of the two muscle bellies on the ventral side of the trachea, then cut through clavicles to remove ribcage fully so entirety of trachea and lungs are exposed.
13. Using microscissors, make an incision in the cricohyoid membrane, cutting through about half the depth of the trachea.
14. Pull up 1 mL of Zamboni's from jar using pipette. Insert pipette tip into the trachea at the site of incision, and slowly fill lungs with 1 mL of Zamboni's. All 5 lung lobes should inflate.
15. Before removing pipette tip, pinch trachea with forceps in left hand to prevent fixative from flowing out. With right hand, cut trachea above thyroid cartilage, then (pulling upward with forceps) make blind cuts behind trachea to remove adhesions, trying not to damage carotid sheath/vagus nerve along the way (if collecting nodose/jugular ganglia). Continue to pull upwards on trachea with forceps so that **lung** is pulled as well, blind cutting adhesions with scissors, and finally cutting through esophagus to remove lungs and trachea from chest cavity. Place in jar of zamboni's.
16. Next remove **head**: using razor blade, cut through head at level of shoulders and posterior to ears. Either:
    a. Place on petri dish on ice for immediate N/J collection, or

    b. Remove skin from head, using scissors and razor blade to remove nose, and place in jar of Zamboni's with lungs/trachea
17. Next remove **spine**: using razor blade, cut through ribs on either side of thoracic spine, leaving about 2mm of ribs intact on either side. Airway nerves are mostly T2-T6. Then use scissors and forceps to remove spine from dorsal skin and to cut posteriorly at beginning of lumbar region. Either:
    a. Place on petri dish on ice for immediate DRG collection, or
    b. Place in jar of Zamboni's with lungs/trachea

Harvesting Dorsal Root Ganglia (DRGs)

1. Move spine to dissecting scope. Bring very fine forceps, razor blade, blunt forceps, and scissors
2. Using your razor blade, cut ribs off close and parallel to the spine
3. Using scissors, cut along the ventral side of the central canal. Gently pull the vertebral bones off the spinal cord.
4. Using blunt forceps, pull up on spinal cord starting at one end to expose the dorsal roots.
5. Using fine forceps, pull on each dorsal root, pulling each ganglion out of its little hidey hole. Do this very gently. Cut off of spinal cord.
6. Put DRGs in TBS O/N at 4^0C (for culturing) or in TBS and then Blocking solution O/N (for staining)

Harvesting Nodose/Jugular Ganglia

1. Bring mouse head to dissecting scope. Bring
2. Lay mouse head on side, with ear facing up and slightly back so the throat is towards you.
3. Use the ear canal as your first landmark. Clear away any remnants of hair.
4. Surgically dissect away tissue to expose the tympanic bullae (the bone dome covering the cochlea) and the carotid sheath. Find the vagus nerve and tie a piece of suture around the end, so you don't lose it later. (Figure 2.7A)
5. Carefully dissect out vagus to make it easier to follow
6. Remove the tympanic bullae: poke through with sharp forceps and then break it off (with practice this can be done all in one piece)
7. Follow vagus to where it dives between the cochlea and the bone spur (Figure 2.7A, labeled). The is where the Nodose/Jugular ganglion is located. Break off bones around the Nodose/Jugular, and carefully separate its adhesions to the cochlea before removing the cochlea completely.
8. You will now see the vagus with the Nodose/Jugular bulb diving into the brainstem. Cut as close to the brainstem as possible, then carefully lift out the N/J with posterior vagus nerve attached. (Figure 2.7B)

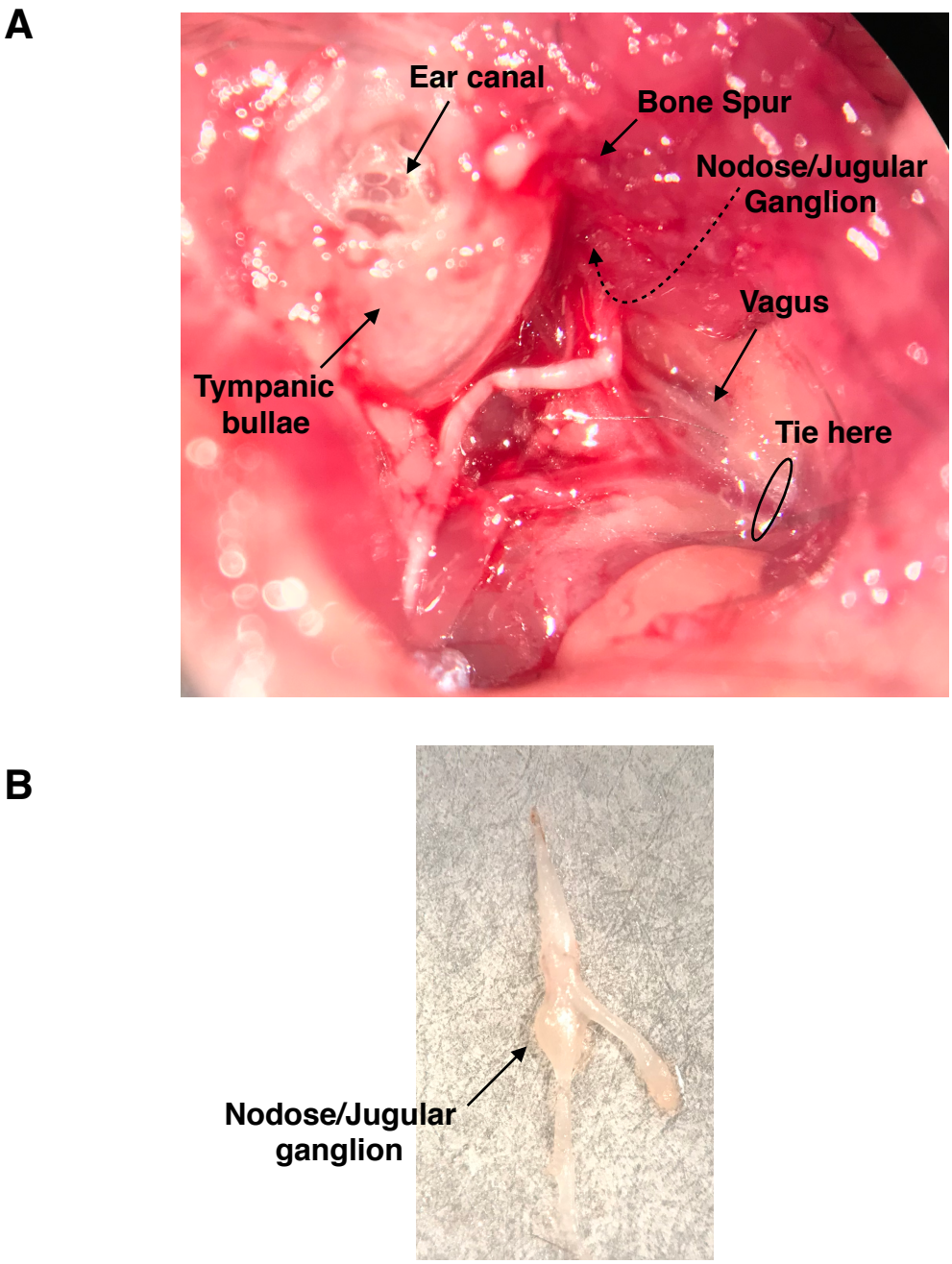

Figure 2.7. Nodose/jugular ganglia dissection. (A) Photograph of mouse head showing left side vagus nerve for dissection. Essential anatomical landmarks are labeled. Note that this mouse was not perfused prior to dissection. (B) Photo of a section of vagus nerve showing the nodose/jugular ganglion as a slight bulge. This was from a perfused mouse. Sometimes the ganglion is less bulgy than seen in this photo, and a microscope is necessary to confirm the presence of nerve soma.

Immunohistochemistry and Clearing of Whole Mount Tissues

Overview: Antibody staining of nerves and other markers and clearing of tissue for immediate imaging

Equipment:

- 1.5 mL eppendorf tubes (2 per sample)
- Tube holder
- Shaker
- Aluminum foil

Reagents:

- Tris buffered saline (TBS), adjust to pH 7.6 using HCl
    - Tris Base: 61 grams
    - NaCl: 90 grams
    - H_2O to 1 liter
- *Blocking solution*: 4% normal goat serum, 1% TritonX 100, 5% powdered milk in TBS

		10 mL	**25 mL**	**30 mL**
Triton X-100	Sigma #X100	100 µL	250 µL	300 µL
Powdered Milk	Carnation instant nonfat dry milk	50 mg	125 mg	150 mL
Normal Goat Serum	Vector #S-1000	400 µL	1 mL	1.2 mL
TBS	See above	9.5 mL	24 mL	29.5 mL

- *Ce3D clearing solution*: Gently melt N-methylacetamide in 37^{0}C water bath until the necessary volume can be obtained. Add to PBS on Heat/Stir pad in chemical fume hood. While stirring and gently heating, add in histodenz little by little. Note: the histodenz takes a long time to fully melt - be patient and don't add too much or the stir bar becomes stuck. Once melted, add Triton X-100 and 1-thioglycerol.

		5mL	**10mL**	**30mL**
N-Methylacetamide (40% v/v)	Aldrich #M26305	2 mL	4 mL	12 mL
PBS	Gibco PBS, pH 7.4	3 mL	6 mL	18 mL
Histodenz (86% w/v)	Sigma #D2158	7.275g	14.55g	43.65g
Triton X-100 (0.1% v/v)	Sigma #X100	5 µL	10 µL	30 µL
1-Thioglycerol (0.5% v/v)	Sigma #M1753	25 µL	50 µL	150 µL

- Primary Antibodies:
    - Rabbit IgG anti-human PGP9.5 Millipore AB1761-I 1:500

    - Rat IgG_{2a} anti-Substance P — BD Pharmigen 556312 — 1:500
    - Chicken IgY anti-GFP — Invitrogen A10262 — 1:500
    - Rabbit Tyrosine Hydroxylase — Pel Freez P40101 — 1:500
    - Rabbit IgG nNOS — Cell Signal C7D7 — 1:100
- Secondary Antibodies:
    - Goat anti-rat Alexa555 IgG (H+L) — Invitrogen #A21428 — 1:1000
    - Goat anti-rabbit Alexa647 IgG — Invitrogen #A21244 — 1:1000
    - Goat anti-chicken Alexa488 — Invitrogen #A11039 — 1:1000

Day 1

- Wash tissue in TBS. 2x2 min at RT, then 1hr at 4^0C until clear.
- Transfer to blocking solution in 1st eppendorf tube. 4^0C O/N.

Day 2

- Pour off blocking solution
- Add 0.5 mL of blocking solution with primary antibodies. 4^0C O/N.

Day 3

- Wash tissue in TBS. 2x2 min at RT, then 5x1hr at 4^0C.
- Pour off TBS. Add 0.5 mL of blocking solution with secondary antibodies. 4^0C O/N.
  (ALL steps after this performed in DARKNESS)

Day 4

- Wash tissue in TBS. 2x2 min at RT, then 5x1hr at 4^0C.
- Take out tissue, wick away extra TBS with kimwipe, and place in fresh eppendorf tube with Ce3D. O/N RT in chemical fume hood.
  NOTE: if doing two antibodies from the same animal (*e.g.* 2 primary rabbit antibodies) then there are additional steps. Instead of clearing tissue, after washing pour off TBS and add blocking solution with special blocking antibody (*e.g.* Goat anti-rabbit IgG, 1:100). 4^0C on shaker O/N.
  Day 5: Wash tissue in TBS. 2x2 min at RT, then 5x1hr at 4^0C on shaker. Pour off TBS. Add 0.5 mL of blocking solution with secondary antibodies. 4^0C on shaker O/N.
  Day 6: Wash tissue in TBS. 2x2 min at RT, then 5x1hr at 4^0C on shaker. Place in Ce3D O/N.
  NOTE: Previous protocols dictated the use of shaking for the O/N steps. This is not necessary.

Analysis of Eosinophil-Nerve Interactions

Overview: Use of Imaris 9.6.0 software to quantify eosinophil-nerve interactions from images of sensory and parasympathetic nerves stained with PGP9.5 (nerves) and antibody against GFP (eosinophils)

Equipment:

- Computer with Imaris 9.6.0 software (available from Advanced Light Microscopy Imaging Core)

Imaris Analysis

1. Use Imaris File Converter (.czi to .ims)
2. Open with Imaris x64 9.6.0
3. Make a Nerve Surface
    a. Add new Surface
    b. Select PGP Channel
    c. Smooth = 2x pixel size = 0.624um for 63x 1024x1024 image
    d. Background subtraction. Maximum object size = 30μm
    e. Set threshold intensity to cover all possible nerves (varies from 1-9 depending on channel intensity, even within the same mouse)
    f. Enable split touching objects: Seed point diameter: 5μm
    g. Quality: Select all
    h. Filter: Intensity Mean Channel 2 (GFP channel): select deviled egg cells (~4.51)*
        i. If there are no deviled egg cells skip this step
    i. No sets (delete). Finish.
    j. Name surface "PGP"
4. Make a Nerve Surface Channel
    a. Nerve Surface: Edit: Mask All
    b. Channel 1 (PGP Channel)
    c. Click on Channel afterward to change channel color if desired for imaging (yellow is nice)
5. Make an Eosinophil Surface
    a. Add new Surface
    b. Select GFP Channel
    c. Smooth = 2x pixel size = 0.624μm for 63x 1024x1024 image
    d. Background subtraction (Max size 8μm)
    e. Set threshold intensity to cover eosinophils completely (1-20)
        i. Unselect PGP Surface and Channels to visualize eosinophils more easily
    f. Enable split touching objects: Seed point diameter: 7μm
        i. 8μm is average eosinophil length - 7μm is just under this, thus enabling optimum splitting of closely aggregated cells in Imaris.
    g. Use Quality to select only eosinophils*
    **Threshold for Intensity Mean Ch GFP and Quality should be same number (e.g. 4.51)*
    h. Filter: Number of Voxels Img=1: set to select whole eosinophils (or leave at minimum above 10 and delete manually in step j)
    i. No Sets (delete). Finish.

    j. If needed: Eos Surface: Edit: click on anything NOT an eosinophil: Delete
    k. Name surface “Eos”
6. Make an Eosinophil Channel
    a. Eosinophil Surface: Edit: Mask All
    b. Channel 2 (GFP Channel)
    c. Click on Channel afterward to change channel color if desired for imaging (light blue is nice)
7. Eosinophil Spots
    a. New Spots
    b. Eosinophil Channel (should be Channel 4)
    c. Estimated Diameter: 8um
    d. Quality: all above 0.01 (excludes common computer glitch of single spot in lower left corner)
    e. Filter x2: Shortest Distance to Surfaces=Nerve.
        i. Set 1 = 15um (Eos within 15um = Class A)
        ii. Set 2 = 8um (Eos within 8um = Class A)
8. Export Data for Analysis
    a. Go to Eosinophil Surface
    b. Statistics: Detailed: Intensity Max Ch (Nerve Surface - should be Ch=3)
        i. “Export statistics on tab display to file”
        ii. Eosinophils with Intensity >0 = Eosinophils touching Nerves
        iii. Export all data (will be saved with file name ending in “Eos_Statistics”)
    c. Go to Eosinophil Spots
    d. Analysis: lower Right: export all data
    e. In Files:
        i. Spots: “Overall” Set 1 and Set 2 Class A = Eosinophils in proximity to nerves;
        ii. Both Spots and Eosinophils: “Shortest Distance to Surfaces=Nerve Surface” is actual distances, can be used to find average. Spots = distance from center of eosinophil, Eosinophils = distance from edge of eosinophil to nerves.

Statistical Analysis

Total number of eosinophils

In “Eos_Statistics” file saved from data export above, go to “Overall” -> “Total number of surfaces.” That is the number of eosinophils (may slightly underestimate real number if the program was unable to separate very closely associated eosinophils, which happens more when there are many eosinophils in the image, as in the HDM condition). Divide this number by the volume of the image: 0.003061458 mm^3 for a single 20x image with 30 μm z stack, 0.01408271037 mm^3 for 5 tiled 20x images with 30 μm z stack and 10% overlap. To compare two groups use Student's t-test (2 tailed). To compare three or more groups use one-way ANOVA with Bonferroni correction for multiple comparisons. P values <0.05 were considered significant.

Percentage of eosinophils touching nerves

In “Eos_Statistics”, go to “Shortest_Distance_to_Surfaces_Surfaces=PGP.” Count number of surfaces for which shortest distance is 0 μm. To compare two groups use Student's t-test (2 tailed). To compare three or

more groups use one-way ANOVA with Bonferroni correction for multiple comparisons. P values <0.05 were considered significant.

Eosinophil distribution

In "Eos_Statistics", go to "Shortest_Distance_to_Surfaces_Surfaces=PGP." Copy all values from each group (saline, HDM) into one long column in Graph Pad Prism. Use Kolmogorov-Smirnov test to compare two frequency distributions without assuming Gaussian distribution. P values <0.05 were considered significant.

Molecular Biology

Quantification of RNA in Mouse Lung Tissue and Submandibular Gland

Brief summary: carefully separate a small sample of frozen tissue, homogenize, then extract RNA using a Qiagen RNeasy kit. Make cDNA, then run 96 well plate with desired primers and 18S as a control in the Applied Biosystems 5500 Fast Thermocycler. Quantify RNA and DNA with NanoDrop.

RNA Isolation from Tissue

Equipment:

- For preparing frozen tissue:
    - Dry ice in large styrofoam container
    - Sterile forceps (clean in between samples with 70% EtOH)
    - 30mg wad of damp paper towel (to help with approximating sample size)
    - For each sample:
        - 1 Sterile petri dish (small)
        - 1 Razor blade
        - 1 Falcon Tube (5 mL round bottom polypropylene - should fit homogenizer)
- Homogenizer
- Ice
- For each sample:
    - 1 50 mL conical tube with 35 mL Ultra Pure H_2O
    - 1 50 mL conical tube with 35 mL Ultra Pure EtOH (plus one extra)
    - Sterile 1.5 mL eppendorf tube (labeled) on ice
    - 600 µL RLT buffer with 6 µL beta-mercaptoethanol (10 µL per 1 mL RLT)
- Box of kimwipes

A. Preparing Frozen Tissue (skip to B for pre-prepared 30mg of tissue in Falcon tube)
    a. Take samples from -80^{0}C freezer and put on dry ice
    b. Label petri dishes and falcon tubes. Put on dry ice.
    c. For each sample:
        i. Clean forceps with 70% EtOH
        ii. Lay out new razor blade on clean paper towel
        iii. Use forceps and gentle warming (with hands through gloves) to remove frozen sample from current container and place in petri dish)
        iv. Move petri dish to bench. Quickly cut off 30mg or less with razor blade. (Refer to pre-weighed wad of damp paper towel for size approximation)
        v. Place the <30mg piece of sample in the Falcon tube. Return remainder to original container. Put both back on dry ice.
        vi. Throw out petri dish and razor blade. Clean forceps.
B. Homogenization
    a. Clean bench space by homogenizer and homogenizer itself with EtOH.

b. Take styrofoam container with dry ice and samples over to homogenizer.
c. For each sample:
    i. Add 600 µL RLT with 6 µL beta-mercaptoethanol to frozen sample
    ii. Run homogenizer until sample is fully puréed (time depends on tissue. ~30sec for lung, 1 minute for submandibular gland). Transfer 600 µL to eppendorf on ice.
    iii. Clean homogenizer by running it in a conical tube with 70% UltraPure EtOH. If this is not the first sample, use the second EtOH from the previous sample as the first wash in this sample.
    iv. Run homogenizer in a second, clean conical tube of 70% UltraPure EtOH
    v. Run homogenizer in a conical tube of UltaPure H_2O.
    vi. Dab clean with kimwipes.
    vii. Spin down final product (in eppendorfs). Transfer supernatant to another eppendorf. Continue to RNA purification. (Or store at -80 degrees)

RNA purification with Qiagen kit

Equipment:

- Centrifuge that holds 1.5 mL eppendorf tubes

Reagents:

- RNA in RLT with beta-mercaptoethanol
- RNeasy Mini Kit (Qiagen, no. 74104)

1. Take eppendorfs with supernatant from *RNA isolation* protocol
2. Add 1 volume (600 µL) of 70% ethanol to the lysate, and mix well by pipetting. Do not centrifuge. Proceed immediately to step 3.
3. Transfer up to 700 µL of the sample, including any precipitate, to an RNeasy Mini spin column placed in a 2 mL collection tube (supplied). Centrifuge for 15 s at ≥8000 x g. Discard the flow through. Transfer any remaining sample to the spin column and centrifuge again.
4. (DNase digestion steps) Add 350 µL Buffer RW1 to the RNeasy spin column. Centrifuge for 15 s at ≥8000 x g. Discard the flow through. Make stock solution of DNase: 10 µL DNase + 70 µL RDD buffer per sample, and mix. Add 80 µL of final solution to each spin column and let sit for 10 min. Then add 350 µL Buffer RW1 to the RNeasy spin column. Centrifuge for 15 s at ≥8000 x g. Discard the flow through.
5. Add 500 µL Buffer RPE to the RNeasy spin volume (note: in preparing the kit, add 4 volumes of ethanol (96-100%) to Buffer RPE for a working solution). Centrifuge for 15 s at ≥8000 x g. Discard the flow through.
6. Add 500 µL Buffer RPE to the RNeasy spin volume. Centrifuge for **2 min** at ≥8000 x g. Place spin column in a new 2 mL collection tube (supplied). Centrifuge at full speed for 1 min to dry the membrane.
7. Place the RNeasy spin column in a new 1.5 mL collection tube (supplied). Add 30-50 µL RNase-free water directly to the spin column membrane. Wait 5 minutes. Centrifuge for 1 min at ≥8000 x g to elute the RNA.

NanoDrop RNA/DNA

Equipment:

- NanoDrop 2000
- 2 µL pipette
- Kim wipes
- Paper and pen

Reagents:

- DNA/RNA to evaluate
- Solution in which DNA/RNA was eluted (exact bottle, if possible)

1. Open NanoDrop and select Nucleic Acids to measure
2. Select either DNA or RNA from drop down menu under sample name
3. Clean NanoDrop pedestal with Kimwipe. Pipette 1 µL elution solution onto pedestal and lower arm
4. Hit "Blank"
5. Wipe off pedestal with clean section of kimwipe. Pipette 1 µL of your first sample onto the pedestal, being sure to completely cover the central hole and not to create bubbles. Type in sample name and hit "Measure."
6. Write down concentration (in ng/µL), 260 value, 260/280 and 260/230 ratios
7. Repeat steps 5-6 for all samples
8. Clean pedestal with dH_2O and dry kim wipe when finished.

Making cDNA from RNA

Equipment:

- Thermocycler

Reagents:

- RNA (see RNA extraction/purification above)
- H_2O (RNase and DNase free)
- Random Primer Hexamer
- dNTP
- 0.1M DTT
- 5x First Strand Buffer

1. Start Thermocycler (so cover heats up)
    a. cDNA Superscript III -> View -> Run
2. Put tubes of Random Primer Hexamer, dNTP, DTT, Buffer, RNAse Out and Superscript III (stored at -20^{0}C) and put in metal tube holder on ice.
3. Using information from NanoDrop on RNA concentration, calculate maximum consistent ng of RNA (should be above 500ng) such that volume of RNA + H_2O = 11.5uL
    a. Ex. For RNA at 43.9 ng/µL, 11.4 µL is 500 ng, plus 0.1 µL H_2O
4. Add RNA, water, Random Primer Hexamer (0.5 µL) and dNTP (1 µL). Put in Thermocycler. Press Run.
5. Make Master Mix of remaining 4 reagents. Add in Superscript III last! (Always add enzyme last)
    a. Ex. For 3 samples, make x4 Master Mix

i. 5x RT Buffer: 4 µL x 4 = 16 µL
ii. 0.1M DTT: 1 µL x 4 = 4 µL
iii. RNAse Out: 1 µL x 4 = 4 µL
iv. Super III: 1 µL x 4 = 4 µL

6. Add 7 µL Master Mix to each tube. Put back in Thermocycler. Press "Skip." Wait 1.5 hrs.
7. Dilute final product with 20 µL water for 40 µL total.

qPCR of cDNA

Equipment:

- Applied Biosystems 5500 Fast Thermocycler
- 96 well plates that fit 5500 Fast Thermocycler, specifically

1. Make a layout of samples in each well. Decide how many replicates, which samples/RNA, *etc.* Negative control should have Master Mix but no RNA. 18S RNA used to assess quantity of overall good RNA in each sample.
2. Make Master Mix of each RNA you want to quantify
   Ex. For PGP9.5

	Forward	**Reverse**	**Water**	**SYBR green**	**Total**
1 reaction	0.6 µL	0.6 µL	6.8 µL	10 µL	18 µL
3 samples x 3 replicates + 1 extra = x10	6 µL	6 µL	68 µL	100 µL	180 µL

3. Add 18 µL Master Mix to each well.
4. Add 2 µL of cDNA (from the 40 µL of sample in Step 7, above) to each well.
5. Seal plates. Add plastic covering, then rub thoroughly with plastic spatula. Overdone is better than underdone.
6. Vortex plates briefly, then centrifuge very briefly at 300g. (Wait until centrifuge hits 300g, then hit stop.)
7. Put plate in Applied Biosystems 5500 Fast Thermocycler.
8. Run plate
   a. Note: in Jacoby lab, go to Users/AD/Desktop/Old 7500 Computer Files/Templates/Templates and click the "Use this - Generic"
   b. Run will take ~4 hours

Plasmid Transformation and Transfection

Brief summary: Make agar plates with antibiotic. Transform plasmid into competent bacteria. Maxi Prep to extract DNA plasmids, then transfect into HEK cells and stain with JaneliaFluor 646 dye. Make sure to prepare the agar plates and unfreeze/passage the HEK cells a few days in advance.

Equipment:

- Autoclave
- 10 cm petri dishes
- Ice
- Dry Ice
- Water bath at 42^{0}C
- 37^{0}C incubator with shaking at 225 rpm
- Centrifuge with 50 mL conical tube holder (>2250 g)
- Nanodrop
- Sterile 12-well plate (or other desired size - see *HEK transfection*)

Reagents:

- LB agar
- LB broth
- Antibiotics (check plasmid - most use ampicillin or kanamycin)
- E. coli (DH5α Cells for heat shock transformation)
- Media for E. Coli (usually comes with the cells)
- Mini Prep Kit (Qiagen; Cat no. 27104)
- Maxi Prep Kit (ChargeSwitch Pro; Cat no. CS31106)
- T4 DNA Ligase (New England Biolabs)
- Lipofectamine 2000 Transduction reagent (Thermo Fisher #11668030)
- Opti-MEM - Reduced Serum Medium (Thermo Fisher #31985070)

Make Agar Plates with antibiotic

1. Add 32g per liter LB Agar to distilled water
2. Autoclave at 121^{0}C for 15 min
3. Wait until agar reaches 50^{0}C, then add the antibiotic
    a. For 100x kanamycin, add 1 mL of 100x stock solution per 100 mL of agar. Final concentration should be 100 μg/mL.
4. Pour into petri dishes
5. Store at 4^{0}C (good for about 1 month)

Transforming Bacteria - Subcloning Efficiency DH5α Cells

1. Thaw on ice one tube of cells. Place 1.5 mL microcentrifuge tubes on wet ice.
2. Gently mix the cells with a pipette tip, then aliquot 50 μL of cells for each transformation into a 1.5 mL microcentrifuge tube.

3. Refreeze any unused cells in dry ice for 5 min before returning to -80 freezer. Do not use liquid nitrogen.
4. Add 1-5 µL (1-10ng) of DNA to the cells and mix gently by stirring. Do not mix by pipetting up and down.
5. Incubate tubes on ice for 30 min
6. Heat-shock the cells for 20 seconds in a 42^{0}C water bath without shaking
7. Place the tubes on ice for 2 minutes
8. Add 950 µL of pre-warmed medium to each tube
9. Incubate the tubes for 1 hour at 37^{0}C, shaking at 225 rpm
10. Spread 20-200 µL from each transformation on pre-warmed agar plates with antibiotics.
    a. It is recommended to plate at two different volumes to ensure that at least one plate will have well-spaced colonies.
    b. It is fun and effective to place the agar plate on a wheel and spin to spread the bacteria. Weeeee!
11. Store the remaining transformation reaction at 4^{0}C. If needed, you can plate additional cells the next day.
12. Incubate the plates overnight at 37^{0}C.

Mini Prep from Plates

1. Mix 5 mL LB broth with antibiotics in Falcon tube - closed to first stop only
2. Take a clean plastic pipette tip with no filter. Touch tip to single colony on bacteria plate, then drop into Falcon tube.
3. Incubate tubes shaking at 225 rpm and 37^{0}C overnight.
4. Look at tubes the next day. LB broth should be pale yellow and cloudy. If needed, remove 500 µL of culture for glycerol stock or Maxi prep and place at 4^{0}C until DNA is sufficiently validated (see Restriction enzyme analysis and Sequencing)
5. Follow instructions for Qiagen QIAprep Spin Miniprep Kit to purify plasmid DNA:
    a. Pellet 1-5 mL bacterial overnight culture by centrifugation at >8000 rps (6800 x g) for 3 min at room temperature.
    b. Resuspend pelleted bacterial cells in 250 µL Buffer P1 and transfer to a 1.5 mL eppendorf tube.
    c. Add 250 µL Buffer P2 and mix thoroughly by inverting the tube 4-6 times until the solution becomes clear. Do not allow the lysis reaction to proceed for more than 5 min. If using LyseBlue reagent, the solution will turn blue.
    d. Add 350 µL Buffer N3 and mix immediately and thoroughly by inverting the tube 4-6 times. If using LyseBlue reagent, the solution will turn colorless.
    e. Centrifuge for 10 min at 13,000 rpm (~17,900 x g) in a table-top microcentrifuge.
    f. Apply 800 µL supernatant from previous step to the QIAprep 2.0 spin column by pipetting. Centrifuge at 13,000 rps for 30-60 s and discard the flow-through.
    g. Wash the spin column by adding 0.5 mL Buffer PB. Centrifuge at 13,000 rps for 30-60 s and discard the flow-through.
    h. Wash the spin column by adding 0.75 mL Buffer PE. Centrifuge at 13,000 rps for 30-60 s and discard the flow-through. Transfer spin column to the collection tube.
    i. Centrifuge for 1 min to remove residual wash buffer.

j. Place the spin column in a clean 1.5 mL eppendorf tube. To elute DNA, add 50 µL Buffer EB (10mM TrisCl, pH 8.5) or water to the center of the spin column, let stand 1 min, and centrifuge for 1 min.

Making Glycerol Stock

1. Add 500 µL of overnight culture (from Mini or Maxi prep) to 500 µL of 50% glycerol in a 2 mL screw top tube or cryovial and gently mix.
2. Freeze at -80^{0}C. When using stock in future, avoid thawing - simply scrape the top of the stock with a pipette or break off a small chip and add to LB broth to re-grow.

Restriction Enzyme Digest

Restriction enzyme (RE) digests are used to cut out specific segments of DNA for identification, amplification, and sometimes future ligation. The protocol will vary slightly based on the REs used. If using for sequence validation, be sure to perform an *in silico* digest before choosing REs: select either a single or multiple REs that will give band sizes different enough to be easily distinguished on a gel. Bands less than 70bp may be hard to see.

1. Calculate how much RE is needed for reaction. One unit of enzyme cuts 1 µg of DNA at 1 site in 1 hour. If you have more cut sites, wait longer for reaction or add more enzyme.
2. For each sample, combine:
    - ~1 µg DNA
    - Buffer (ex. CutSmart Buffer from NEB - check appropriate buffer for each enzyme)
    - dH_2O (to make 20 µL total reaction)
    - Restriction enzymes (~ 1 µL each)
3. Incubate for at least 1 hour (but longer is better) at the appropriate temperature (ex. TaqI incubates at 60^{0}C for as long as possible, DraI and HincIII incubate at 37^{0}C.)
4. Put RE digests on ice
5. Run reaction on a gel (see earlier section, “Gel electrophoresis”) to visualize results.

PCR Amplification of Larger DNA sequences

- 5 µL of 2ng/µL DNA for 10ng total DNA
- 1 µL of 20 uM of each primer - forward and reverse (2 µL total) (dilute 100uM stock 1:5)
- 18 µL of H_2O
- 25 µL DNA polymerase (Platinum SuperFi)
- Make one Master Mix for each fragment of DNA you wish to amplify. Master Mix should contain DNA polymerase, H2O, and primers.

PCR Thermocycler parameters:

95^{0}C x 2 min

35 cycles of :

95 x 15 sec

55 x 30 sec

72 x 30 sec
72^0C x 5 min
4^0C x infinity

Ligation

1. For ligation, calculate the volume needed of each DNA fragment based on size in kb. For example, for inserting 1.4 kb PGP9.5 promoter into 4.8 kp AAV-GFP backbone you need a 3:1 molar ratio of PGP:AAV, and slightly less for the larger TUBA1 promoter. Ex.

   1.5 μL AAV-GFP backbone
   5 μL PGP9.5 (4 μL TUBA)
   2 μL Buffer
   1 μL T4 DNA Ligase
   11.5 or 10.5 μL H_2O
   20 μL total

2. Ligate at room temp for at least 1 hour. Then transform product into bacteria (see "Transforming Bacteria") and Mini Prep.

Maxi Prep using Invitrogen ChargeSwitch Pro Filter kit

1. **Before starting**: for a new kit, add the RNase A provided to the Resuspension buffer and mix. If necessary, warm the Lysis Buffer to 37^0C to dissolve any precipitate.
2. **Preparing the Sample**: Take cells from Mini Prep or Glycerol stock and grow in LB broth with antibiotics overnight.
3. Pellet cells from overnight culture. Up to 100 mL fit in one bucket.
4. Re-suspend cells in 7 mL Resuspension Buffer premixed with RNase A. No cell clumps should remain.
5. Add 7 mL Lysis Buffer. Mix well by gentle inversion 10 times. Do not vortex!
6. Incubate at room temp for 5 minutes. But NOT more than 5 minutes.
7. Add 7 mL Precipitation Buffer and mix well until white precipitate forms.
8. **Clearing/Binding the DNA**: Transfer the lysate from the previous step onto the Filter Column inserted in a 50 mL conical tube.
9. Incubate for 2-3 minutes to allow precipitate to float to the surface.
10. Centrifuge the column at >2250 x g for 2-3 minutes
11. Gently remove the column from the tube and discard the flow-through
12. Remove and discard inner Lysate Clarification Column. Re-insert column in the same tube.
13. **Washing the Column**: Add 15 mL of Wash Buffer 1 to the column
14. Centrifuge the column at >2250 x g for 1 minute
15. Remove the column from the tube. Discard flow-through. Re-insert the column in the tube.
16. Add 15 mL of Wash Buffer 2 to the column.
17. Centrifuge the column at >2250 x g for 1 minute.
18. Remove column from tube. Discard flow-through AND 50 mL conical tube.

19. **Eluting the DNA**: Insert column into a clean 50 mL conical tube.
20. Add 1-2 mL Elution Buffer onto the column.
21. Centrifuge the column at >2250 x g for 1 minute.
22. Remove column from tube.
23. Transfer the eluate from the tube back onto the same column. Replace in tube.
24. Centrifuge the column at >2250 x g for 1 minute. The eluate contains the purified DNA.
25. Discard the used column. Store DNA at 4^0C or -20^0C.

Transfecting HEK/Neuro 2a cells

1. Nano Drop to assess concentration of purified DNA. Calculate volume needed per well (see below)
2. Verify that cells are at desired level of confluence (aim for 50% for nice images of individual cells)
3. Prepare tissue culture hood: spray everything with 70% EtOH and wipe thoroughly
4. Warm OptiMEM in 37^0C water bath

	8 well slide	**24 well plate**	**12 well plate**	**6 well plate**
DNA	200 ng	0.5 ug	1 ug	2 ug
Lipofectamine	0.7 µL	2 µL	4 µL	8 µL
OptiMEM	40 µL	100 µL	200 µL	500 µL

5. Per DNA plasmid: make one tube with DNA plus OptiMEM. Add Lipofectamine, swirl to mix, and let sit 30 min at room temperature in culture hood.
6. Add DNA-Lipofectamine-OptiMEM to each well. Rock gently to mix. Incubate at 37^0C 24-48hrs.

JaneliaFluor Dye Stain

1. Treat cells with 33nM JaneliaFluor for 15 min in their home dish
    a. Make stock solution of 1 mM. Use 0.2 µL of this in 6 mL of medium for an effective concentration of about 33.3 nM.
2. Wash cells 2x with imaging medium or sterile PBS (with calcium to preserve adhesion)
3. Transfer coverslip into fresh medium for 15 min
4. Wash 2x with imaging medium or PBS (with calcium)
5. Mount coverslip in chamber and walk it to the microscope

Electrophysiology

Trachea Preparation

Reagents:

- Room temperature Krebs buffer containing (in mM): 125 NaCl, 21.4 NaHCO3, 11.1 D-glucose, 2.5 KCl, 1.2 MgCl2, 2.4 CaCl2, 1.2 NaH2PO4, z305 mOsm and 0.02 mg/ml Liberase (Thermolysin Medium; Roche)
- Artificial cerebrospinal fluid (aCSF)

1. Anesthetize mice with 100 mg/kg i.p. ketamine and 10 mg/kg i.p. xylazine
2. Do NOT perfuse with saline
3. Rapidly remove trachea using forceps and scissors while partner applies washes of Krebs.
4. Move trachea to dissection scope to clean as much tissue from outside of trachealis as possible. Do not let trachea dry out, keep it bathed in Krebs the whole time.
5. Submerge dissected trachea in room temperature Krebs buffer with Liberase for 30 minutes.
6. Wash trachea in artificial cerebrospinal fluid (aCSF) for another 20 minutes while saturating with 95% O2/5% CO2

Preparing Pipette Tips

Purpose: for patching airway postganglionic parasympathetic mouse neurons with Sweta Adhikary

Equipment:

- Borosilicate pipettes (2.5–3 MOhms; Sutter Instruments)
    - Outside diameter (O.D.) 1.5mm, inside diameter (I.D.) 1.1mm
- John Williams Lab pipette puller (the one with the plastic pig on top)

1. Put pipette in pipette puller
2. Make sure left knob is in “UP” position
3. Hold the swinging door so it stops pipette from dropping too far
4. Close the clear plastic protective shield
5. Press start
    a. Coil should turn orange
    b. Watch for small first drop
6. Move left knob to “DOWN” position
7. Keep swinging door open and out of the way. Keep plastic protective shield closed
8. Press start
    a. Wait for second drop
9. You’re done! Don’t let the pipette tips touch anything as you take them out, or they will break.

Chapter 3. Optogenetic Control of Airway Cholinergic Neurons *in vivo*

Background

Development of optogenetics

Optogenetics utilizes genetic expression of light-sensitive ion channels to activate (with cation channels) or inactivate (with chloride and other modified channels) specific populations of neurons in response to light. The system was originally developed by Deisseroth and colleagues (Deisseroth *et al.*, 2006), who saw potential in a light-sensitive ion channel that had been identified in bacteria (Nagel, 2002). The cation channel, which they named channelrhodopsin, successfully expressed in mammalian cells, trafficked to the plasma membrane, opened in response to photons of 405 nm light, and activated neurons (Boyden *et al.*, 2005). After demonstrating the feasibility of this technique, optogenetics was first used in the central nervous system, where it was used to activate neurons in the motor cortex (Aravanis *et al.*, 2007), orexin producing neurons in the hypothalamus (Adamantidis *et al.*, 2007), and dopamine neurons in the ventral tegmental region in awake, behaving mice (Tsai *et al.*, 2009). It is now almost ubiquitously used in studying nerve populations in the central nervous system, with applications for circuit mapping (Gradinaru *et al.*, 2007, Petreanu *et al.*, 2007), restoring functionality of retinal cells (van Wyk *et al.*, 2015), understanding mouse emotions and facial expressions (Dolensek *et al.*, 2020), and much more.

Use of optogenetics in the peripheral nervous system

Optogenetics has more recently been adapted to the peripheral nervous system as well. Researchers have used this technique in many innovative ways: inhibiting cardiac sympathetic nerve activity to suppress arrhythmias (Yu *et al.*, 2017) and even using different frequencies of nerve activation to inhibit motor neurons *in vivo* (Liske *et al.*, 2013). Despite this, only a small amount of studies have been done using optogenetics to study the airways.

Optogenetic activation of airway nerves

Much has been learned using traditional methods to study airway nerve activation, either by direct electrical stimulation of airway nerves *in vivo* or by activating nerves in airway segments in vitro with electrical field stimulation. Varying stimulus parameters gives some degree of selectivity to which nerves are activated (Ellis and Undem, 1990), but that selectivity is limited. Selectivity in activating neurons can be greatly enhanced by using optogenetics. Because of its ability to target subpopulations of neurons, both through promoter selectivity and physical limitations of light penetration, it is ideally suited to target specific components of nerve pathways, including the reflex bronchoconstriction pathway. Nerves are activated within milliseconds within an intact system, providing a significant advantage over other approaches. Though a relatively new technique, optogenetics has been used with airway sensory neurons to identify subpopulations that regulate patterns of breathing (Chang *et al.*, 2015), and to identify a subpopulation of sensory nerves expressing TRPV1 and

sphingosine-1-phosphate receptor 3 (S1PR3) that are important contributors to airway hyperreactivity in antigen challenged mice (Tränkner *et al.*, 2014). Currently these techniques are used in anesthetized, ventilated animals, but advances in the field of miniaturized implantable light diodes may make it possible to expand this technology and investigate airway nerve function in awake, behaving animals in the future.

Abstract

Dysregulation of airway nerves leads to airway hyperreactivity, a hallmark of asthma. Although changes in nerve density and phenotype have been described in asthma, the relevance of these changes in nerve function has not been investigated due to anatomical limitations where afferent and efferent nerves run in the same nerve trunk, making it difficult to assess their independent contributions. I developed a unique and accessible system to activate specific airway nerves to investigate their function in mouse models of airway disease. I describe a method to specifically activate cholinergic neurons using light, resulting in immediate, measurable increases in airway inflation pressure and decreases in heart rate. Expression of light-activated channelrhodopsin 2 in these neurons is governed by Cre expression under the endogenous choline acetyltransferase promoter, and I describe a method to decrease variability in channelrhodopsin expression in future experiments. Optogenetic activation of specific subsets of airway neurons will be useful for studying the functional relevance of other observed changes, such as changes in nerve morphology and protein expression, across many airway diseases, and may be used to study the function of subpopulations of autonomic neurons in lungs and other organs.

This chapter has been published as:

Pincus, A. B., Adhikary, S., Lebold, K. M., Fryer, A. D., & Jacoby, D. B. (2020). Optogenetic control of airway cholinergic neurons *in vivo*. *American Journal of Respiratory Cell and Molecular Biology*, *62*(4). https://doi.org/10.1165/rcmb.2019-0378MA

Part of the work presented within this chapter (Figure 3.7) was done in collaboration with Sweta Adhikary from the John Williams laboratory.

Introduction

Airway nerves are dysfunctional in asthma (Minette *et al.*, 1989). In the lungs, parasympathetic nerves provide the dominant autonomic control of airway tone and mediate bronchoconstriction (Nadel and Barnes, 1984). They are also part of a reflex arc that is triggered by sensory nerves and relayed via the central nervous system. Our lab has shown that epithelial sensory nerve density is increased in asthma (Drake *et al.*, 2018), while blocking parasympathetic nerves reduces airway tone and blocks vagally-mediated and reflex-mediated bronchoconstriction. Studies in animals have shown that airway hyperreactivity is mediated by parasympathetic nerves after antigen sensitization and challenge, infection with parainfluenza, exposure to ozone or organophosphate pesticides, and obesity (Fryer and Jacoby, 1991, Adamko *et al.*, 1999, Fryer *et al.*, 2004, Verhein *et al.*, 2013, Nie *et al.*, 2014). Gi-coupled M2 muscarinic receptors on postganglionic parasympathetic nerves normally limit acetylcholine release in healthy airways, but in animal models of airway hyperreactivity, and in humans with allergic asthma, M2 receptors decrease their inhibition of acetylcholine release, resulting in increased bronchoconstriction (Minette *et al.*, 1989, Fryer and Wills-Karp, 1991, Fryer and Jacoby, 1992, Evans *et al.*, 1997).

Electrical stimulation of the vagus nerve is the most common method for studying its function *in vivo*, but results obtained with this method are complicated by the many different types of neurons in the vagus, including multiple types of both sensory and autonomic neurons, and by regulatory effects of vagal activation on sympathetic outflow (Rajendran *et al.*, 2019). Current methods rely on pharmacological blockade or tight control of electrical stimulation parameters, but there is always a concern about specificity of action even with these controls. Therefore, there is a need for better tools to study nerves in the peripheral nervous system and, given the important role that nerves play in asthma, in airways in particular.

In this chapter, I have used optogenetics (Boyden *et al.*, 2005), or light activation of neurons, to specifically activate cholinergic nerves *in vivo*. Simultaneously, I recorded bronchoconstriction caused by the specific activation of these cholinergic neurons. This method can additionally be adapted to target other nerve populations. This new technique will allow us to evaluate the contribution of cholinergic parasympathetic neurons, as well as other nerve populations, to airway responses in asthma and other airway diseases.

Experimental Design

Animals

All animal procedures complied with Oregon Health & Science University's Institutional Animal Care and Use Committee guidelines. Transgenic mice expressing a floxed stop codon before channelrhodopsin 2 (CH2) fused to enhanced yellow fluorescent protein (EYFP; CH2–EYFP mice, #024109; Jackson Laboratory) and mice expressing Cre recombinase driven by the choline acetyltransferase (CHAT) promoter (CHAT-Cre mice, #028861; Jackson Laboratory) were bred to create mice with CH2 expressed in cholinergic neurons (CHAT-CH2 mice). Heterozygous mice were crossed with one another to form a homozygous CHAT-CH2 line. All mice were on a C57BL/6 background. Male and female mice 12 weeks of age and older were used for experiments.

Tissue Optical Clearing and Imaging of Airway Nerves

Mice were perfused with PBS and airways were excised and left at 4°C in Zamboni fixative (Newcomer Supply) overnight. Tracheas were blocked overnight with 4% normal goat serum, 1% Triton X-100, and 5% powdered milk, and then incubated overnight with antibodies to EYFP (anti-GFP chicken IgY, 1:500; Invitrogen) and pan-neuronal marker protein gene product 9.5 (PGP9.5, rabbit IgG, 1:500; Millipore) on a shaker at 4°C. Tissues were washed and incubated overnight in secondary antibodies (Alexa goat anti-rabbit 647, 1:1,000; Invitrogen; Alexa goat anti-chicken 488, 1:1,000; Invitrogen) before optical clearing for 12 hours in N-methylacetamide/Histodenz (Ce3D) (Li *et al.*, 2017). Tracheas were mounted in Ce3D on slides in silicon imaging wells and imaged using an LSM 880 confocal microscope. Samples were illuminated with 488 nm and 633 nm light, and images were acquired as z-stacks and converted to maximum intensity projections. Tiled images were obtained of each trachea, extending from the posterior cricoarytenoid muscle to the carina. All PGP9.5-positive and EYFP-positive nerve cell bodies within the area were quantified (Figure 3.1). All EYFP-positive cell bodies were PGP9.5 positive.

Ventilation and Physiological Measurements

Mice were anesthetized with ketamine (100 mg/kg i.p.) and xylazine (10 mg/kg i.p.), tracheotomized, and ventilated as previously described (Brown *et al.*, 1999). A 21-gauge catheter was inserted into the cricothyroid membrane to the level of the second cartilage ring. Mice were mechanically ventilated with 100% oxygen at 120 breaths/min with a tidal volume of 150 μl and a positive end-expiratory pressure of 2 cm H_2O. Mice were paralyzed with succinylcholine (0.05 mg in 0.05 ml i.p.) to eliminate respiratory effort. Some mice were injected with the cholinesterase inhibitor, physostigmine (0.5 mg/kg i.p.), and/or the muscarinic antagonist atropine (3 mg/kg i.p.). Body temperature was maintained at 37°C with a heat lamp, homeothermic blanket, and rectal probe. Heart rate and rhythm were measured by electrocardiogram recorded with three needle electrodes placed subcutaneously on the right hindpaw, left forepaw, and left shoulder. Airway pressure, heart rate, respiratory rate, tidal volume,

body temperature, and flow were all measured using LabChart Pro acquisition software (ADInstruments).

Optogenetic Activation of Nerves *In Vivo*

A midline skin incision was made extending 1 cm caudally from the base of the neck over the thorax. Soft tissue and muscle were retracted to expose the sternum to the level of the first two ribs, and this section of sternum was removed without lacerating the major blood vessels. If the thymus was visible, a 2-mm section from the proximal end was removed to allow a clear light path to the trachea. Muscle around the trachea was resected, and tissue was held to each side with clamps. Damp gauze was placed over the exposed trachea between light stimulations to prevent desiccation.

A high-power 454-nm light-emitting diode (LED) light source (Prizmatix) coupled to an optic fiber with a 500-μm core diameter was attached to a collimator (numerical aperture = 0.63) to create a 1-cm circle of light with 8.9-mW/mm2 intensity. A 555-nm LED light source was also used as a control. The light was positioned immediately ventral to the exposed trachea, centered midway between the larynx and carina (Figure 3.2). Light activation, frequency, pulse width, and pulse number were controlled by a Master-8 system pulse stimulator (A.M.P.I.).

Quantitative PCR of Lung Tissue and Submandibular Glands

Sections of lung tissue and submandibular gland were surgically excised. RNA was extracted by Qiagen RNeasy mini kit (Qiagen), and reverse transcribed with SuperScript III (Invitrogen). cDNA was amplified using QuantiTect SYBR Green on the Veriti 96-well Thermal Cycler (Applied Biosystems). Primers specific for EYFP, PGP9.5, and Cre recombinase were synthesized (Table 3.1; Integrated DNA Technologies), and the cycle thresholds (CT values) for PCR products were measured with 7,500 Fast Real-Time PCR System (Applied Biosystems).

Electrophysiology Recording of Parasympathetic Neurons

Tracheas were removed from anesthetized mice and were submerged in room temperature Krebs buffer containing (in mM): 125 NaCl, 21.4 NaHCO3, 11.1 D-glucose, 2.5 KCl, 1.2 MgCl2, 2.4 CaCl2, 1.2 NaH2PO4, ~305 mOsm, and incubated in 0.02 mg/ml Liberase (Thermolysin Medium; Roche) for 30 minutes. Tracheas were then washed in artificial cerebrospinal fluid (aCSF) for another 20 minutes while being saturated with 95% O2/5% CO2. Recordings were obtained at near-physiological temperature (32–34°C) from slices superfused with oxygenated aCSF.

Table 3.1. Primers used for PCR RNA analysis.

RNA target	Forward	Reverse
EYFP	CCA CCT ACG GCA AGC TGA CC	GGT AGC GGG CGA AGC ACT
PGP9.5	GAA GCA GAC CAT CGG AAA CTC C	GGA CAG CTT CTC CGT TTC AGA C
Cre	TCT CAC GTA CTG ACG GTG G	ACC AGC TTG CAT GAT CTC C
18S	GTA ACC CGT TGA ACC CCA TT	CCA TCC AAT CGG TAG TAG CG

Electrophysiology Data Acquisition

Borosilicate pipettes (2.5–3 MΩ; Sutter Instruments) were filled with potassium gluconate-based internal solution (in mM): 110 potassium gluconate, 10 KCl, 15 NaCl, 1.5 MgCl2, 10 HEPES, 1 EGTA, 2 Na2ATP, 0.3 Na2GTP, 7.8 phosphocreatine; pH 7.35–7.40; ~280 mOsm. Tracheal parasympathetic ganglionic neurons were identified by morphology and by their expression of EYFP. Optically evoked inward currents were recorded in whole-cell voltage-clamp mode at −70 mV holding potential. Optically evoked depolarizations were recorded in whole-cell current clamp mode.
All recordings were acquired using an Axopatch 200A amplifier (Molecular Devices), digitized at 20 kHz (Instrutech ITC-16), and recorded (Axograph X software). Optically evoked currents were elicited by LED illumination through the microscope objective (Olympus, BX51W with 60×, 1.0 numerical aperture water immersion objective. For LED stimulation a transistor to transistor logic (TTL)-controlled LED driver and 470 nm LED (Thorlabs) were used to illuminate the slice directly over the recorded cell generally with approximately 1 mW of power for 1 ms.

Statistical Analysis

One-way ANOVA with Bonferroni post hoc test was used for airway pressure and heart rate data. Linear regressions were used for assessment of CH2 expression in both imaging and quantitative PCR (qPCR) analysis. Data were analyzed using GraphPad Prism 8 (GraphPad Software).

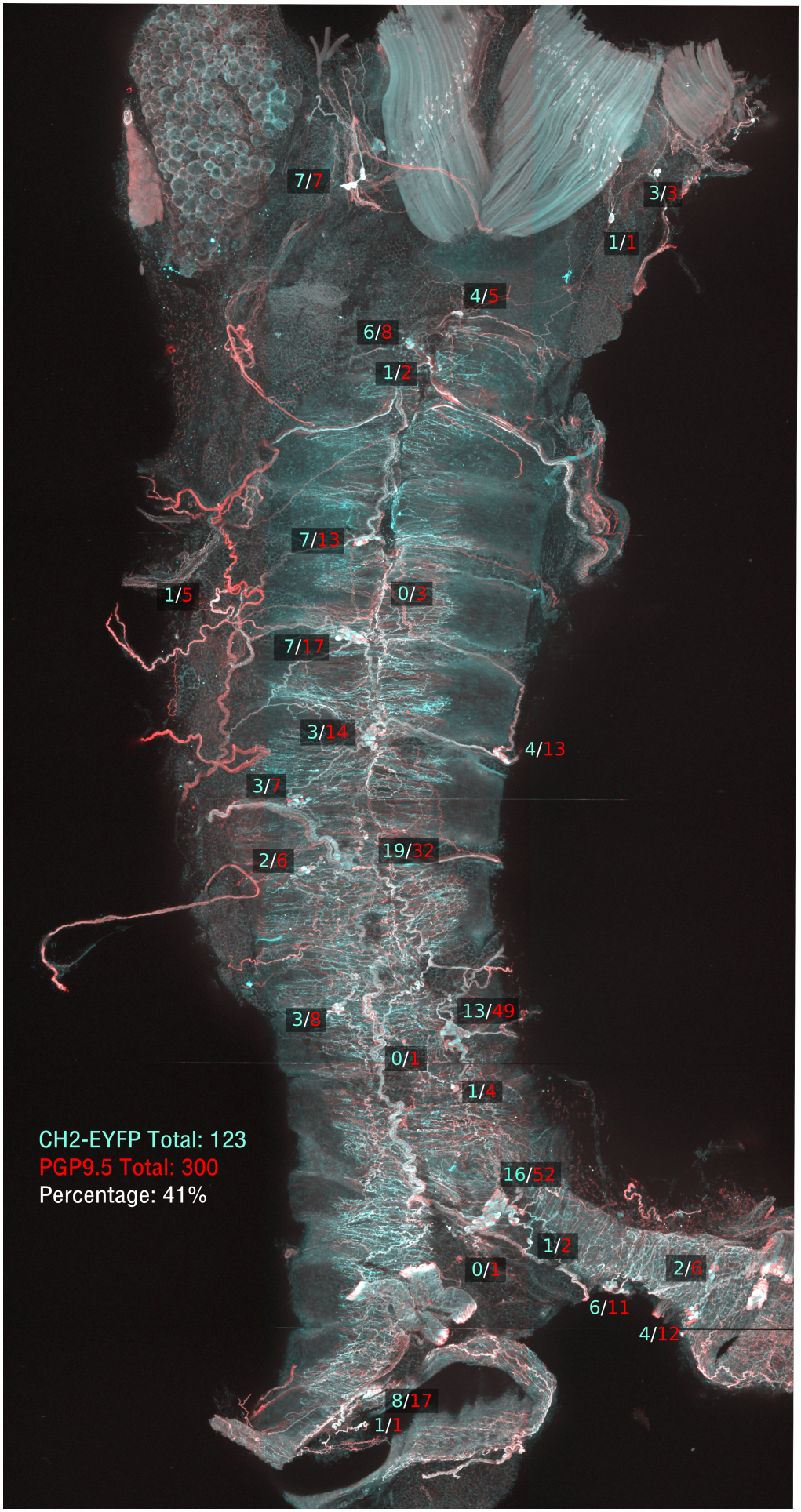
7/7
3/3
1/1
4/5
6/8
1/2
7/13
1/5
0/3
7/17
3/14
4/13
3/7
2/6
19/32
3/8
13/49
0/1
1/4
CH2-EYFP Total: 123
PGP9.5 Total: 300
Percentage: 41%
16/52
1/2
0/1
2/6
6/11
4/12
8/17
1/1

Figure 3.1. Representative image illustrating quantification of CH2 expression. Whole tracheas, from the posterior cricoarytenoid muscle (top) to the carina bifurcation (bottom) showing expression of PGP9.5 (red) and EYFP fused to CH2 (cyan). Parasympathetic nerve cell bodies in the trachea were identified by location along nerve fibers, cellular morphology, and PGP9.5 staining. All identifiable nerve cells in each trachea were counted (PGP9.5 positive cells, red). Number of cells co-expressing CH2-EYFP were recorded (CH2-EYFP positive cells, cyan). This trachea from a heterozygous CHAT-CH2 mouse has 41% expression of CH2 in airway parasympathetic nerves. PGP9.5 = protein gene product 9.5.

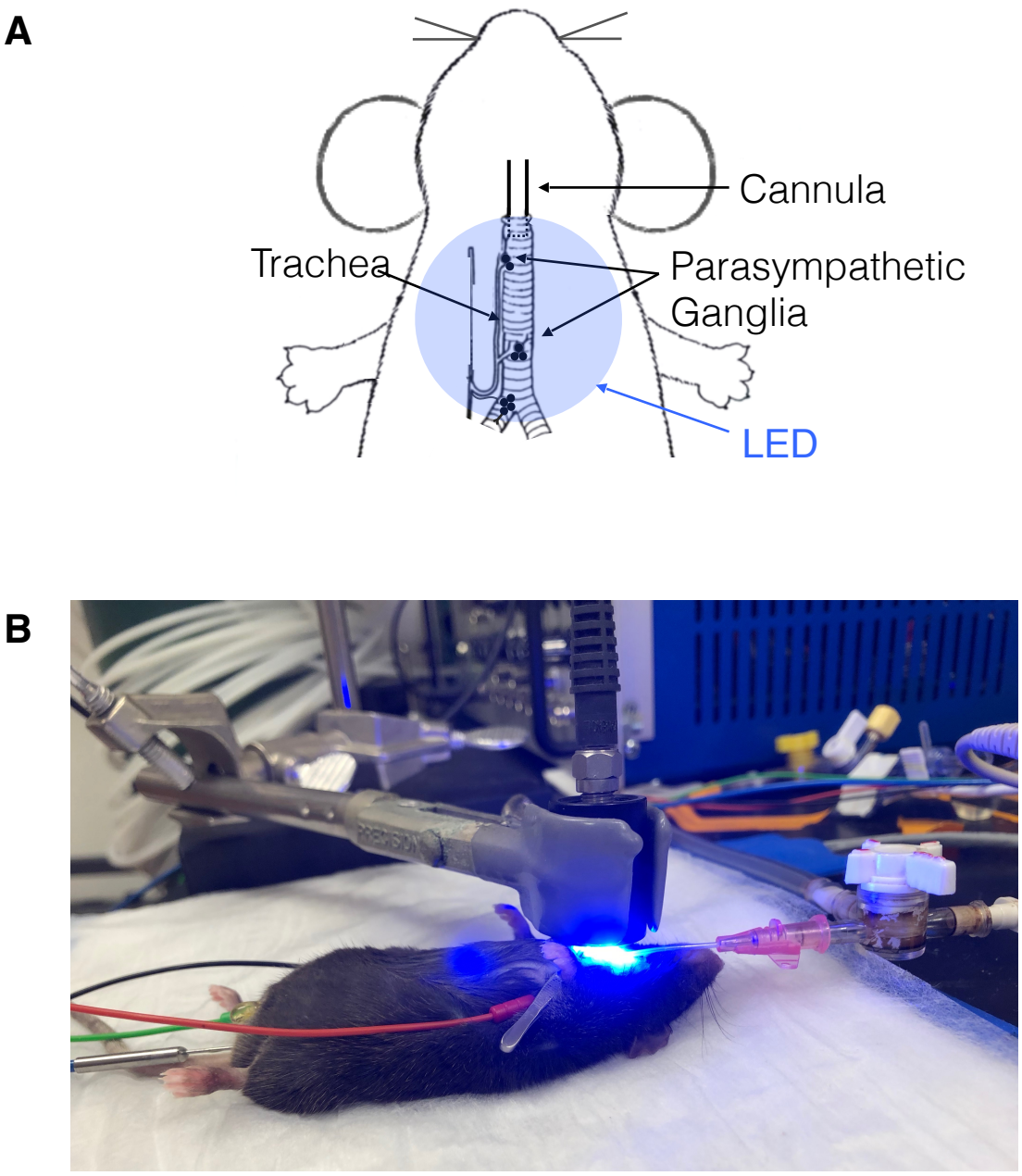

Figure 3.2. (A) Diagram of ventilated mouse showing area of light-emitting diode (LED) illumination. The area of illumination covers the majority of the trachea. Light must be of sufficient intensity to travel through the trachea to parasympathetic ganglia located on the dorsal aspect. (B) Image of cannulated mouse on ventilator with LED turned on. EKG needle electrodes are attached to right leg, left arm, and right back.

Results

Optogenetic Activation of Thoracic Cholinergic Nerves Leads to Bronchoconstriction and Heart Rate Reduction

Bronchoconstriction and bradycardia were measured during 30 seconds of light at increasing pulse frequencies (2–40 Hz) and pulse widths (1–15 ms) in the presence of physostigmine. Light of 20-Hz frequency and 5-ms pulse width caused the largest increase in airway pressure (Figure 3.3), and was used in subsequent experiments. Each CHAT-CH2 mouse was exposed to three pulse trains of light over 20 minutes: an initial pulse train (light), a pulse train given 15 minutes after intraperitoneal injection of 0.1 mg/ml physostigmine to block degradation of acetylcholine by cholinesterase (light + physostigmine), and a pulse train given 5 minutes after a further intraperitoneal injection of 1 mg/ml atropine to block muscarinic receptors (light + physostigmine + atropine). Without pharmacological intervention, light caused small increases in airway pressure. Physostigmine dramatically increased the response to light (Figures 3.4 and 3.5). In both the absence and presence of physostigmine, light-induced bronchoconstriction and bradycardia reversed rapidly upon cessation of light stimulation. In addition, both bronchoconstriction and bradycardia were blocked by atropine, confirming these effects were mediated by release of acetylcholine onto muscarinic receptors. Wildtype animals had no airway pressure or heart rate response when exposed to light, even after giving physostigmine, and CHAT-CH2 mice had no response when the 454-nm LED light was replaced with light in the red spectrum (555 nm; Figure 3.6).

Electrophysiologic Recordings Confirm Light Response of CH2-Expressing Parasympathetic Neurons

To verify CH2 effect in parasympathetic neurons, I collaborated with Sweta Adhikary to perform whole cell patch-clamp recording of parasympathetic neurons in homozygous mice (CH2+/+ CHAT+/+). We observed inward currents (Figure 3.7A) and cell depolarization equivalent to that obtained with current injection (Figure 3.7B) in response to 1-ms pulses of 470-nm light in neurons expressing CH2-EYFP, as indicated by fluorescence with 488-nm light. Light did not elicit either inward currents or depolarization in neurons that did not express CH2-EYFP within the same animals.

Whole-Mount Fluorescence Microscopy of Tracheal Parasympathetic Nerves Reveals Variable Expression of CH2 in Heterozygous CHAT-CH2 Mice

Overlap of fluorescent labeling for EYFP and PGP9.5 confirmed that CH2 was expressed within parasympathetic neurons. However, high variability in the proportion of postganglionic parasympathetic neurons expressing CH2 was observed between breeding pairs and even within litters

(Figure 3.8, Table 3.2). A linear relationship ($R2 = 0.681$, $P < 0.001$) was found between the percentage of nerves expressing CH2 and the maximum light-induced increase in airway peak pressure (Figure 3.9). This relationship demonstrates that observed increases in airway pressure are the direct result of activation of CH2-expressing airway parasympathetic neurons.

qPCR of Lung Tissue Is a Fast and Reliable Method of Determining CH2 Expression

Although reliable, immunohistochemistry and imaging of every mouse trachea is both an expensive and time-intensive process. To quantify CH2 expression without imaging I extracted RNA from lung tissue in heterozygous mice with variable CH2 expression. Quantification of mRNA showed that the ratio of expression of EYFP to the neuronal marker, PGP9.5, in lung tissue correlated well with the percentage of CH2-positive neurons in the tracheas (Figure 3.10A). Because the submandibular gland is also supplied by parasympathetic innervation, I took samples of this tissue to test whether the level of CH2 expression might be assessed in a nonlethal tissue biopsy. However, the ratio of EYFP to PGP9.5 in these qPCR reactions did not correlate as well to CH2 expression from imaging (Figure 3.10B). To assess whether variability in CH2 expression was due more to a lack of Cre efficiency or Cre expression, I correlated PCR results of Cre mRNA expression to PGP9.5 and EYFP expression in lung homogenates (Figure 3.11). Cre expression was aligned more closely with PGP9.5 compared with EYFP, indicating that Cre is consistently expressed in nerves, but variably efficient at facilitating CH2-EYFP transcription.

Mice Homozygous for CHAT-Cre Have Higher and Less Variable CH2 Expression

In an effort to produce animals with less variability in CH2 expression, heterozygous mice (genotype CH2+/−CHAT+/−) were bred together, resulting in some mice that were homozygous for both genes (CH2+/+ CHAT+/+). These mice had two copies of the CHAT-Cre gene as well as two copies of floxed CH2. CH2 expression was quantified using imaging, and homozygous mice were found to have a higher percentage of CH2-expressing nerves in parasympathetic ganglia ($95 \pm 4.4\%$) than heterozygotes ($53 \pm 4.8\%$), $P = 0.0006$; Figure 3.12).

Parasympathetic nerve activation is sensitive to dosage of anesthesia but not mouse age

Other potential sources of airway pressure variability were investigated. Increasing the dose of administered ketamine/xylazine anesthetic decreased the maximum observed change in airway pressure (Figure 3.13). The effect of mouse age on channelrhodopsin expression was also investigated. No correlation was found between the age of mice (16 -42 weeks) and either channelrhodopsin expression in airway nerves (Figure 3.14A) or maximum observed change in peak airway pressure (Figure 3.14B).

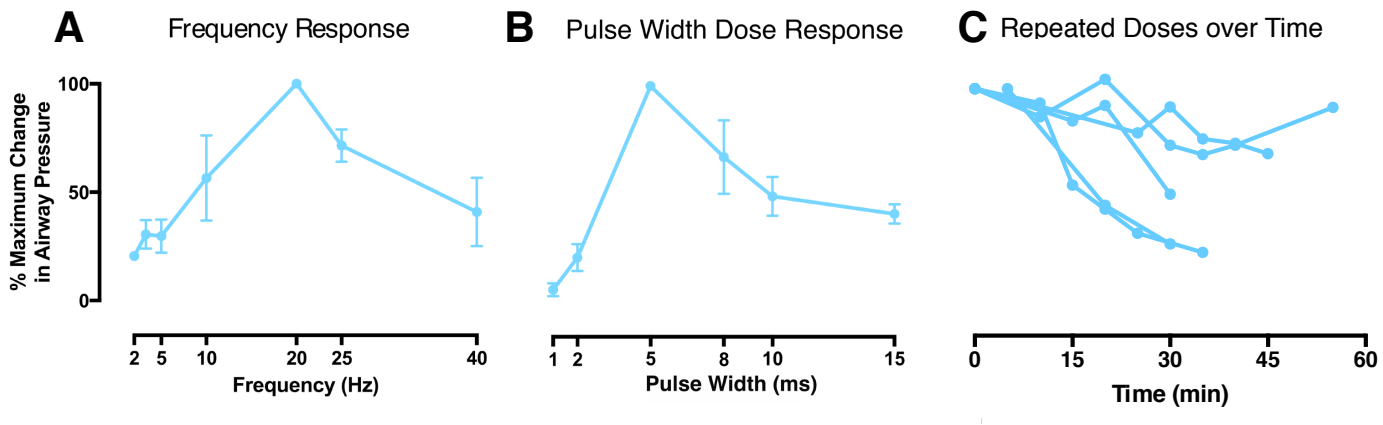

Figure 3.3. (A-B) Increase in peak pressure during light activation at different frequencies and pulse widths, reported as a percentage of the maximum peak airway pressure increase for each mouse. Maximum increases in airway pressure were achieved using 20-Hz light with a pulse width of 5 ms. (C) Repeated light exposure resulted in a decrease in pressure change over time, which varied widely between mice.

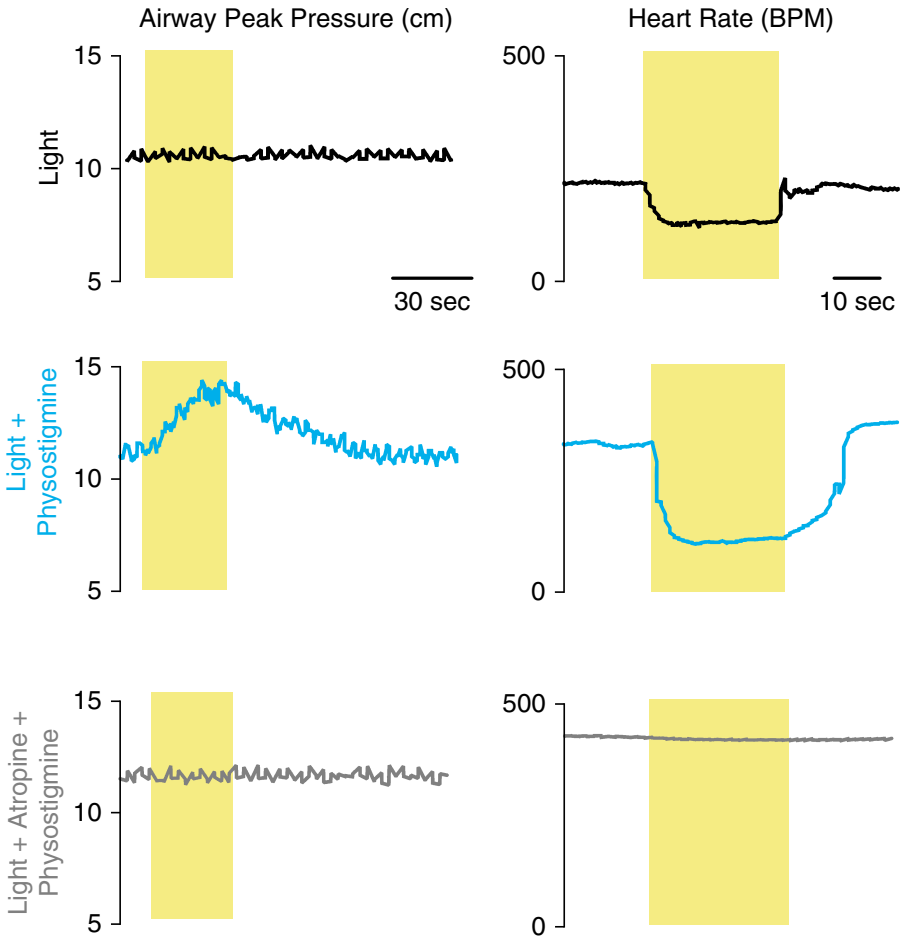

Figure 3.4. Optogenetic activation of airway cholinergic neurons leads to bronchoconstriction. Representative traces of airway peak pressure and heart rate effects after optogenetic activation. Airway peak pressures increased substantially in the presence of physostigmine. This effect, as well as the decrease in heart rate, was blocked by atropine.

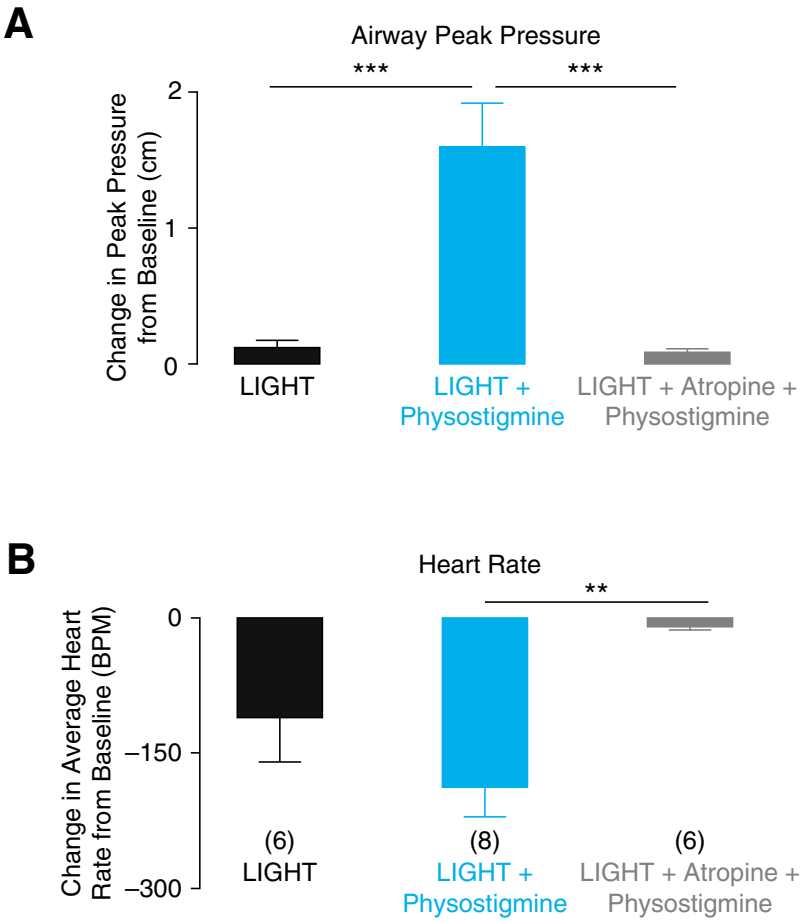

Figure 3.5. Airway peak pressures increased substantially in the presence of physostigmine. This effect was blocked by atropine. (A and B) Maximum peak airway pressure increases (A) and heart rate decreases (B) over the 30-second period of light activation (n = 6–8 as indicated; mean ± SEM; **P , 0.01 and ***P , 0.001). Columns show mean ± SEM. BPM = beats per minute.

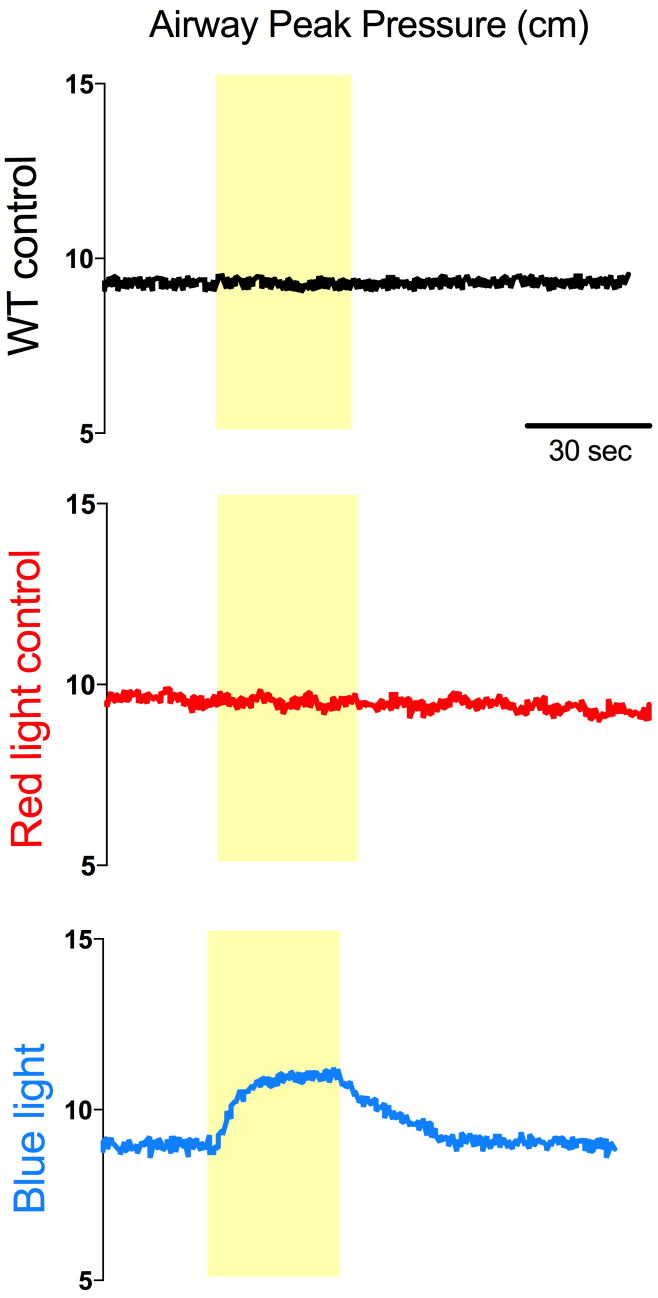

Figure 3.6. Optogenetic controls. WT C57/B6 mice in the presence of physostigmine do not respond to 454nm light- activation. CH2+/+ CHAT+/+ mice do not respond to 555nm light-activation, but subsequently responded to 454nm light.

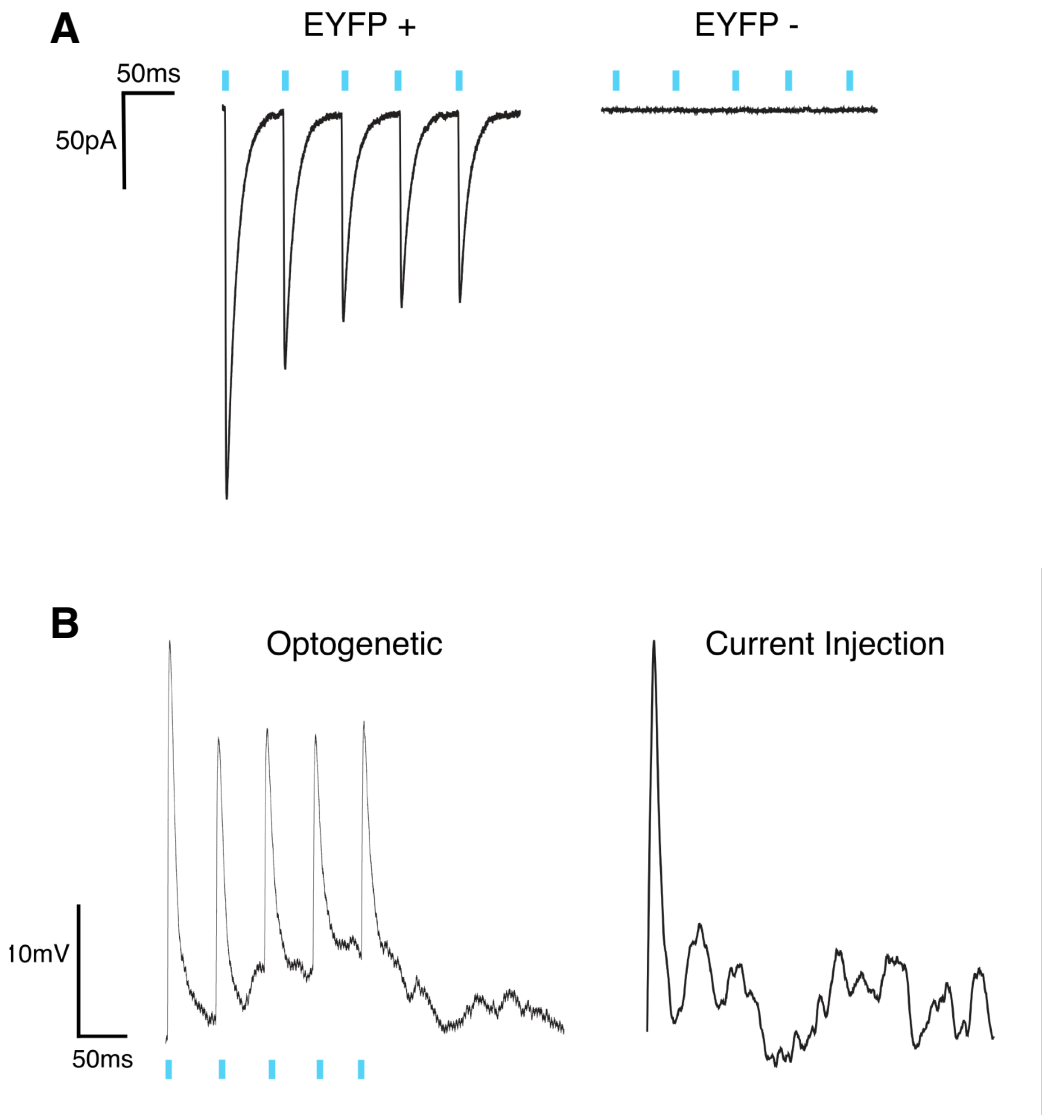

Figure 3.7. (A) Whole-cell patch clamp of enhanced yellow fluorescent protein (EYFP)-positive cells showed light-induced inward currents, which were absent in neurons not expressing channelrhodopsin 2 (CH2)-EYFP. (B) Optogenetic activation of airway neurons and current injection led to similar levels of depolarization in EYFP-positive cells.

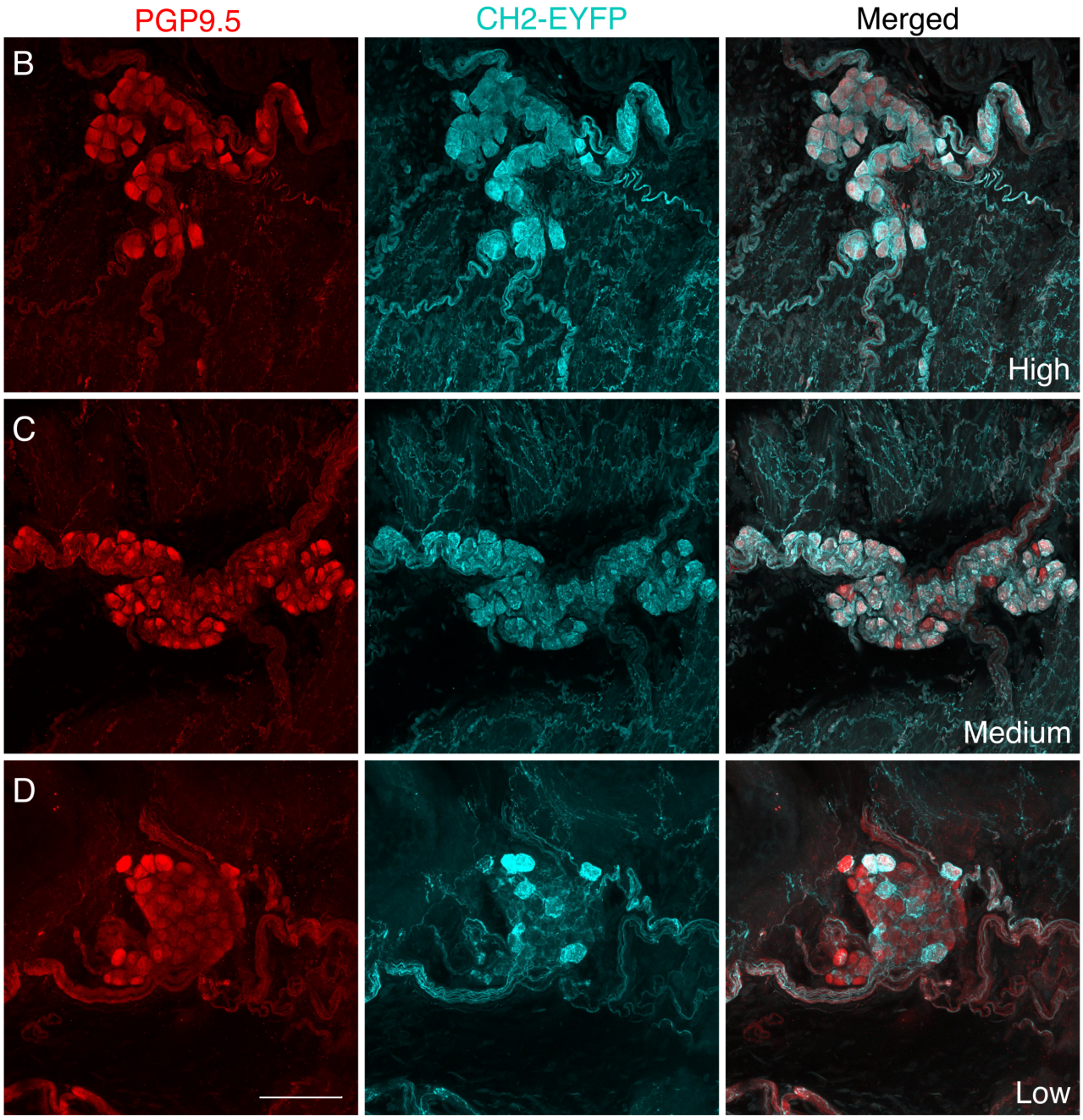

Figure 3.8. Light-induced bronchoconstriction is proportional to airway CH2 expression. Parasympathetic ganglia from mice expressing CH2 in 96% (A), 84% (B), and 16% (C) of postganglionic parasympathetic airway neurons. Scale bar: 50 mm. Tracheas labeled with antibody against PGP9.5 and GFP. Images taken using laser-scanning confocal microscopy, showing maximum intensity orthogonal projections.

Table 3.2. High variability in CH2 expression is found between breeding pairs (all pairs female CHAT-Cre mated to male CH2-EYFP) and within litters.

	% Neurons expressing CH2	
Breeding Pair 1	**Per Mouse**	**Average**
Litter 1	30	20.3
	21	
	10	
Litter 2	10	57.4
	57	
	89	
	38	
	93	
	Average:	43.5
Breeding Pair 2		
Litter 1	85	64.5
	44	
	Overall Average:	47.7%

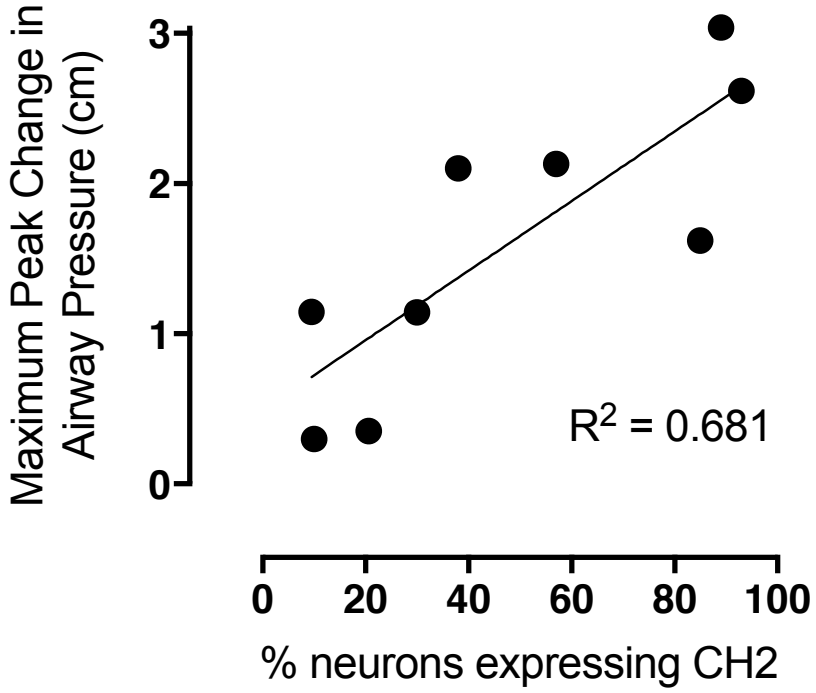

Figure 3.9. Linear relationship between the percentage of CH2 expression in airway postganglionic parasympathetic neurons and the maximum increase in airway peak pressure with 30 seconds of light in the presence of physostigmine (P = 0.0062).

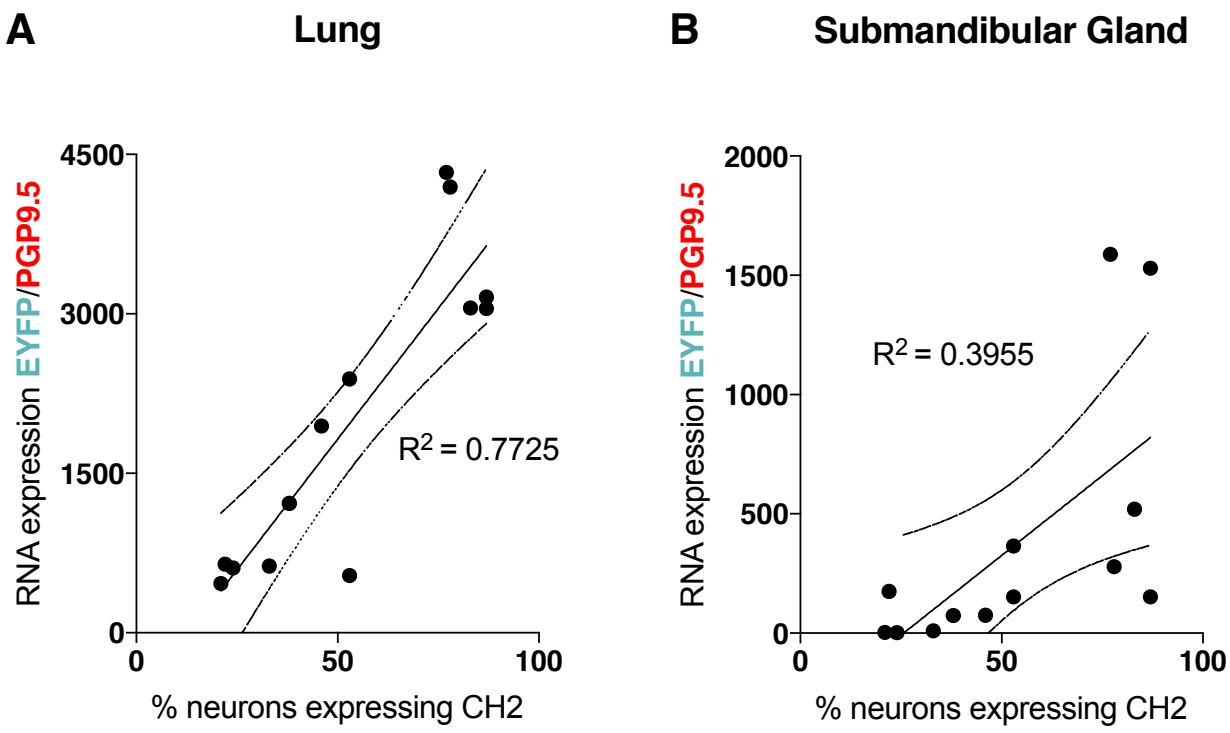

Figure 3.10. (A) PCR analysis of mRNA expression in lung homogenates represents an alternative method of assessing CH2 expression that is proportional to imaging (P , 0.0001, dashed lines represent 95% confidence interval). (B) PCR of EYFP/PGP9.5 does not correlate to lung CH2 expression in submandibular gland biopsy. RNA was extracted from lung homogenates as well as submandibular gland homogenates, and the ratio of EYFP to PGP9.5 expression was compared to imaging data of CH2-EYFP expression in the mouse trachea. The abundance of other nerve types in the submandibular gland likely led to the lower overall ratios in this tissue type, and prevents it from being used as a non-lethal quantification of airway neuronal CH2 expression in the mice.

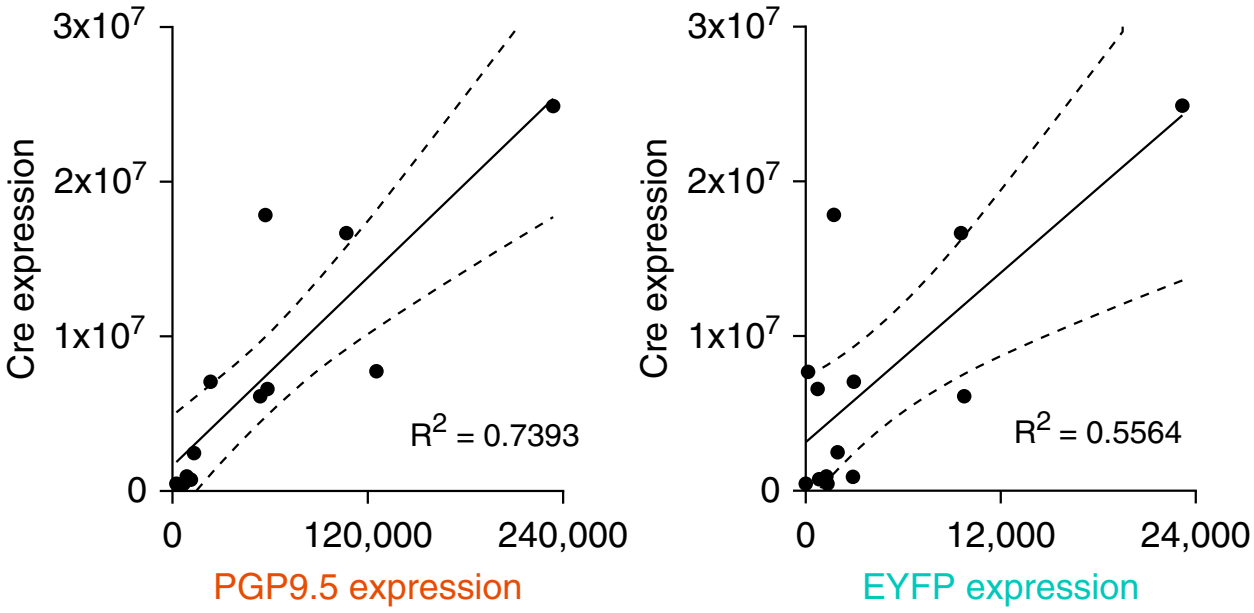

Figure 3.11. PCR analysis of Cre expression in lung homogenates shows a closer relationship to PGP9.5 expression than EYFP expression, indicating that variability in the efficiency of Cre protein rather than variability in expression may be more responsible for CH2 variability overall.

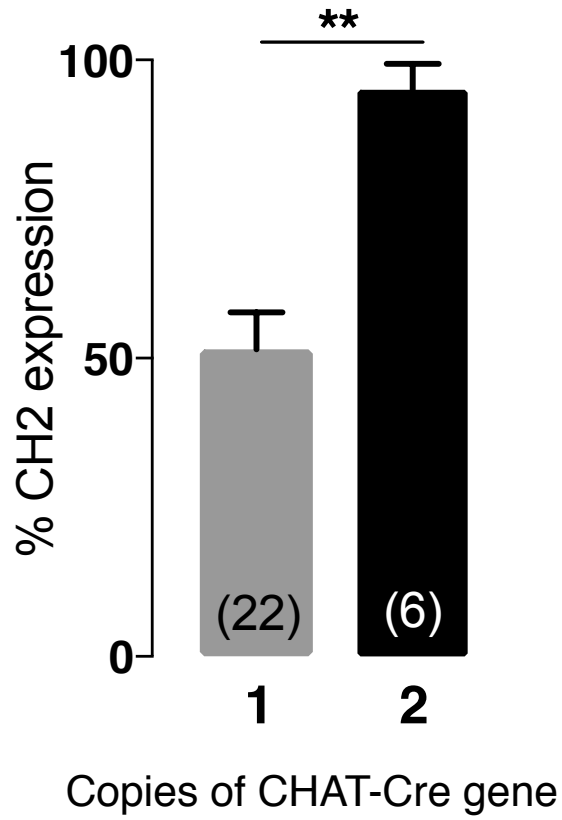

Figure 3.12. Mice with two copies of Cre driven by the choline acetyltransferase (CHAT) promoter had higher CH2 expression in the airways (sample size in parentheses; t test, **P = 0.0006). Columns show mean ± SEM.

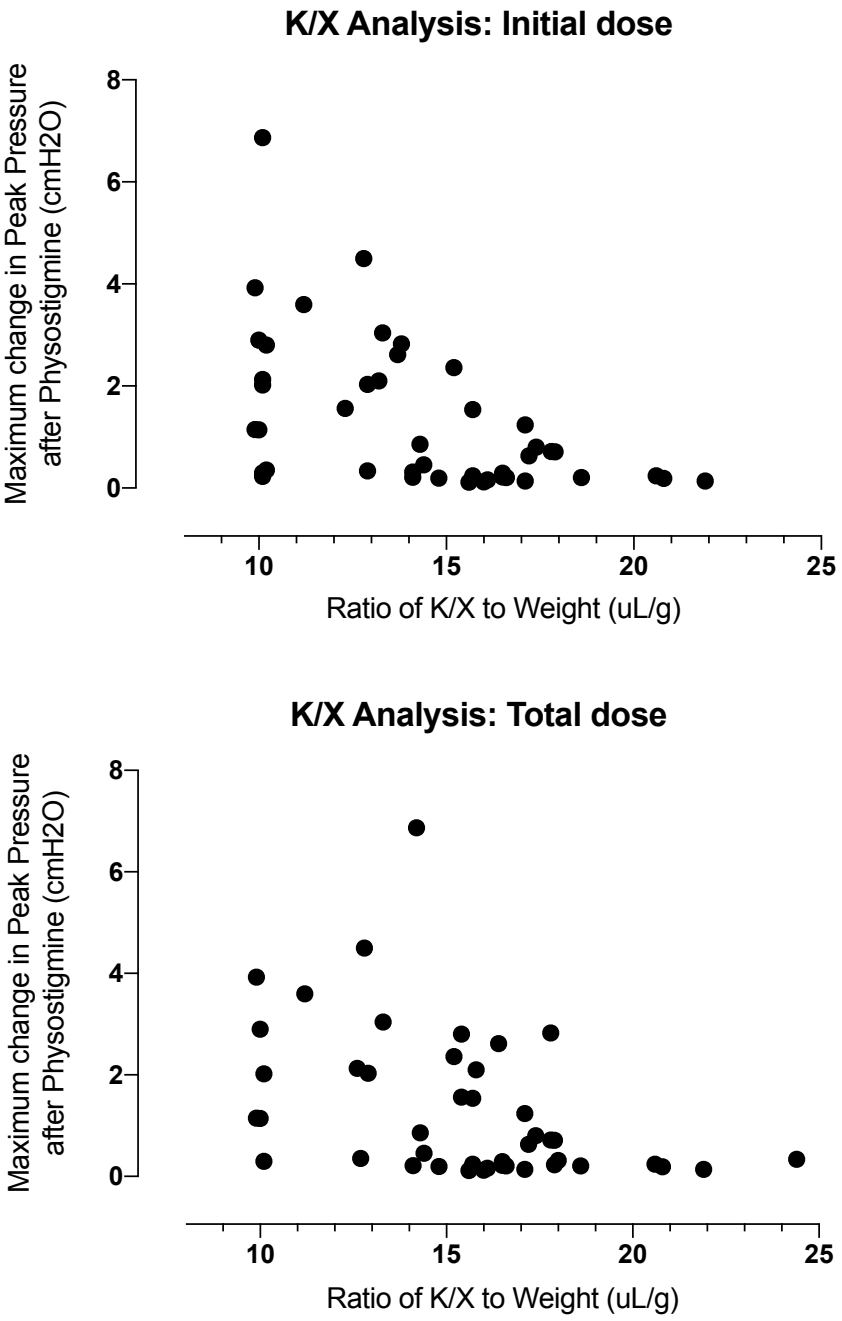

Figure 3.13. Increasing dosage of ketamine/xylazine anesthesia decreases peak airway pressure response to light activation. Ketamine/xylazine was given at variable doses as determined by ratio of anesthetic (μL) to mouse weight (grams). The maximum bronchoconstriction response to light activation of parasympathetic nerves decreased as anesthesia dosage increased. Some mice received a bolus of anesthesia after the initial dose - both initial and total doses are graphed.

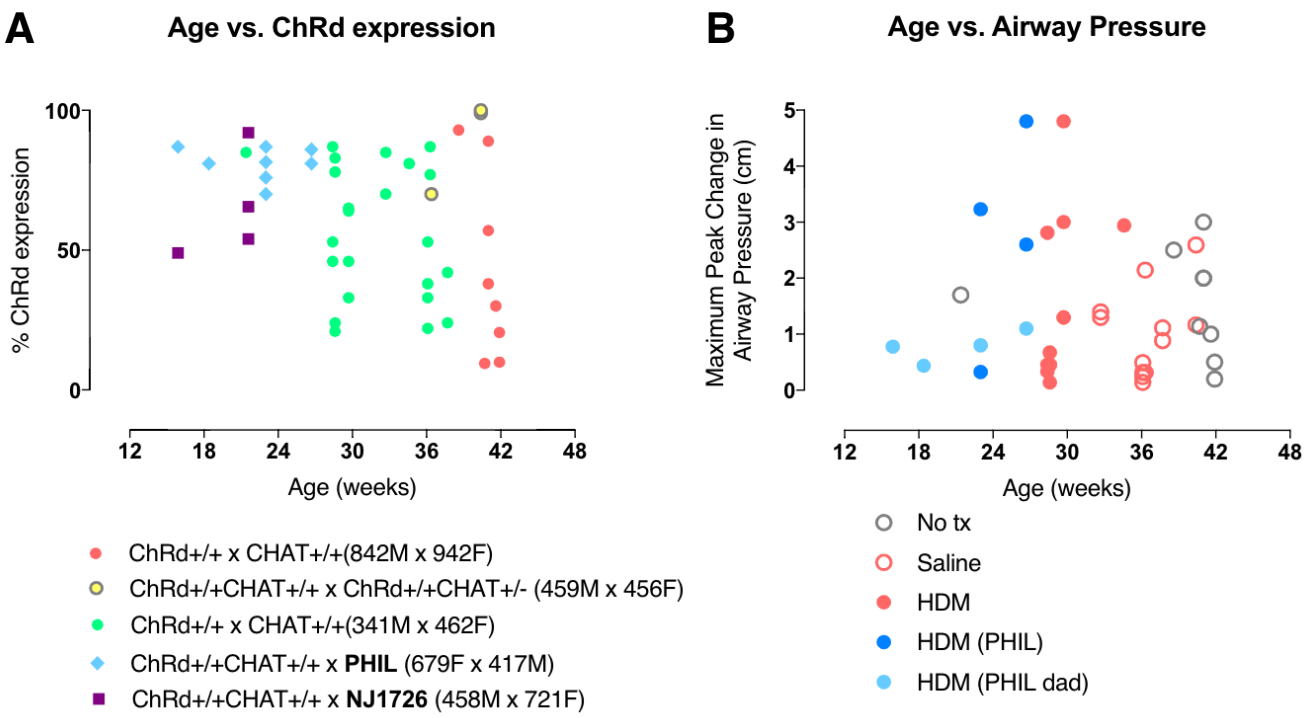

Figure 3.14. Effect of mouse age and parental lineage on channelrhodopsin expression and maximum change in peak airway pressure. (A) Channelrhodopsin expression in heterozygous (ChRd+/-CHAT+/-) mice from different parental breeding pairs was graphed as a function of age. Although greater variability was seen in the older age groups, this could not be distinguished from the parental lineage, and mice with high channelrhodopsin expression were seen at all ages. (B) Maximum peak change in airway pressure was graphed as a function of age, treatment, and genetic lineage. No obvious correlation was noted between mouse age and parasympathetic nerve mediated airway pressure changes. PHIL = eosinophil deficient mice. NJ1726 = IL-5tg mice. HDM = house dust mite treatment. Numbers next to lineage refer to parental mouse ear tags.

Discussion

Here, I show that it is possible to express CH2 in airway nerves and use these channels to specifically stimulate a single nerve population, in this case parasympathetic nerves, which are anatomically tangled with sensory nerves within the vagus. The method presented in this article is a novel and readily accessible technique for studying the function of airway neurons. Light activation of airway nerves may be achieved through the use of an intense, collimated LED light source after surgical exposure of the trachea. Furthermore, functional effects of that nerve activation can be measured using basic mouse ventilator parameters. Pharmacological enhancement, such as the administration of physostigmine, may be necessary to see the full effects of nerve activation. Expression of endogenous opsins that cause muscle relaxation in response to 430-nm light has been previously demonstrated in airway smooth muscle (Yim *et al.*, 2019). I did not observe bronchodilation in response to 454-nm light in these experiments, likely because our light source was focused on the trachea, and primarily activated the light-sensitive channels in airway nerves to cause peripheral airway smooth muscle contraction.

Although variability in the effectiveness of Cre within cells is a well-reported phenomenon, I had not anticipated that variability of CH2 expression in CHAT-positive neurons would impact physiological measurements. Many mechanisms may underlie expression variability in Cre-lox systems (Turlo *et al.*, 2010). The likeliest explanation in our system, given that the expression of Cre mRNA was proportional to pan neuronal marker PGP9.5 mRNA in lung tissue, is that Cre was being produced in cells, but was unable to efficiently cut the lox sites. Given that variable expression had physiological impact, it will be important to assess expression in animals before using this or any other technique that requires a new Cre-lox mouse line. This will be extremely important to assess in model systems of disease, where changes in transcriptional regulation may affect expression in experimental animals differently than controls. Our finding, that homozygosity for Cre produced higher and less variable expression of CH2, suggests that homozygous mice should be preferentially used in future experiments. If heterozygous mice are used, results from these mice must always be interpreted in the context of expression level, and treatment groups should be large enough to account for a wide range of natural variability. PCR analysis of EYFP/PGP9.5 expression in lungs may be performed to eliminate mice with the lowest expression from analysis.

Studies of airway nerve physiology have described many distinct subpopulations of airway neurons (Tränkner *et al.*, 2014, Chang *et al.*, 2015), the functions of which are difficult to study using traditional nerve activation techniques. A subset of sensory neurons that produce the neuropeptide substance P has long been implicated in asthma pathophysiology (Ollerenshaw *et al.*, 1991, Drake *et al.*, 2018), and neurons with receptors for P2X3 have more recently been linked to chronic cough (Abdulqawi *et al.*, 2015, Morice *et al.*, 2019). For many of these nerves, mouse lines are already

available in which Cre is expressed under the relevant promoter, which means research using our method could advance rapidly. Although our study used only one light-activated protein channel, CH2, it is possible to use multiple channels responding to different wavelengths of light within the same mouse (Zhang *et al.*, 2008). Inhibition of nerves through light-activated chloride channels (such as halorhodopsin) (Zhang *et al.*, 2007) is a variation of this technique that may prove useful. It is also worth noting that robust heart rate decreases were seen in addition to airway pressure increases in response to light. Indeed, the heart rate responses were more sensitive than changes in airway pressure, with no physostigmine necessary to elicit a measurable decrease. Parasympathetic nerves are important regulators of physiologic function for many organs, including the highly complex gastrointestinal system, and continuing to develop techniques to study parasympathetic nerves will advance our ability to interrogate these other systems and increase our understanding of disease beyond the airways.

Work from our laboratory and others has consistently demonstrated changes in nerve architecture (Drake *et al.*, 2018), neurotransmitter expression (de Vries *et al.*, 2006) and excitability (Lötvall *et al.*, 1998) in humans with asthma and in animal models of airway disease. The relevance of these morphological and molecular changes to airway function *in vivo* has been difficult to assess, as traditional methods, such as vagal nerve stimulation, can nonspecifically activate many different nerve fibers within a nerve bundle. Although this technique of nerve activation would be challenging to apply directly to humans for therapeutic purposes, results from studying the activation of specific nerve subtypes in animal models will give us more precise knowledge of the function of these nerves, and may reveal targets for future pharmacological treatments. I hope this method will prove useful for elucidating the relevant nerve contributions to airway hyperreactivity in many animal models of asthma and airway hyperreactivity, including allergen challenge, viral infection, ozone exposure, organophosphate exposure, and obesity (Fryer and Jacoby, 1991, Fryer and Wills-Karp, 1991, Adamko *et al.*, 1999, Fryer *et al.*, 2004, Verhein *et al.*, 2013, Nie *et al.*, 2014).

Chapter 4. Sensory and parasympathetic contributions to airway hyperreactivity in eosinophilic asthma

Abstract

Airway hyperreactivity in asthma is mediated by airway nerves, including sensory nerves in the airway epithelium and parasympathetic nerves innervating airway smooth muscle. In the past it has been difficult to study these nerve populations separately *in vivo*, and thus difficult to distinguish how each is affected by inflammatory processes and contributes to hyperreactivity in asthma. In this study I use optogenetic activation of airway nerves *in vivo* to study sensory and parasympathetic contributions to airway hyperreactivity in two mouse models of asthma. I use both an acute allergen challenge model and a chronic airway hypereosinophilia model to explore the disparate effects of acute inflammatory responses and long term eosinophilia on sensory and parasympathetic nerve sensitization. Using whole mount tissue immunofluorescence, I examine in three dimensions the interactions between eosinophils and parasympathetic nerves in our asthma mouse models, and underscore the key role these interactions play in mediating nerve sensitivity. As a whole, this study demonstrates divergent effects of acute airway inflammation compared to chronic eosinophilia on airway nerve sensitization, and points to eosinophil-nerve interactions as a key regulator of airway hyperreactivity.

Introduction

Asthma is a disease of the airways characterized by inflammation, increased mucus production, airway smooth muscle hypertrophy, and airway hyperreactivity. Airway hyperreactivity is defined as increased bronchoconstriction in response to inhaled irritants, and is mediated by airway nerves (Hargreave *et al.*, 1986). Sensory nerves endings detect chemical and mechanical stimuli in the airway and send activation signals to neurons in the brainstem. These activation signals are passed along to airway parasympathetic nerves, which release acetylcholine onto muscarinic receptors on smooth muscle and cause contraction. This pathway is known as reflex bronchoconstriction (McCaig, 1987, Costello *et al.*, 1999, McAlexander *et al.*, 2015). Asthma therapies that block this nerve-mediated bronchoconstriction, such as muscarinic antagonists, improve symptoms and lung function in asthma (Peters *et al.*, 2010, Kerstjens *et al.*, 2012). Despite the importance of this pathway to asthma pathology, much about the underlying changes to airway nerves remains to be understood.

The most common phenotype of asthma, the type 2 high phenotype, is characterized by an abundance of eosinophils in the airways (Lötvall *et al.*, 2011). Previous studies in humans and guinea pigs have shown that eosinophils cluster around airway parasympathetic nerves and decrease the function of inhibitory M2 muscarinic receptors on the nerves, which increases acetylcholine release and reflex bronchoconstriction (Fryer and Wills-Karp, 1991, Costello *et al.*, 1997). Studies have also shown that eosinophils increase sensory nerve length and branching in airways of patients with severe eosinophilic asthma (Drake *et al.*, 2018), which may also contribute to hyperactivity. It is not known whether eosinophils lead to parasympathetic hyperreactivity in mice, or whether the increases in sensory innervation observed in humans correspond to functional increases in sensory nerve responsiveness.

A variety of risk factors lead patients to develop asthma, including in utero exposures (Liu *et al.*, 2018, Morten *et al.*, 2018), genetic susceptibility, and environmental exposures (Wenzel, 2012, Beasley *et al.*, 2015). Two commonly studied mouse models of airway hyperreactivity capture these different exposures: antigen sensitization and challenge models, in which airway hyperreactivity develops as a result of acute environmental exposures, and interleukin 5 transgenic (IL-5tg) mouse models, in which airway hyperreactivity develops as a result of in utero and chronic overexpression of IL-5 recruiting eosinophils to the airways. Both of these mouse models display histological changes consistent with asthma, including goblet cell hyperplasia and airway eosinophilia, but previous research from our laboratory has shown differences between sensory nerve length and branching in the models, which is increased in IL-5tg mice but remains unchanged after acute antigen exposure. This suggests potential differences in sensory and parasympathetic nerve pathology underlying airway hyperreactivity in these systems.

In the past, it has been challenging to specifically study sensory or parasympathetic nerve function *in vivo*. Methods developed by our lab to optogenetically activate airway nerves have overcome these

challenges (Chapter 3). I used optogenetics, or light activation of neurons, to specifically activate parasympathetic nerves in ventilated mice and measure increases in bronchoconstriction. In this study, I again use optogenetics to activate airway parasympathetic nerves, and compare the bronchoconstriction response in untreated mice, IL-5tg mice, mice sensitized and challenged with the antigen house dust mite (HDM), and control mice exposed to saline. I further develop this method to allow activation of sensory airway nerves, and again compare the bronchoconstriction response in our models (Figure 4.1). I show differences in parasympathetic hyperreactivity in antigen-challenged compared to IL-5tg mice despite similarities in airway hyperreactivity to inhaled agonists. These results suggest different eosinophil-dependent airway nerve remodeling pathways mediate airway hyperreactivity in chronic inflammatory states compared to acute antigen exposure.

I also use tissue clearing and immunostaining followed by quantitative three dimensional image analysis to measure the interactions of eosinophils with parasympathetic nerves in our two models. Previous studies into eosinophil-nerve interactions have relied on thin tissue sections that do not capture the complex architecture of airway nerve networks. I have overcome these limitations by using confocal laser scanning microscopy to image eosinophils and nerves in whole mouse tracheas that have been passively cleared in solution. Using Imaris software, I quantify the location of airway eosinophils in relation to parasympathetic nerves within ganglia and airway smooth muscle, and find increased proximity of eosinophils to nerves in the smooth muscle layer of house dust mite treated mice compared to controls.

Overall, these studies reveal differences in airway nerve remodeling underlying airway hyperreactivity mediated by eosinophils. This underscores the complex pathology of airway disease and the need for greater understanding of eosinophil-nerve interactions to treat eosinophilic asthma.

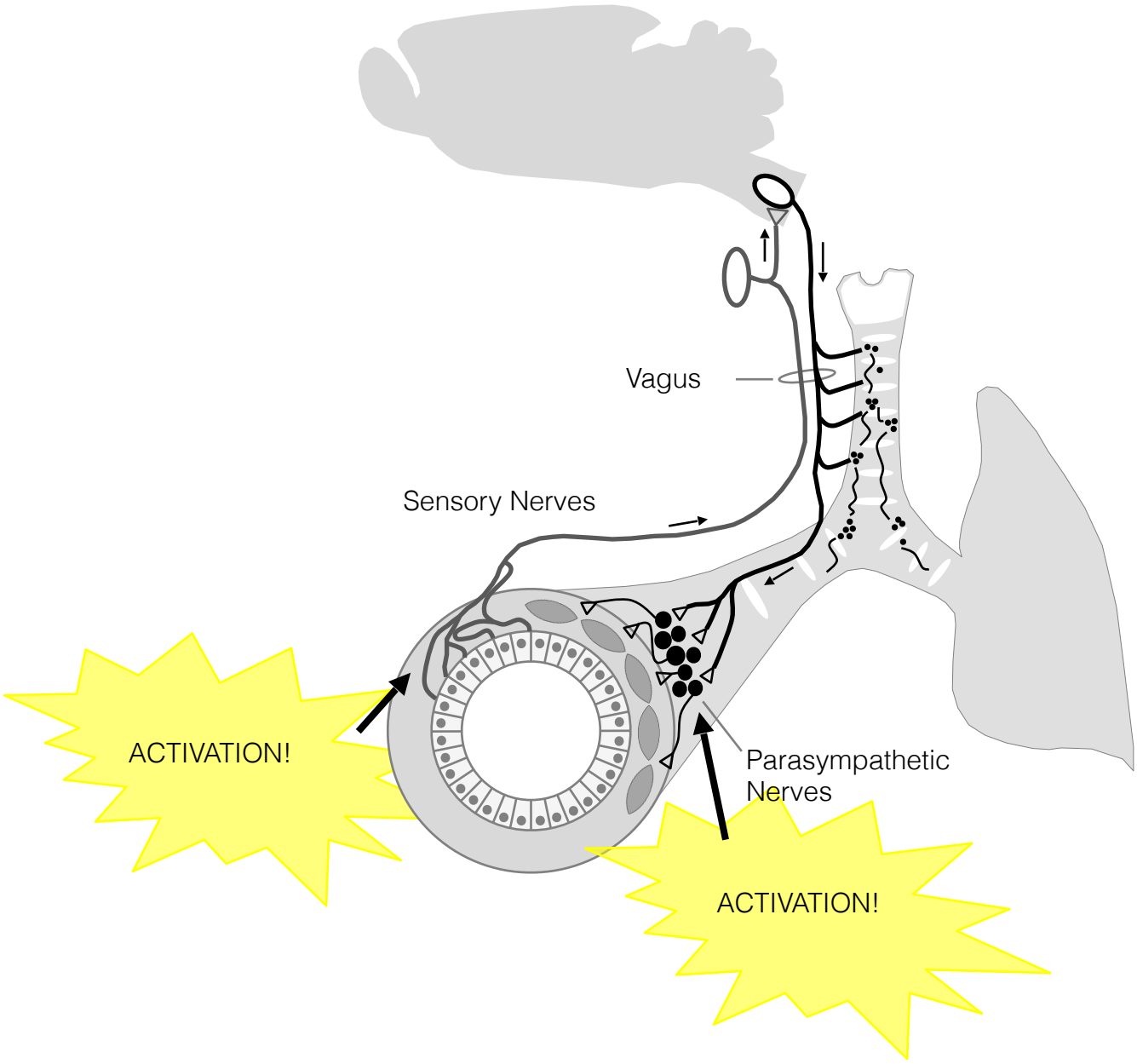

Figure 4.1. Diagram illustrating primary study question. In this study we use light activation of sensory and parasympathetic neurons in mouse models of asthma to examine underlying differences in nerve-mediated airway hyperreactivity.

Experimental Design

Animals

All animal procedures complied with Oregon Health & Science University's Institutional Animal Care and Use Committee guidelines. For optogenetic activation of parasympathetic nerves in the acute asthma model: transgenic mice expressing a floxed stop codon before channelrhodopsin 2 (CH2) fused to enhanced yellow fluorescent protein (EYFP; CH2–EYFP mice, #024109; Jackson Laboratory) and mice expressing Cre recombinase driven by the choline acetyltransferase (CHAT) promoter (CHAT-Cre mice, #028861; Jackson Laboratory) were bred to create mice with CH2 expressed in cholinergic neurons (CHAT-CH2 mice). Heterozygous mice were crossed with one another to form a homozygous CHAT-CH2 line. For optogenetic activation of sensory nerves in the acute asthma model: CH2 mice were crossed with mice expressing Cre recombinase driven by the advillin promoter and dependent on tamoxifen activation (Advillin-iCre mice, #032027; Jackson Laboratory) to create mice with CH2 expressed in sensory neurons (Advillin-CH2 mice). Heterozygous mice were crossed with one another to form a homozygous Advillin-CH2 line.

For optogenetic activation of parasympathetic and sensory nerves in chronic model: homozygous CHAT-CH2 and Advillin-CH2 mice were crossed with an IL-5 transgenic line (IL-5tg; gift of James and Nancy Lee; Lee et al., 1997) expressing IL-5 driven by the CC10 promoter, which is specific to airway epithelium. IL-5tg offspring of this cross had lung-specific expression of IL-5, upregulation of eosinophil production, and increased recruitment of eosinophils to airways, in addition to light-activatable airway nerves.

For studies of eosinophil-nerve interactions, mice expressing Cre recombinase driven by the endogenous eosinophil peroxidase promoter (eoCre mice; gift of James and Nancy Lee; Doyle et al., 2013) were crossed with a mouse line in which GFP follows a floxed stop codon, leading to GFP expression specifically in eosinophils. These mice were also crossed with the IL-5tg line. All mice were on a C57BL/6 background. Male and female mice 12 weeks of age and older were used for experiments.

House Dust Mite (HDM) sensitization and challenge

For the acute allergen sensitization and challenge model, mice were anesthetized with 5% isofluorane and given intranasal doses of house dust mite (HDM; Greer Laboratories). Sensitization: 50 μg in 25 μl PBS (Days 0, 1). Challenge: 25 μg in 25 μl PBS (Days 14, 15, 16, 17). Control animals were given intranasal saline. Airway physiology measurements were taken one day after final challenge (Day 18) (Figure 2.3). Lung lavage was collected by flushing three times with 0.5mL PBS. Collected cells were counted by hemocytometry and spun onto slides. Wright stain was used to differentiate white blood

cells for quantification. Airway inflammation and eosinophilia were evaluated by analyzing the total count and differential of white blood cells in lung lavage.

Ventilation and Physiological Measurements

Mice were anesthetized with ketamine (100 mg/kg i.p.) and xylazine (10 mg/kg i.p.), tracheotomized, and ventilated as previously described (Brown *et al.*, 1999). A 21-gauge catheter was inserted into the cricothyroid membrane to the level of the second cartilage ring. Mice were mechanically ventilated with 100% oxygen at 120 breaths/min with a tidal volume of 150 μl and a positive end-expiratory pressure of 2 cm H_2O. Mice were paralyzed with succinylcholine (0.05 mg in 0.05 ml i.p.) to eliminate respiratory effort. Body temperature was maintained at 37°C with a heat lamp, homeothermic blanket, and rectal probe. Heart rate and rhythm were measured by electrocardiogram recorded with three needle electrodes placed subcutaneously on the right hindpaw, left forepaw, and left shoulder. Airway pressure, heart rate, respiratory rate, tidal volume, body temperature, and flow were all measured using LabChart Pro acquisition software (ADInstruments). Airway peak pressures were measured 60 s after administering aerosolized PBS (baseline) and each increasing dose of serotonin (5HT; 10 μL at 10, 30, and 100 mM).

Optogenetic Activation of Nerves *In Vivo*

Optogenetic activation of airway parasympathetic nerves was performed as previously described (Chapter 3; Pincus et al., 2020). Briefly: while ventilated the mouse trachea was surgically exposed by retracting soft tissue and muscle and removing a section of proximal sternum. Damp gauze protected the tissue against desiccation between light stimulations. Light was delivered to the trachea via a high-power 454-nm light-emitting diode (LED) light source (Prizmatix) coupled to an optic fiber with a 500-μm core diameter attached to a collimator (numerical aperture = 0.63), creating a 1-cm circle of light with 8.9-mW/mm2 intensity. The light was positioned ventral to the exposed trachea, centered midway between the larynx and carina. Light activation, frequency, pulse width, and pulse number were controlled by a Master-8 system pulse stimulator (A.M.P.I.). Parasympathetic nerves were activated with 20Hz light with a pulse width of 5ms for 30seconds, while sensory nerves were activated with 50Hz light for the same time period (Figure 4.2). For optogenetic activation of sensory nerves, indomethacin (2mg/kg i.p.) and L-NAME (30mg/kg i.p.) were administered 30 minutes before light stimulation to inhibit the production of prostaglandins and nitric oxide by bronchodilatory nerves, guanethidine (5mg/kg i.p.) was administered 20 minutes before to prevent release of guanethidine by sympathetic nerves, and physostigmine (0.5mg/kg i.p.) was administered 15 minutes before to block acetylcholinesterase activity and enhance reflex bronchoconstriction. All mice were given the muscarinic antagonist atropine (3 mg/kg i.p.) 5 minutes prior to final light activation to block muscarinic receptors and to verify that any measured bronchoconstriction effects were due to acetylcholine release.

Tissue Optical Clearing and Imaging of Airway Nerves

Mice were perfused with PBS and airways were excised and left at 4°C in Zamboni fixative (Newcomer Supply) overnight. Tracheas were blocked overnight with 4% normal goat serum, 1% Triton X-100, and 5% powdered milk, and then incubated overnight with antibodies to EGFP (anti-GFP chicken IgY, 1:500; Invitrogen) and protein gene product 9.5 (PGP9.5, rabbit IgG, 1:500; Millipore) on a shaker at 4°C. Tissues were washed and incubated overnight in secondary antibodies (Alexa goat anti-rabbit 647, 1:1,000; Invitrogen; Alexa goat anti-chicken 488, 1:1,000; Invitrogen) before optical clearing for 12 hours in N-methylacetamide/Histodenz (Ce3D) (Li et al., 2017). Tracheas were mounted in Ce3D on slides in silicon imaging wells and imaged using an LSM 900 confocal microscope. Samples were illuminated with 488 nm and 640 nm light, and 20x images were acquired as 30μm z-stacks and converted to maximum intensity projections. Five consecutive tiles with 10% overlap were taken of the smooth muscle layer of trachealis, as well as five individual tiles of ganglia, identified using the PGP9.5 channel without viewing EGFP.

Quantitative Analysis of Eosinophil-Nerve Interactions

Z-stack images of airway nerves and eosinophils were analyzed using Imaris software (version 9.6.0). Surfaces were created covering PGP9.5 positive voxels for nerves and EGFP positive voxels for eosinophils. Investigators were blinded to treatment group during image analysis. Smoothing was set at 2x pixel size, background subtraction was enabled with maximum object size of 30μm for PGP9.5 and 8μm for EGFP, split touching objects enabled with seed point diameter of 5μm for PGP9.5 surface and 7μm for EGFP surface. The quality filter was used to eliminate spots of fluorescence that were unlikely to represent eosinophils, due to shape or size. Data on the number of eosinophil surfaces, distance between eosinophil and nerve surfaces, and number of eosinophils touching nerves (shortest distance between eosinophil and nerve surface = 0 μm) were recorded for analysis.

Statistical Analysis

Two tailed unpaired t-tests were used to compare two groups for analysis, as in light response and white blood cell counts. Two-way ANOVA with Sidak's multiple comparisons test was used to compare serotonin dose response curves. Kolmogorov-Smirnov test was used to compare cumulative frequency distributions of eosinophils around airway nerves. Data presented in text as mean ± SD. P values <0.05 were considered significant.

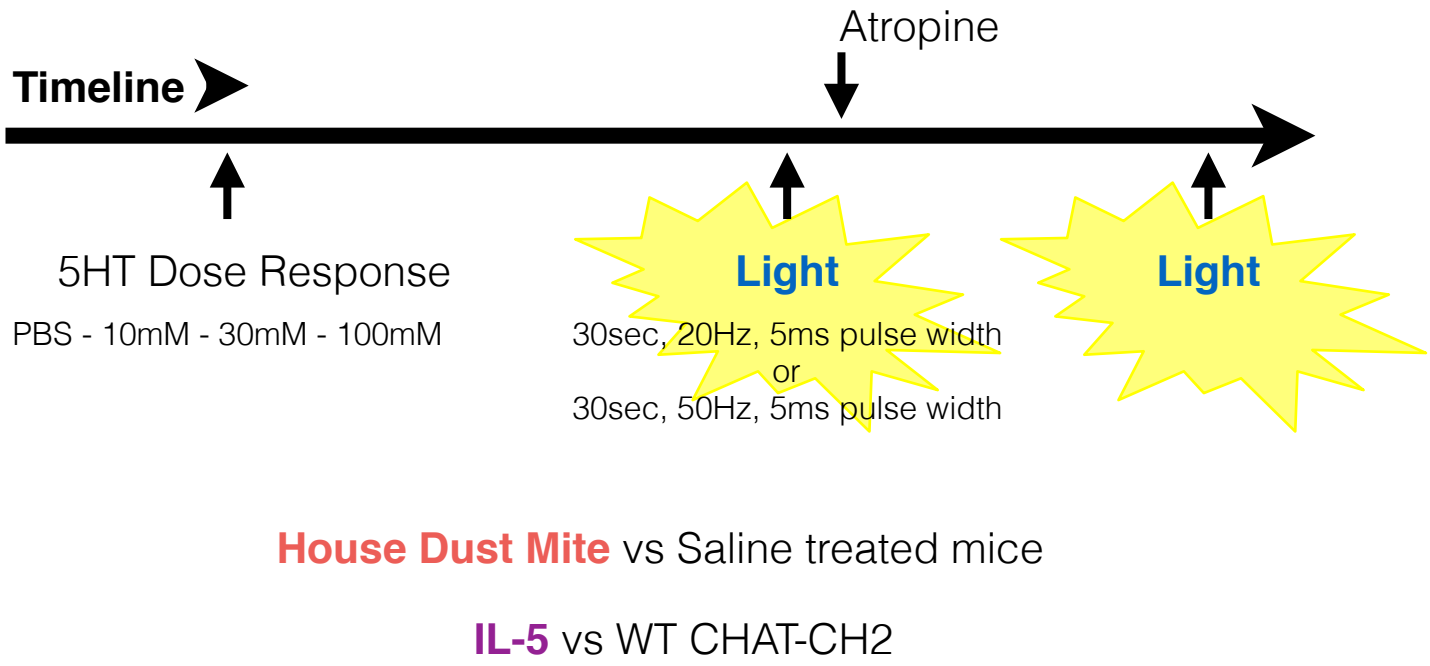

Figure 4.2. Timeline of optogeneticics experiments. Airway hyperreactivity is tested by serotonin (5HT) dose response curve, then by light activation of either parasympathetic (20Hz) or sensory (50Hz) nerves. Atropine blocks muscarinic receptors, so there should be no airway pressure response to light after administration of atropine.

Results

Airway Hyperreactivity in House Dust Mite Challenged and IL5tg Mice

CHAT-CH2 mice were treated with acute house dust mite (HDM) exposure or saline exposure control. CHAT-CH2-IL-5tg (IL-5tg) mice and a control group of CHAT-CH2 (WT) mice were untreated. HDM exposed mice had increased airway white blood cells (t test HDM vs. Saline ***$p<0.001$) and a higher percentage of eosinophils (***$p<0.001$) than saline controls (Figure 4.3), and IL5-tg mice had a higher percentage of eosinophils than controls (*$p<0.05$). Mice were anesthetized and ventilated, and airway pressure response to increasing doses of inhaled aerosolized serotonin was measured. HDM treated mice had greater hyperreactivity to serotonin than saline controls (two-way ANOVA main effect of treatment **$p<0.01$; Figure 4.4A), and IL-5tg mice had greater hyperreactivity to serotonin than untreated WT mice (Figure 4.4B; two-way ANOVA main effect of treatment *$p<0.05$).

Parasympathetic Hyperreactivity in House Dust Mite Challenged but not IL5tg Mice

Parasympathetic nerves were activated in all mouse groups using 454nm LED light at 20Hz for 30 seconds. Airway response was measured as change in peak pressure during the period of light compared to peak pressures prior to light. HDM treated animals had greater responses to parasympathetic nerve activation than saline treated animals, indicating parasympathetic hyperreactivity in these animals (HDM 1.665±1.17 cm H_2O, Saline 0.101±0.076 cm H_2O, **$p<0.01$). In contrast, IL-5tg mice did not have a greater response than untreated WT mice (IL-5tg 0.252±0.376 cm H_2O, WT 0.493±0.282 cm H_2O, $p=0.09$; Figure 4.4C). Atropine eliminated the airway response to light in all groups (mean HDM 0.088, saline 0.025, IL-5tg 0.026, WT 0.063 cm H_2O; Figure 4.4D), confirming that airway pressure changes were due to acetylcholine release onto airway smooth muscle. Since previous studies have shown expression of channelrhodopsin to be variable in parasympathetic nerves of CHAT-Cre mice, PCR studies were performed to confirm similar ranges of channelrhodopsin expression between experimental and control groups (Figure 4.5).

Sensory Hyperreactivity in House Dust Mite Challenged Mice

A new mouse line was created by breeding CH2-EYFP mice Advillin-iCre mice to express CH2 in sensory neurons (Advillin-CH2 mice). Expression of CH2 was confirmed through imaging of endogenous EYFP fluorescence in vagal ganglia (Figure 4.6). Since previous studies had reported leaky expression of the advillin promoter in autonomic nerves (Hunter *et al.*, 2018), tracheas from these mice were labeled with antibodies against EYFP and PGP9.5 and imaged. The number of parasympathetic nerves expressing CH2 was found to range from 4-23% (Figure 4.7). Vagotomy experiments in which the vagus nerves are cut bilaterally were performed in Advillin-CH2 mice to

differentiate the effects of direct parasympathetic activation from that of sensory activation leading to bronchoconstriction through the reflex pathway.

Advillin-CH2 mice were treated with acute HDM exposure or saline exposure control. As with CHAT-CH2 mice, HDM exposed animals had increased airway white blood cells (t test HDM vs. Saline *$p<0.05$) and a higher percentage of eosinophils (*$p<0.0001$) than saline controls (Figure 4.8). HDM animals also had greater hyperreactivity to serotonin than saline treated mice (***$p=0.001$; Figure 4.9A). Sensory nerves were activated in HDM and saline treated mice using 454nm LED light at 50Hz for 30 seconds after administration of guanethidine, indomethacin, L-NAME and physostigmine. HDM treated animals demonstrated greater bronchoconstriction in response to sensory nerve activation than saline treated mice, which was eliminated with atropine (*$p<0.05$; Figure 4.9B). Bronchoconstriction was also eliminated when mice underwent vagotomy prior to light stimulation, demonstrating that the light response is due to sensory and not parasympathetic nerve activation (Figure 4.10).

Eosinophil-Nerve Interactions in House Dust Mite Challenged and IL5tg Mice

To evaluate the potential role that eosinophil-nerve interactions play in sensory and parasympathetic nerve hyperreactivity, eoCre-GFP mice were treated with HDM and saline and crossed with IL-5tg mice. Tracheas from these mice were harvested, labeled with antibodies against GFP and PGP9.5, cleared using passive tissue clearing techniques and imaged using fluorescent confocal microscopy. 3D images were taken of airway smooth muscle and around airway parasympathetic ganglia, and Imaris software was used to create surfaces around the GFP (eosinophil) and PGP9.5 (nerve) fluorescence and analyze interactions (Figure 4.11). Preliminary results show differences between eosinophil-nerve interactions in HDM vs. saline treated mice around nerves in airway smooth muscle. HDM treated animals had a greater percentage of eosinophils touching nerves (HDM 49.75±6%, Saline 21.05±0.3%, **$p<0.01$). A cumulative frequency distribution revealed that eosinophils were also closer to nerve surfaces in the HDM treated group compared to controls (**$p<0.01$; Figure 4.12). This was not true for eosinophils around parasympathetic ganglia, where the cell bodies of these same nerves are located.

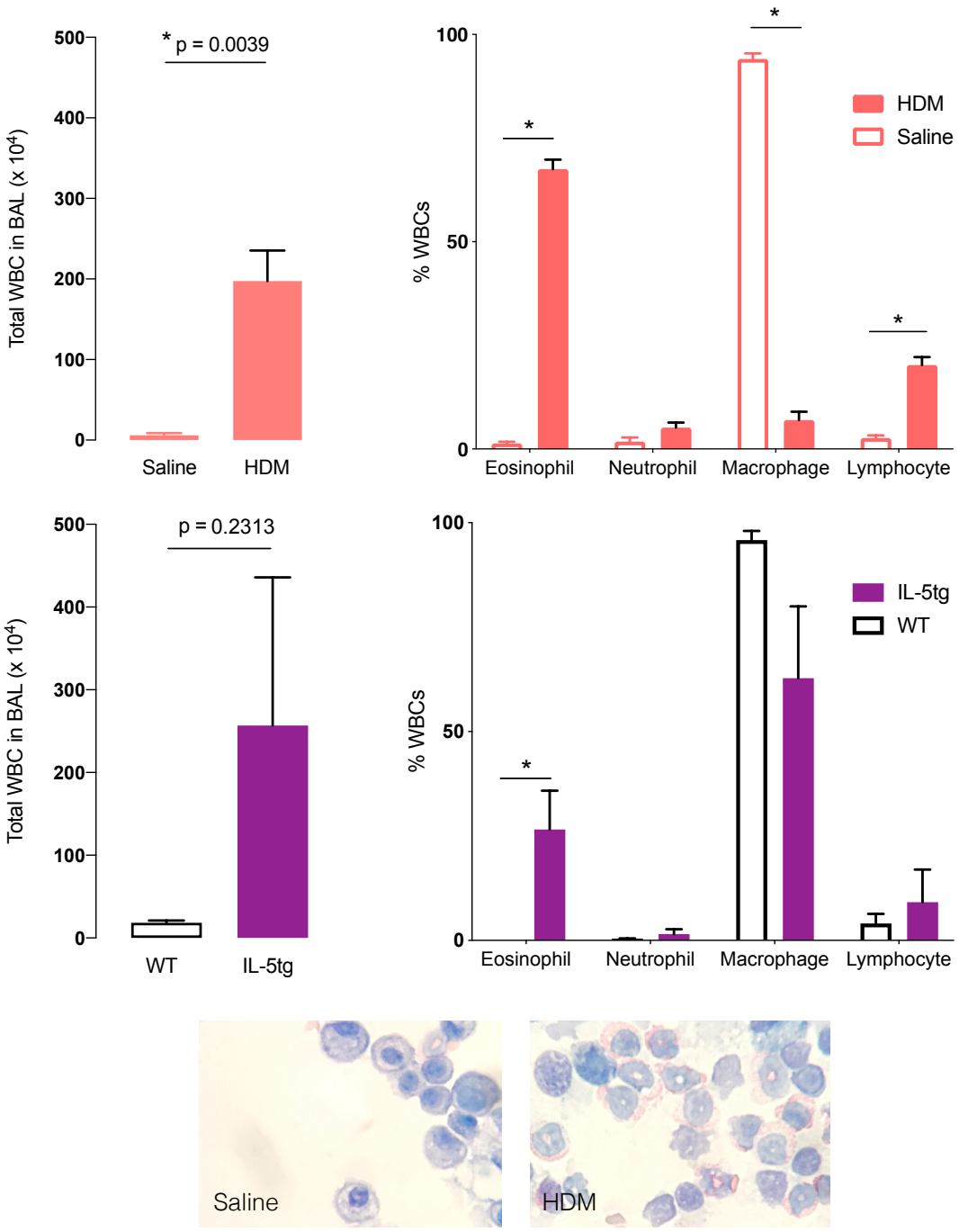

Figure 4.3. Immune response in house dust mite treated (HDM) and interleukin 5 transgenic mice (IL-5tg) compared to controls. Total white blood cell (WBC) count in HDM vs Saline and IL-5tg vs WT mice were analyzed by unpaired t test. WBC differential was analyzed using multiple t tests. *$p<0.05$. Columns show mean ± SEM. Representative images of a control and eosinophilic slide used for analyzing differentials is shown in the bottom panel.

Parasympathetic Activation

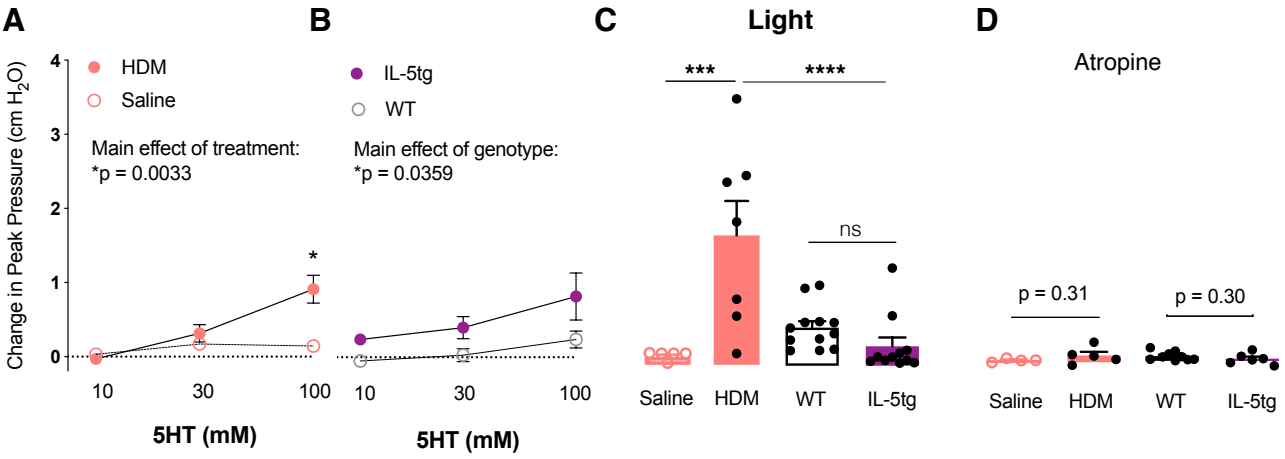

Figure 4.4. Parasympathetic Hyperreactivity in House Dust Mite Challenged but not IL5tg Mice. (A) HDM mice have greater hyperreactivity to serotonin (5HT) than saline controls (**p<0.01), and (B) IL-5tg mice had greater hyperreactivity to serotonin than untreated WT mice (*p<0.05). Data analyzed by two-way ANOVA with Sidak's multiple comparisons test. HDM vs saline mice different at 100mM 5HT dose, *p<0.05. (C) HDM mice have greater parasympathetic hyperreactivity than saline controls (***p=0.0002) or IL-5tg mice (****p<0.0001). IL-5tg mice are not statistically different than WT controls (p=0.74). (D) Atropine abolishes light response in all animals. Data analyzed by two-way ANOVA with Tukey's multiple comparisons test. Columns show mean ± SEM.

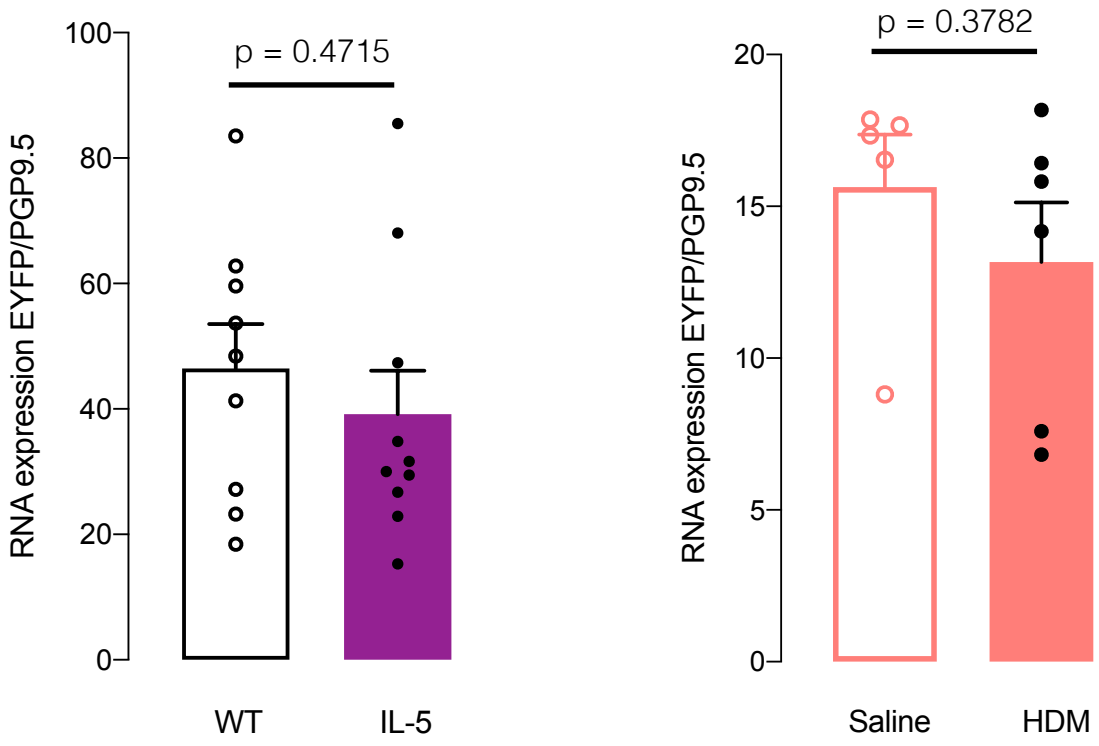

Figure 4.5. No difference between experimental and control groups in proportion of airway nerves expressing channelrhodopsin as measured by PCR. Previous studies (chapter 3) found a high degree of variation in the expression of channelrhodopsin when driven by the CHAT promoter. Measurements of channelrhodopsin (fused to EYFP protein) as a proportion of nerves (PGP9.5) in a lung tissue sample were validated using imaging studies. These data show no difference between HDM vs saline animals and IL-5tg vs WT animals. Data analyzed by two-tailed unpaired t test. Columns show mean ± SEM.

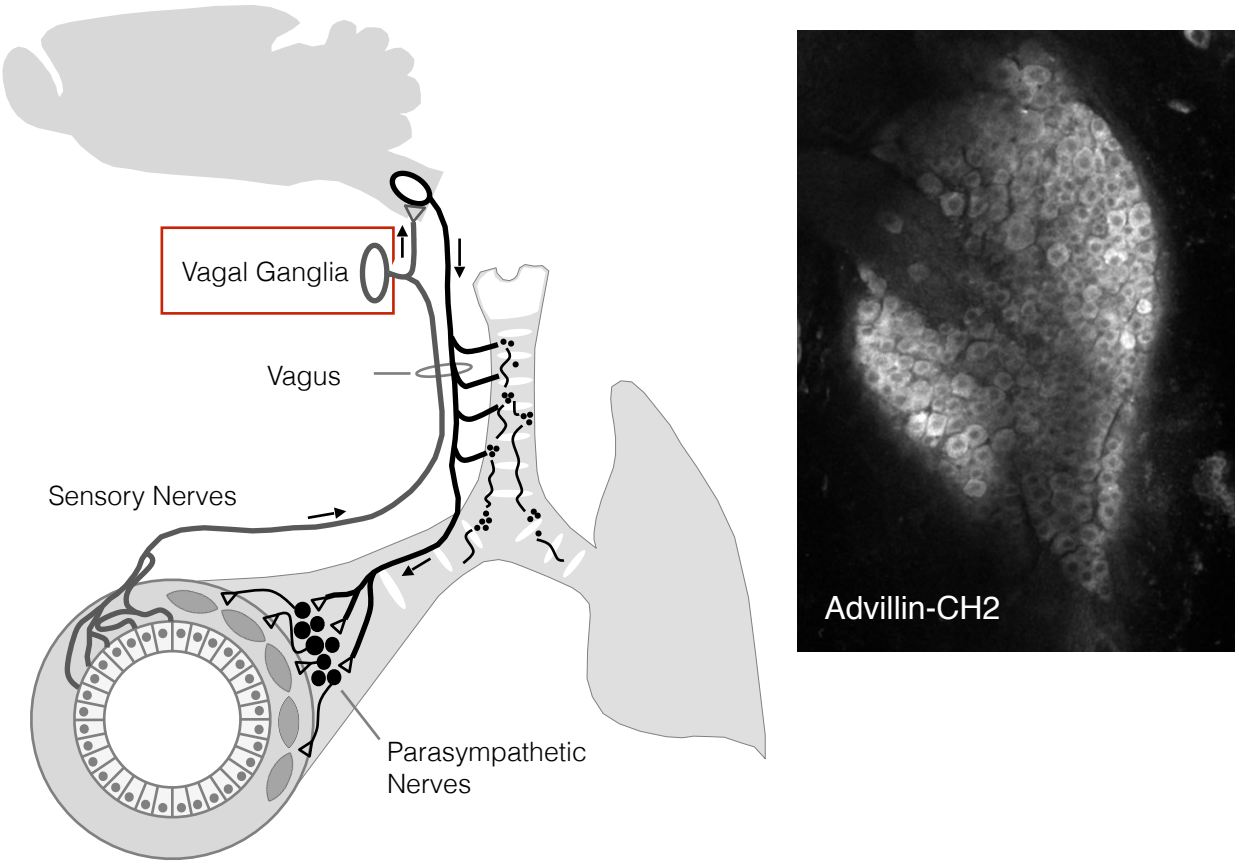

Figure 4.6. Imaging of channelrhodopsin expression in airway sensory neurons in the vagal ganglia. On the left the location of vagal ganglia is shown in a diagram, while on the right is shown an image of endogenous CH2-EYFP expression in sensory nerve cell bodies. The pattern of fluorescence is consistent with expression in all vagal ganglia neurons.

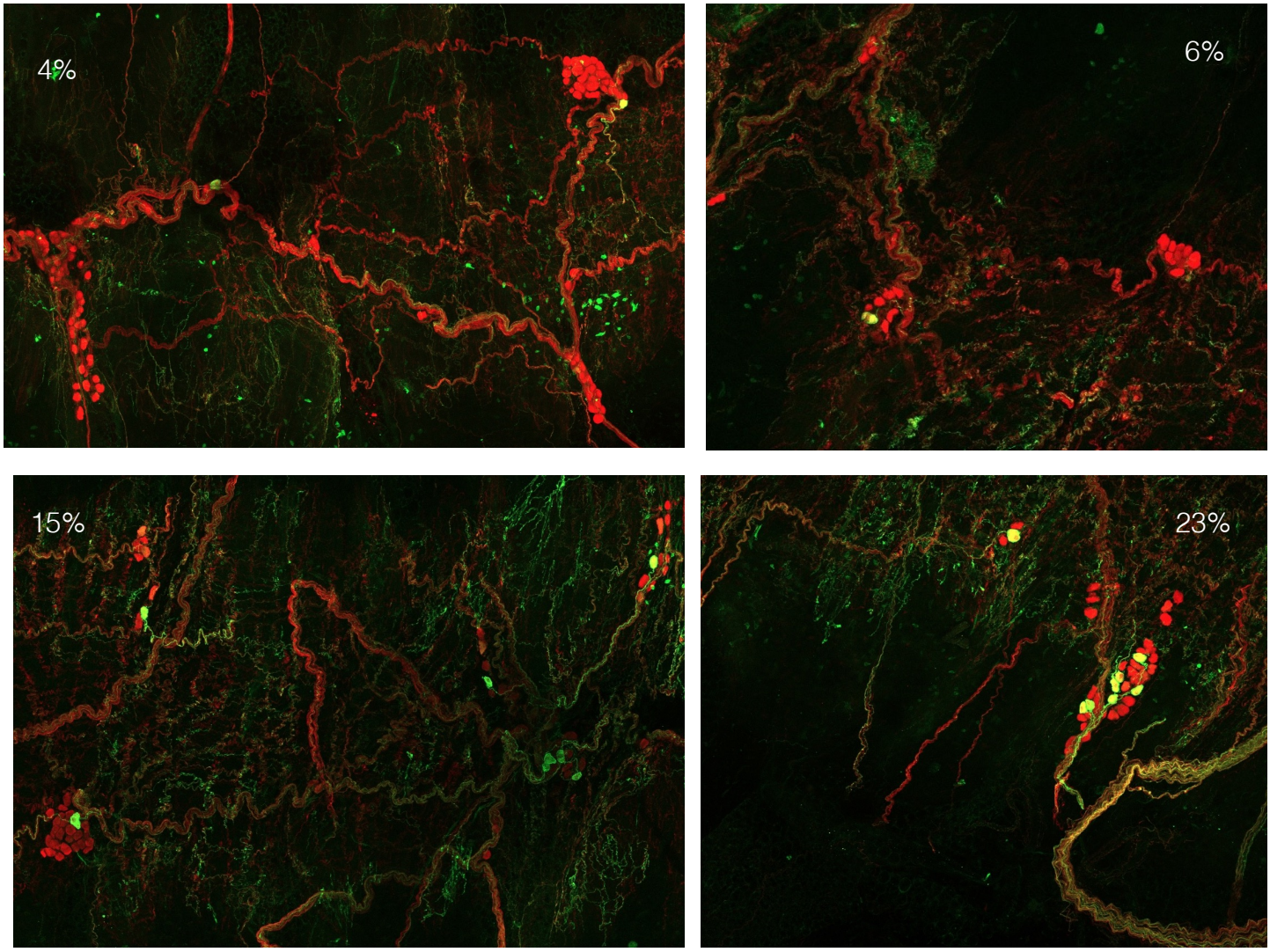

Figure 4.7. Channelrhodopsin 2 is expressed at low frequency in parasympathetic neurons in Advillin-CH2 mice. Tracheas from Advillin-CH2 mice were labeled with antibodies against PGP9.5 (red) and GFP to label CH2 (green). The number of postganglionic parasympathetic cells expressing CH2 were divided by total number of parasympathetic cell bodies imaged to quantify expression. Representative images spanning the range of expression are shown.

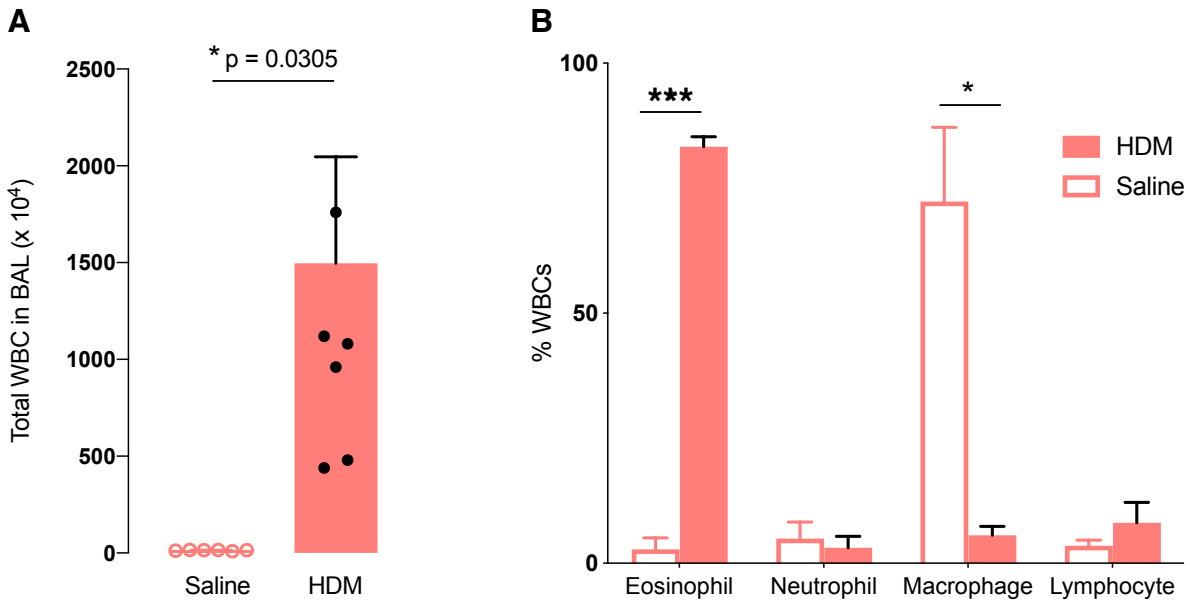

Figure 4.8. Advillin-CH2 mice treated with HDM had increased airway white blood cells and a higher percentage of eosinophils in bronchoalveolar lavage fluid (BAL) than saline controls. (A) Total white blood cell (WBC) count in HDM vs Saline mice were analyzed by unpaired t test. *p<0.05. (B) WBC differential was analyzed using multiple t tests. *p<0.05, ***p<0.0001. Columns show mean ± SEM.

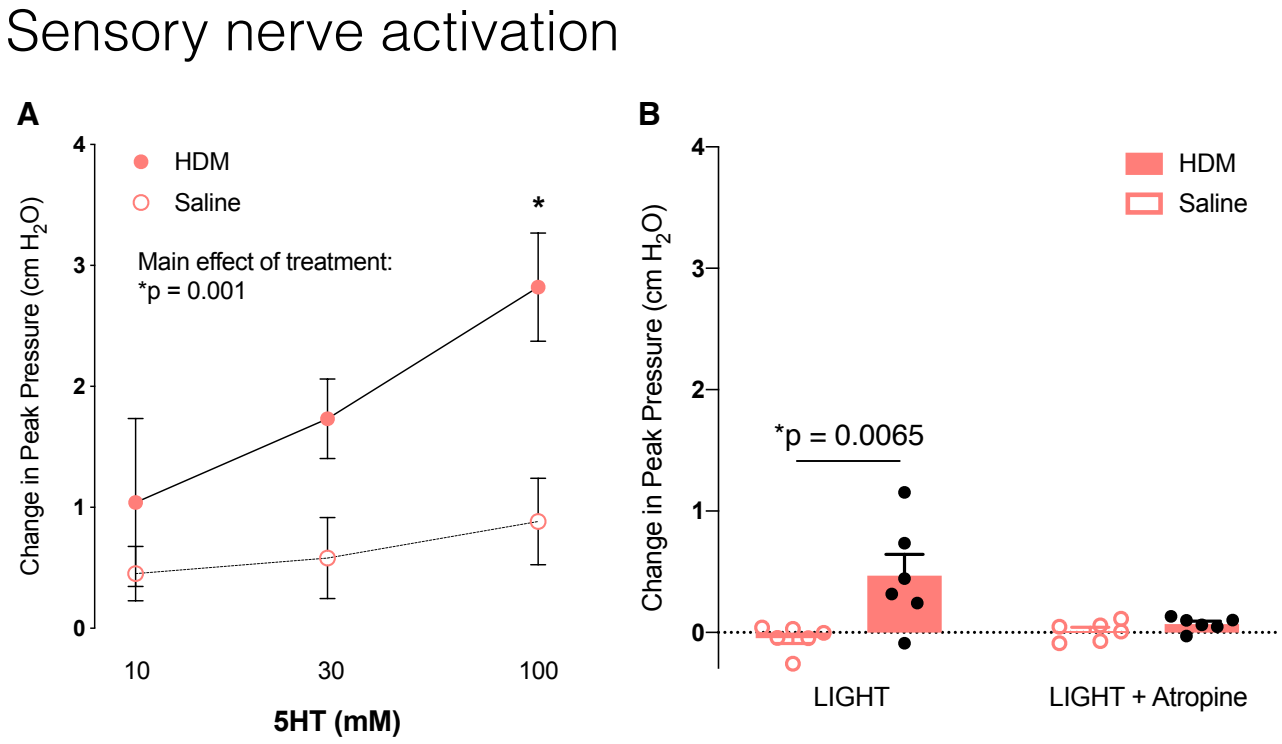

Figure 4.9. House dust mite increases airway hyperreactivity and optogenetically-mediated sensory activity in Advillin-CH2 mice. (A) HDM animals also had greater hyperreactivity to serotonin than saline treated mice. Two way ANOVA, main effect of treatment (HDM vs. saline) ***p=0.001. Sidak's post hoc test for multiple comparisons different at 100mM 5HT dose, *p<0.05. (B) HDM treated animals demonstrated greater bronchoconstriction in response to sensory nerve activation than saline treated mice (two way ANOVA with Sidak's post hoc, **p<0.01), which was eliminated with atropine (p = 0.9757). Columns show mean ± SEM.

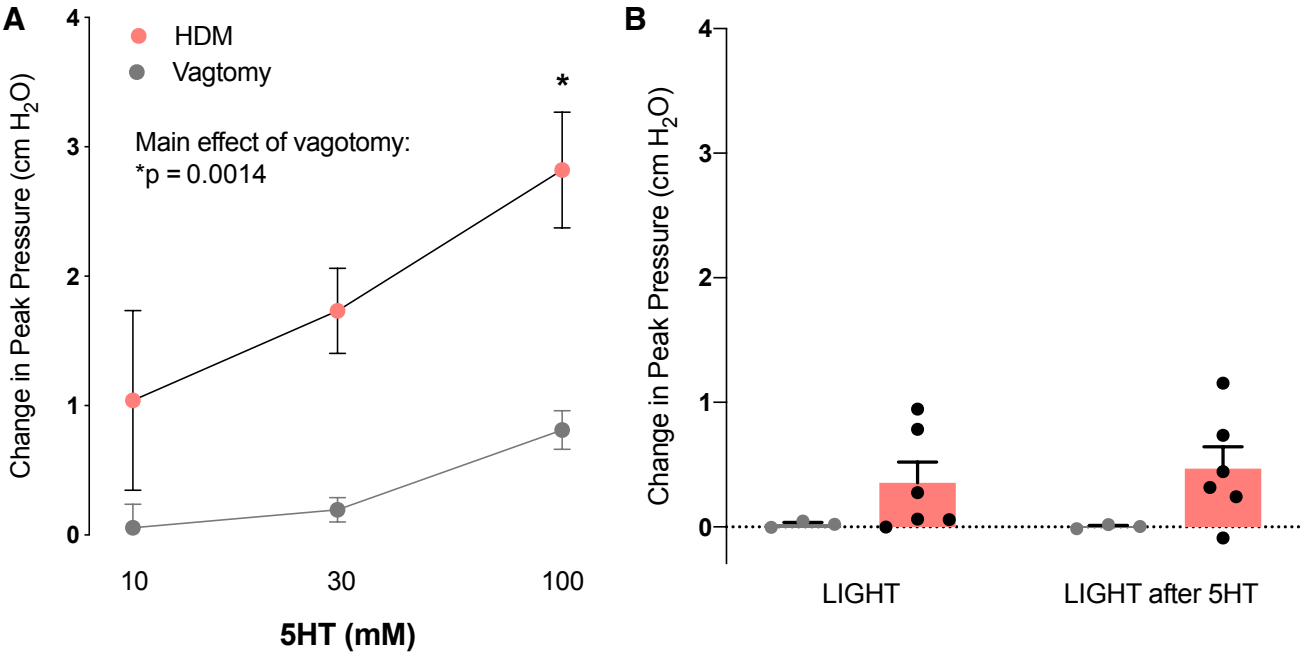

Figure 4.10. Vagotomy eliminates serotonin and light response in HDM treated Advillin-CH2 mice. Mice underwent vagotomy prior to serotonin (5HT) dose response and light stimulation. (A) Two way ANOVA, main effect of treatment (vagotomy vs. no vagotomy) **p<0.01. Sidak's post hoc test for multiple comparisons different at 100mM 5HT dose, *p=0.0284. (B) Mice after vagotomy had no airway response to light, indicating that light response is mediated by reflex bronchoconstriction and not direct activation of parasympathetic neurons. Two way ANOVA main effect of vagotomy *p = 0.0268. Columns show mean ± SEM.

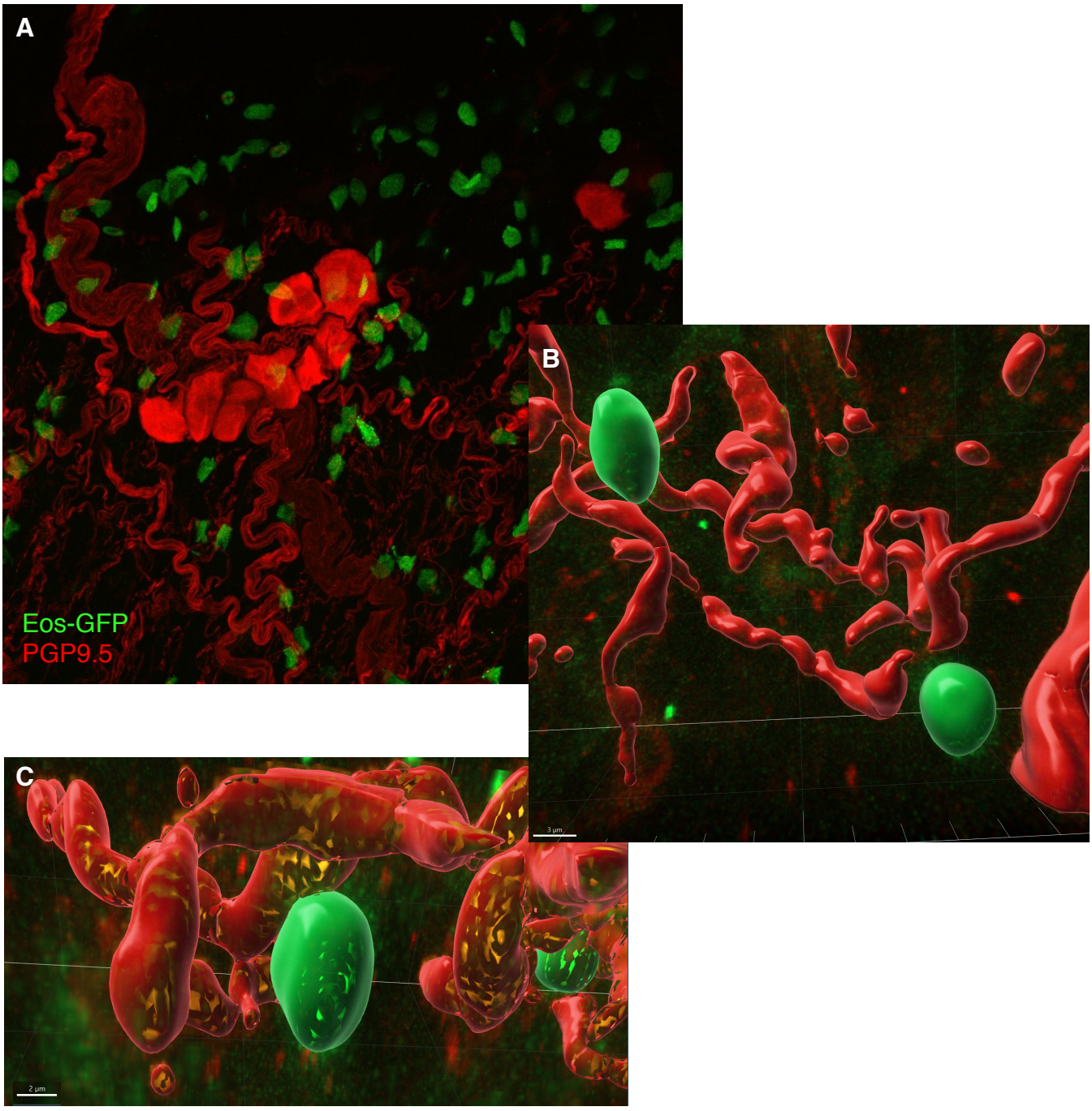

Figure 4.11. Analysis of eosinophil-nerve interactions. (A) Maximum projection image of eosinophils (anti-GFP antibody, green) surrounding a parasympathetic ganglion (anti-PGP9.5 antibody, red). (B) 3D images of airway nerves and eosinophils were analyzed using Imaris software (version 9.6.0). Surfaces were created covering PGP9.5 positive voxels for nerves and EGFP positive voxels for eosinophils. (C) Example of overlap between eosinophil and nerve surfaces where eosinophil was marked as touching airway nerves.

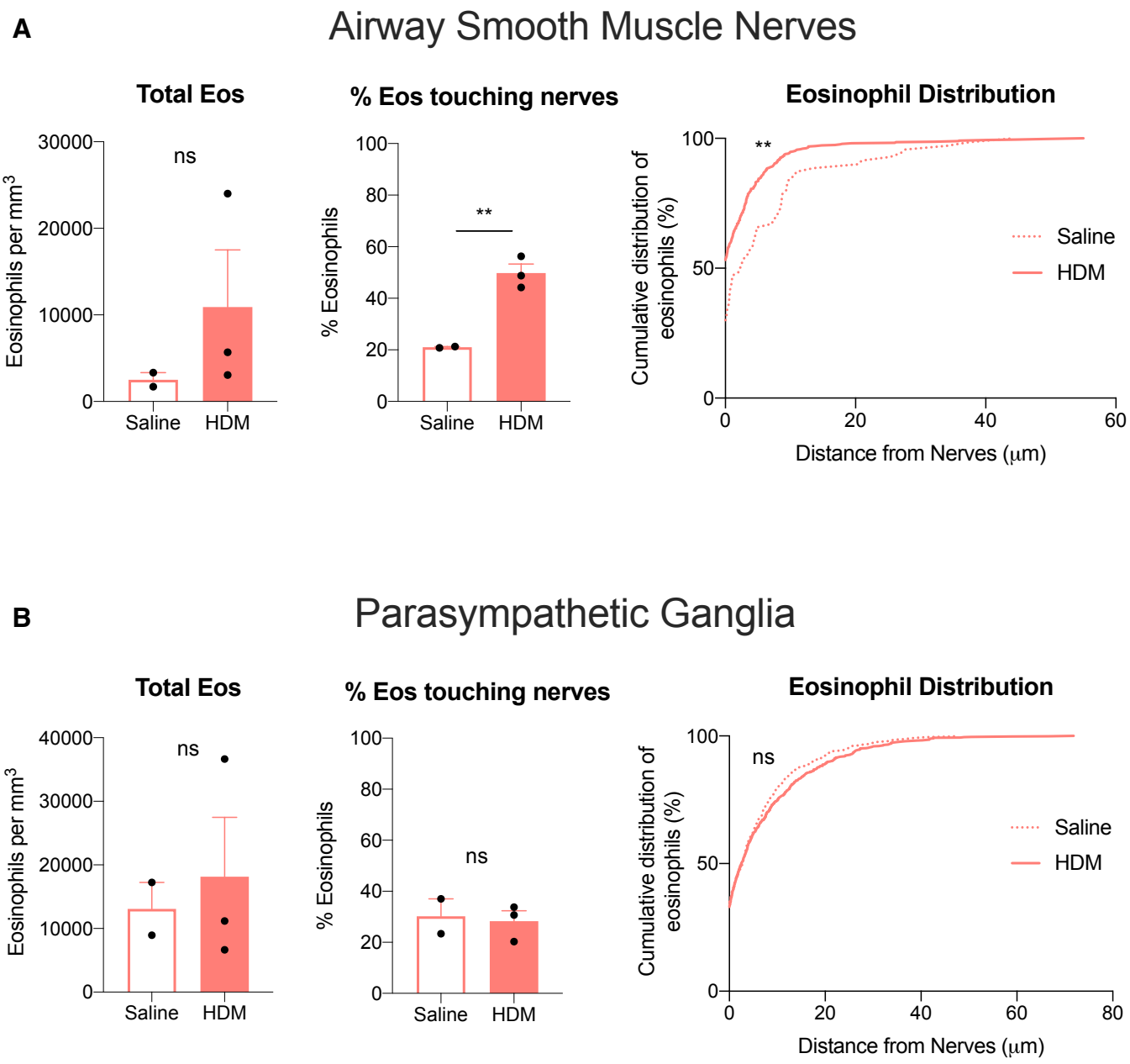

Figure 4.12. Differences between eosinophil-nerve interactions in HDM vs. saline treated mice around nerves in airway smooth muscle but not around parasympathetic ganglia. (A) Around nerve fibers in airway smooth muscle, HDM treated animals had a greater percentage of eosinophils touching nerves (**$p<0.01$) and increased cumulative frequency of eosinophils close to nerve surfaces (**$p<0.01$) compared to saline controls. (B) No difference was found between eosinophil-nerve associations around parasympathetic ganglia. Columns show mean ± SEM.

Discussion

In this study I show fundamental differences in the mechanism of airway hyperreactivity in two asthma mouse models. In a mouse model of acute environmental antigen exposure, HDM treatment led to parasympathetic nerve hyperreactivity that was absent in a mouse model of chronic eosinophilia. HDM treatment also led to modest sensory hyperreactivity, while sensory hyperreactivity in IL-5tg mice remains to be investigated (Figure 4.13). These observed differences may be due to a number of factors. One mechanism that could potentially lead to increased sensory hyperreactivity in the IL-5tg model is increased sensory innervation in the epithelium in IL-5tg mice. Like humans with severe eosinophilic asthma, an increase in sensory innervation has been previously shown in IL-5tg (Drake *et al.*, 2018) but not HDM treated mice (Lebold, 2018). The results of my forthcoming experiments will help determine whether or not these increases are functionally relevant in sensory hyperreactivity.

Another key mechanism that may underlie differences in airway hyperreactivity is compartmentalization of eosinophils and eosinophil-nerve interactions. Previous research in antigen challenged guinea pigs and humans with asthma has shown that eosinophils traffic to nerve compartments and preferentially cluster around airway nerves (Costello *et al.*, 1997). In this study, I have analyzed eosinophil-nerve interactions in three dimensions and shown that eosinophils gather more closely around airway parasympathetic nerves in the HDM treated animals compared to controls. It is my prediction that eosinophils will not cluster as strongly around parasympathetic nerves in IL-5tg mice, both because of the lack of parasympathetic hyperreactivity and because the promoter in the mouse model drives IL-5 expression in airway epithelium, so I would expect eosinophils to be trafficked in higher numbers to that compartment compared to airway smooth muscle. Ongoing experiments will address this question.

Previous work from our lab and others has consistently demonstrated the critical role of eosinophil-nerve interactions in airway hyperreactivity and asthma. In healthy airways parasympathetic hyperreactivity is held in check by inhibitory M_2 muscarinic receptors on postganglionic parasympathetic nerves (Fryer and Maclagan, 1984), which exert negative feedback control over acetylcholine release. Humans with asthma (Ayala and Ahmed, 1989, Minette *et al.*, 1989) and guinea pig models of acute antigen challenge (Fryer and Wills-Karp, 1991) both show loss of M_2 receptor function on parasympathetic neurons, due to endogenous antagonism of the M_2 receptor by eosinophil major basic protein released from eosinophils as they cluster adjacent to airway nerves (Jacoby *et al.*, 1993, Elbon *et al.*, 1995, Evans *et al.*, 1997). The close proximity of eosinophils to parasympathetic nerve endings in the airway smooth muscle suggests that eosinophils may be acting on M_2 muscarinic receptors in a similar capacity in this model. In contrast, in the IL-5tg model eosinophils are being recruited to sensory nerve endings in the airway epithelium, and may not be interacting as closely with parasympathetic nerves. Nevertheless, eosinophils in the IL-5tg model markedly increase sensory innervation (Drake *et al.*, 2018). It is likely that both of these effects are in

play in patients with severe eosinophilic asthma, and both should be considered as we continue to understand the pathology of this disease and identify future targets for treatment.

The experiments in this study have begun the work of understanding how different nerve subtypes - sensory and parasympathetic neurons - are affected in different conditions leading to airway disease. The categories of 'sensory' and 'parasympathetic' in fact encompass a wide variety of nerve subpopulations, which may be better defined by transcriptome analysis (Kupari *et al.*, 2019) or by the expression of key neurotransmitters or receptors (Han *et al.*, 2018). The optogenetic approach will be applied to further understanding these nerve populations, either through activation (with channelrhodopsin) or through light-dependent silencing (as with halorhodopsin) of specific subsets of nerves. Furthermore, this approach to three dimensional imaging of eosinophil-nerve interactions can be applied to understand eosinophil nerve interactions in different patient populations. Such studies will assist developing future treatments for airway disease, building on an understanding of the acute and long-lasting effects of eosinophils on airway nerves.

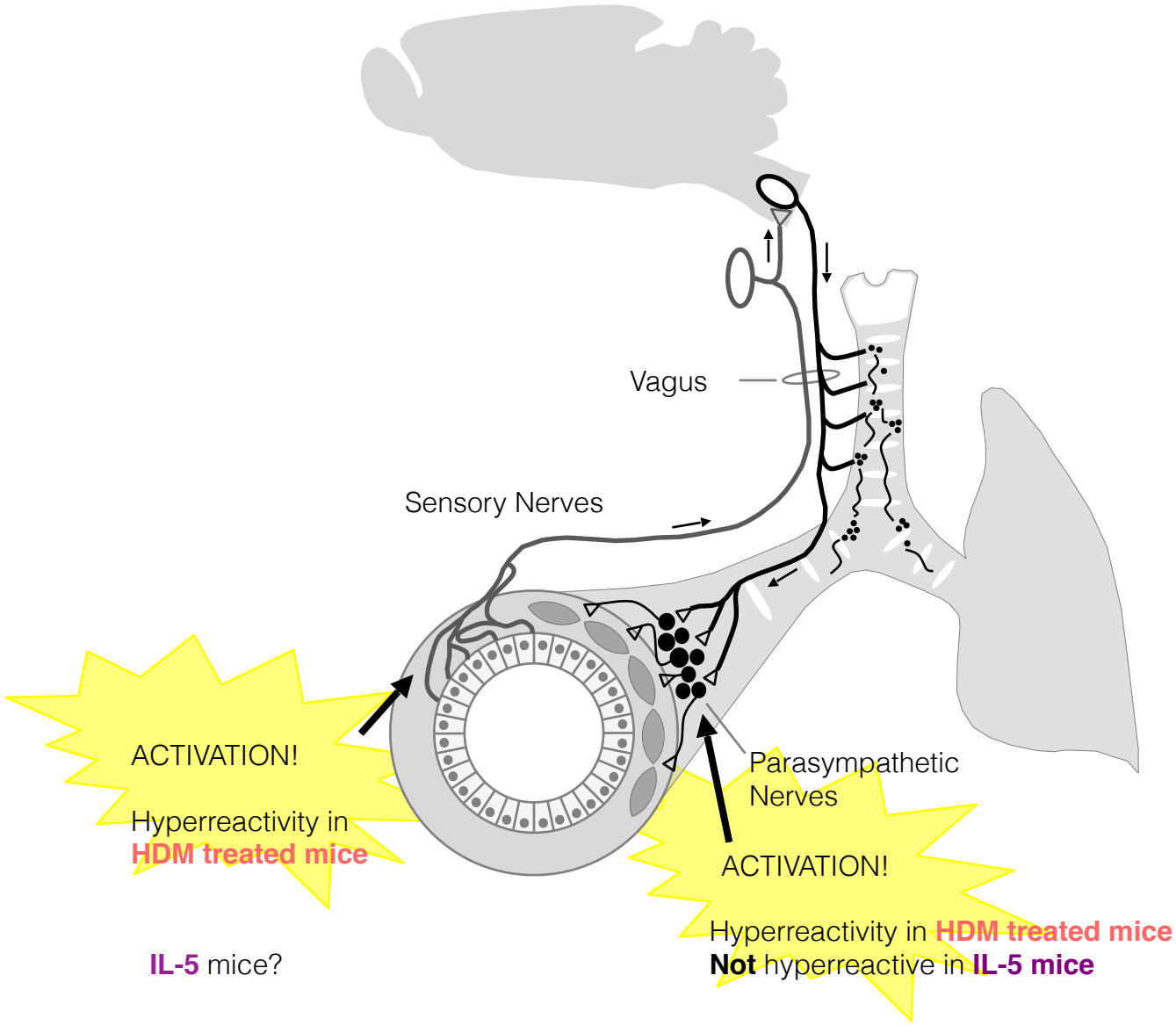

Figure 4.13. Diagram illustrating study findings. Optogenetic activation of sensory and parasympathetic neurons reveals parasympathetic hyperreactivity in HDM treated but not IL-5tg mice. Sensory hyperreactivity is present in HDM treated mice compared to saline controls. Parasympathetic hyperreactivity in HDM treated animals is accompanied by increased eosinophil-nerve interactions in this group. Future experiments will examine sensory hyperreactivity and eosinophil-nerve interactions in IL-5tg animals.

Chapter 5. Multicolor labeling of airway neurons and immunohistochemical analysis of parasympathetic heterogeneity

A. Multicolor Nerve Labeling with AAV9

B. Creation of a transgenic mouse with peripheral multicolor nerve capability

Background

Imaging airway nerves

Histological analysis of airway nerves complements the functional, pharmacological, and electrophysiological study of neural control of the airways. Histological work has traditionally relied on the study of thin tissue sections, which generated important data, but could not fully capture the extraordinary, complex architecture of airway nerves. Fine nerves that wind through airway smooth muscle were often lost in thin sections, which led to contradictory findings between studies. These limitations have been overcome through advances in tissue clearing - the process of rendering tissues transparent through the removal of lipids or equilibration in an immersion medium with refractive index matched to the tissue components. Today tissue clearing solutions are easy to use, inexpensive, generate excellent transparency in lung tissue and are compatible with both endogenous fluorescence and antibody-based immunolabeling (Li *et al.*, 2017). The application of tissue clearing to airway whole mounts combined with optical sectioning in confocal microscopy allows for accurate analysis of full thickness mouse airways and unsectioned bronchoscopic biopsies from humans, with all nerves intact (Scott *et al.*, 2013, 2014). Detailed examination of anatomical structures in three dimensions has allowed for the discovery of new nerve populations, including a subset of myelinated afferent fibers in humans that do not express the peripheral nerve marker protein gene product 9.5 (PGP9.5) (West *et al.*, 2015), and for accurate quantification of nerves in disease models, where increased sensory innervation has recently been shown in humans with eosinophilic asthma (Drake *et al.*, 2018) and with chronic cough (Shapiro *et al.*, 2020).

The study of airway sensory nerves has also benefited from advances in two photon microscopy and calcium indicators, which have been combined with sophisticated ex vivo tissue preparations (Kollarik *et al.*, 2003) to study subgroups of airway C-fibers in different conditions. Patil et al. (2019) provides a detailed account of these experiments. Using this technique, they investigated the response of airway sensory nerves to sphingosine-1-phosphate, a signaling lipid elevated in asthmatic bronchoalveolar lavage fluid. They demonstrate that sphingosine-1-phosphate relies on S1PR3 specifically for activation of mouse vagal C-fibers (Patil *et al.*, 2019), which aligns with data from single-cell RNA transcriptome studies that found S1PR3 on pulmonary chemosensitive sensory nerves (Kupari *et al.*, 2019). In the end, a combination of molecular, functional, and imaging studies will all be necessary to understand the critical role of nerves in the lung, and how changes in nerve architecture, neurotransmitters and receptor expression all contribute to airway hyperreactivity.

Multicolor imaging of nerves

One recent advance in nerve imaging and tracing studies that has not yet reached the airways is multicolor labeling and analysis of nerves. This technique was demonstrated in the central nervous system with a transgenic mouse line called Brainbow 1.0 (Livet *et al.*, 2007). This mouse expressed a

cassette of three fluorescent proteins under a Thy1 promoter - red fluorescent protein (RFP), yellow fluorescent protein (YFP), and membrane-tethered cyan fluorescent protein (M-CFP). RFP was expressed by default, while lox sites flanked both this protein and the YFP protein. A slight variation, Brainbow 1.1, had four fluorescent proteins: the same three as Brianbow 1.0, plus an orange fluorescent protein (OFP) at the beginning of the cassette, making expression of OFP the default in nerves not expressing Cre protein. There are some drawbacks to this system: because a fluorescent protein is the default state there are always more red (1.0) or orange (1.1) neurons than the other colors. However, for researchers of airway nerves the more concerning drawback is that the Thy1 promoter does not drive fluorophore expression in all neurons. A study evaluating different Thy1 fluorescent reporter lines found no expression in superior cervical ganglia, variable expression in dorsal root ganglia (2-20%), and expression in only a small subset of parasympathetic neurons (Feng *et al.*, 2000).

Brainbow continued to be worked on and improved, and six years later the same group published their creation of Brainbow 3.0, 3.1, and 3.2 mice (Cai *et al.*, 2013). They had identified a problem: the original Brainbow fluorophores were difficult to target with antibodies, because they are all modifications of GFP, and the similarity of those protein structures leads to a high level of antibody cross-reactivity. Furthermore, the original fluorophores had a tendency to aggregate in the cell body of the neuron, known as the soma, rather than migrating out into the cell processes as desired. To address these concerns, they chose three new fluorophores for the new mouse lines: mOrange, jellyfish n-GFP, and mKate2. These fluorophores have low levels of fluorescence but are antigenically distinct, have high stability after fixation, and have low aggregation. Furthermore, they constructed Brainbow 3.1 and 3.2 to have a non-fluorescent but still antigenically distinct protein, mutated YFP, as the default, so that one color would not predominate. And they improved the stability of the fluorophores in 3.2 by adding a woodchuck hepatitis virus post-translational regulatory element (WPRE). Further modifications to the Brainbow genetic cassette and the creation of a Brainbow-like mouse for studying airway neurons is described in Chapter 5B.

A novel AAV-based approach has also been used for multicolor labeling of neurons. AAV vectors have the ability to infect and express protein in fully differentiated neurons. However, the small viruses have limited capacity to hold genetic material, and with a genome limit of around 4kb only two fluorescent proteins can be expressed at the same time. Researchers have circumvented this problem by co-transducing with multiple viruses, each with a different fluorophore or set of fluorophores. If individual neurons are infected with multiple copies of each virus then many color combinations are possible. Using this method, researchers have been able to target nerve populations not reached by the canonical Brainbow mice, including parasympathetic nerves in the heart and enteric systems (Chan *et al.*, 2017, Rajendran *et al.*, 2019).

An important matter for consideration in using an AAV approach is which serotype of AAV would work best to target the desired cells. AAV9 is an AAV capsid that has high tropism for nervous tissue, and variations of AAV9 have recently been developed to improve crossing of the blood brain barrier (PHP.B) and to target peripheral nerves (PHP.S), among others (Chan *et al.*, 2017). AAV9 has been previously shown to successfully infect peripheral nerves in the gastrointestinal system (Gombash *et al.*, 2014) as well as sensory nerves in the dorsal root ganglia and nodose ganglia (Schuster *et al.*, 2014). No prior publications report whether AAV9 can successfully infect airway parasympathetic neurons.

A. Multicolor Nerve Labeling with AAV9

Abstract

Postganglionic parasympathetic neurons within the airway regulate airway muscle tone and control bronchoconstriction, and become dysregulated in airway diseases such as asthma. Although there have been reports of acetylcholinergic parasympathetic neurons expressing non-cholinergic neurotransmitters in both healthy and disease states, airway postganglionic neurons are still broadly considered to be a homogenous population, and the potential for subgroups with distinct regulatory functions within this population has never been explored in depth. In this study I report a series of experiments that highlight the heterogeneity of this nerve population in regards to promoter regulation and neurotransmitter expression. I report sparse subpopulations in healthy C57Bl/6 mice in which the promoter synapsin 1 (Syn1), Thy1, and tubulin alpha 1 (TUBA1) are active, as well as ubiquitous activity of an abbreviated version of the PGP9.5 promoter. I further report subpopulations expressing substance P, neuronal nitric oxide synthase, and tyrosine hydroxylase. Using multicolor nerve labeling and digital tracing techniques I begin to characterize the subpopulations expressing these unexpected neurotransmitters, and confirm that their innervation targets extend outside the parasympathetic ganglia and into the airways. Collectively, my experiments confirm extensive heterogeneity within postganglionic parasympathetic neurons, the understanding of which may aid in our investigations of asthma and other airway diseases.

AAV9 vectors were produced by Samuel Huang and the Hiroyuki Nakai lab. Plasmid construction was performed in collaboration with this laboratory. Thanks to Dr. Dawen Cai for assistance with nTracer software. The distribution of nTracer is partially supported by grant funding from NSF-1707316 Neunex MINT.

Introduction

In the airways, sensory neurons innervate airway epithelium and send signals centrally to the brainstem. Preganglionic parasympathetic neurons within the brainstem are activated by these signals, and in turn activate postganglionic parasympathetic neurons within the trachea and primary bronchi. Parasympathetic nerves are primarily cholinergic: postganglionic nerves release acetylcholine onto muscarinic receptors on airway smooth muscle to cause tonic smooth muscle tone as well as bronchoconstriction.

In parasympathetic ganglia throughout the body, subpopulations of neurons have been found that express a variety of neurotransmitters beyond acetylcholine. A population of cardiac parasympathetic neurons has been found to express tyrosine hydroxylase (TH) (Horackova *et al.*, 1999, Hoard *et al.*, 2008), while a separate population expresses neuronal nitric oxide synthase (nNOS) (Calupca *et al.*, 2000, Richardson *et al.*, 2003). Non-overlapping subpopulations of nNOS and TH expressing parasympathetic neurons are also found in the uterus (Papka *et al.*, 1995), and over half of all parasympathetic postganglionic neurons are reactive for NOS in the bladder (Zhou and Ling, 1998). This suggests functional specialization for postganglionic parasympathetic neurons across many organs that remains to be understood.

In the airways, substance P immunoreactive parasympathetic neurons have been found in cats, ferrets, and humans (Dey *et al.*, 1988, 1991, 1996, Scott *et al.*, 2014), nNOS has been reported in ferrets and humans (Dey *et al.*, 1996, Fischer *et al.*, 1996), and TH has been seen in human airway intrinsic ganglia after lung transplant (Springall *et al.*, 1990). In an animal model, the number of substance P positive nerves in parasympathetic nerves has been seen to increase in ozone exposure and contribute to airway hyperreactivity (Wu *et al.*, 2003), but as a whole these nerve subpopulations remain understudied in the context of development and disease. Understanding parasympathetic subpopulations and their functions will improve our understanding of airway function and nerve dysregulation in airway hyperreactivity. Since mice are a valuable model currently in use for studying the airways, I have sought to determine whether substance P, nNOS, and TH expression exists in postganglionic parasympathetic nerves within these animals.

A useful tool in understanding the function of novel nerve populations in the peripheral system is to identify their targets of innervation. Within the airways, nerves may innervate airway epithelium, smooth muscle, mucus glands, vascular endothelium, or other airway neurons. Postganglionic parasympathetic neurons within the trachea have been shown to innervate airway smooth muscle, mucus glands, and other airway neurons (Baker *et al.*, 1986). However, these studies were performed using cholinergic markers to label parasympathetic nerves. The innervation targets of specific neurotransmitter-expressing subpopulations have yet to be identified.

Recent innovations in the field of neuroscience have provided elegant tools for identifying nerve subpopulations and their innervation targets. Multicolor labeling of nerves, such as in Brainbow mice (Livet *et al*., 2007)(Livet *et al.*, 2007) or combinatorial viral vector labeling (Chan *et al.*, 2017), allows for the axons and processes of nerves in close proximity to each other to be distinguished and traced to their terminal destinations. These techniques rely on the expression of random combinations of three fluorophores to generate bright, fluorescent labeling over a wide spectrum of colors in neurons within a system. Brainbow mice are an especially useful tool since they may be bred with Cre-lox mice to endogenously express fluorophores in specific nerves, driven by a genetic promoter. However, these mice were created with studies of the central nervous system in mind, and the Thy1 promoter that drives fluorescent expression in Brainbow mice does not appear to drive expression in postganglionic parasympathetic nerves (Tsuriel *et al.*, 2015).

With this in mind, I collaborated with Samuel Huang and the Nakai lab to investigate whether an alternative approach to multicolor labeling would work to target airway parasympathetic neurons. Viral vector strategies have been employed in other organs to label parasympathetic nerves with many colors, including cardiac and enteric ganglia (Rajendran *et al.*, 2019). This approach involves injecting individual mice with three adeno-associated viruses (AAVs) with neural tropism, each of which express a different, spectrally-distinct fluorophore: at an appropriate viral dosage, the randomness of transduction results in a wide variety of colors within neurons, similar to the Brainbow mice. Previous studies in the periphery have suggested that specially engineered AAV capsids, such as AAV-PHP.S, are necessary to achieve the desired tropism for peripheral nerves (Chan *et al.*, 2017). I investigated the tropism both of this capsid and of the more readily available AAV9 capsid for parasympathetic nerves in the airways. I then used viral vector multicolor nerve labeling and simultaneous immunohistochemistry to identify the cell bodies of SP, nNOS, and TH expressing neurons within parasympathetic ganglia and trace their nerve processes within the airway.

For my final experiments, I sought to understand the ability of different promoters - each widely considered to be pan-neuronal - to drive expression of protein markers within postganglionic parasympathetic airway neurons. Using a combination of Cre-lox mouse lines and a viral-vector approach, and again in collaboration with Dr. Huang I examined the expression of fluorescent proteins driven by the thymus cell antigen 1 (Thy1), synapsin 1 (Syn1), tubulin alpha 1 (TUBA1), and protein gene product 9.5 (PGP9.5) promoters. I co-labeled these airways with antibodies against our previously studied neurotransmitter-expressing subpopulations to highlight the vast heterogeneity of gene regulation and expression in parasympathetic airway neurons.

Materials and Methods

Animals

All animal procedures complied with Oregon Health & Science University's Institutional Animal Care and Use Committee guidelines. C57BL/6 mice from Jackson Labs were used for viral injection experiments. Male and female mice were used at 8 weeks of age and older. For evaluation of promoters in parasympathetic neurons, I used transgenic Thy1 mice (Jackson Labs #003709), with expression of yellow fluorescent protein driven by the thymus cell antigen 1 promoter, as well as the offspring of Syn1-Cre mice (Jackson Labs #003966) and tdTomato reporter mice (Jackson Labs #007909), with expression of tdTomato driven by the rat synapsin 1 promoter.

Plasmid selection and construction

mNeonGreen, mRuby2, and mTurquoise2 plasmids were purchased as bacteria stabs from Addgene. pAAV-CAG-mNeonGreen was a gift from Pantelis Tsoulfas (RRID:Addgene_124101). pAAV-CAG-mTurquoise2 (RRID:Addgene_99122) and pAAV-CAG-mRuby2 (RRID:Addgene_99123) were a gift from Viviana Gradinaru .

TUBA1 and PGP9.5 promoter-enhancer clones were purchased from GeneCopoeia and promoter sequences were PCR-amplified using Platinum Pfx polymerase and the following primers:

Table 5.1. Primers for promoter amplification

Promoter	Forward	Reverse
TUBA1	CTA AAC TAG TAG CCC AGC TGC GGA AAG GGG	TCT TGG TAC CCT GCC GGG TGG ATG GCG GAG
PGP9.5	TAA ACT AGT CCC AAG CTC AGT GAC CAG TG	TCT TGG TAC CTC GCG GAT GGC ACC TGC AGA

PCR products were cloned into pAAV-CAG-NLS-GFP, a kind gift from Viviana Gradinaru (Addgene #104061), using SpeI and KpnI restriction sites. Plasmid authentication included restriction enzyme characterization with BglI, which cuts within the ITRs, and Taq(alpha)I. (Figure 5.1). In addition, junctions between the insert and vector were Sanger sequenced (sequences for pAAV-TUBA1-NLS-GFP and pAAV-PGP9.5-NLS-GFP available in appendix). Transgene expression was confirmed by transient transfection of the plasmids into Neuro 2a cells (mouse albino neuroblastoma).

Cell culture conditions and experiments

HEK293 cells were grown in Dulbecco's Modified Eagle's Medium (DMEM, Lonza) supplemented with 10% fetal bovine serum, L-glutamine and penicillin–streptomycin. mNeonGreen, mRuby2, and mTurquoise2 plasmids were separately transduced into HEK293 cells plated on an 8 well glass slide using Lipofectamine 2000 Transduction reagent (Thermo Fisher). Cells were imaged using confocal microscopy 48h later. Microscope settings were optimized for acquisition of each fluorophore's emission spectra (Figure 5.2). The same settings were later used for multicolor nerve imaging and analysis.

AAV9 vector production, purification, titration, and administration

Dr. Huang produced AAV9 vectors by adenovirus-free triple transfection of HEK293 cells (Stratagene) using polyethyleneimine (PEI) transfection. In brief, 15μg each of pITR (*e.g.* pAAV-TUBA1-NLS-GFP, pAAV-PGP9.5-NLS-GFP), AAV9 Helper (Stratagene), and pladeno5 was delivered to each T225 flask using a DNA:PEI mass ratio of 1:2. In total, 25 flasks (1L culture) were used per vector prep. Cells and media were harvested five days post-transfection and underwent a single freeze-thaw cycle. Virus was precipitated from the cleared lysate by adding NaCl to a final concentration of 500mM and polyethylene glycol (PEG) to a final concentration of 8% and incubating on ice for 3 hours. PEG pellets were resuspended in 50mM HEPES, 150mM NaCl, 1% Sarkosyl, pH8.0 (Resuspension Buffer) and purified by two rounds of cesium chloride ultracentrifugation in a 50.2Ti rotor (Beckman) spun at 45,000rpm x 22hr and 65,000rpm x 16hr. Fractions were collected and combined based on refractory index and dot blot titers. Pooled fractions were then dialyzed against PBS supplemented with 0.001% Pluronic-F68 using Slide-a-lyzer 10K MWCO (Thermo Fisher). Three buffer changes were performed, each with 400x excess of buffer relative to the dialyzed volume. Finally, the buffer was exchanged with a 5% sorbitol in PBS supplemented with 0.001% Pluronic-F68. Vector recovered from the dialysis cassette was filter-sterilized using a 0.22um filter, aliquoted, and stored at -80C. Vector titers were ~3 x 10^{13} vg/mL and determined using a radioactive dot blot assay probing the GFP transgene (Powers *et al.*, 2018). For pAAV-TUBA1-nls-GFP and pAAV-PGP9.5-nls-GFP, C57BL/6 mice were injected intravenously at a dose of 5 × 10^{12} vg per mouse. For mNeonGreen, mRuby2, and mTurquoise2, AAV9 vectors were combined in equal proportions and injected intravenously at a total dose of 3 × 10^{11} to 3 × 10^{12} vg per mouse.

Tissue Immunohistochemistry, Optical Clearing and Imaging of Airway Nerves

Mice were perfused with PBS and airways were excised and left at 4°C in Zamboni fixative (Newcomer Supply) overnight. For imaging of endogenous fluorescence, tracheas were washed with TBS and then moved to optical clearing solution N-methylacetamide/Histodenz (Ce3D) (Li *et al.*, 2017) overnight. For immunohistochemistry experiments, tracheas were blocked overnight with 4% normal goat serum, 1% Triton X-100, and 5% powdered milk, and then incubated for 4 hours with antibodies to EGFP

(anti-GFP chicken IgY, 1:500; Invitrogen) and protein gene product 9.5 (PGP9.5, rabbit IgG, 1:500; Millipore) (expression experiments) or substance P (rat anti-SP, 1:500; BD Pharmigen 556312), neuronal nitric oxide synthase (rabbit anti-nNOS, 1:100; Cell Signal C7D7), or tyrosine hydroxylase (rabbit anti-TH, 1:500, Pel Freez P40101) (multicolor labeling experiments) at 4°C. Tissues were washed and incubated overnight in secondary antibodies (Alexa goat anti-rat 647, 1:1,000; Alexa goat anti-rabbit 647, 1:1,000; Alexa goat anti-chicken 488, 1:1,000; Invitrogen) before optical clearing overnight in Ce3D. Tracheas were mounted in Ce3D on slides in silicon wells (Grace Labs) and imaged using an LSM 900 confocal microscope. Samples were illuminated with four different wavelengths of light on separate tracks: 405 nm (detection wavelengths 467-503), 488 nm (516-526), 561 nm (576-619) and 640 nm (645-700). Images were acquired as z-stacks: z stacks were used for subsequent tracing studies while maximum intensity projections were used for visualization.

nTracer analysis of parasympathetic nerve morphology

Tracing studies were performed on 8-bit images using FIJI software with the nTracer plugin (Roossien *et al.*, 2019). Cell bodies for neurons of interest were identified through immunofluorescent labeling. Traces were created around the cell bodies of these neurons and following their axons across the image. User inputs for points along each axon were verified through three-channel color intensity analysis in nTracer, and a path was created in the software of pixels with matching intensity in each of the three color channels between the user identified points. This semi-manual tracing allowed individual axons to be followed through each image. In some cases overlapping images were taken: cell bodies and axons were traced individually, and traces were combined using the overlapping region.

Statistical Analysis

Fluorescence intensity data for multicolor cell bodies was not normally distributed, as analyzed by A D'Agostino and Pearson normality test ($p<0.001$ for medium and low doses). Data was analyzed using a Kruskal-Wallis test with Dunn's post hoc ($p^{**}<0.01$, $p^{***}<0.001$).

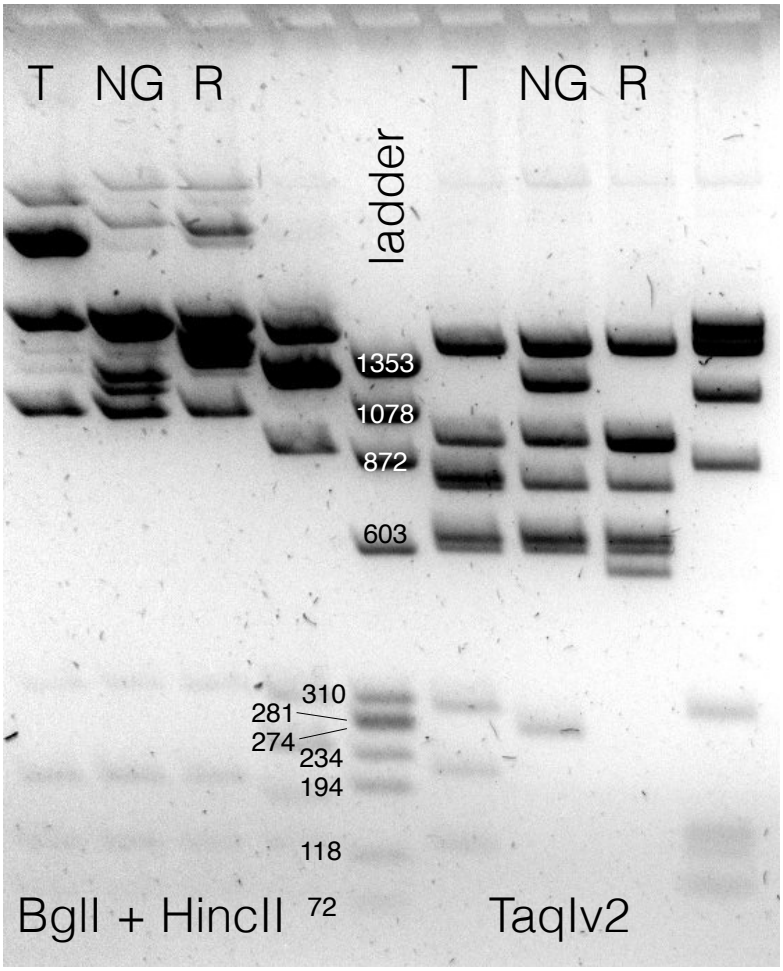

Figure 5.1. Restriction enzyme digests to validate purchased Addgene plasmids for mNeonGreen, mRuby2 and mTurquoise2 AAV vectors. BglI + HincII and TaqI-v2 enzymes were used for digestion. Bands matched prediction from *in silico* digest. T = mTurquoise2, NG = mNeonGreen, R = mRuby2.

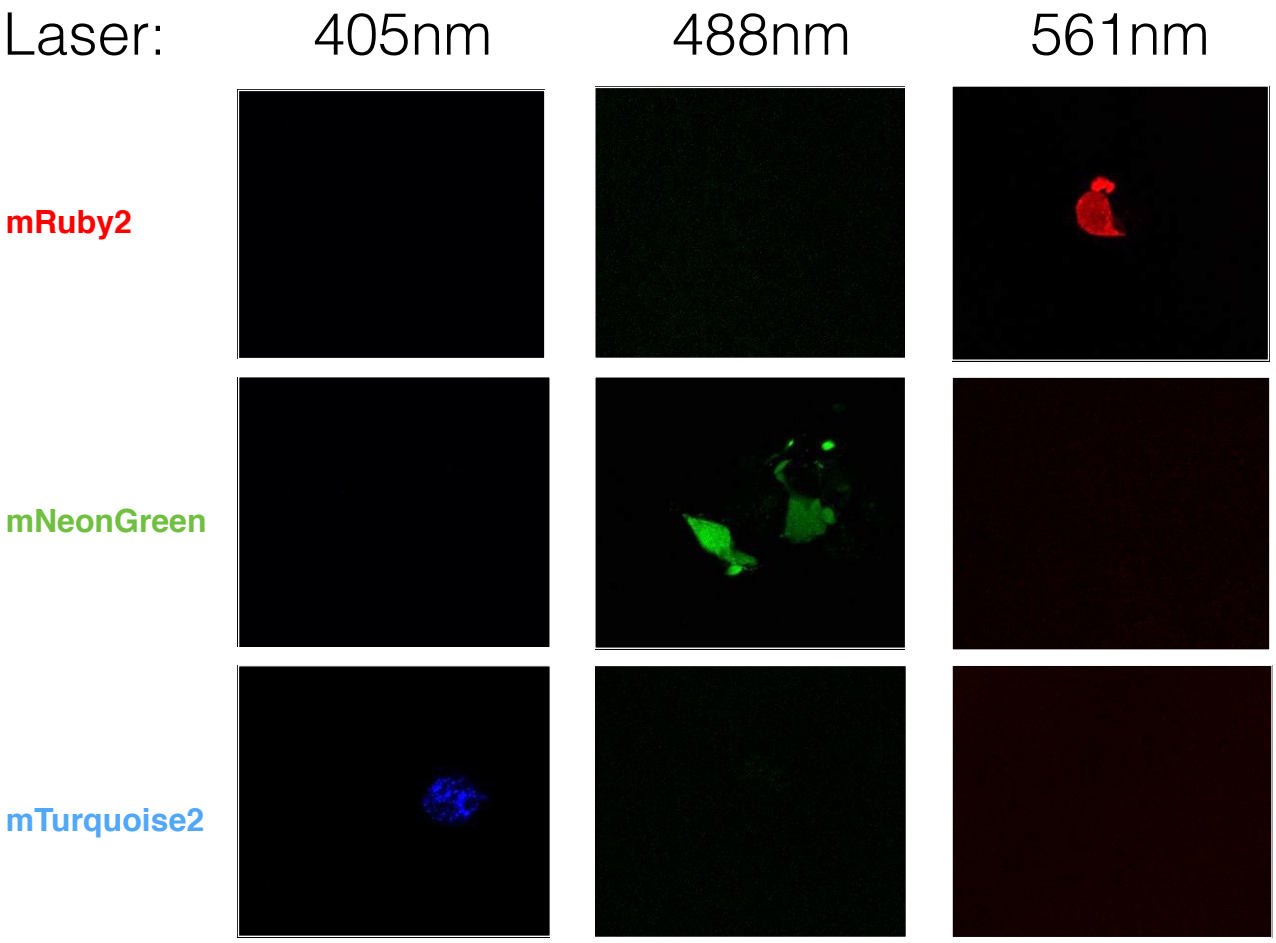

Figure 5.2. Validated microscope settings in HEK293 cells. Groups of cells in separate wells were transfected with plasmids for each of the three fluorophores. Windows for detection of emitted light were narrowed such that each channel only detected light from a single flurophore. Final microscope settings were laser 405 nm (detection wavelengths 467-503 nm), 488 nm (516-526 nm), and 561 nm (576-619 nm).

Results

Airway Postganglionic Parasympathetic Neurons Express Substance P, neuronal Nitric Oxide Synthase, and Tyrosine Hydroxylase

Trachea and primary bronchi from wild type C57BL/6 mice were labeled with antibodies against PGP9.5 and either SP, nNOS, or TH. Small numbers of cell bodies identified as belonging to postganglionic parasympathetic neurons (based on morphology and location within tissue) stained positively for each of these neurotransmitter markers (Figure 5.3). The number of positive neurons varied between mice, with SP positive neurons representing (7 ± 2.0), nNOS (19.1 ± 6.6), and TH (7.2 ± 3.1) per mouse (Figure 5.4).

AAV9 Virus Transduces Airway Parasympathetic Neurons

Next we investigated the efficacy of using AAV9 viral capsids to transduce airway parasympathetic neurons. AAV9 viral capsids containing a nuclear-localized GFP sequence driven by a ubiquitous CAG promoter were injected intravenously into 8 week old C57BL/6 mice at variable doses. Expression (number of postganglionic parasympathetic cell bodies expressing GFP) was low for a viral titer of 5×10^{10}, but increased to close to one hundred percent expression with a viral titer of 5×10^{11}. Expression with a viral injection of 5×10^{12} reached one hundred percent (Figures 5.5-5.7). This successful transduction included postganglionic neurons expressing SP (Figure 5.8). The viral capsid AAV-PHP.S was also tested for expression in airway parasympathetic neurons. A low dose of 1×10^{9} AAV-PHP.S driving GFP expression was injected into 21 day old C57BL/6 mice, with successful but sparse expression detected 21 days later (Figure 5.9).

Multicolor Labeling Identifies Soma and Processes of Individual Airway Parasympathetic Neurons

Previous studies have identified spectrally distinct fluorescent proteins (Chan *et al.*, 2017) that may be packaged into AAV capsids for multicolor nerve labeling. I selected three of these proteins, available as AAV plasmids from Addgene: mNeonGreen, mRuby2, and mTurquoise2 (Figure 5.10; see also Figure 1.14). These were packaged into AAV9 viral capsids and injected intravenously into mouse tail veins. Tissues were passively cleared by immersion in Ce3D solution to preserve endogenous fluorescence. Imaging mouse airways revealed successful multicolor labeling of parasympathetic neurons using this system (Figure 5.11) Three viral doses were tested, with varying results for fluorescence color and intensity (Figure 5.12 and 5.13).

Next I tested whether individual neurons could be traced to their innervation targets. I imaged ganglia and surrounding nerve fibers in whole mount mouse airways (Figure 5.14). I used software specific for analyzing the color ratios of different pixels (nTracer plugin for FIJI) to semi-manually trace axons as they exited cell bodies and traveled through the tissue (Figure 5.15). I found that only the brightest

axons could be traced in this way, and that the physics of optical microscopy limited our ability to follow axons all the way to their innervation targets. Specifically, high magnification (63x) was needed to accurately differentiate closely associated axons of similar colors, yet the working distance of this lens (180 μm) was not sufficient to capture the full depth that axons traveled into the tissue (Figure 5.16). Nevertheless, this imaging was sufficient to assess whether neurons synapse onto other neurons within their own ganglia, in the manner of interneurons, or whether their axons left ganglia to travel elsewhere in the airways.

Axons of Substance P, nNOS, and Tyrosine Hydroxylase Neurons Leave Ganglia

Multicolor mouse tissues were next labeled via immunohistochemistry with antibodies against SP, nNOS, or TH. The three proteins selected for multicolor labeling left an opening in the far red spectrum, which was used for the secondary antibody in labeling neurons with specific neurotransmitters. Only one parasympathetic neuron was found in the tissue labeled with SP (Figures 5.17-5.19), while two neurons labeled with nNOS and TH were found in their respective tissues. The SP positive neuron formed its own single neuron ganglia. Axons of the nNOS and TH positive neurons were traced, and each were found to exit the ganglion in which they were located (Figures 5.20 and 5.21).

PGP9.5 Promoter Drives Ubiquitous Expression in Airway Postganglionic Parasympathetic Neurons while Syn1, Thy1, and TUBA1 Promoters Do Not

Long term studies of airway parasympathetic neurons would benefit from the ease and economy of endogenous multicolor labeling in a transgenic mouse line, similar to what Brainbow mice provide the central nervous system. I investigated different promoters that might prove to be effective drivers of protein expression in airway parasympathetic neurons, including Syn1, TUBA1, and PGP9.5. I examined the airways of a Thy1-GFP mouse line and confirmed that, similar to postganglionic parasympathetic ganglia in other areas of the organism, Thy1 did not drive expression in our neurons of interest. Examining the airway of a mouse with Syn1 driving tdTomato expression produced similar results: in both of these mice, only a rare subset (1 Thy1, 2 Syn1) of parasympathetic neurons expressed the fluorophore, while the remaining three to four hundred airway parasympathetic neurons did not. I next used viral vectors to drive fluorescent protein expression using abbreviated forms of the TUBA1 and PGP9.5 promoters. A viral titer of 3×10^{12} was used for experiments. TUBA1 drove expression in the vast majority of parasympathetic neurons but not all, while the PGP9.5 promoter drove robust expression in all neurons (Figure 5.22).

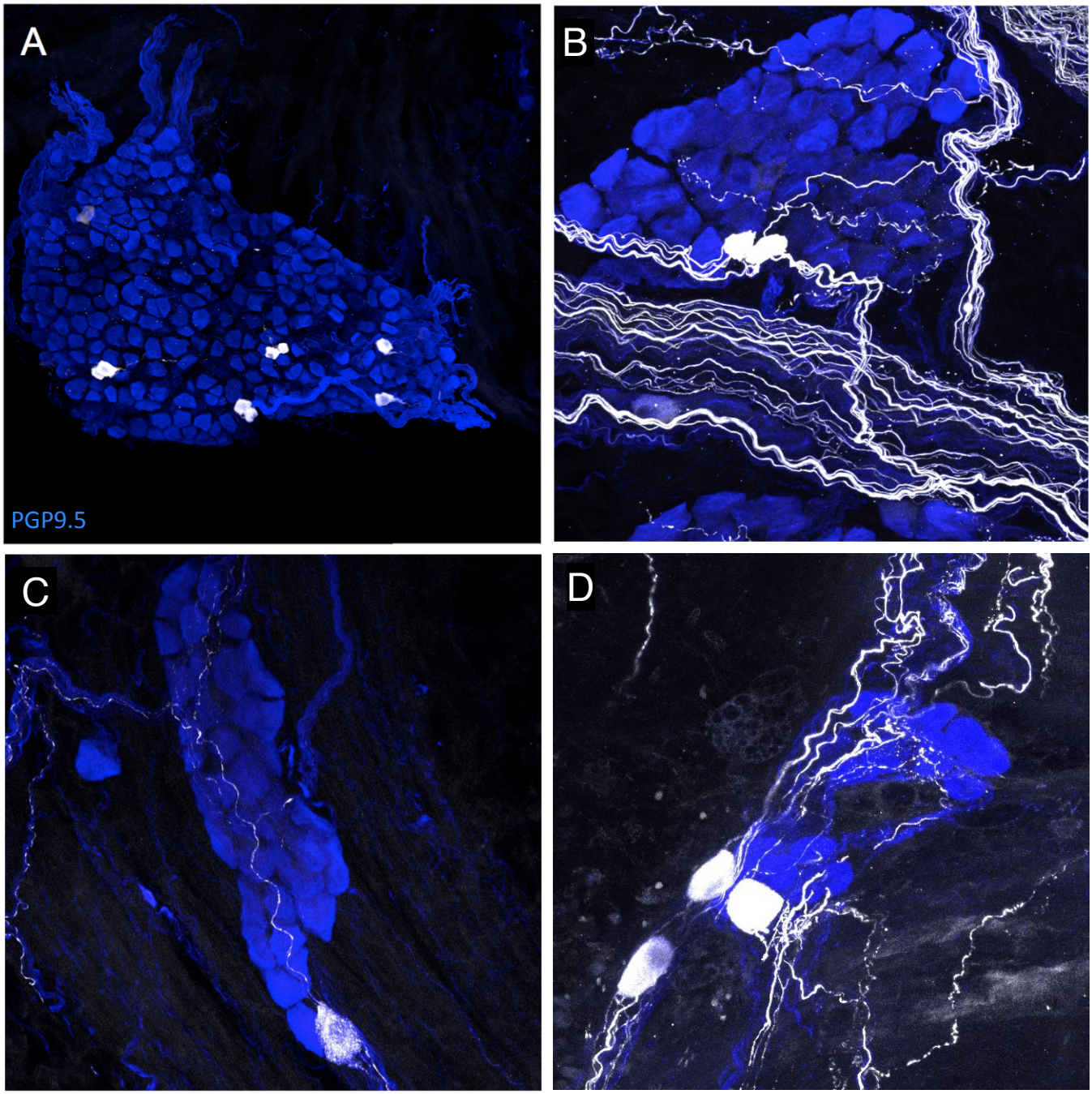

Figure 5.3. Parasympathetic nerve heterogeneity in mouse airways. Subpopulations of airway nerves express neuronal nitric oxide synthase (nNOS) (A), tyrosine hydroxylase (TH) (B), and substance P (SP) (C-D). Figures A-C from Lebold, 2018.

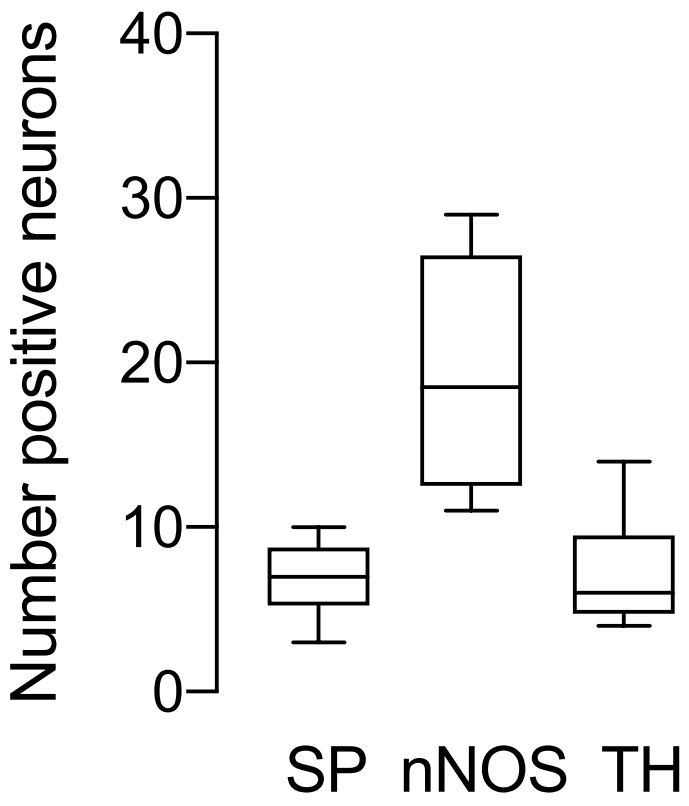

Figure 5.4. Small subsets of postganglionic parasympathetic neurons express substance P (SP), neuronal nitric oxide synthase (nNOS), and tyrosine hydroxylase (TH). The number of neurons expressing these transmitters was quantified in wild type C57BL/6 mice: SP positive neurons (7 ± 2.0), nNOS (19.1 ± 6.6), and TH (7.2 ± 3.1) per mouse (mean ± SD). Data acquired in collaboration with Dr. Katherine Lebold, presented in Lebold, 2018.

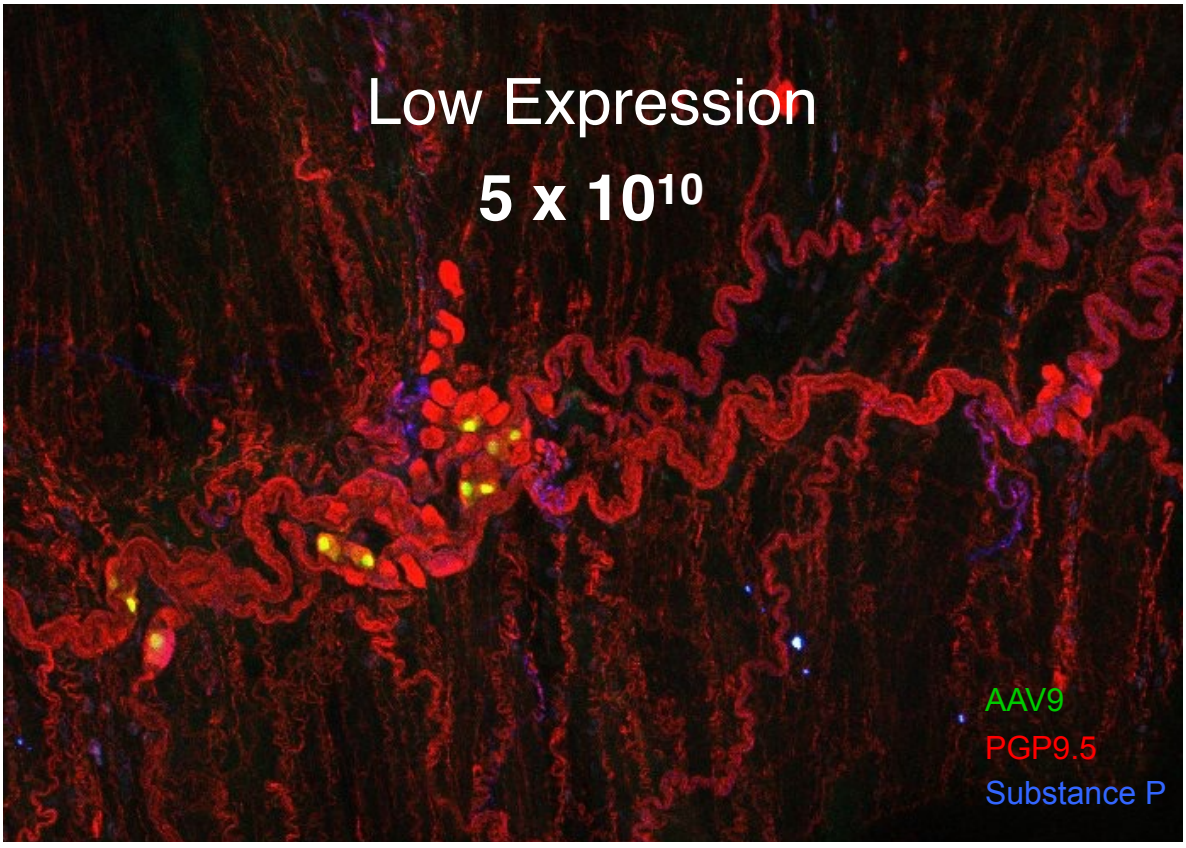

Figure 5.5. Representative image of immunofluorescent labeling showing few parasympathetic neurons (red, rabbit anti-PGP9.5) expressing GFP (green; chicken anti-GFP) with an injected AAV9-CAG-GFP viral titer of 5 x 10^{10} in C57BL/6 mice.

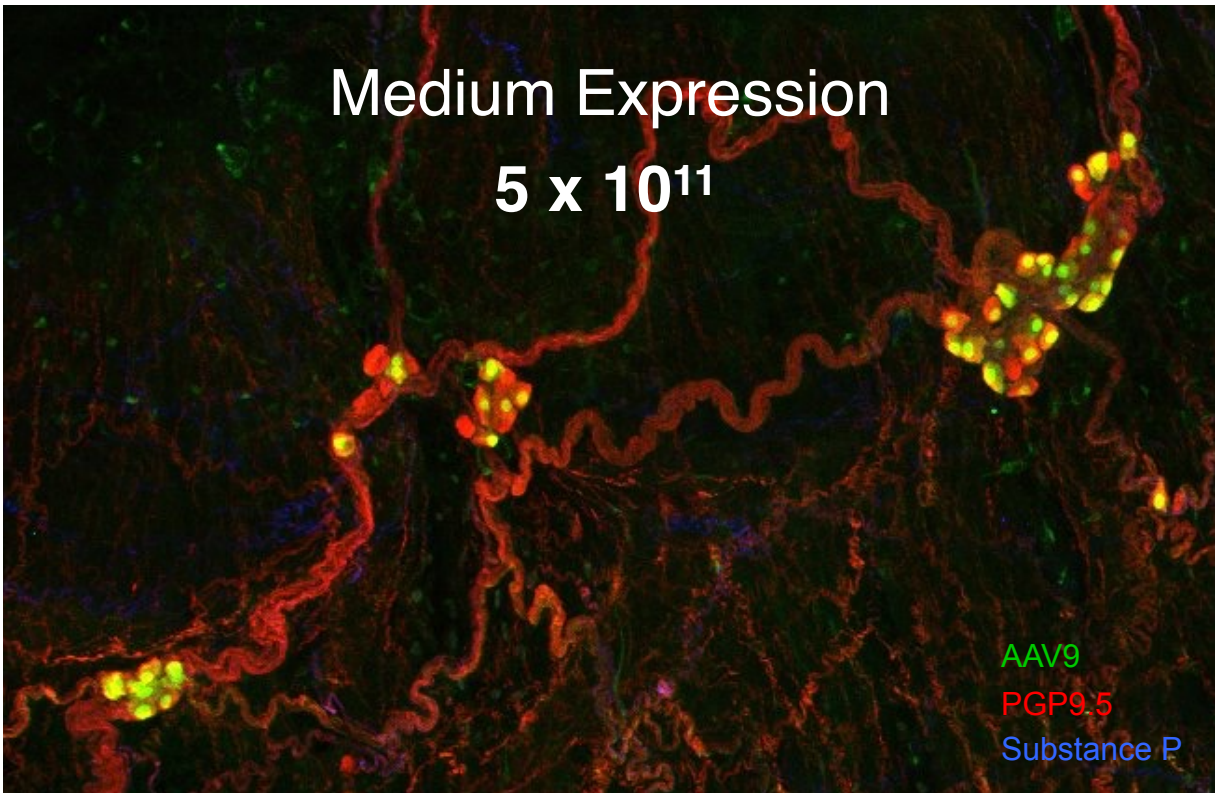

Figure 5.6. Representative image of immunofluorescent labeling showing many parasympathetic neurons (red, rabbit anti-PGP9.5) expressing GFP (green; chicken anti-GFP) with an injected AAV9-CAG-GFP viral titer of 5 x 10^{11} in C57BL/6 mice.

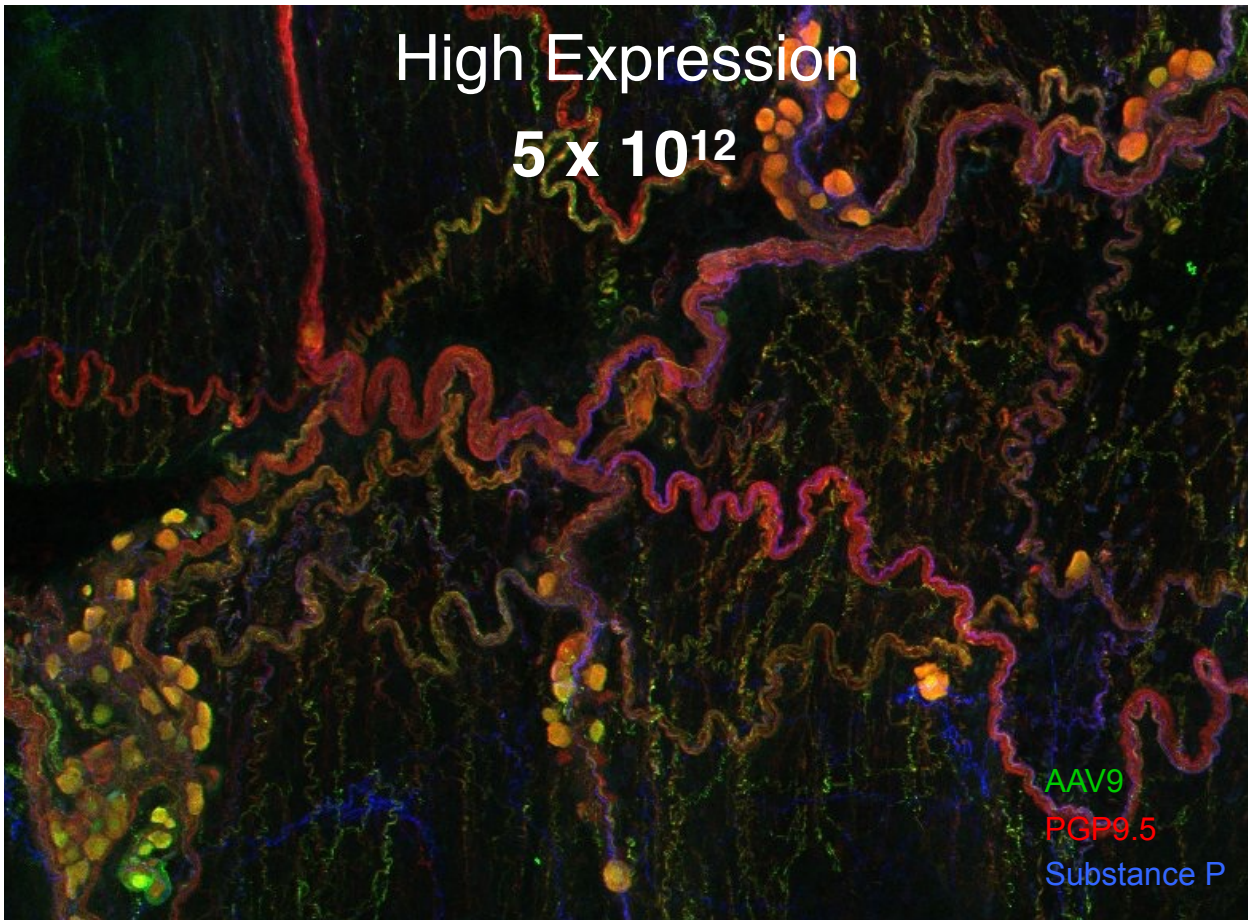

Figure 5.7. Representative image of immunofluorescent labeling showing all parasympathetic neurons (red, rabbit anti-PGP9.5) expressing GFP (green; chicken anti-GFP) with an injected AAV9-CAG-GFP viral titer of 5×10^{12} in C57BL/6 mice.

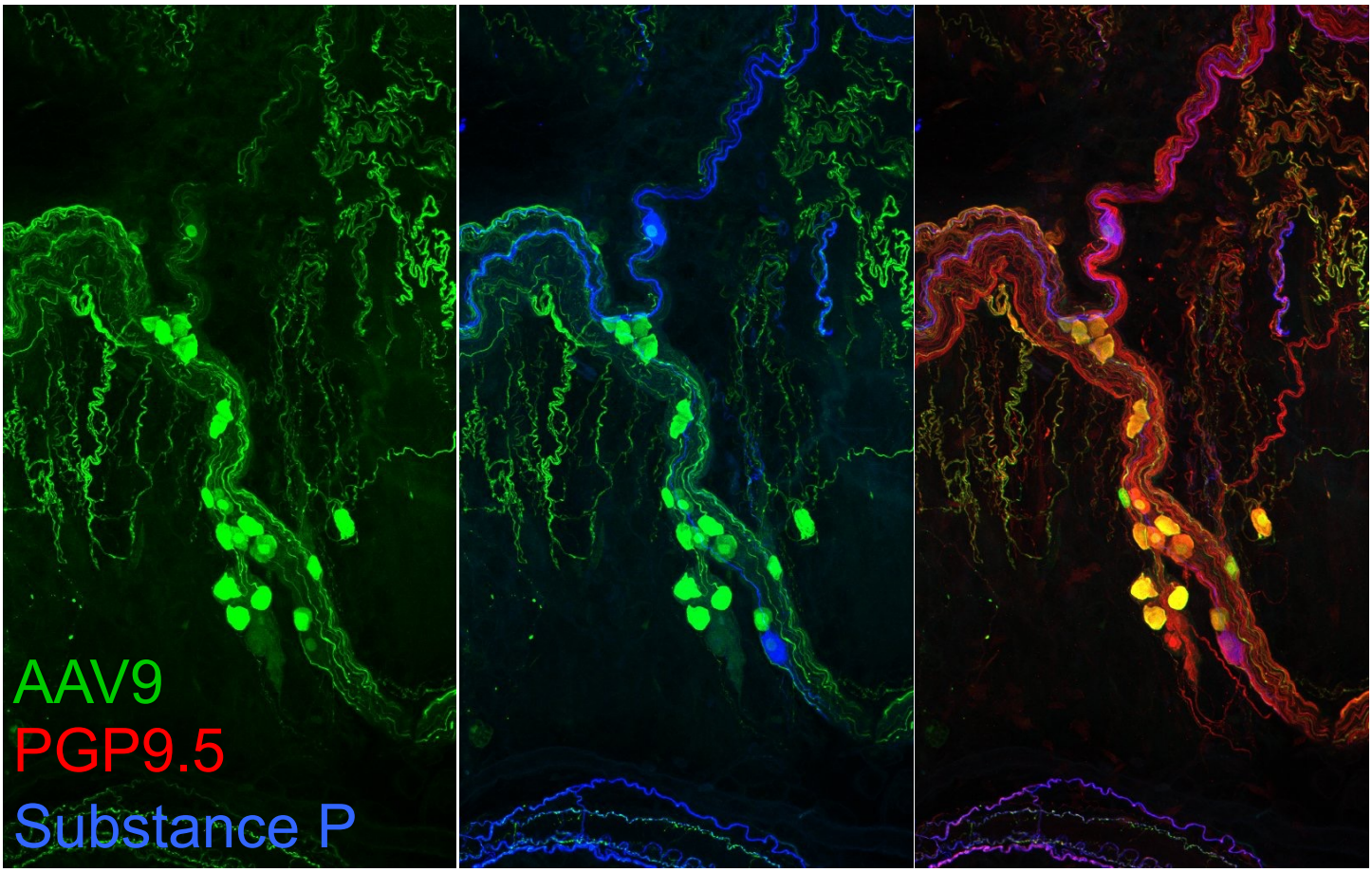

Figure 5.8. Substance P (blue) expression in transduced postganglionic parasympathetic neurons (neurons in red, PGP9.5; AAV9-CAG-GFP expression in green).

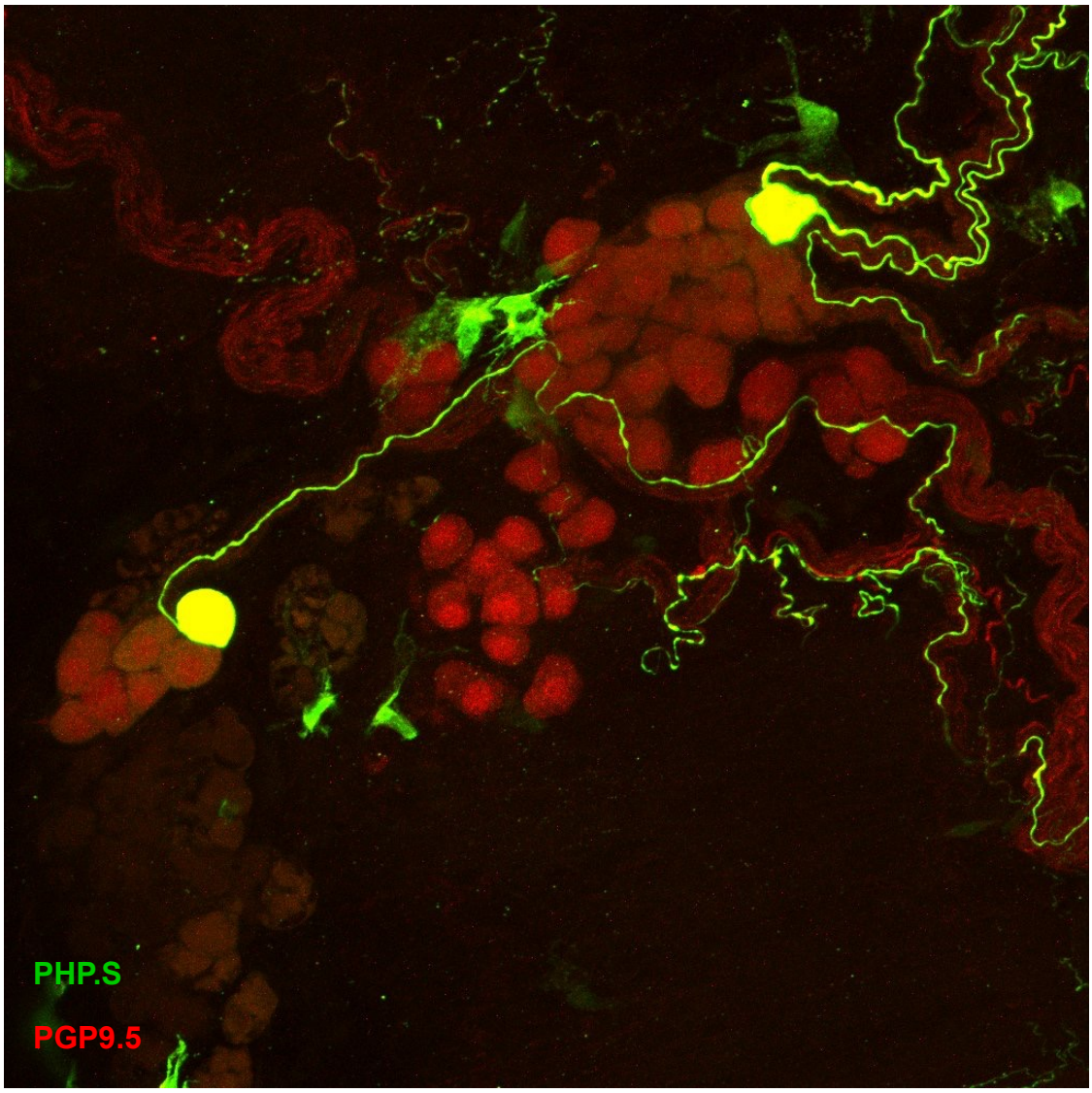

Figure 5.9. PHP.S transduces airway parasympathetic neurons. Two postganglionic parasympathetic neurons and their axons (green, anti-GFP) in mouse trachea were successfully transfected using PHP.S capsid.

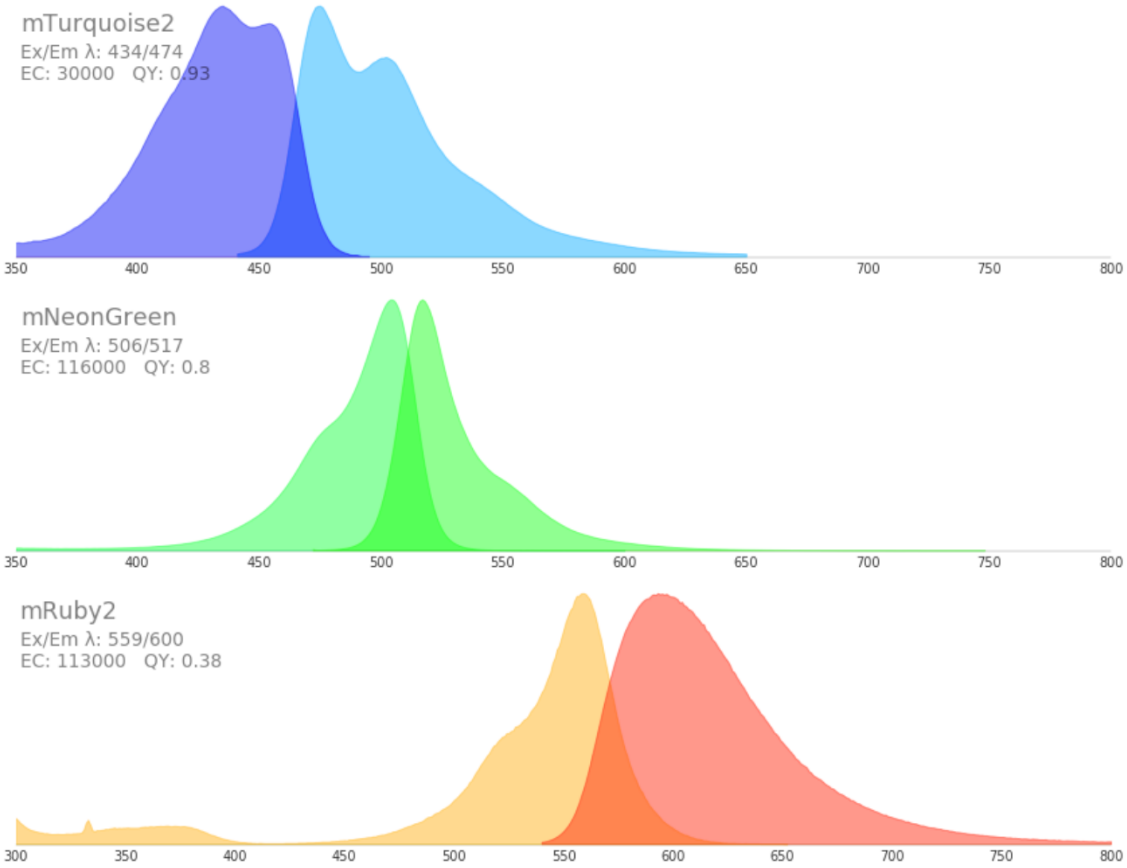

fpbase.com

Figure 5.10. Excitation and emission spectra of fluorophores used for multicolor labeling. Images from fpbase.com. Note that the far red spectrum is free for labeling subpopulations of neurons, such as substance P.

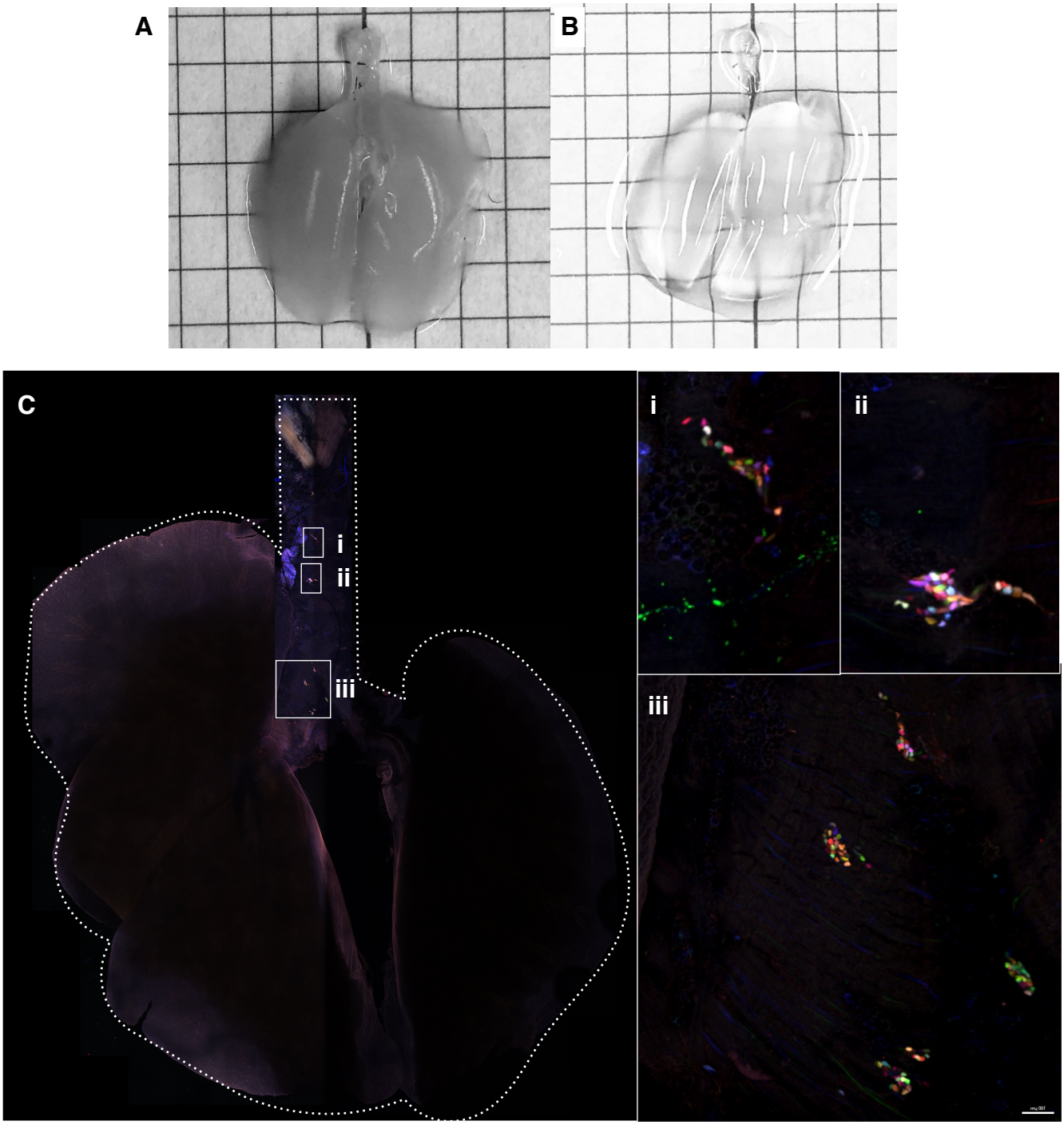

Figure 5.11. Successful multicolor labeling of postganglionic parasympathetic neurons with multicolors. (A) Mouse trachea and lungs. (B) Same mouse airways, cleared with Ce3D. (C) Confocal microscopy of whole trachea and lungs, showing parasympathetic ganglia with multicolor labeling within the trachea (i, ii) and primary bronchi (iii).

Viral dose: 3 x 10^{12} (High) 1 x 10^{12} (Medium) 3 x 10^{11} (Low)

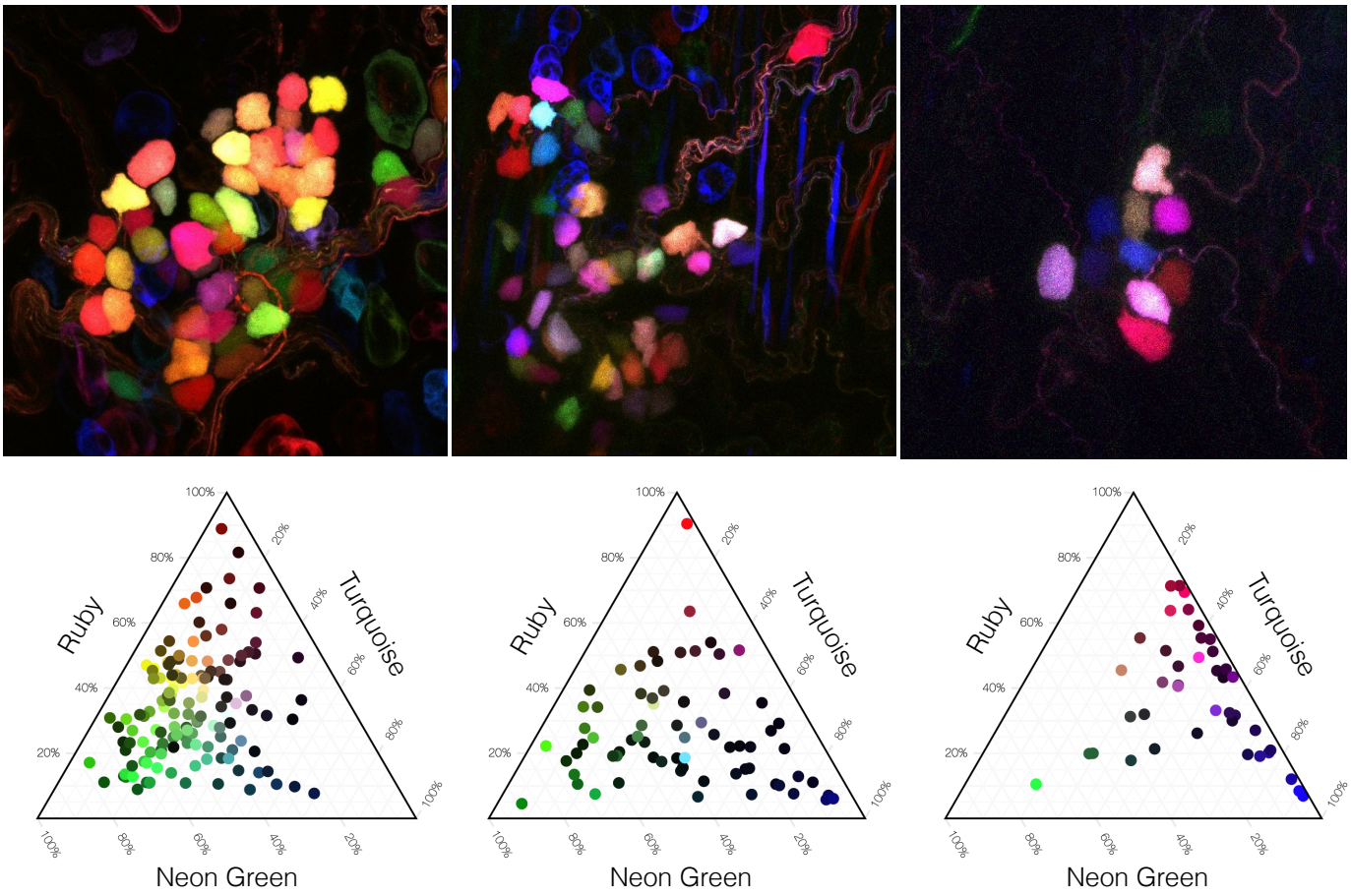

Figure 5.12. Test of three doses of virus for multicolor nerve labeling. Equal titers of each virus were used, and total overall titer is labeled. Representative image of a parasympathetic ganglion and ternary plot showing color spread shown for each image. Fluorescence intensities at neuronal cell bodies were used for ternary plots. Fluorescence intensities were vector normalized for each image and color. Color spread was most even using middle dose.

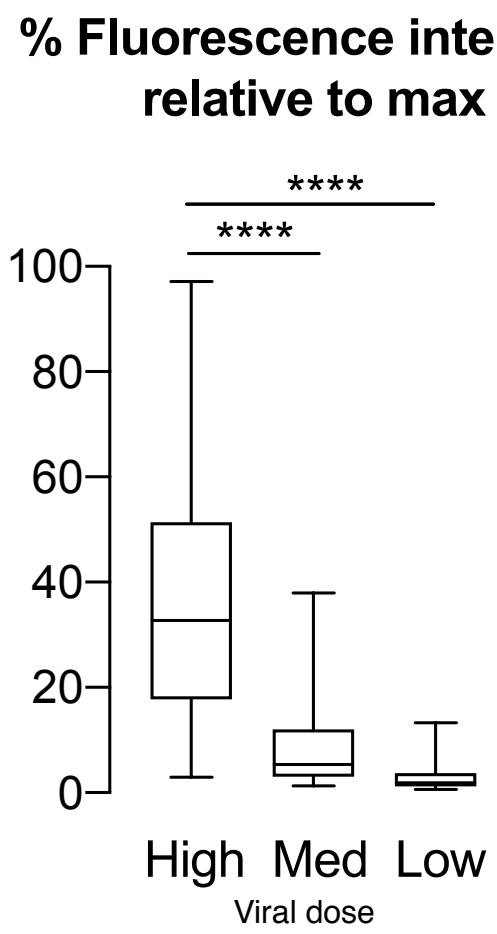

Figure 5.13. Test of three doses of virus for multicolor nerve labeling. Fluorescence intensity was dose dependent. Doses were compared using a Kruskal-Wallis test with Dunn's post-hoc test. Fluorescence intensity represents the average intensity in a single nerve soma with the three color channels added together. ****$p<0.0001$. n = 41-139.

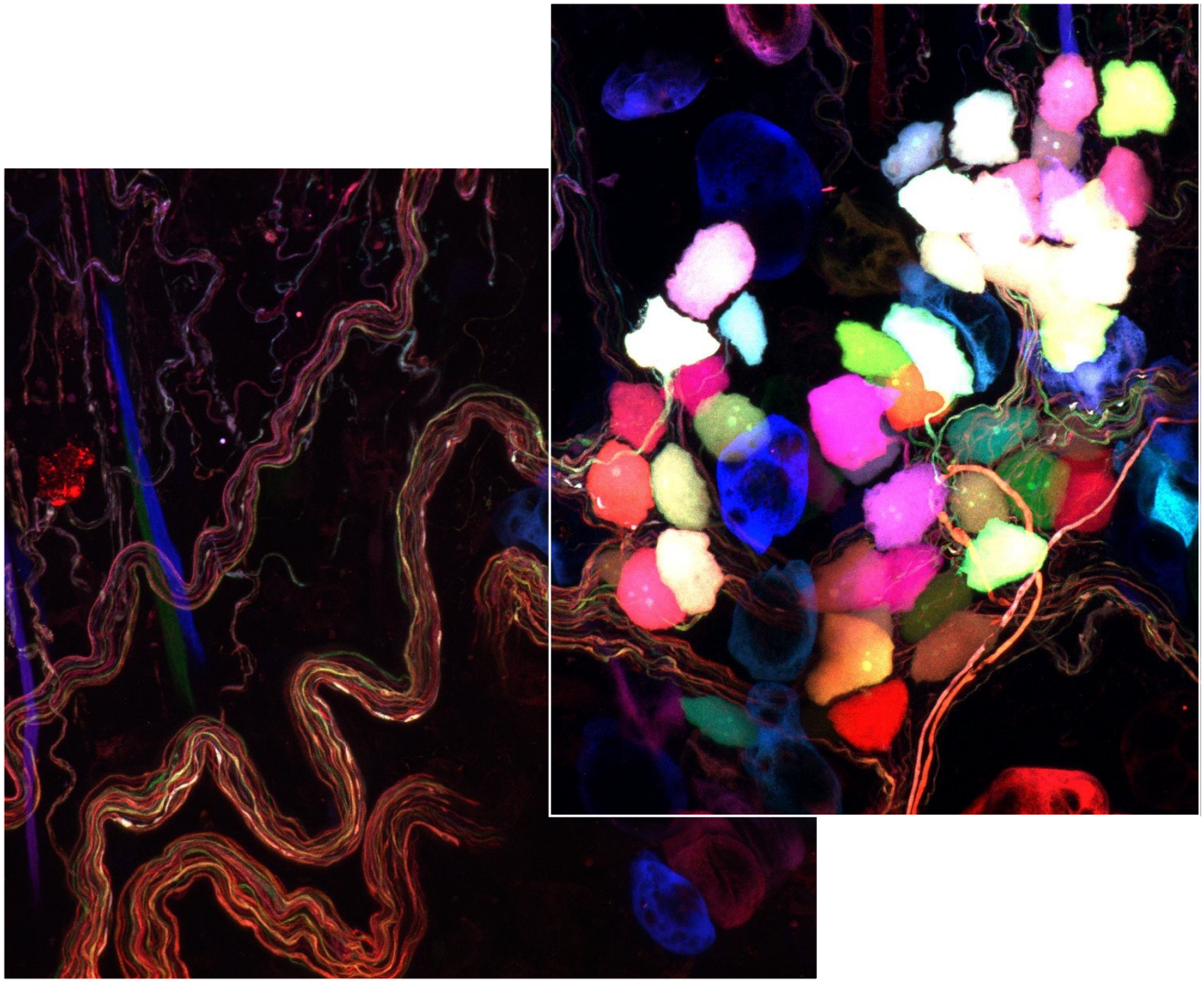

Figure 5.14. Imaging of ganglia and nerve fibers labeled with many colors. Ganglia is the same as seen in the high dose mouse of figure 5.12. These images show the ganglia and the path of a nerve bundle exiting the ganglia and traveling to the left out of the first image. Images can be taken at different times and then later combined for tracing studies. Trace of these neurons using FIJI nTracer plugin shown in figure 5.15.

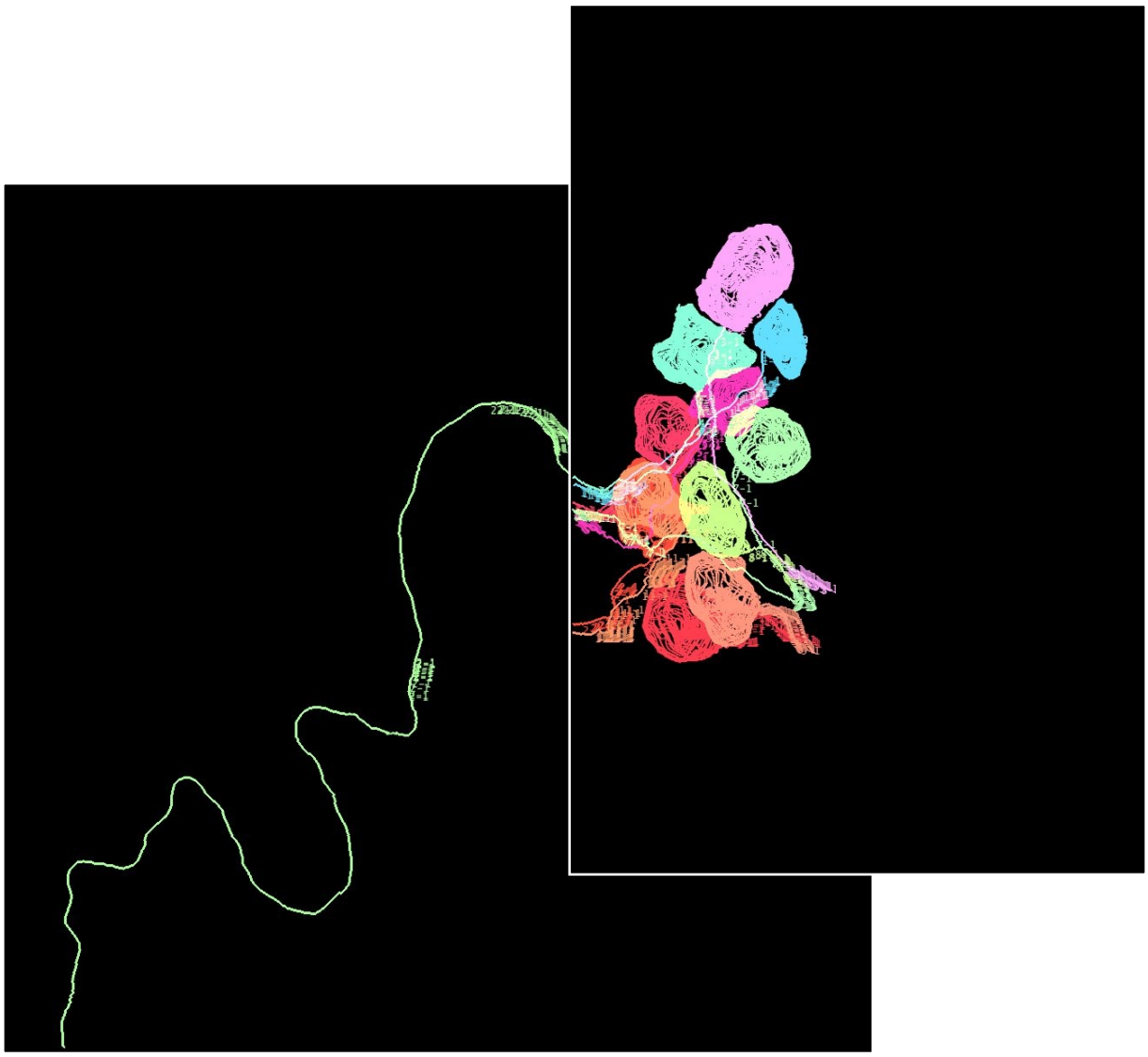

Figure 5.15. Trace of subset of neurons shown in figure 5.14, including on axon traced all the way out of the ganglia and through to its exit in the image on the left. Image made using nTracer plugin for FIJI.

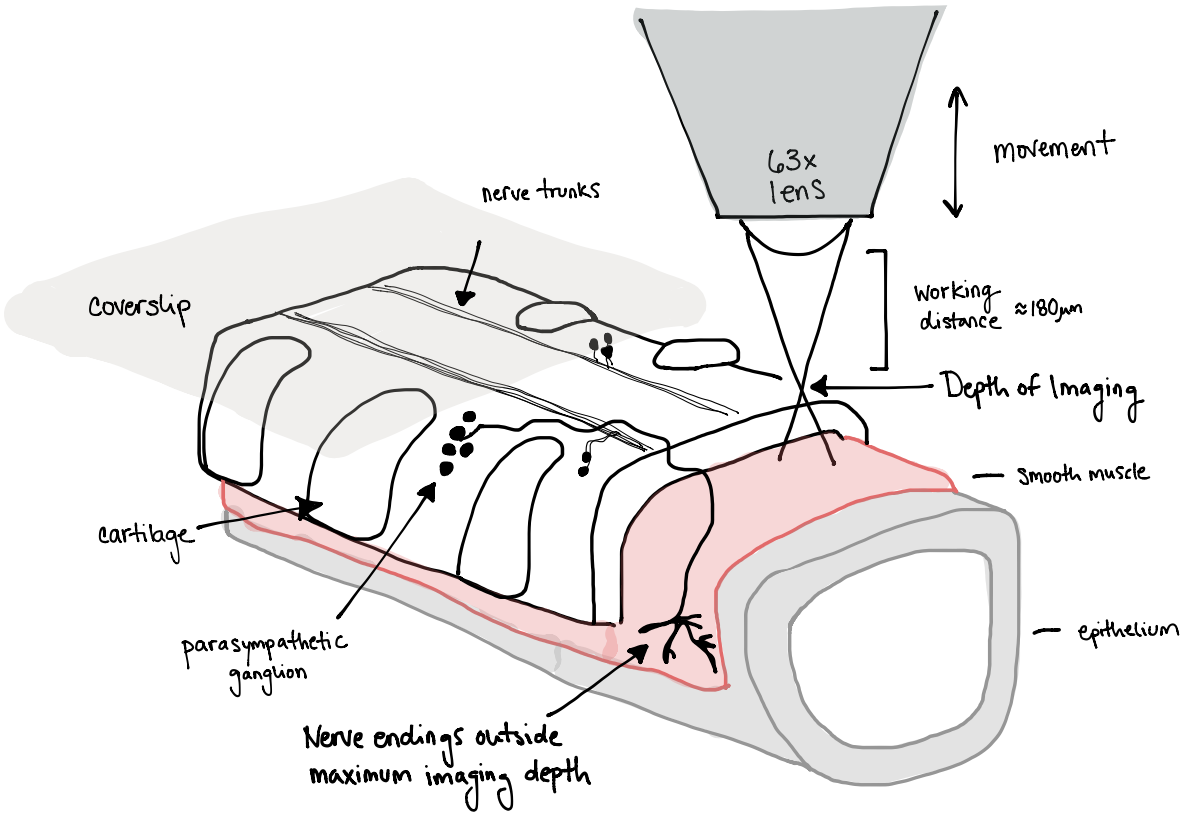

Figure 5.16. Diagram showing a whole mount trachea underneath a coverslip and a 63x lens with working distance of 180 μm. This working distance is not sufficient to capture the full depth that axons of parasympathetic nerves travel into the tissue, which makes it difficult to trace nerves to their innervation targets. Adapted from Widdicombe 2001.

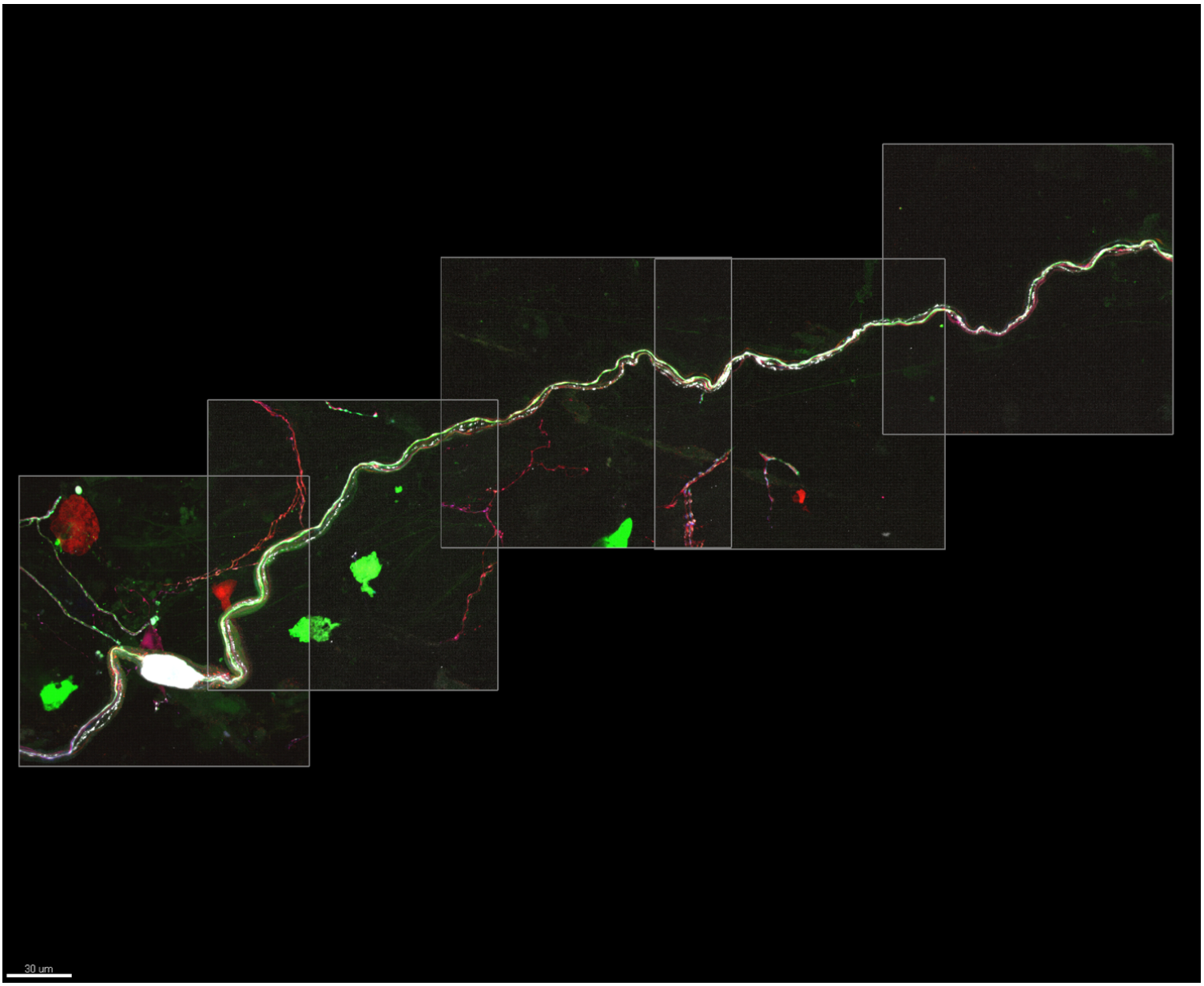

Figure 5.17. Nerve labeled with multicolors and with antibody against substance P (white). Many overlapping images were taken at 63x and later stitched together to trace the axon through the tissue. Image created using Imaris Stitcher.

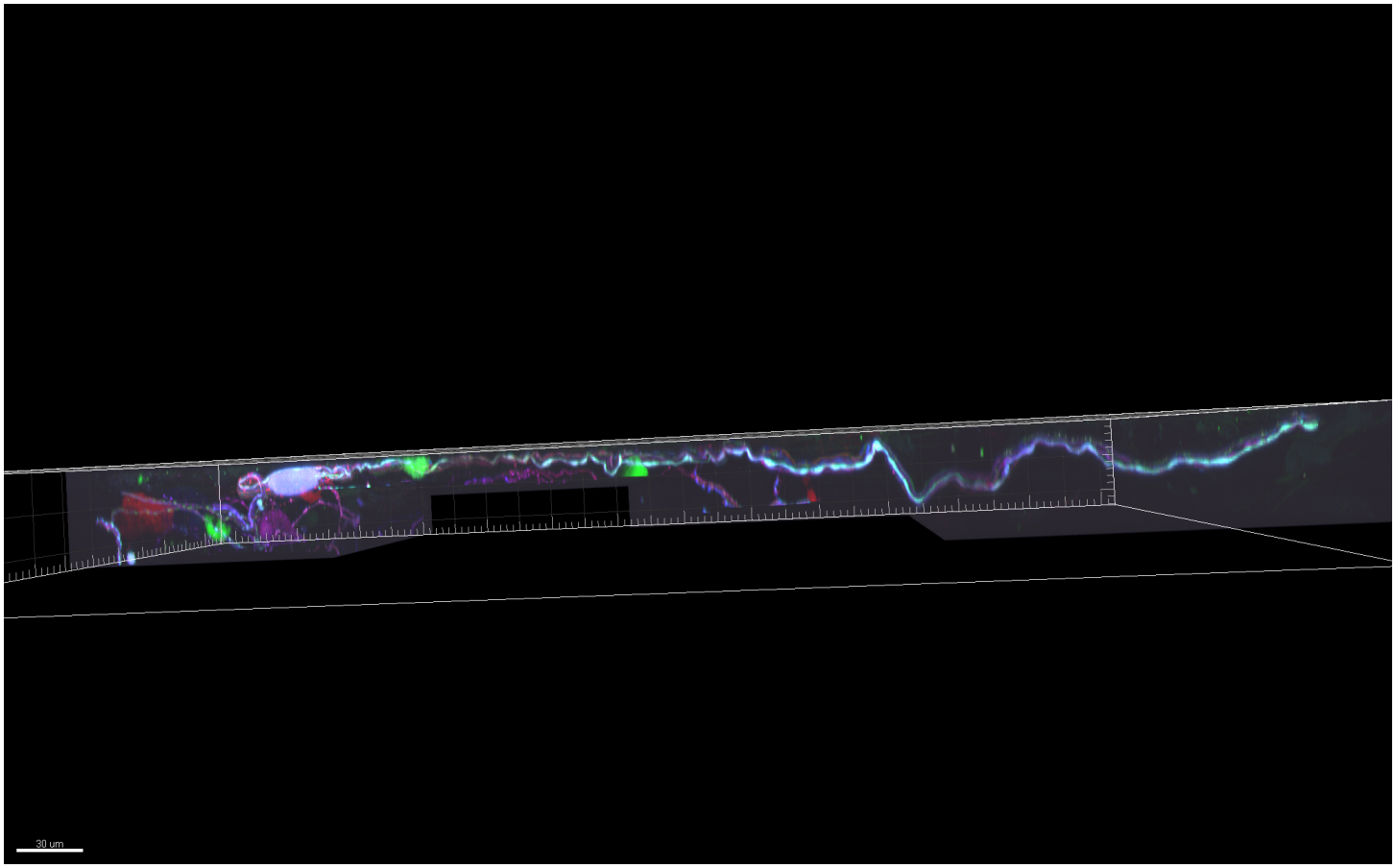

Figure 5.18. Orthogonal view of substance P positive multicolor neuron shown in figure 5.17. Image created using Imaris software.

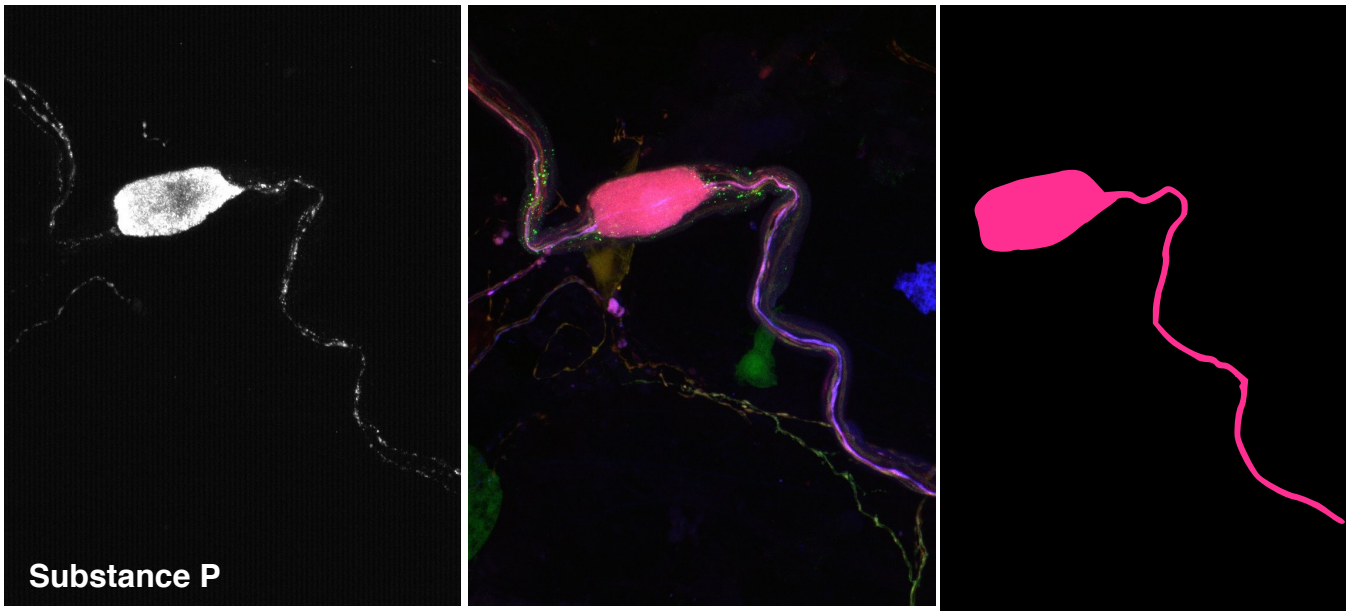

Figure 5.19. Substance P labeling in mouse airway with multicolor nerves. Left panel shows immunofluorescent labeling with antibodies against substance P (white). Middle panel shows same image with multicolor nerve fluorescence. This substance P positive neuron formed its own single-neuron ganglion and its axon exits to the right of the image, as shown in the nTracer trace in the panel on the right.

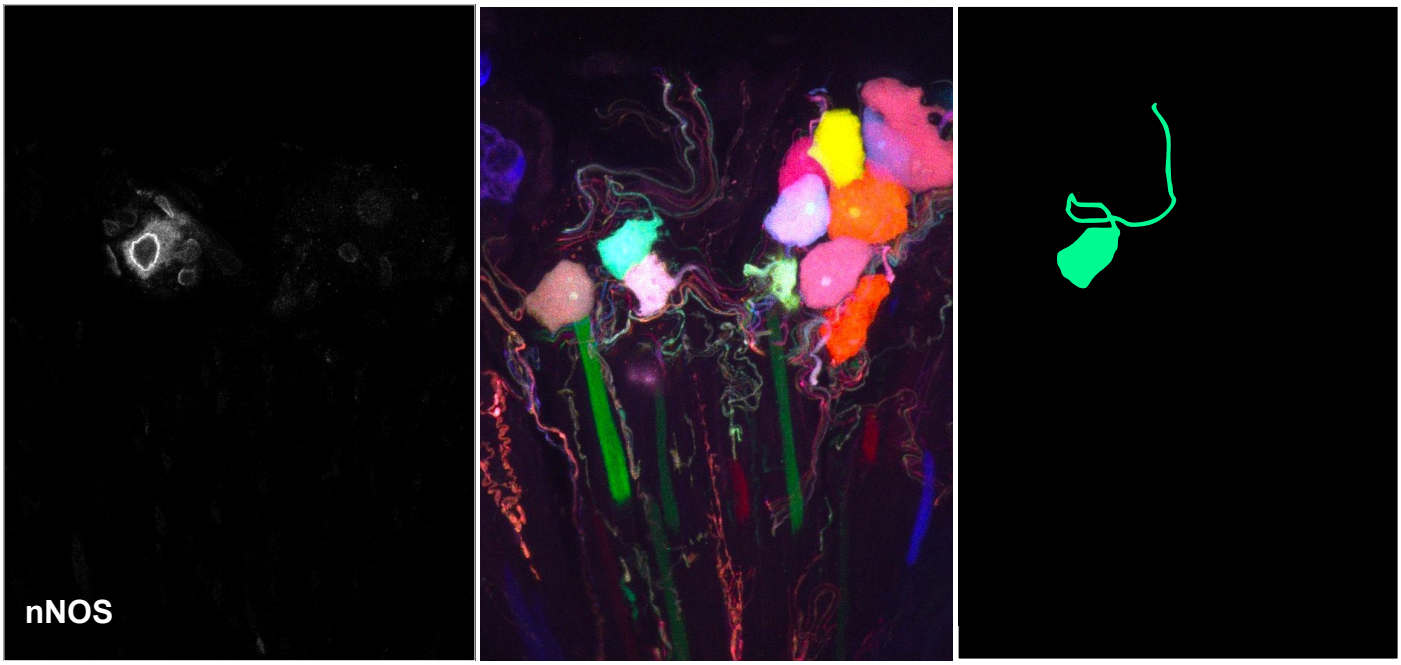

Figure 5.20. nNOS labeling in mouse airway with multicolor nerves. Left panel shows immunofluorescent labeling with antibodies against nNOS (white). Middle panel shows same image with multicolor nerve fluorescence. This nNOS positive neuron is green and its axon exits at the top of the image and outside of the acquired z plane, as shown in the nTracer trace in the panel on the right.

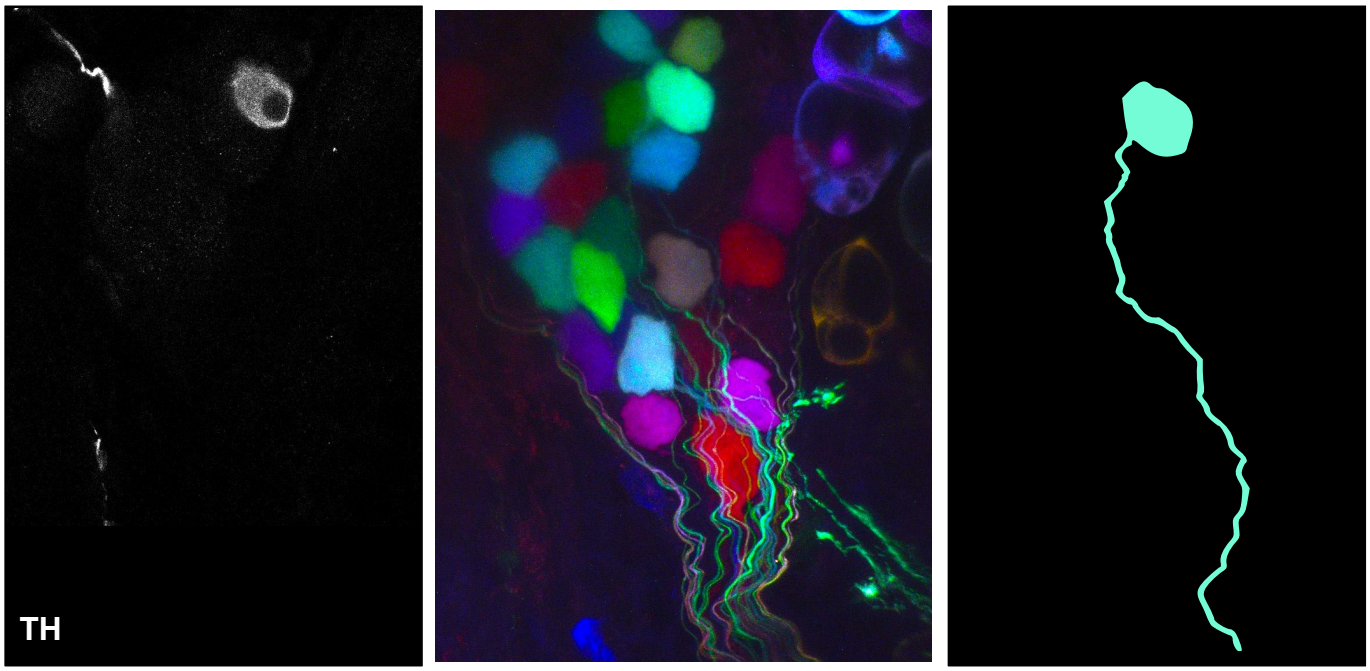

Figure 5.21. Tyrosine hydroxylase (TH) labeling in mouse airway with multicolor nerves. Left panel shows immunofluorescent labeling with antibodies against TH (white). Middle panel shows same image with multicolor nerve fluorescence. This TH positive neuron is bright green with a blue tint, and its axon exits at the bottom of the image, as shown in the nTracer trace in the panel on the right.

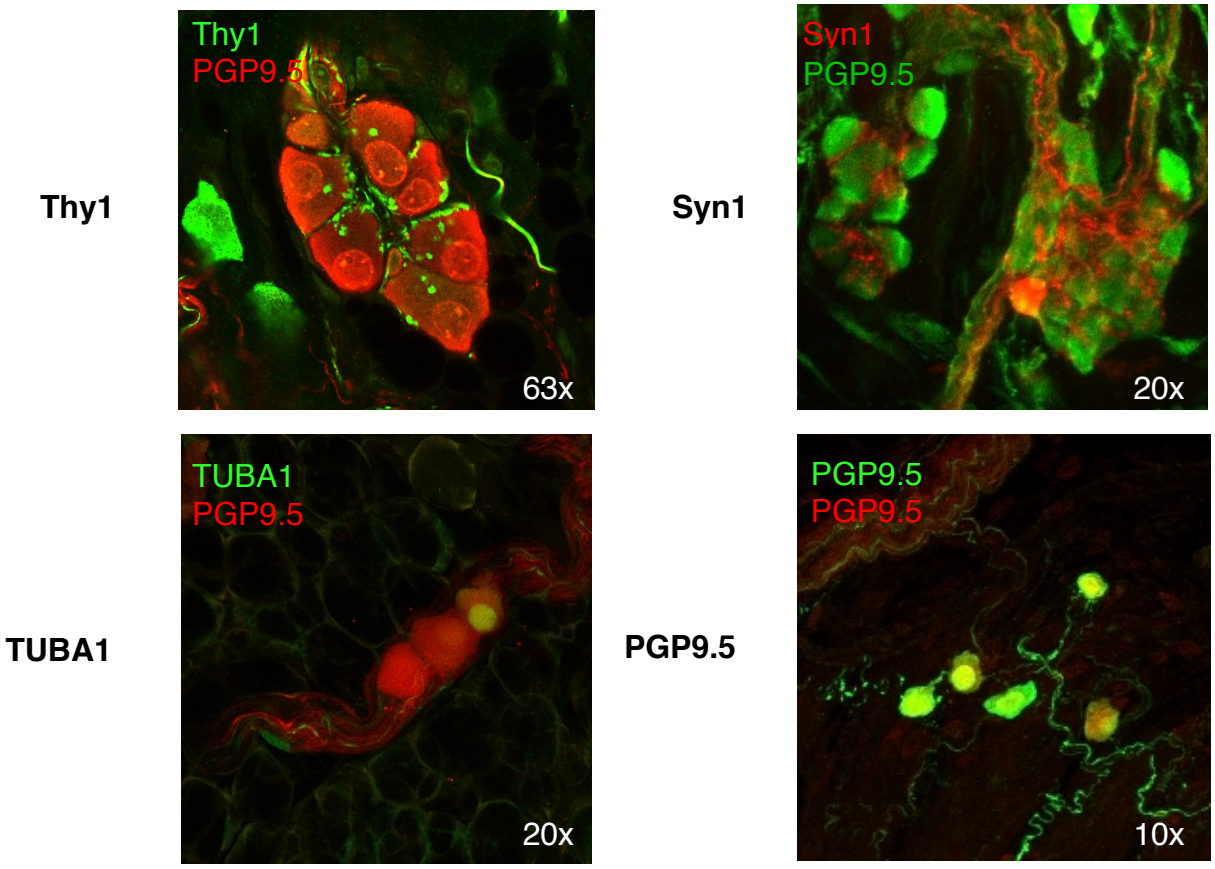

Figure 5.22. Promoters driving expression in parasympathetic ganglia. Similar to postganglionic parasympathetic ganglia in other areas of the organism, Thy1 did not drive expression in our neurons of interest. Syn1 drove fluorescent protein expression in only a few neurons in the trachea. TUBA1 drove expression in the vast majority of parasympathetic neurons but not all, as shown. PGP9.5 drove robust expression in all neurons. Tissues labeled with PGP9.5 antibody and antibodies against fluorescent proteins driven by specific promoters.

Discussion

This study presents the first reported identification of airway postganglionic parasympathetic neurons expressing nNOS and TH. This opens up exciting possibilities for differential function roles of these nerve subpopulations, and perhaps even more importantly differential regulation and importance for airway diseases. Previous studies of substance P expression in airway parasympathetic neurons have suggested a role in airway hyperreactivity (Wu et al., 2003), but more research is needed to understand this nerve subset. Future studies, such as single cell RNA sequencing and optogenetic nerve activation, could shed more light on the characteristics and role of these nerve subgroups.

This study is also the first to report the successful infection of airway parasympathetic neurons using viral vector strategies. I show that the capsid AAV9 is capable of driving expression of fluorescent proteins in airway nerves after intravenous injection, and at viral titers equivalent to that used for other peripheral organs (Rajendran et al., 2019). The capsid AAV-PHP.S has been previously recommended for studies of peripheral nerves requiring viral infection, and although I found it more expedient to produce viruses using AAV9 I did observe some infection outside of neural tissue. It is possible that AAV-PHP.S would offer improved specificity for future studies.

The role of SP, nNOS, and TH neurotransmitters in other nerve populations may shed some light onto their potential function in airway parasympathetic nerves. Substance P is a neuropeptide involved in inflammation, the axon reflex, and sensory hyperreactivity. Neuronal nitric oxide is a bronchodilator, usually produced by a separate population of parasympathetic neurons with cell bodies located in the esophagus. Tyrosine hydroxylase is an enzyme necessary for the production of dopamine, epinephrine, and norepinephrine, and is usually found in sympathetic nerves, which synapse onto parasympathetic nerves in the airways and act to inhibit bronchoconstriction. It is possible that these small subgroups of neurons are serving similar functions to their sensory, esophageal, and sympathetic counterparts. One hypothesis is that these may represent a population of interneurons, synapsing onto other parasympathetic nerves within the airway and serving to modulate their function. However, the results from our tracing study show that if these SP, TH, and nNOS positive cells are indeed functioning as interneurons, they are not doing so within a single ganglia.

In this study I show that multicolor labeling of airway neurons is feasible using viral vector strategies. This represents a significant step forward for the field of airway neuron research, especially as viral vectors can be employed with larger animal models for which transgenic organisms are not readily available, such as guinea pigs and rats. Yet there are also disadvantages to this approach. A large dose of administered virus is necessary to achieve transduction with multiple copies of virus in all airway neurons, as needed for multicolor labeling. This may lead to inflammatory reactions within animals, and high titers means that experiments with multiple animals become increasingly expensive. For imaging purposes, it should be noted that the randomness of transduction leads to different copy

numbers of fluorescent protein in each neuron, which leads to unevenness in fluorescence intensity. All of these downsides would be alleviated by the creation of a Brainbow-like mouse that could drive expression in parasympathetic nerves. The creation of such a mouse would require an alternative promoter to Thy1, one that is able to express in all nerve types within the airway but is also nerve specific. Our research suggests that an abbreviated version of the PGP9.5 promoter is an ideal candidate. Once transgenic mice are created they are relatively inexpensive to reproduce, and the nature of the genetic insertions used to create Brainbow mean that each neuron expresses the same number of fluorophores, only in different ratios, thus achieving uniform fluorescence. Importantly, such mice could also be bred with Cre-lox lines to endogenously express fluorophores in specific subtypes of nerves, expanding the utility of this tool. In summary, I hope this research paves the way towards further studies into airway parasympathetic nerves and the key role they play in airway disease.

B. Creation of a transgenic mouse with peripheral multicolor nerve capability

Introduction

Brainbow mice provide the field of neuroscience a facile and accessible method for multicolor labeling of neurons, which allows researchers to easily distinguish clusters of nerve cell bodies and tracks of nerve axons even when they are in close proximity to one another (Livet *et al*., 2007). I sought to use Brainbow mice to study nerves in the airways, including populations of sensory and parasympathetic neurons that play an important role in asthma and airway pathology. However, Brainbow mice rely on the Thy1 promoter to drive nerve specificity, and imaging studies from our lab showed this promoter was unable to drive protein expression in postganglionic parasympathetic neurons (Figure 5.22), one of the nerve populations I was particularly interested in studying. To address this, I am creating a novel mouse line that will better facilitate the study of peripheral nerves. I will be referring to this as the PANbow mouse line, which stands for Peripheral Autonomic Nerve rainbow mouse.

Brainbow mice rely on the expression of random combinations of three fluorophores to generate bright, fluorescent labeling over a wide spectrum of colors within neurons. Transgenic mice represent an improvement over other methods of multicolor nerve labeling, such as viral vector methods, in that they have a more consistent expression level of fluorophores within each nerve cell. For PANbow, I am attempting to create a mouse line very similar in genetic construction to the Brainbow 3.2 line (Cai *et al.*, 2013). I have kept the same construction of a single neuronal promoter driving expression of four potential proteins: one expressed as a default, and three which may be randomly chosen instead of the default by Cre-lox recombination. I selected fluorophores optimized for bright and non-overlapping endogenous fluorescence. For the default protein, I used a large non-fluorescent globular protein (HaloTag; Los et al., 2008) that has click chemistry with small fluorescent molecules (Janelia Fluor; Grimm et al., 2015). Finally, a limiting factor in the PANbow design was finding a promoter that would drive protein expression in both sensory and parasympathetic airway neurons. Testing promoters with different mouse lines, as well as AAV vectors, revealed an abbreviated version of the PGP9.5 promoter as the most promising candidate (Chapter 5A). I used Thermo Fisher's GeneArt program to create the complete PANbow gene construct, including promoter sequence and all fluorescent protein sequences, and will begin the process of validation prior to pronuclear injection as soon as it arrives (Figure 5.23). Additionally, I created a second gene construct using the same PGP9.5 promoter to drive expression of tamoxifen-inducible Cre protein (Figure 5.24). I will also validate this construct and use it to create a second mouse line, PGP9.5-iCre mice, which could be bred with the PANbow mouse to activate multicolor labeling in all PGP9.5-expressing neurons. Together, I hope these new mouse lines will provide useful tools for studying airway disease.

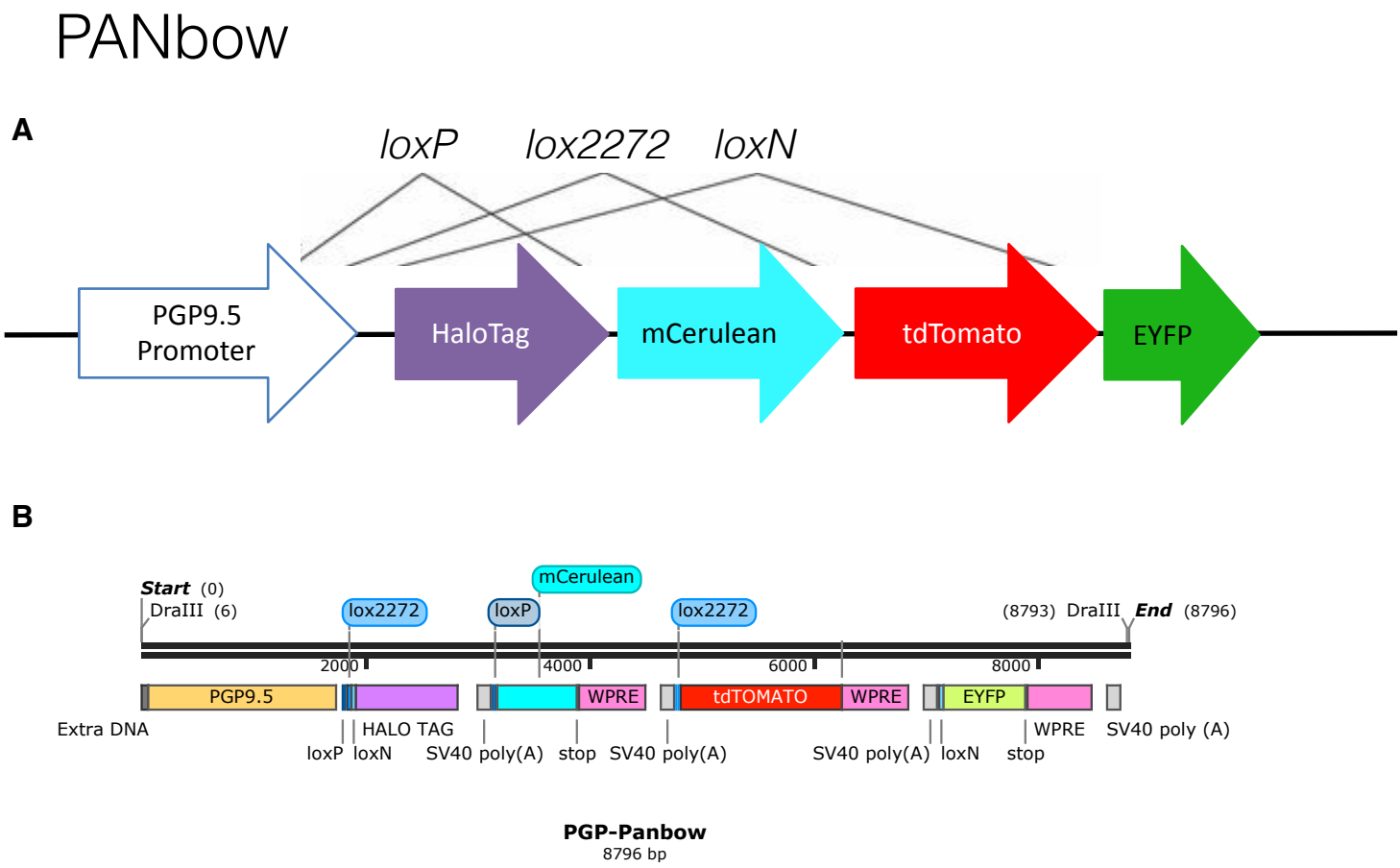

Figure 5.23. Genetic construct used to produce PANbow mouse. This construct is designed to be inserted multiple times into the genome, and to be combined with Cre recombinase systems for multicolor labeling of subsets of neurons. (A) Basic structure. (B) Detailed map. Full sequence available in appendix. Map made using SnapGene.

PGP9.5-iCre

A

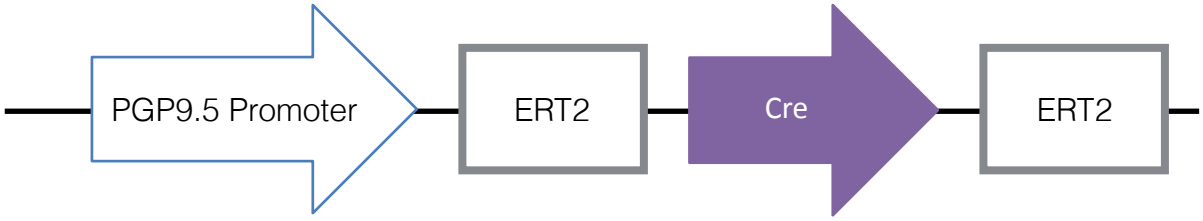

B

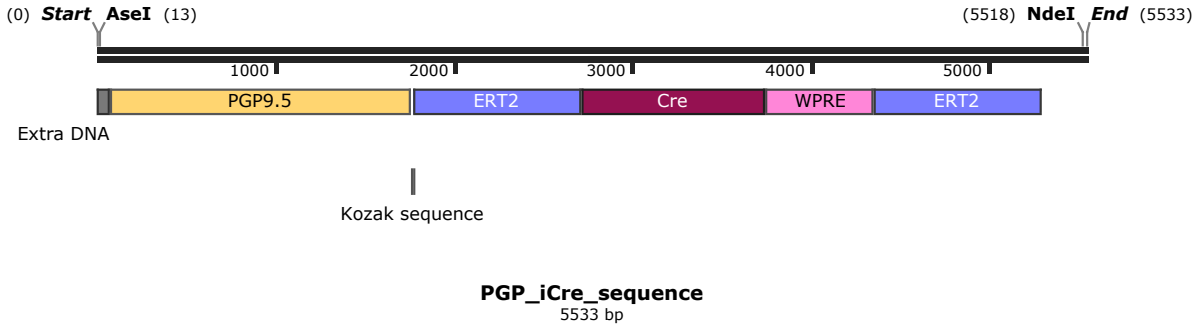

Figure 5.24. Genetic construct used to produce PGP9.5-iCre mouse. This construct is designed to be combined with floxxed systems to drive expression of a protein in peripheral neurons. Flanking ERT2 sites ensure Cre is only active after tamoxifen is introduced to the system, allowing for temporal control over expression. (A) Basic structure. (B) Detailed map. Full sequence available in appendix. Map made using SnapGene.

Experimental Design

Validation of PGP9.5 with AAV9

See Chapter 5A for information of the creation of AAV9 vectors to test promoter expression in parasympathetic ganglia. AAV9 with an abbreviated version of the PGP9.5 promoter driving GFP expression was injected into C57BL/6 mice at a viral titer of 3×10^{12}. The PGP9.5 promoter drove robust expression in all observed parasympathetic neurons, and was selected as the best promoter for PANbow.

Design of PANbow construct

Brainbow 3.2 scaffolding

The Brainbow 3.2 sequence was used for the overall structure of PANbow. This included: three pairs of nested incompatible lox sites (loxP, loxN, and lox2272) set between the fluorophores to allow stochastic expression of only one fluorescent protein after Cre-lox recombination, Kozak sequences preceding each fluorophore to initiate transcription, polyadenylation sequences following each fluorophore to halt transcription, and woodchuck hepatitis virus post-transcriptional regulatory elements (WPRE) to enhance expression. To the ends of the construct I added restriction enzyme sites (DraIII) to facilitate easy linearization of DNA for pronuclear injection.

Fluorophores

The three fluorophores selected for PANbow were mCerulean, EYFP, and tdTomato. These were selected to maximize intensity and contrast on a confocal laser-scanning microscope with excitation lasers at 405 nm, 488 nm, and 561 nm, and to leave an opening for labeling other cells or structures in the far-red spectrum (Figure 5.25). TGA stop codons were used for each fluorophore to optimize efficiency in mice.

HaloTag

I chose HaloTag (Los et al., 2008) as the default protein to be expressed in all cells without Cre recombinase under the PGP9.5 promoter. HaloTag is a large, globular protein - a modified haloalkane dehalogenase that forms a covalent bond with synthetic ligands using a chloroalkane linker. HaloTag is not fluorescent, but the chloroalkane linker has been added to a variety of fluorescent proteins (Grimm et al., 2015) with the ability to traverse cell membranes in both fresh and chemically fixed tissue and form stable bonds with HaloTag protein. Thus, HaloTag acts as a docking site where other molecules bind using click chemistry. I anticipate situations where a certain population of nerves, as selected by breeding to a Cre-lox mouse line, has been labeled with many colors, yet where it is still desirable to visualize the other nerves around this population. In such a situation, Janelia Fluor HaloTag ligands in

the far red spectrum could be rapidly washed over the tissue, efficiently labeling all non-multicolor neurons more easily and quickly than using immunofluorescence.

Sequencing validation

To validate our sequences, primers will be designed that span the full constructs in both the 5' to 3' and 3' to 5' directions. Primers will be spaced ~600bp apart with overlapping regions of at least 50bp. The online platform NIH BLAST will be used to compare sequence results to *in silico* constructs (see appendix for full PANbow and PGP9.5-iCre sequences). The functional effects of any discrepancies will be evaluated using transfection and imaging in a neuroblastoma cell line.

Neuroblastoma cell line transfection and imaging

In order to verify correct functionality of the PANbow construct I will transfect a neuroblastoma cell line with both PANbow and Cre plasmids. Neuroblastoma cells will be grown to 50% confluence, then cells and DNA plasmids will be combined with Lipofectamine 2000 (Thermo Fisher) according to manufacturer instructions. A range of PANbow DNA concentrations will be used such that some cells will likely be transfected with only one copy of the plasmid while others will have multiple. It is important to ensure both that all fluorophores (and HaloTag) are expressed, and that fluorophores may be expressed individually, to ensure the construct is not "leaky". For an 8 well tissue culture slide, 40 μL OptiMEM should be combined with 0.7 μL Lipofectamine and 20-200 ng of each DNA plasmid. Post-transfection, cells should be incubated at 37^0C for 48 hours to visualize fluorescent protein expression.

Linearization and purification

PANbow and PGP9.5-iCre plasmids will be linearized using restriction enzymes to produce DNA with sticky ends. Results of restriction enzyme digest will be gel extracted, and intactness of DNA will be verified using mini gel electrophoresis. Frozen DNA will be submitted to OHSU Transgenic Mouse core, where it will be inserted into embryos via pronuclear microinjection and used to create the PANbow and PGP9.5-iCre mouse lines.

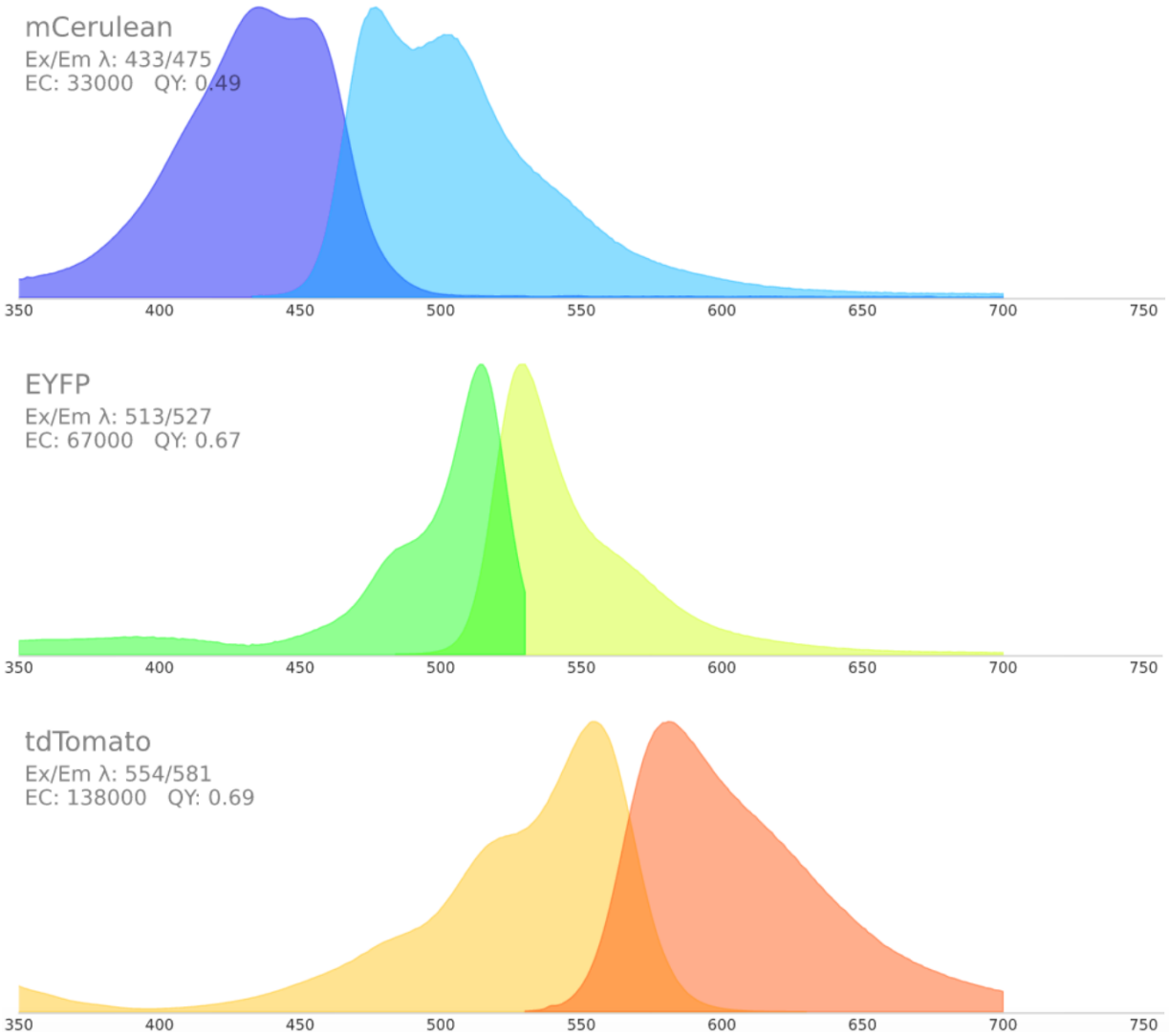

Figure 5.25. Excitation and emission spectra of fluorophores used for PANbow mouse. Images from fpbase.com. Note that the far red spectrum is free for labeling all neurons using Janelia Fluor Halo Tag or for labeling other structures of interest.

Discussion

Identifying targets of innervation is a key step in understanding the function of novel nerve populations, especially in the peripheral system. Multicolor nerve labeling and tracing studies have the capacity to identify innervation targets for subpopulations of nerves within complex pathways, but the tools for such studies have not yet been developed for airway nerves. Our goal in making the PANbow mouse line is to provide tools for further understanding airway nerve subpopulations relevant to airway diseases. By breeding PANbow mice with Cre-lox lines, I will be able to limit the expression of multicolor fluorophores to specific subsets of nerves, and such sparse labeling of individual neurons will allow for comprehensive anatomical characterization that is not currently possible.

Airway parasympathetic nerves containing substance P, neuronal nitric oxide synthase, and tyrosine hydroxylase are some of the nerve populations I hope to study in the future using PANbow mice. Substance P expressing nerves in parasympathetic ganglia are differentially expressed in mouse models of asthma, and my preliminary studies suggest that multiple populations exist even among this subset of nerves (Figure 5.26 and 5.27). Tracing the targets of innervation would help us begin to establish functional differences among these nerve subsets, with the eventual goal of developing an atlas of airway parasympathetic nerves, similar to that available for the brain.

Within the airways, different nerves innervate airway epithelium, airway smooth muscle, mucus glands, vascular endothelium, and other airway neurons. Any of these tissues may be potential innervation targets for airway nerve subpopulations. When the PANbow mice are ready for analysis, it will be essential that innervation studies maintain as much of the integrity and complexity of airway tissues as possible in order to ascertain the true innervation targets for the nerves in question. At the same time, some tissue manipulations will likely be needed for high magnification imaging of individual nerve fibers, including potentially unmounting and rotating the tissue in order to keep axons close to the coverslip. Tissue clearing will be essential, and it is likely that multiple rounds of tissue imaging will be necessary to fully capture nerve pathways.

In summary, the PANbow mouse line is a tool that I hope will advance studies into the complex architecture of airway nerves and the key role they play in airway disease.

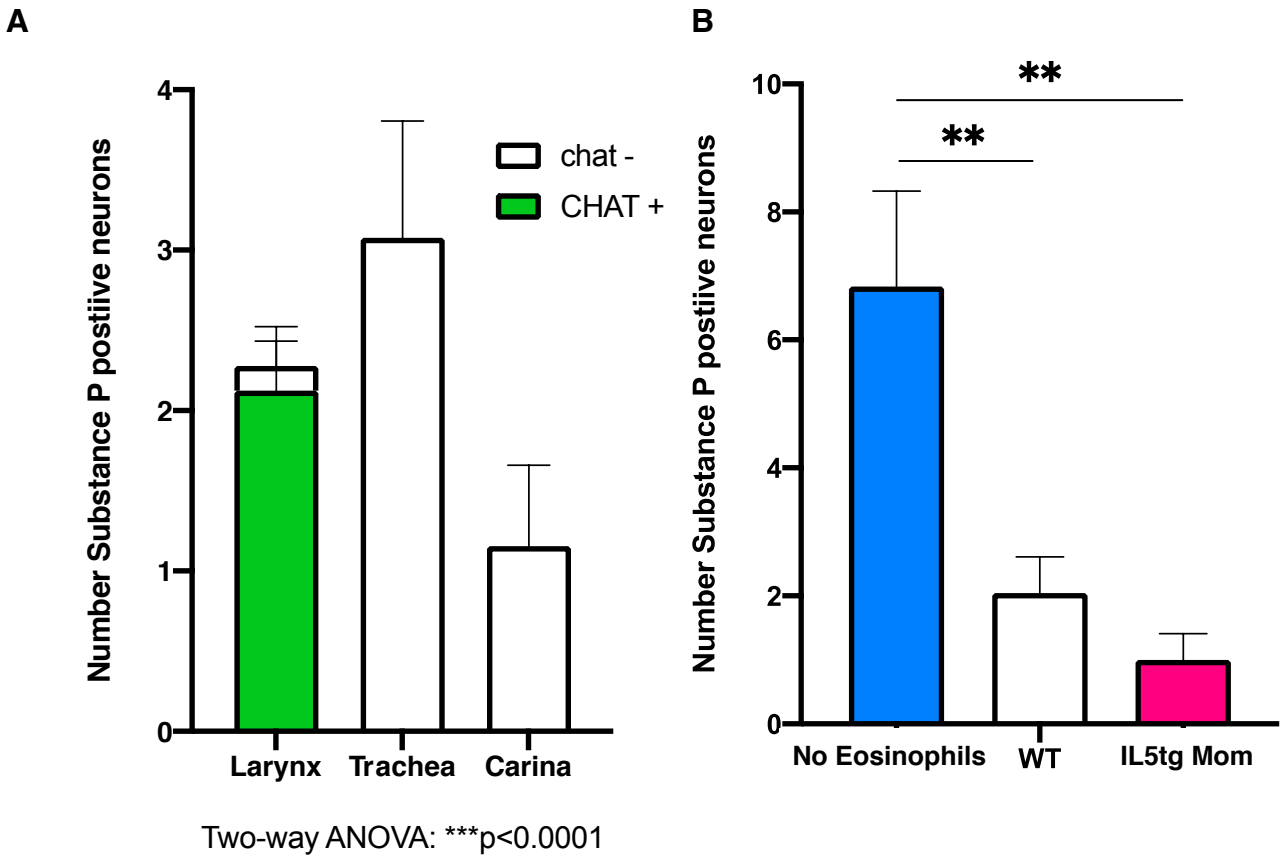

Figure 5.26. Evidence for subtypes of substance P-expressing airway nerves. (A) In heterozygous CHAT-CH2 mice (described in chapter 3), which had parasympathetic neurons both with and without CH2 expression due to variability in efficacy of CHAT-Cre, it was noted that neurons labeled with both substance P and CH2 (therefore with an active CHAT promoter) were always located near the larynx, while many mice had neurons that labeled with substance P but not CH2 in the trachea and carina regions. Examples shown in figure 5.27. (B) Mice with no eosinophils and wild type mice born to a father with no eosinophils had greater substance P positive nerves in their parasympathetic ganglia than wild type mice born to wild type parents or mice born to mothers with IL-5 driving eosinophilia. One way ANOVA with Sidak post-hoc test. **p<0.01.

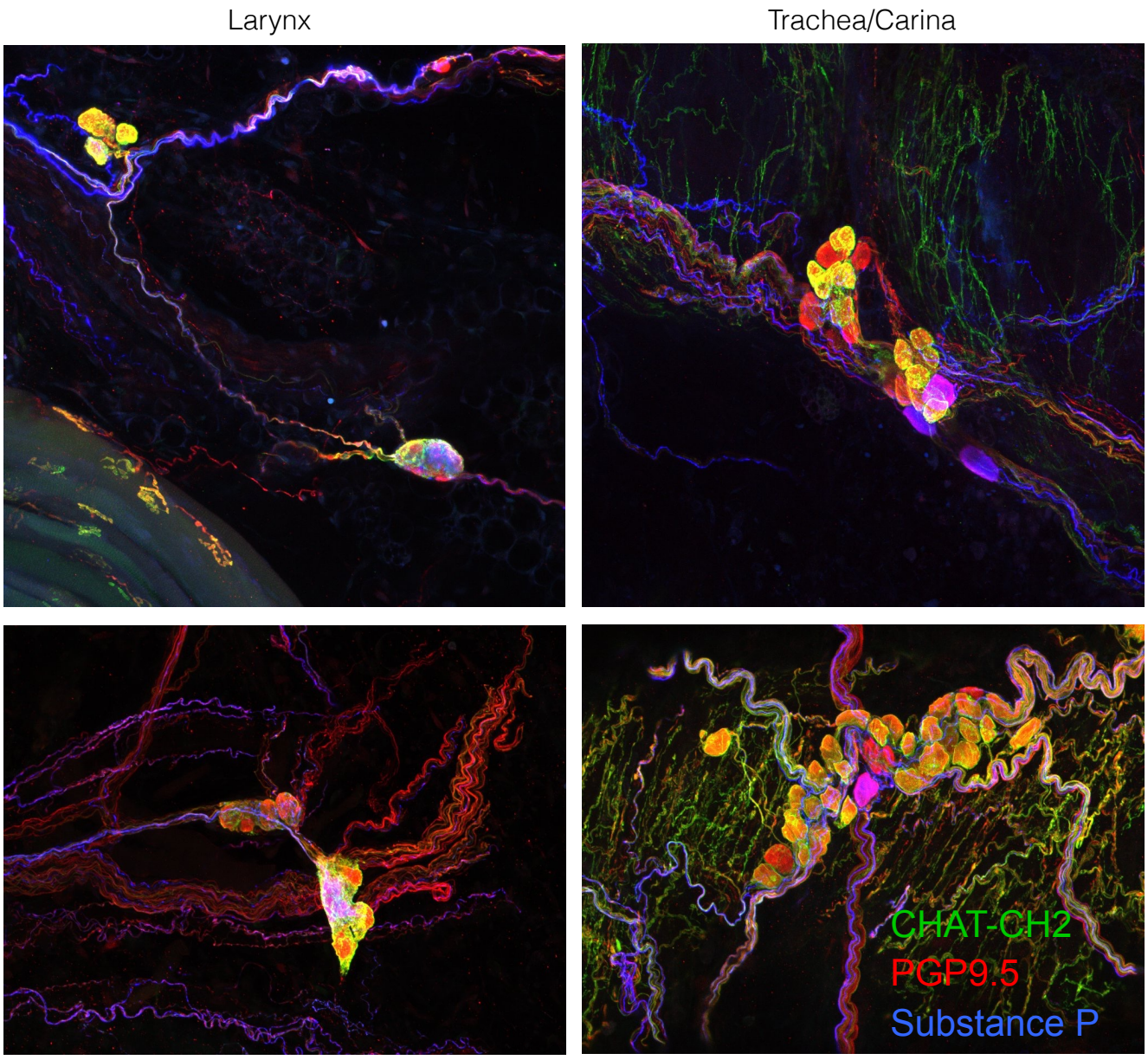

Figure 5.27. Examples of substance P nerves in parasympathetic ganglia in CHAT-CH2 heterozygous mice. Nerves near the larynx labeled with PGP9.5 (red), substance P (blue), and CH2 (green), while substance P nerves in the trachea and carina region were never CH2 positive, suggesting the possibility that these nerves may not express acetylcholine, and that substance P expressing nerves in these two anatomical regions may serve different functions.

Chapter 6. Summary and Conclusions

Asthma is a highly prevalent airway disease for which treatment, despite many recent advances, remains inadequate for many patients. Research has revealed long term structural changes to the airways that would need to be understood and reversed in order for treatments to return lung function to healthy levels in all patients. Airway hyperreactivity is a fundamental characteristic of asthma, defined as increased bronchoconstriction in response to inhaled agonists, and is mediated by airway nerves. Although some of the neural mechanisms underlying this hyperreactivity are well understood, such as the key role played by eosinophils in mediating M_2 muscarinic receptor dysfunction, much more remains to be studied. Recent research has found increases in sensory innervation (Drake *et al.*, 2018) and cholinergic innervation (Dragunas *et al.*, 2020) in severe asthmatics and chronic mouse models of asthma. It remains unclear how these morphological changes relate to nerve function.

It is my hypothesis that structural changes to the sensory and parasympathetic nervous systems contribute to airway hyperreactivity associated with asthma. However, the complexity of the sensory and autonomic nervous systems makes it difficult to identify a role for specific nerves in airway hyperreactivity. In this dissertation, I describe the development of novel tools to depolarize specific nerve populations and image individual nerves in the airways. My data demonstrates that these tools can be used successfully to identify the role of unique subsets of nerves in airway hyperreactivity. I use a combination of optogenetics and imaging to demonstrate that differences in eosinophil localization and nerve interactions leads to parasympathetic nerve hyperreactivity in an acute antigen challenge asthma mouse model but not in a mouse model of chronic airway hyperreactivity and eosinophilia. Overall, my dissertation 1) demonstrates a successful protocol for optogenetic activation of airway nerves, both parasympathetic and sensory, 2) uses optogenetics to show differences between different mouse models of eosinophilic asthma in the mechanism of hyperreactivity, 3) assesses eosinophil localization around airway nerves to explain hyperreactivity differences, 4) optimizes tools for multicolor labeling and nerve tracing that can be used to image airway nerves and their connections, and 5) develops a brainbow-like genetic construct with utility for labeling autonomic nerves in the airways and other systems, which will be used to improve analysis of parasympathetic nerve subpopulations in the future.

Optogenetic activation of airway nerves

My data demonstrate the capability of optogenetics to interrogate nerve subpopulations in airway hyperreactivity. Optogenetic activation of airway parasympathetic neurons in mouse models of asthma, as well as in healthy mice given physostigmine, produces robust and measurable bronchoconstriction that is directly correlated to the proportion of parasympathetic neurons expressing channelrhodopsin (Figure 3.9). Although the protocol requires some specialized equipment, the widespread use of optogenetics in the central nervous system means the technology is

readily accessible from many commercial sources, and is easy to adapt for any laboratory with an established mouse ventilation apparatus. The most technical aspects involve placement of the cannula in the mouse trachea, which should be placed as proximally as possible to allow unimpeded light transmission through to the dorsal aspect of the tissue, and the surgical resection of tissue above the trachea, during which the operator must be sure to avoid severing any major blood vessels. As with any surgical technique, some practice will be required, yet the advantage of the large collimated light source is that once this basic surgery has been learned the placement of the light source is impossible to mistake (unlike the precise placement of fiber optic light sources necessary in other optogenetic surgeries), and so the technique is more easily accessible to new users. Although other studies (Chang *et al.*, 2015) have previously used optogenetics to activate airway sensory nerves, our study (Chapter 3) (Pincus *et al.*, 2020) was the first to activate airway parasympathetic nerves, thus expanding our ability to interrogate nerve mechanisms underlying airway hyperreactivity.

Parasympathetic hyperreactivity in mouse models of eosinophilic asthma

I used optogenetics to investigate sensory and parasympathetic nerve hyperreactivity in two mouse models of eosinophilic asthma. House dust mite (HDM) treatment is a model of acute antigen sensitization and challenge that causes wildtype animals to develop airway hyperreactivity within 3 weeks. Interleukin-5 transgenic (IL-5tg) mice are a genetically engineered mouse line where eosinophils are chronically overproduced and recruited to airway epithelial tissue. Both mouse models have neurally-mediated airway hyperreactivity to inhaled serotonin. I activated parasympathetic nerves in both of these models, and my data demonstrate that while parasympathetic nerves in the HDM treatment model are hyperreactive, those in the IL-5tg model are not (Figure 4.4). This finding has not previously been reported, and suggests different underlying mechanisms drive airway hyperreactivity in the two mouse models, which is important for our understanding of neural hyperreactivity in the more complicated landscape of human asthma. My finding of different pathways resulting in airway hyperreactivity is consistent with previous research into airway hyperreactivity in virus infected, obesity-related, and organophosphate exposure models, in which different immunological pathways all lead in the end to airway hyperresponsiveness (Fryer and Jacoby, 1991, Fryer *et al.*, 2004, Nie *et al.*, 2014).

Eosinophil localization around airway nerves

My data demonstrate that in the HDM treatment model, eosinophils associate closely with parasympathetic nerves (Figure 4.12), which may be a key driver for airway hyperreactivity. This finding is consistent with previous data from humans and guinea pig asthma models (Costello *et al.*, 1997), which analyzed thin histology sections and also demonstrated eosinophils clustering around airway nerves. One novel finding from my study is the anatomical localization of these eosinophil-nerve interactions: I found eosinophils in close proximity to nerves within the airway smooth muscle layer in HDM treated mice compared to saline controls, but I did not find any difference in eosinophil

localization around parasympathetic ganglia between these two groups. This has not previously been reported, likely because the method of three dimensional imaging in whole mount tissues allowed me to characterize eosinophil-nerve interactions with more precision than was previously possible. However, the possibility that eosinophil localization is different in my mouse model compared to humans and guinea pig models cannot be ruled out.

Future directions: optogenetics in parasympathetic and sensory nerves

Our original impetus for testing sensory vs parasympathetic nerves was to investigate whether increases in sensory innervation that had been previously observed in IL-5tg mice (Drake *et al.,* 2018) were mediating airway hyperreactivity in those animals. The sensory nerve increases were seen in both IL-5tg mice and humans with severe eosinophilic asthma, but were not seen in the HDM treated mouse model. My data from activation of sensory nerves in Advillin-CH2 mice demonstrate a moderate degree of hyperreactivity in HDM compared to saline treated mice (Figure 4.9).

Experiments on IL-5tg mice are underway. There are three possibilities for what this data will look like compared with HDM treated animals. One is that the airway bronchoconstriction to sensory stimulation will be higher in IL-5tg animals, due to increased sensory innervation causing hyperreactivity that is detectable by activating sensory but not parasympathetic nerves. A second possibility is that IL-5tg and HDM bronchoconstriction will look the same after sensory activation. This makes sense given the pathway of reflex bronchoconstriction: sensory nerves activate nerves in the brainstem, which in turn activate parasympathetic neurons, such that hyperreactivity anywhere in this pathway should increase the final output of bronchoconstriction. If sensory nerves are hyperreactive in IL-5tg mice and parasympathetic nerves are hyperreactive in HDM treated animals, then activating sensory nerves may result in similar levels of bronchoconstriction in both models, as seen with the serotonin dose response curves. The third possibility is that sensory activation in IL-5tg mice may be lower than in HDM treated animals. This data would be more challenging to interpret, but could be explained by differences in the relative proportion of sensory nerve subtypes, as described in the next paragraph.

In optogenetic experiments with Advillin-CH2 mice, all sensory nerves within our column of light are activated simultaneously. This may not be the optimal way to cause reflex bronchoconstriction - in fact, it is likely that activating only a subset of these nerves would be more effective. A recently published atlas of vagal sensory nerves defined 24 nerve subtypes based on single cell RNA transcriptome analysis (Kupari *et al.,* 2019). Of these, 7 subgroups express receptors for serotonin (presumably the groups activated by inhaled serotonin), including the subgroup responsible for sensing pulmonary volume, a group of polymodal mechanoreceptors, and a group involved in detecting satiety signals from the gut. Not, in other words, the optimal group for inducing bronchoconstriction. On the other hand, 6 subtypes (2 of which expressed serotonin receptors) were

identified as chemosensors potentially relevant to the pulmonary system, and I would venture to speculate that activating all of *these* nerves simultaneously would generate the strongest possible bronchoconstriction response. Instead, in Advillin-CH2 mice I am activating all subtypes simultaneously. On the one hand, this is limiting in that it 1) elicits a response which is unlikely to be seen under normal physiological circumstances, and 2) invites the potential for nerves activated simultaneously to act at cross-purposes to one another. On the other hand, in the emerging field of optogenetic activation of airway nerves, the results of our Advillin studies provide an important baseline for comparison for future studies to activate select subgroups of sensory nerves. It is also worth noting that the Kupari *et al.* study was performed on mouse ganglia that were naive to environmental allergens, and that the molecular profiles of mouse neurons exposed to house dust mite or a life of airway eosinophilia would likely look significantly different. A relevant follow-up study could investigate whether and how those categories of nerves changed after allergen sensitization, especially the subgroups of pulmonary chemosensors.

Multicolor labeling and tracing of parasympathetic nerves

Unlike sensory nerves, there is no atlas for parasympathetic nerves in the airways, and heterogeneity in this nerve population is severely understudied. Tools for multicolor labeling of nerves, such as the Brainbow mouse, can be used to study novel nerve populations, but such tools have not previously been described for use in airway nerves. Previous studies have advocated for the use of a specialized AAV capsid, PHP.S, for transducing peripheral sensory and parasympathetic neurons (Chan *et al.,* 2017, Rajendran *et al.*, 2019). My data demonstrate the viral capsid AAV9, which is far more readily available, successfully transduces airway parasympathetic neurons for tools such as multicolor labeling (Figure 5.12). I describe a pipeline for simultaneous imaging of endogenous multicolor expression and immunolabeled subsets of airway postganglionic parasympathetic nerves in optically cleared whole mount tracheas. Multiple clearing solutions, including BABB and ECi, were tested before finding Ce3D, which is the optimal clearing solution for my purposes because it preserves endogenous fluorescence, does not degrade silicone imaging wells, does not have an unpleasantly pungent aroma, and only requires a single emersion step rather than a more lengthy clearing protocol. I determined a range of working doses for intravenous administration of viruses to achieve 100% transduction and substantial color variation, and I demonstrate tracing of individual nerve axons within a limited range in airway tissue (Figure 5.15). The creation of this tool is a foundational step in the characterization and study of heterogeneous airway parasympathetic nerves.

My data validate previous unpublished studies from our laboratory (Lebold, 2018) that found substance P, neuronal nitric oxide synthase (nNOS), and tyrosine hydroxylase (TH) expression in mouse airway parasympathetic neurons. These findings are consistent with human studies, which have previously reported sparse staining of each of these proteins in parasympathetic ganglia (Scott *et al.*, 2014; Fischer *et al.*, 1996; Springall *et al.*, 1990). There is much that we still don't understand about

parasympathetic neurons, including why they form ganglia, whether or not the exact location of those ganglia is functionally relevant, and what function is performed by the subpopulations expressing substance P and other neurotransmitters. Interneurons, or neurons that form synapses and transmit signals between other neurons, are an important component of circuits in the central nervous system. I had hypothesized that one reason for the clustering of parasympathetic neurons into ganglia might be to group together neurons with slightly different functions, including perhaps interneurons that could tune up or tune down input from preganglionic parasympathetic, sympathetic, and sensory nerves. While previous studies have seen parasympathetic neurons synapsing onto one another (Coburn and Kalia, 1986), they used acetylcholinesterase activity for staining, and did not identify whether those nerves expressed any other neurotransmitters of interest. Using multicolor and antibody labeling, I was able to trace axons from parasympathetic neurons expressing substance P, nNOS, and TH in C57BL/6 mouse airways (Figures 5.19-5.21). None of these neurons projected to other parasympathetic neurons within their own ganglia, although projection to parasympathetic neurons in other ganglia cannot be ruled out. It is also possible that interganglionic interneurons exist in the airways, but if so they are not specifically characterized by substance P, nNOS, or TH. Other neuropeptides, such as VIP and NPY, have also been identified in rodent and human parasympathetic ganglia (Dey *et al.,* 1996; Fischer *et al.,* 1996; Richardson *et al.,* 2003). It will be interesting to look at these in mouse parasympathetic ganglia, and to use this new analysis method to investigate these populations as well.

PANbow and PGP9.5-iCre mouse lines

In order to improve further upon our pipeline for airway multicolor nerve labeling and analysis, I decided to create mouse lines that could label only select nerve populations with many colors. I based this mouse construct on the Brainbow 3.2 mouse, which does almost exactly what I want to do but in the central nervous system. Published literature shows that the Thy1 promoter that Brainbow mice use to drive nerve-specific fluorescent protein expression unfortunately fails to drive expression in postganglionic parasympathetic neurons (Feng *et al.,* 2000), and my studies validate this finding. A search of the literature did not yield any information on promoters that would definitively drive expression in all airway neurons. I therefore tested candidate promoters for expression in parasympathetic neurons.

The one promoter that I knew drove expression in parasympathetic ganglia was the choline acetyltransferase (CHAT) promoter - used to drive channelrhodopsin expression in chapters 3 and 4. Although general consensus states that this promoter should drive expression in all parasympathetic neurons, since one of their defining features is use of acetylcholine as a neurotransmitter, there are studies that suggest otherwise (El-Bermani, 1973), and my data on substance P labeled neurons in the trachea and carina region is consistent with these studies (Figure 5.26). Future studies could test this by co-labeling tracheas with PGP9.5 and an antibody against CHAT, however it is important to note that all commercially available antibodies target cCHAT - the splice variant of CHAT expressed in the

central nervous system - rather than pCHAT - the splice variant of CHAT expressed in the periphery. A collaboration with laboratories producing pCHAT antibody would therefore be necessary (Nakajima *et al.*, 2000, Koga *et al.*, 2013). For the purposes of creating the PANbow mouse, the CHAT promoter was non-ideal for a different reason, which is that it would restrict the possibilities of fluorescent expression in our mouse to cholinergic nerves only, and in the interest of maximizing utility I was looking for a promoter that could drive expression in sensory neurons as well.

Three options for "pan-neuronal" promoters with some evidence in the literature of parasympathetic expression were the rat synapsin 1 ((Zhu *et al.*, 2001)), rat tubulin alpha 1 (TUBA1) (Gloster *et al.*, 1994) and 1.6kp abbreviated mouse PGP9.5 promoter (the gene PGP9.5 is also called UCHL1). My data demonstrate that neither synapsin 1 nor TUBA1 promoters drive expression of fluorescent protein in all parasympathetic neurons, although the TUBA1 promoter came close. The PGP9.5 promoter did successfully drive expression in all labeled neurons (Figure 5.22), and I proceeded to use this promoter in genetic constructs for the PANbow and PGP9.5-iCre mice. One possible limitation for this study is that the standard used for definitive labeling of airway neurons was an antibody against PGP9.5. This means that if there are any airway neurons that do not express PGP9.5, they would not have been detected by either the antibody or the promoter driving fluorescent expression. However, the PGP9.5 antibody was used to label airway neurons in all studies throughout this dissertation, including co-labeling with CHAT-CH2 expression, substance P, tyrosine hydroxylase, nNOS, Syn1, Thy1, and AAV9-CAG-GFP. No neurons were seen in any of these studies that stained with one method but not with PGP9.5, so it seems likely that mouse airway parasympathetic neurons not expressing PGP9.5 do not exist. I thus have high hopes for the continued development and utility of the PANbow and PGP9.5-iCre mouse lines.

Conclusions

In conclusion, I have demonstrated that optogenetics and multicolor nerve imaging are powerful tools for studying airway nerve architecture and function. Using these methods, I have shown hyperreactivity to acute antigen sensitization and challenge is mediated by parasympathetic nerves, and that eosinophils cluster around parasympathetic nerve processes in airway smooth muscle but not around parasympathetic cell bodies after acute antigen sensitization and challenge. These are important considerations for understanding the therapeutic potential of eosinophil-reducing treatment for patients with long term asthma, and may explain why anti-IL-5 drugs largely reduce asthma exacerbations without improving baseline lung function. My data also suggest that development of drugs that can reverse or limit sensory nerves overgrowth may work synergistically with anti-IL-5 therapies in patients with chronic asthma. Studies described in this dissertation reveal fundamental differences between neural mechanisms of airway hyperreactivity in chronic asthma compared with asthma exacerbations, and provide groundbreaking tools for dissecting the morphological, functional, and pharmacological changes to airway nerves in disease.

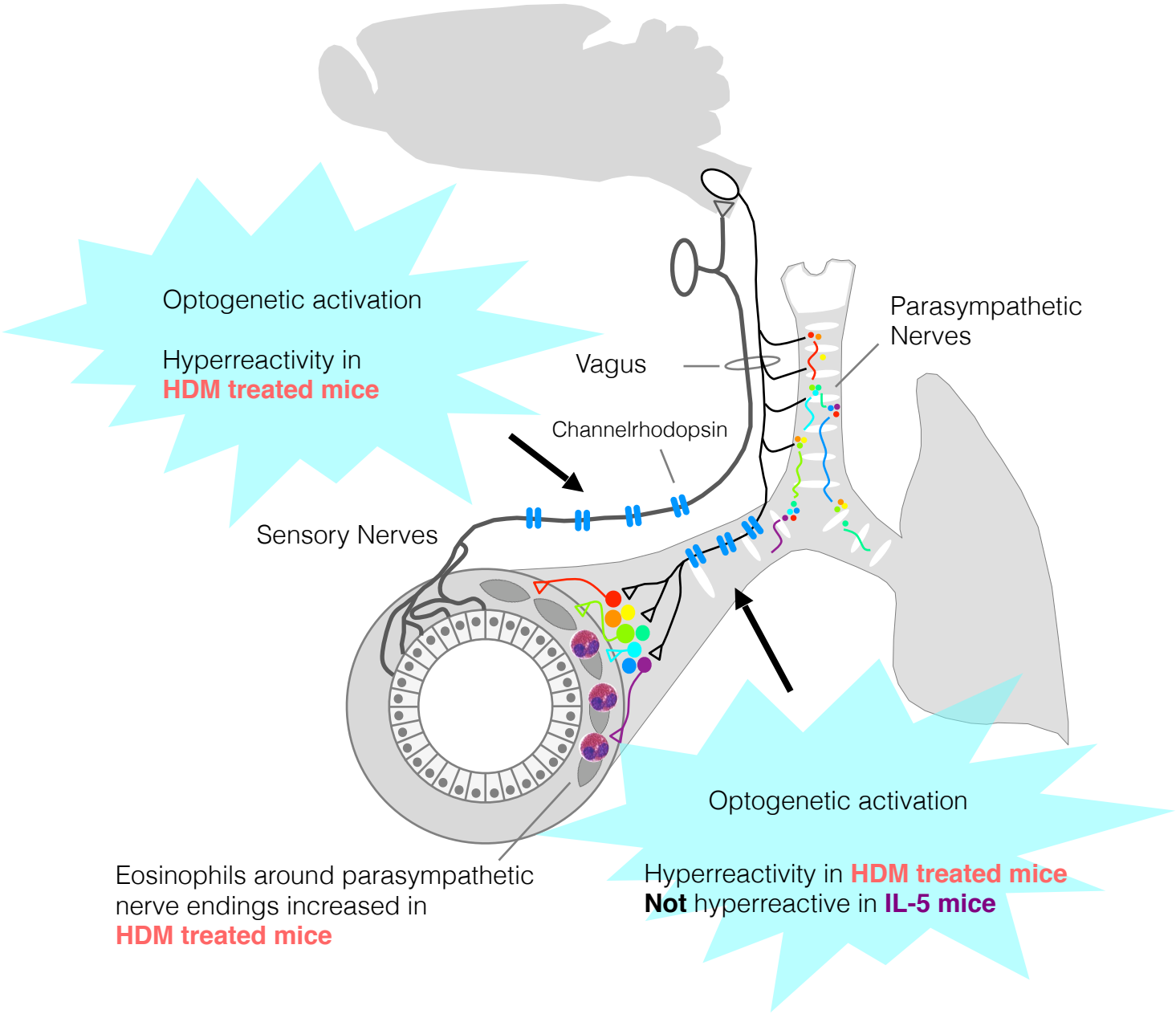

Figure 6.1. Summary of Dissertation Findings. I have developed a successful protocol using optogenetics in both parasympathetic (Ch 3) and sensory airway nerves to selectively and independently stimulate these arms of the reflex bronchoconstriction pathway. I have demonstrated there are important differences in the mechanism of hyperreactivity between two different, commonly used mouse models of eosinophilic asthma, which may depend on unique eosinophil localization around airway nerves (Ch 4), and which may explain why eosinophil depletion prevents acute asthma exacerbations but not chronic airway hyperreactivity. I have optimized tools for multicolor labeling of individual autonomic nerves and used nerve tracing to identify airway nerves and their connections (Ch 5). In summary, I have developed several new methodological approaches that can be used to study airway nerves in asthma, and demonstrated their utility in two mouse models of airway hyperreactivity.

References

Abdulqawi, R., Dockry, R., Holt, K., Layton, G., McCarthy, B. G., Ford, A. P., Smith, J. A., 2015. P2X3 receptor antagonist (AF-219) in refractory chronic cough: a randomised, double-blind, placebo-controlled phase 2 study, *The Lancet*, 385, 9974, 1198–1205. doi: 10.1016/S0140-6736(14)61255-1.

Adamantidis, A. R., Zhang, F., Aravanis, A. M., Deisseroth, K., de Lecea, L., 2007. Neural substrates of awakening probed with optogenetic control of hypocretin neurons, *Nature*, 450, 7168. doi: 10.1038/nature06310.

Adamko, D. J., Yost, B. L., Gleich, G. J., Fryer, A. D., Jacoby, D. B., 1999. Ovalbumin sensitization changes the inflammatory response to subsequent parainfluenza infection. Eosinophils mediate airway hyperresponsiveness, m(2) muscarinic receptor dysfunction, and antiviral effects., *The Journal of experimental medicine*, 190, 10, 1465–78. doi: 10.1084/jem.190.10.1465.

Adrian, E. D., 1933. Afferent impulses in the vagus and their effect on respiration, *The Journal of Physiology*, 79, 3, 332–358. doi: 10.1113/jphysiol.1933.sp003053.

Agache, I., 2019. Severe asthma phenotypes and endotypes, *Seminars in Immunology*, 46. doi: 10.1016/j.smim.2019.101301.

Aizawa, H., Tanaka, H., Sakai, J., Takata, S., Hara, N., Ito, Y., 1997. L-NAME-sensitive and -insensitive nonadrenergic noncholinergic relaxation of cat airway in vivo and in vitro, *European Respiratory Journal*, Eur Respir J, 10, 2, 314–321. doi: 10.1183/09031936.97.10020314.

Aravanis, A. M., Wang, L.-P., Zhang, F., Meltzer, L. A., Mogri, M. Z., Schneider, M. B., Deisseroth, K., 2007. An optical neural interface: in vivo control of rodent motor cortex with integrated fiberoptic and optogenetic technology, *Journal of Neural Engineering*, 4, 3. doi: 10.1088/1741-2560/4/3/S02.

Atmar, R. L., Guy, E., Guntupalli, K. K., Zimmerman, J. L., Bandi, V. D., Baxter, B. D., Greenberg, S. B., 1998. Respiratory tract viral infections in inner-city asthmatic adults, *Archives of Internal Medicine*, American Medical Association, 158, 22, 2453–2459. doi: 10.1001/archinte.158.22.2453.

Aven, L., Paez-Cortez, J., Achey, R., Krishnan, R., Ram-Mohan, S., Cruikshank, W. W., Fine, A., Ai, X., 2014. An NT4/TrkB-dependent increase in innervation links early-life allergen exposure to persistent airway hyperreactivity, *FASEB Journal*, FASEB, 28, 2, 897–907. doi: 10.1096/fj.13-238212.

Ayala, L. E., Ahmed, T., 1989. Is there loss of a protective muscarinic receptor mechanism in asthma?, *Chest*, Chest, 96, 6, 1285–1291. doi: 10.1378/chest.96.6.1285.

Baker, C. V. H., Schlosser, G., 2005. Editorial: The evolutionary origin of neural crest and placodes, in, *Journal of Experimental Zoology Part B: Molecular and Developmental Evolution*, J Exp Zool B Mol Dev Evol, pp. 269–273. doi: 10.1002/jez.b.21060.

Baker, D., 1986. Parasympathetic Motor Pathways to the Trachea: Recent Morphologic and Electrophysiologic Studies, *Clinics in chest medicine*, Clin Chest Med, 7, 2.

Baker, D. G., Mcdonald, D. M., Rasbaum, C. B., Mitchell, R. A., 1986. *The Architecture of Nerves and Ganglia of the Ferret Trachea as Revealed by Acetylcholinesterase Histochemistry*, *THE JOURNAL OF COMPARATIVE NEUROLOGY*, pp. 513–526. (online: https://onlinelibrary.wiley.com/doi/pdf/10.1002/cne.902460408).

Balentova, S., Conwell, S., Myers, A. C., 2013. Neurotransmitters in parasympathetic ganglionic neurons and nerves in mouse lower airway smooth muscle, *Respiratory Physiology and Neurobiology*, Elsevier, 189, 1, 195–202. doi: 10.1016/j.resp.2013.07.006.

Barnes, P. J., 2001. Neurogenic inflammation in the airways, *Respiration Physiology*, 125, 1, 145–154. doi: 10.1016/S0034-5687(00)00210-3.

Beasley, R., Semprini, A., Mitchell, E. A., 2015. Risk factors for asthma: is prevention possible?, *The Lancet*, 386, 9998, 1075–1085. doi: 10.1016/S0140-6736(15)00156-7.

Bel, E. H., Wenzel, S. E., Thompson, P. J., Prazma, C. M., Keene, O. N., Yancey, S. W., Ortega, H. G., Pavord, I. D., 2014. Oral Glucocorticoid-Sparing Effect of Mepolizumab in Eosinophilic Asthma, *New England Journal of Medicine*, 371, 13. doi: 10.1056/NEJMoa1403291.

Belvisi, M. G., Birrell, M. A., Khalid, S., Wortley, M. A., Dockry, R., Coote, J., Holt, K., Dubuis, E., Kelsall, A., Maher, S. A., Bonvini, S., Woodcock, A., Smith, J. A., 2016. Neurophenotypes in airway diseases: Insights from translational cough studies, *American Journal of Respiratory and Critical Care Medicine*, American Thoracic Society, 193, 12, 1364–1372. doi: 10.1164/rccm.201508-1602OC.

Belvisi, M. G., Motohiko, M., Stretton, D., Barnes, P. J., 1993. Endogenous vasoactive intestinal peptide and nitric oxide modulate cholinergic neurotransmission in guinea-pig trachea, *European Journal of Pharmacology*, Eur J Pharmacol, 231, 1, 97–102. doi: 10.1016/0014-2999(93)90689-F.

Birks, R. I., Macintosh, F. C., 1957. Acetylcholine metabolism at nerve-endings, *British Medical Bulletin*, 13, 3, 157–161. doi: 10.1093/oxfordjournals.bmb.a069605.

Bleecker, E. R., FitzGerald, J. M., Chanez, P., Papi, A., Weinstein, S. F., Barker, P., Sproule, S., Gilmartin, G., Aurivillius, M., Werkström, V., Goldman, M., 2016. Efficacy and safety of benralizumab for patients with severe asthma uncontrolled with high-dosage inhaled corticosteroids and long-acting β2-agonists (SIROCCO): a randomised, multicentre, placebo-controlled phase 3 trial, *The Lancet*, 388, 10056. doi: 10.1016/S0140-6736(16)31324-1.

Bonham, A. C., Chen, C. Y., Sekizawa, S. I., Joad, J. P., 2006. Plasticity in the nucleus tractus solitarius and its influence on lung and airway reflexes, *Journal of Applied Physiology*, 101, 1, 322–327. doi: 10.1152/japplphysiol.00143.2006.

Boyden, E. S., Zhang, F., Bamberg, E., Nagel, G., Deisseroth, K., 2005. Millisecond-timescale, genetically targeted optical control of neural activity, *Nature Neuroscience*, 8, 9. doi: 10.1038/nn1525.

Britt, R. D., Thompson, M. A., Wicher, S. A., Manlove, L. J., Roesler, A., Fang, Y. H., Roos, C., Smith, L., Miller, J. D., Pabelick, C. M., Prakash, Y. S., 2019. Smooth muscle brain-derived neurotrophic factor contributes to airway hyperreactivity in a mouse model of allergic asthma, *FASEB Journal*, FASEB, 33, 2, 3024–3034. doi: 10.1096/fj.201801002R.

Brown, R. H., Walters, D. M., Greenberg, R. S., Mitzner, W., 1999. A method of endotracheal intubation and pulmonary functional assessment for repeated studies in mice, *Journal of Applied Physiology*, 87, 6. doi: 10.1152/jappl.1999.87.6.2362.

Buels, K., Jacoby, D., Fryer, A., 2012. Non-bronchodilating mechanisms of tiotropium prevent airway hyperreactivity in a guinea-pig model of allergic asthma, *British Journal of Pharmacology*, 165, 5. doi: 10.1111/j.1476-5381.2011.01632.x.

Burnstock G, A. T., Hassall CJ., 1987. The electrophysiologic and neurochemical properties of paratracheal neurones in situ and in dissociated cell culture., *Am Rev Respir Dis*, 136, (6 Pt 2), S23–S26. doi: 10.1164/ajrccm/136.6_Pt_2.S23.

Busse, W. W., Morgan, W. J., Gergen, P. J., Mitchell, H. E., Gern, J. E., Liu, A. H., Gruchalla, R. S., Kattan, M., Teach, S. J., Pongracic, J. A., Chmiel, J. F., Steinbach, S. F., Calatroni, A., Togias, A., Thompson, K. M., Szefler, S. J., Sorkness, C. A., 2011. Randomized Trial of Omalizumab (Anti-IgE) for Asthma in Inner-City Children, *New England Journal of Medicine*, 364, 11. doi: 10.1056/NEJMoa1009705.

Cai, D., Cohen, K. B., Luo, T., Lichtman, J. W., Sanes, J. R., 2013. Improved tools for the Brainbow toolbox, *Nature Methods*, 10, 6, 540–547. doi: 10.1038/nmeth.2450.

Calupca, M. A., Vizzard, M. A., Parsons, R. L., 2000. Origin of neuronal nitric oxide synthase (NOS)-immunoreactive fibers in guinea pig parasympathetic cardiac ganglia, *The Journal of Comparative Neurology*, 426, 3. doi: 10.1002/1096-9861(20001023)426:3<493::AID-CNE10>3.0.CO;2-P.

Canning, B. J., Fischer, A., 2001. Neural regulation of airway smooth muscle tone, *Respiration Physiology*, Elsevier, 125, 1–2, 113–127. doi: 10.1016/S0034-5687(00)00208-5.

Canning, B. J., Spina, D., 2009. Sensory nerves and airway irritability, *Handbook of Experimental Pharmacology*,

Nature Publishing Group, 194, 139–183. doi: 10.1007/978-3-540-79090-7_5.
Canning, B. J., Undem, B. J., 1993. Evidence that distinct neural pathways mediate parasympathetic contractions and relaxations of guinea-pig trachealis, *The Journal of Physiology*, 471, 25–40. doi: 10.1113/jphysiol.1993.sp019889.
Castro, M., Mathur, S., Hargreave, F., Boulet, L.-P., Xie, F., Young, J., Wilkins, H. J., Henkel, T., Nair, P., 2011. Reslizumab for Poorly Controlled, Eosinophilic Asthma, *American Journal of Respiratory and Critical Care Medicine*, 184, 10. doi: 10.1164/rccm.201103-0396OC.
Castro, M., Zangrilli, J., Wechsler, M. E., Bateman, E. D., Brusselle, G. G., Bardin, P., Murphy, K., Maspero, J. F., O'Brien, C., Korn, S., 2015. Reslizumab for inadequately controlled asthma with elevated blood eosinophil counts: results from two multicentre, parallel, double-blind, randomised, placebo-controlled, phase 3 trials, *The Lancet Respiratory Medicine*, 3, 5. doi: 10.1016/S2213-2600(15)00042-9.
Cates, E. C., Fattouh, R., Wattie, J., Inman, M. D., Goncharova, S., Coyle, A. J., Gutierrez-Ramos, J.-C., Jordana, M., 2004. Intranasal Exposure of Mice to House Dust Mite Elicits Allergic Airway Inflammation via a GM-CSF-Mediated Mechanism, *The Journal of Immunology*, 173, 10. doi: 10.4049/jimmunol.173.10.6384.
Chan, K. Y., Jang, M. J., Yoo, B. B., Greenbaum, A., Ravi, N., Wu, W.-L., Sánchez-Guardado, L., Lois, C., Mazmanian, S. K., Deverman, B. E., Gradinaru, V., 2017. Engineered AAVs for efficient noninvasive gene delivery to the central and peripheral nervous systems, *Nature Neuroscience*, 20, 8, 1172–1179. doi: 10.1038/nn.4593.
Chang, R. B., Strochlic, D. E., Williams, E. K., Umans, B. D., Liberles, S. D., 2015. Vagal sensory neuron subtypes that differentially control breathing, *Cell*, Cell Press, 161, 3, 622–633. doi: 10.1016/j.cell.2015.03.022.
Chen, C. Y., Bonham, A. C., Joad, J. P., Gershwin, L. J., Schelegle, E. S., Plopper, C. G., Plopper, C. G., 2001. Extended allergen exposure in asthmatic monkeys induces neuroplasticity in nucleus tractus solitarius, *Journal of Allergy and Clinical Immunology*, J Allergy Clin Immunol, 108, 4, 557–562. doi: 10.1067/mai.2001.118132.
Choi, H. K., Finkbeiner, W. E., Widdicombe, J. H., 2000. A comparative study of mammalian tracheal mucous glands, *Journal of Anatomy*, Wiley-Blackwell, 197, 3, 361–372. doi: 10.1046/j.1469-7580.2000.19730361.x.
Choi, J. Y., Lee, H. Y., Hur, J., Kim, K. H., Kang, J. Y., Rhee, C. K., Lee, S. Y., 2018. TRPV1 Blocking Alleviates Airway Inflammation and Remodeling in a Chronic Asthma Murine Model, *Allergy, Asthma & Immunology Research*, 10, 3. doi: 10.4168/aair.2018.10.3.216.
Chuaychoo, B., Lee, M.-G., Kollarik, M., Undem, B. J., 2005. Effect of 5-hydroxytryptamine on vagal C-fiber subtypes in guinea pig lungs, *Pulmonary Pharmacology & Therapeutics*, 18, 4. doi: 10.1016/j.pupt.2004.12.010.
Coburn, R. F., Kalia, M. P., 1986. Morphological features of spiking and nonspiking cells in the paratracheal ganglion of the ferret, *The Journal of Comparative Neurology*, 254, 3. doi: 10.1002/cne.902540307.
Corren, J., Lemanske, R. F., Hanania, N. A., Korenblat, P. E., Parsey, M. V., Arron, J. R., Harris, J. M., Scheerens, H., Wu, L. C., Su, Z., Mosesova, S., Eisner, M. D., Bohen, S. P., Matthews, J. G., 2011. Lebrikizumab Treatment in Adults with Asthma, *New England Journal of Medicine*, 365, 12. doi: 10.1056/NEJMoa1106469.
Corren, J., Weinstein, S., Janka, L., Zangrilli, J., Garin, M., 2016. Phase 3 Study of Reslizumab in Patients With Poorly Controlled Asthma, *Chest*, 150, 4. doi: 10.1016/j.chest.2016.03.018.
Costello, R. W., Evans, C. M., Yost, B. L., Belmonte, K. E., Gleich, G. J., Jacoby, D. B., Fryer, A. D., 1999. Antigen-induced hyperreactivity to histamine: Role of the vagus nerves and eosinophils, in, *American Journal of Physiology - Lung Cellular and Molecular Physiology*, American Physiological Society. doi: 10.1152/ajplung.1999.276.5.l709.

Costello, R. W., Schofield, B. H., Kephart, G. M., Gleich, G. J., Jacoby, D. B., Fryer, A. D., 1997. Localization of eosinophils to airway nerves and effect on neuronal M2 muscarinic receptor function, *American Journal of Physiology - Lung Cellular and Molecular Physiology*, Am J Physiol, 273, 1 17-1. doi: 10.1152/ajplung.1997.273.1.l93.

Deisseroth, K., Feng, G., Majewska, A. K., Miesenbock, G., Ting, A., Schnitzer, M. J., 2006. Next-Generation Optical Technologies for Illuminating Genetically Targeted Brain Circuits, *Journal of Neuroscience*, 26, 41. doi: 10.1523/JNEUROSCI.3863-06.2006.

Dey, R. D., Altemus, J. B., Michalkiewicz, M., 1991. Distribution of vasoactives intestinal peptide- and substance P-containing nerves originating from neurons of airway ganglia in cat bronchi, *The Journal of Comparative Neurology*, 304, 2. doi: 10.1002/cne.903040213.

Dey, R. D., Altemus, J. B., Rodd, A., Mayer, B., Said, S. I., Coburn, R. F., 1996. Neurochemical characterization of intrinsic neurons in ferret tracheal plexus., *American Journal of Respiratory Cell and Molecular Biology*, 14, 3. doi: 10.1165/ajrcmb.14.3.8845170.

Dey, R. D., Hoffpauir, J., Said, S. I., 1988. Co-localization of vasoactive intestinal peptide- and substance P-containing nerves in cat bronchi, *Neuroscience*, 24, 1. doi: 10.1016/0306-4522(88)90330-2.

Dinh, Q. T., Mingomataj, E., Quarcoo, D., Groneberg, D. A., Witt, C., Klapp, B. F., Braun, A., Fischer, A., 2005. Allergic airway inflammation induces tachykinin peptides expression in vagal sensory neurons innervating mouse airways, *Clinical and Experimental Allergy*, 35, 6, 820–825. doi: 10.1111/j.1365-2222.2005.02264.x.

Dixon, M., Jackson, D. M., Richards, I. M., 1980. The effects of 5-hydroxytryptamine, histamine and acetylcholine on the reactivity of the lung of the anaesthetized dog., *The Journal of Physiology*, 307, 1. doi: 10.1113/jphysiol.1980.sp013425.

Dolensek, N., Gehrlach, D. A., Klein, A. S., Gogolla, N., 2020. Facial expressions of emotion states and their neuronal correlates in mice, *Science*, 368, 6486. doi: 10.1126/science.aaz9468.

Doyle, A. D., Jacobsen, E. A., Ochkur, S. I., Willetts, L., Shim, K., Neely, J., Kloeber, J., LeSuer, W. E., Pero, R. S., Lacy, P., Moqbel, R., Lee, N. A., Lee, J. J., 2013. Homologous recombination into the eosinophil peroxidase locus generates a strain of mice expressing Cre recombinase exclusively in eosinophils, *Journal of Leukocyte Biology*, 94, 1. doi: 10.1189/jlb.0213089.

Dragunas, G., Woest, M. E., Nijboer, S., Bos, S. T., van Asselt, J., de Groot, A. P., Vohlídalová, E., Vermeulen, C. J., Ditz, B., Vonk, J. M., Koppelman, G. H., van den Berge, M., ten Hacken, N. H. T., Timens, W., Munhoz, C. D., Prakash, Y. S., Gosens, R., Kistemaker, L. E. M., 2020. Cholinergic neuroplasticity in asthma driven by TrkB signaling, *The FASEB Journal*, Wiley. doi: 10.1096/fj.202000170r.

Drake, M. G., Scott, G. D., Blum, E. D., Lebold, K. M., Nie, Z., Lee, J. J., Fryer, A. D., Costello, R. W., Jacoby, D. B., 2018. Eosinophils increase airway sensory nerve density in mice and in human asthma, *Science Translational Medicine*, 10, 457, eaar8477–eaar8477. doi: 10.1126/scitranslmed.aar8477.

Dürk, T., Duerschmied, D., Müller, T., Grimm, M., Reuter, S., Vieira, R. P., Ayata, K., Cicko, S., Sorichter, S., Walther, D. J., Virchow, J. C., Taube, C., Idzko, M., 2013. Production of Serotonin by Tryptophan Hydroxylase 1 and Release via Platelets Contribute to Allergic Airway Inflammation, *American Journal of Respiratory and Critical Care Medicine*, 187, 5. doi: 10.1164/rccm.201208-1440OC.

Dusser, D. J., Djokic, T. D., Borson, D. B., Nadel, J. A., 1989. Cigarette smoke induces bronchoconstrictor hyperresponsiveness to substance P and inactivates airway neutral endopeptidase in the guinea pig. Possible role of free radicals., *Journal of Clinical Investigation*, 84, 3, 900–906. doi: 10.1172/JCI114251.

Dusser, D. J., Jacoby, D. B., Djokic, T. D., Rubinstein, I., Borson, D. B., Nadel, J. A., 1985. Virus induces airway hyperresponsiveness to tachykinins: role of neutral endopeptidase, *Journal of Applied Physiology*, 67, 4, 1504–1511. doi: 10.1152/jappl.1989.67.4.1504.

El-Bermani, A.-W. I., 1973. Innervation of the rat lung. Acetylcholinesterase-containing nerves of the bronchial tree, *American Journal of Anatomy*, John Wiley & Sons, Ltd, 137, 1, 19–29. doi:

10.1002/aja.1001370103.
Elbon, C. L., Jacoby, D. B., Fryer, A. D., 1995. Pretreatment with an antibody to interleukin-5 prevents loss of pulmonary M2 muscarinic receptor function in antigen-challenged guinea pigs., *American journal of respiratory cell and molecular biology*, Am J Respir Cell Mol Biol, 12, 3, 320–328. doi: 10.1165/ajrcmb.12.3.7873198.
Ellis, J. L., Undem, B. J., 1990. Non-adrenergic, non-cholinergic contractions in the electrically field stimulated guinea-pig trachea, *British Journal of Pharmacology*, John Wiley & Sons, Ltd, 101, 4, 875–880. doi: 10.1111/j.1476-5381.1990.tb14174.x.
Evans, C. M., Fryer, A. D., Jacoby, D. B., Gleich, G. J., Costello, R. W., 1997. Pretreatment with antibody to eosinophil major basic protein prevents hyperresponsiveness by protecting neuronal M2 muscarinic receptors in antigen-challenged guinea pigs, *Journal of Clinical Investigation*, American Society for Clinical Investigation, 100, 9, 2254–2262. doi: 10.1172/JCI119763.
Feldberg, W., Mann, T., 1946. Properties and distribution of the enzyme system which synthesizes acetylcholine in nervous tissue, *The Journal of Physiology*, 104, 4, 411–425.
Feng, G., Mellor, R. H., Bernstein, M., Keller-Peck, C., Nguyen, Q. T., Wallace, M., Nerbonne, J. M., Lichtman, J. W., Sanes, J. R., 2000. Imaging neuronal subsets in transgenic mice expressing multiple spectral variants of GFP, *Neuron*, Cell Press, 28, 1, 41–51. doi: 10.1016/S0896-6273(00)00084-2.
Fischer, A., McGregor, G. P., Saria, A., Philippin, B., Kummer, W., 1996. Induction of tachykinin gene and peptide expression in guinea pig nodose primary afferent neurons by allergic airway inflammation, *Journal of Clinical Investigation*, American Society for Clinical Investigation, 98, 10, 2284–2291. doi: 10.1172/JCI119039.
Fisher, J. T., Vincent, S. G., Gomeza, J., Yamada, M., Wess, J., 2004. Loss of vagally mediated bradycardia and bronchoconstriction in mice lacking M2 or M3 muscarinic acetylcholine receptors., *The FASEB journal : official publication of the Federation of American Societies for Experimental Biology*, FASEB J, 18, 6, 711–713. doi: 10.1096/fj.03-0648fje.
FitzGerald, J. M., Bleecker, E. R., Nair, P., Korn, S., Ohta, K., Lommatzsch, M., Ferguson, G. T., Busse, W. W., Barker, P., Sproule, S., Gilmartin, G., Werkström, V., Aurivillius, M., Goldman, M., 2016. Benralizumab, an anti-interleukin-5 receptor α monoclonal antibody, as add-on treatment for patients with severe, uncontrolled, eosinophilic asthma (CALIMA): a randomised, double-blind, placebo-controlled phase 3 trial, *The Lancet*, 388, 10056. doi: 10.1016/S0140-6736(16)31322-8.
Fryer, A. D., Jacoby, D. B., 1991. Parainfluenza virus infection damages inhibitory M2 muscarinic receptors on pulmonary parasympathetic nerves in the guinea-pig., *British journal of pharmacology*, 102, 1, 267–71. doi: 10.1111/j.1476-5381.1991.tb12164.x.
Fryer, A. D., Jacoby, D. B., 1992. Function of pulmonary M2 muscarinic receptors in antigen-challenged guinea pigs is restored by heparin and poly-L-glutamate, *Journal of Clinical Investigation*, 90, 6, 2292–2298. doi: 10.1172/JCI116116.
Fryer, A. D., Lein, P. J., Howard, A. S., Yost, B. L., Beckles, R. A., Jett, D. A., 2004. Mechanisms of organophosphate insecticide-induced airway hyperreactivity., *American journal of physiology. Lung cellular and molecular physiology*, 286, 5, L963-9. doi: 10.1152/ajplung.00343.2003.
Fryer, A. D., Maclagan, J., 1984. Muscarinic inhibitory receptors in pulmonary parasympathetic nerves in the guinea-pig, *British Journal of Pharmacology*, Br J Pharmacol, 83, 4, 973–978. doi: 10.1111/j.1476-5381.1984.tb16539.x.
Fryer, A. D., Stein, L. H., Nie, Z., Curtis, D. E., Evans, C. M., Hodgson, S. T., Jose, P. J., Belmonte, K. E., Fitch, E., Jacoby, D. B., 2006. Neuronal eotaxin and the effects of CCR3 antagonist on airway hyperreactivity and M2 receptor dysfunction, *Journal of Clinical Investigation*, J Clin Invest, 116, 1, 228–236. doi: 10.1172/JCI25423.
Fryer, A. D., Wills-Karp, M., 1991. Dysfunction of M2-muscarinic receptors in pulmonary parasympathetic nerves after antigen challenge, *Journal of Applied Physiology*, 71, 6, 2255–2261. doi:

10.1152/jappl.1991.71.6.2255.
Fryer, A. D., Yarkony, K. A., Jacoby, D. B., 1994. The effect of leukocyte depletion on pulmonary M2 muscarinic receptor function in parainfluenza virus-infected guinea-pigs, *British Journal of Pharmacology*, Br J Pharmacol, 112, 2, 588–594. doi: 10.1111/j.1476-5381.1994.tb13115.x.
Garcia, G., Magnan, A., Chiron, R., Contin-Bordes, C., Berger, P., Taillé, C., Devouassoux, G., de Blay, F., Couderc, L.-J., Didier, A., O'Callaghan, D. S., Girodet, P.-O., Bourdeix, I., Le Gros, V., Humbert, M., 2013. A Proof-of-Concept, Randomized, Controlled Trial of Omalizumab in Patients With Severe, Difficult-to-Control, Nonatopic Asthma, *Chest*, 144, 2. doi: 10.1378/chest.12-1961.
Gleich, G. J., Loegering, D. A., Kueppers, F., Bajaj, S. P., Mann, K. G., 1974. Physiochemical and biological properties of the major basic protein from guinea pig eosinophil granules, *Journal of Experimental Medicine*, J Exp Med, 140, 2, 313–332. doi: 10.1084/jem.140.2.313.
Gloster, A., Wu, W., Speelman, A., Weiss, S., Causing, C., Pozniak, C., Reynolds, B., Chang, E., Toma, J. G., Miller, F. D., 1994. The T alpha 1 alpha-tubulin promoter specifies gene expression as a function of neuronal growth and regeneration in transgenic mice, *The Journal of Neuroscience: The Official Journal of the Society for Neuroscience*, 14, 12, 7319–7330.
Gombash, S. E., Cowley, C. J., Fitzgerald, J. A., Hall, J. C. E., Mueller, C., Christofi, F. L., Foust, K. D., 2014. Intravenous AAV9 efficiently transduces myenteric neurons in neonate and juvenile mice, *Frontiers in Molecular Neuroscience*, Frontiers Media S.A., 7, OCT. doi: 10.3389/fnmol.2014.00081.
Gordon, T., Venugopalan, C. S., Amdur, M. O., Drazen, J. M., 1984. Ozone-induced airway hyperreactivity in the guinea pig, *Journal of Applied Physiology*, 57, 4. doi: 10.1152/jappl.1984.57.4.1034.
Gradinaru, V., Thompson, K. R., Zhang, F., Mogri, M., Kay, K., Schneider, M. B., Deisseroth, K., 2007. Targeting and Readout Strategies for Fast Optical Neural Control In Vitro and In Vivo, *Journal of Neuroscience*, 27, 52. doi: 10.1523/JNEUROSCI.3578-07.2007.
Gregory, L. G., Causton, B., Murdoch, J. R., Mathie, S. A., O'Donnell, V., Thomas, C. P., Priest, F. M., Quint, D. J., Lloyd, C. M., 2009. Inhaled house dust mite induces pulmonary T helper 2 cytokine production, *Clinical & Experimental Allergy*, 39, 10. doi: 10.1111/j.1365-2222.2009.03302.x.
Hadziefendic, S., Haxhiu, M. A., 1999. CNS innervation of vagal preganglionic neurons controlling peripheral airways: a transneuronal labeling study using pseudorabies virus, *Journal of the Autonomic Nervous System*, 76, 2–3. doi: 10.1016/S0165-1838(99)00020-X.
Hamad, A. M., Sutcliffe, A. M., Knox, A. J., 2004. Aspirin-Induced Asthma, *Drugs*, 64, 21, 2417–2432. doi: 10.2165/00003495-200464210-00004.
Han, L., Limjunyawong, N., Ru, F., Li, Z., Hall, O. J., Steele, H., Zhu, Y., Wilson, J., Mitzner, W., Kollarik, M., Undem, B. J., Canning, B. J., Dong, X., 2018. Mrgprs on vagal sensory neurons contribute to bronchoconstriction and airway hyper-responsiveness, *Nature Neuroscience*, Nature Publishing Group, 21, 3, 324–328. doi: 10.1038/s41593-018-0074-8.
Hanania, N. A., Alpan, O., Hamilos, D. L., Condemi, J. J., Reyes-Rivera, I., Zhu, J., Rosen, K. E., Eisner, M. D., Wong, D. A., Busse, W., 2011. Omalizumab in Severe Allergic Asthma Inadequately Controlled With Standard Therapy, *Annals of Internal Medicine*, 154, 9. doi: 10.7326/0003-4819-154-9-201105030-00002.
Hanania, N. A., Korenblat, P., Chapman, K. R., Bateman, E. D., Kopecky, P., Paggiaro, P., Yokoyama, A., Olsson, J., Gray, S., Holweg, C. T. J., Eisner, M., Asare, C., Fischer, S. K., Peng, K., Putnam, W. S., Matthews, J. G., 2016. Efficacy and safety of lebrikizumab in patients with uncontrolled asthma (LAVOLTA I and LAVOLTA II): replicate, phase 3, randomised, double-blind, placebo-controlled trials, *The Lancet Respiratory Medicine*, 4, 10. doi: 10.1016/S2213-2600(16)30265-X.
Hanania, N. A., Noonan, M., Corren, J., Korenblat, P., Zheng, Y., Fischer, S. K., Cheu, M., Putnam, W. S., Murray, E., Scheerens, H., Holweg, C. T., Maciuca, R., Gray, S., Doyle, R., McClintock, D., Olsson, J., Matthews, J. G., Yen, K., 2015. Lebrikizumab in moderate-to-severe asthma: pooled data from two randomised placebo-controlled studies, *Thorax*, 70, 8. doi: 10.1136/thoraxjnl-2014-206719.

Hargreave, F. E., Dolovich, J., O'Byrne, P. M., Ramsdale, E. H., Daniel, E. E., 1986. The origin of airway hyperresponsiveness, *The Journal of Allergy and Clinical Immunology*, 78, 5 PART 1, 825–832. doi: 10.1016/0091-6749(86)90226-5.

Hau, J., 2008. Animal models for human diseases: An overview, in, *Source Book of Models for Biomedical Research*, Humana Press, pp. 3–8. doi: 10.1007/978-1-59745-285-4_1.

Haxhiu, M. A., Kc, P., Neziri, B., Yamamoto, B. K., Ferguson, D. G., Massari, V. J., 2003. Catecholaminergic microcircuitry controlling the output of airway-related vagal preganglionic neurons, *Journal of Applied Physiology*, 94, 5. doi: 10.1152/japplphysiol.01066.2002.

Haxhiu, M. A., Rust, C. F., Brooks, C., Kc, P., 2006. CNS determinants of sleep-related worsening of airway functions: Implications for nocturnal asthma, *Respiratory Physiology & Neurobiology*, 151, 1. doi: 10.1016/j.resp.2005.07.009.

Haxhiu, M. A., Yamamoto, B., Dreshaj, I. A., Bedol, D., Ferguson, D. G., 2000. Involvement of glutamate in transmission of afferent constrictive inputs from the airways to the nucleus tractus solitarius in ferrets, *Journal of the Autonomic Nervous System*, J Auton Nerv Syst, 80, 1–2, 22–30. doi: 10.1016/S0165-1838(99)00088-0.

Hoard, J. L., Hoover, D. B., Mabe, A. M., Blakely, R. D., Feng, N., Paolocci, N., 2008. Cholinergic neurons of mouse intrinsic cardiac ganglia contain noradrenergic enzymes, norepinephrine transporters, and the neurotrophin receptors tropomyosin-related kinase A and p75, *Neuroscience*, 156, 1. doi: 10.1016/j.neuroscience.2008.06.063.

Hong, J.-L., Ho, C.-Y., Kwong, K., Lee, L.-Y., 1998. Activation of pulmonary C fibres by adenosine in anaesthetized rats: role of adenosine A 1 receptors, *The Journal of Physiology*, 508, 1. doi: 10.1111/j.1469-7793.1998.109br.x.

Horackova, M., Armour, J. A., Byczko, Z., 1999. Distribution of intrinsic cardiac neurons in whole-mount guinea pig atria identified by multiple neurochemical coding, *Cell and Tissue Research*, 297, 3. doi: 10.1007/s004410051368.

Hunter, D. V., Smaila, B. D., Lopes, D. M., Takatoh, J., Denk, F., Ramer, M. S., 2018. Advillin is expressed in all adult neural crest-derived neurons, *eNeuro*, Society for Neuroscience, 5, 5. doi: 10.1523/ENEURO.0077-18.2018.

Irvin, C. G., Boileau, R., Tremblay, J., Martin, R. R., Macklem, P. T., 1980. Bronchodilatation: Noncholinergic, nonadrenergic mediation demonstrated in vivo in the cat, *Science*, Science, 207, 4432, 791–792. doi: 10.1126/science.7352292.

Jacoby, D. B., Gleich, G. J., Fryer, A. D., 1993. Human eosinophil major basic protein is an endogenous allosteric antagonist at the inhibitory muscarinic M2 receptor, *Journal of Clinical Investigation*, The American Society for Clinical Investigation, 91, 4, 1314–1318. doi: 10.1172/JCI116331.

Jacoby, D. B., Tamaoki, J., Borson, D. B., Nadel, J. A., 1985. Influenza infection causes airway hyperresponsiveness by decreasing enkephalinase, *Journal of Applied Physiology*, 64, 6, 2653–2658. doi: 10.1152/jappl.1988.64.6.2653.

Jarial, M. S., 2005. Ultrastructural study of the blood cells of the coelacanth Latimeria chalumnae (Rhipidistia: Coelacanthini), *Journal of Submicroscopic Cytology and Pathology*, 37, 1.

Johnston, N. W., Johnston, S. L., Duncan, J. M., Greene, J. M., Kebadze, T., Keith, P. K., Roy, M., Waserman, S., Sears, M. R., 2005. The September epidemic of asthma exacerbations in children: A search for etiology, *Journal of Allergy and Clinical Immunology*, Mosby Inc., 115, 1, 132–138. doi: 10.1016/j.jaci.2004.09.025.

Johnston, S. L., Pattemore, P. K., Sanderson, G., Smith, S., Lampe, F., Josephs, L., Symington, P., Toole, S. o., Myint, S. H., Tyrrell, D. A. J., Holgate, S. T., 1995. Community study of role of viral infections in exacerbations of asthma in 9-11 year old children, *BMJ*, BMJ Publishing Group, 310, 6989, 1225–1225. doi: 10.1136/bmj.310.6989.1225.

Jones, J. T., Tassew, D. D., Herrera, L. K., Walton-Filipczak, S. R., Montera, M. A., Chand, H. S., Delgado, M.,

Mebratu, Y. A., Tesfaigzi, Y., 2017. Extent of allergic inflammation depends on intermittent versus continuous sensitization to house dust mite, *Inhalation Toxicology*, 29, 3. doi: 10.1080/08958378.2017.1311389.

Kajekar, R., Proud, D., Myers, A. C., Meeker, S. N., Undem, B. J., 1999. Characterization of vagal afferent subtypes stimulated by bradykinin in guinea pig trachea, *The Journal of Pharmacology and Experimental Therapeutics*, 289, 2, 682–687.

Kajekar, R., Rohde, H. K., Myers, A. C., 2001. The Integrative Membrane Properties of Human Bronchial Parasympathetic Ganglia Neurons, *American Journal of Respiratory and Critical Care Medicine*, 164, 10. doi: 10.1164/ajrccm.164.10.2106073.

Karczewski, W., Widdicombe, J. G., 1969. The role of the vagus nerves in the respiratory and circulatory responses to intravenous histamine and phenyl diguanide in rabbits, *The Journal of Physiology*, 201, 2, 271–291. doi: 10.1113/jphysiol.1969.sp008755.

Kerstjens, H. A. M., Engel, M., Dahl, R., Paggiaro, P., Beck, E., Vandewalker, M., Sigmund, R., Seibold, W., Moroni-Zentgraf, P., Bateman, E. D., 2012. Tiotropium in Asthma Poorly Controlled with Standard Combination Therapy, *New England Journal of Medicine*, 367, 13. doi: 10.1056/NEJMoa1208606.

Kips, J. C., Anderson, G. P., Fredberg, J. J., Herz, U., Inman, M. D., Jordana, M., Kemeny, D. M., Lotvall, J., Pauwels, R. A., Plopper, C. G., Schmidt, D., Sterk, P. J., Van Oosterhout, A. J. M., Vargaftig, B. B., Chung, K. F., 2003. Murine models of asthma, *European Respiratory Journal*, 22, 2. doi: 10.1183/09031936.03.00026403.

Knowlton, G. C., Larrabee, M. G., 1946. A unitary analysis of pulmonary volume receptors, *American Journal of Physiology-Legacy Content*, American Physiological Society, 147, 1, 100–114.

Ko, W. C., Lai, Y. L., 1988. The tracheal nonadrenergic noncholinergic inhibitory system during antigen challenge, *Respiration Physiology*, Respir Physiol, 74, 2, 129–138. doi: 10.1016/0034-5687(88)90099-0.

Koga, T., Bellier, J.-P., Kimura, H., Tooyama, I., 2013. Immunoreactivity for Choline Acetyltransferase of Peripheral-Type (pChAT) in the Trigeminal Ganglion Neurons of the Non-Human Primate Macaca fascicularis, *Acta Histochemica Et Cytochemica*, 46, 2, 59–64. doi: 10.1267/ahc.12044.

Kollarik, M., Dinh, Q. T., Fischer, A., Undem, B. J., 2003. Capsaicin-sensitive and -insensitive vagal bronchopulmonary C-fibres in the mouse, *Journal of Physiology*, Wiley-Blackwell, 551, 3, 869–879. doi: 10.1113/jphysiol.2003.042028.

Kubin, L., Alheid, G. F., Zuperku, E. J., McCrimmon, D. R., 2006. Central pathways of pulmonary and lower airway vagal afferents, *Journal of Applied Physiology*, American Physiological Society, 101, 2, 618–627. doi: 10.1152/japplphysiol.00252.2006.

Kummer, W., Fischer, A., Kurkowski, R., Heym, C., 1992. The sensory and sympathetic innervation of guinea-pig lung and trachea as studied by retrograde neuronal tracing and double-labelling immunohistochemistry., *Neuroscience*, 49, 3, 715–37.

Kupari, J., Häring, M., Agirre, E., Castelo-Branco, G., Ernfors, P., 2019. An Atlas of Vagal Sensory Neurons and Their Molecular Specialization, *Cell Reports*, Elsevier B.V., 27, 8, 2508-2523.e4. doi: 10.1016/j.celrep.2019.04.096.

Lamb, J. P., Sparrow, M. P., 2002. Three-Dimensional Mapping of Sensory Innervation with Substance P in Porcine Bronchial Mucosa: Comparison with Human Airways, *American Journal of Respiratory and Critical Care Medicine*, 166, 9, 1269–1281. doi: 10.1164/rccm.2112018.

Lau, J., Minett, M. S., Zhao, J., Dennehy, U., Wang, F., Wood, J. N., Bogdanov, Y. D., 2011. Temporal Control of Gene Deletion in Sensory Ganglia Using a Tamoxifen-Inducible Advillin-CreERT2 Recombinase Mouse, *Molecular Pain*, 7. doi: 10.1186/1744-8069-7-100.

Laviolette, M., Gossage, D. L., Gauvreau, G., Leigh, R., Olivenstein, R., Katial, R., Busse, W. W., Wenzel, S., Wu, Y., Datta, V., Kolbeck, R., Molfino, N. A., 2013. Effects of benralizumab on airway eosinophils in asthmatic patients with sputum eosinophilia, *Journal of Allergy and Clinical Immunology*, 132, 5. doi: 10.1016/j.jaci.2013.05.020.

Lebold, K. M., 2018. *Pre and postnatal determinants of airway hyperreactivity*, Oregon Health & Science University.

Lebold, K. M., Drake, M. G., Hales-Beck, L. B., Fryer, A. D., Jacoby, D. B., 2020. IL-5 exposure in utero increases lung nerve density and airway reactivity in adult offspring, *American Journal of Respiratory Cell and Molecular Biology*, American Thoracic Society, 62, 4, 493–502. doi: 10.1165/rcmb.2019-0214OC.

Lee, J. J., Dimina, D., Macias, M. P., Ochkur, S. I., McGarry, M. P., O'Neill, K. R., Protheroe, C., Pero, R., Nguyen, T., Cormier, S. A., Lenkiewicz, E., Colbert, D., Rinaldi, L., Ackerman, S. J., Irvin, C. G., Lee, N. A., 2004. Defining a link with asthma in mice congenitally deficient in eosinophils., *Science (New York, N.Y.)*, 305, 5691, 1773–6. doi: 10.1126/science.1099472.

Lee, J. J., Jacobsen, E. A., McGarry, M. P., Schleimer, R. P., Lee, N. A., 2010. Eosinophils in health and disease: The LIAR hypothesis, *Clinical and Experimental Allergy*, Clin Exp Allergy, 40, 4, 563–575. doi: 10.1111/j.1365-2222.2010.03484.x.

Lee, J. J., Jacobsen, E. A., Ochkur, S. I., McGarry, M. P., Condjella, R. M., Doyle, A. D., Luo, H., Zellner, K. R., Protheroe, C. A., Willetts, L., Lesuer, W. E., Colbert, D. C., Helmers, R. A., Lacy, P., Moqbel, R., Lee, N. A., 2012. Human versus mouse eosinophils: 'That which we call an eosinophil, by any other name would stain as red', *Journal of Allergy and Clinical Immunology*, Mosby Inc., 130, 3, 572–584. doi: 10.1016/j.jaci.2012.07.025.

Lee, J. J., McGarry, M. P., Farmer, S. C., Denzler, K. L., Larson, K. A., Carrigan, P. E., Brenneise, I. E., Horton, M. A., Haczku, A., Gelfand, E. W., Leikauf, G. D., Lee, N. A., 1997. Interleukin-5 expression in the lung epithelium of transgenic mice leads to pulmonary changes pathognomonic of asthma., *The Journal of experimental medicine*, 185, 12, 2143–56.

Lee, L.-Y., Lin, R.-L., Khosravi, M., Xu, F., 2018. Reflex bronchoconstriction evoked by inhaled nicotine aerosol in guinea pigs: role of the nicotinic acetylcholine receptor, *Journal of Applied Physiology*, 125, 1. doi: 10.1152/japplphysiol.01039.2017.

Li, W., Germain, R. N., Gerner, M. Y., 2017. Multiplex, quantitative cellular analysis in large tissue volumes with clearing-enhanced 3D microscopy (Ce3D)., *Proceedings of the National Academy of Sciences of the United States of America*, 114, 35, E7321–E7330. doi: 10.1073/pnas.1708981114.

Lieu, T. M., Myers, A. C., Meeker, S., Undem, B. J., 2012. TRPV1 induction in airway vagal low-threshold mechanosensory neurons by allergen challenge and neurotrophic factors, *American Journal of Physiology - Lung Cellular and Molecular Physiology*, 302, 9, L941-8. doi: 10.1152/ajplung.00366.2011.

Liske, H., Qian, X., Anikeeva, P., Deisseroth, K., Delp, S., 2013. Optical control of neuronal excitation and inhibition using a single opsin protein, ChR2, *Scientific Reports*, 3, 1. doi: 10.1038/srep03110.

Liu, X., Agerbo, E., Schlünssen, V., Wright, R. J., Li, J., Munk-Olsen, T., 2018. Maternal asthma severity and control during pregnancy and risk of offspring asthma, *Journal of Allergy and Clinical Immunology*, 141, 3, 886-892.e3. doi: 10.1016/j.jaci.2017.05.016.

Livet, J., Weissman, T. A., Kang, H., Draft, R. W., Lu, J., Bennis, R. A., Sanes, J. R., Lichtman, J. W., 2007. Transgenic strategies for combinatorial expression of fluorescent proteins in the nervous system, *Nature*, 450, 7166, 56–62. doi: 10.1038/nature06293.

Lötvall, J., Akdis, C. A., Bacharier, L. B., Bjermer, L., Casale, T. B., Custovic, A., Lemanske Jr., R. F., Wardlaw, A. J., Wenzel, S. E., Greenberger, P. A., 2011. Asthma endotypes: A new approach to classification of disease entities within the asthma syndrome, *Journal of Allergy and Clinical Immunology*, 127, 2. doi: 10.1016/j.jaci.2010.11.037.

Lötvall, J., Inman, M., O'Byrne, P., 1998. *Measurement of airway hyperresponsiveness: new considerations*.

Lötvall, J., Lunde, H., Augustinson, L.-E., Hedner, T., Svedmyr, N., Ben-Menachem, E., 1994. Airway effects of direct left-sided cervical vagal stimulation in patients with complex partial seizures, *Epilepsy Research*, 18, 2. doi: 10.1016/0920-1211(94)90007-8.

Lundy, J. A., McNary, T., 2019. *Neuroanatomy, Pterygopalatine Ganglion*, *StatPearls*, StatPearls Publishing.

(online: http://www.ncbi.nlm.nih.gov/pubmed/31424892).
Maarsingh, H., Leusink, J., Zaagsma, J., Meurs, H., 2006. Role of the l-citrulline/l-arginine cycle in iNANC nerve-mediated nitric oxide production and airway smooth muscle relaxation in allergic asthma, *European Journal of Pharmacology*, Eur J Pharmacol, 546, 1–3, 171–176. doi: 10.1016/j.ejphar.2006.07.041.
Madisen, L., Mao, T., Koch, H., Zhuo, J., Berenyi, A., Fujisawa, S., Hsu, Y.-W. A., Garcia, A. J., Gu, X., Zanella, S., Kidney, J., Gu, H., Mao, Y., Hooks, B. M., Boyden, E. S., Buzsáki, G., Ramirez, J. M., Jones, A. R., Svoboda, K., Han, X., Turner, E. E., Zeng, H., 2012. A toolbox of Cre-dependent optogenetic transgenic mice for light-induced activation and silencing, *Nature Neuroscience*, 15, 5. doi: 10.1038/nn.3078.
Marsh, B. J., Fryer, A. D., Jacoby, D. B., Drake, M. G., 2020. TRPA1 causes rapid bronchodilation via non-epithelial PGE 2, *American Journal of Physiology-Lung Cellular and Molecular Physiology*, American Physiological Society. doi: 10.1152/ajplung.00277.2019.
Mazzone, S., Canning, B., 2002. Central nervous system control of the airways: pharmacological implications, *Current Opinion in Pharmacology*, 2, 3. doi: 10.1016/S1471-4892(02)00151-0.
McAlexander, M. A., Gavett, S. H., Kollarik, M., Undem, B. J., 2015. Vagotomy reverses established allergen-induced airway hyperreactivity to methacholine in the mouse, *Respiratory Physiology and Neurobiology*, Elsevier, 212–214, 20–24. doi: 10.1016/j.resp.2015.03.007.
McCaig, D. J., 1987. Comparison of autonomic responses in the trachea isolated from normal and albumin-sensitive guinea-pigs, *British Journal of Pharmacology*, Wiley-Blackwell, 92, 4, 809–816. doi: 10.1111/j.1476-5381.1987.tb11385.x.
McGovern, A. E., Davis-Poynter, N., Yang, S. K., Simmons, D. G., Farrell, M. J., Mazzone, S. B., 2015. Evidence for multiple sensory circuits in the brain arising from the respiratory system: an anterograde viral tract tracing study in rodents, *Brain Structure and Function*, Springer Verlag, 220, 6, 3683–3699. doi: 10.1007/s00429-014-0883-9.
McGovern, A. E., Driessen, A. K., Simmons, D. G., Powell, J., Davis-Poynter, X., Michael, X., Farrell, J., Mazzone, S. B., 2015. Systems/Circuits Distinct Brainstem and Forebrain Circuits Receiving Tracheal Sensory Neuron Inputs Revealed Using a Novel Conditional Anterograde Transsynaptic Viral Tracing System. doi: 10.1523/JNEUROSCI.5128-14.2015.
Mendez-Enriquez, E., Alvarado-Vazquez, P. A., Abma, W., Simonson, O. E., Rodin, S., Feyerabend, T. B., Rodewald, H., Malinovschi, A., Janson, C., Adner, M., Hallgren, J., 2021. Mast cell-derived serotonin enhances methacholine-induced airway hyperresponsiveness in house dust mite-induced experimental asthma, *Allergy*. doi: 10.1111/all.14748.
Meurs, H., McKay, S., Maarsingh, H., Hamer, M. A. M., Macic, L., Molendijk, N., Zaagsma, J., 2002. Increased arginase activity underlies allergen-induced deficiency of cNOS-derived nitric oxide and airway hyperresponsiveness, *British Journal of Pharmacology*, 136, 3, 391–398. doi: 10.1038/sj.bjp.0704725.
Michoud, M. C., Fraser, R. S., Pare, P. D., Hogg, J. C., 1976. Effect of indomethacin and atropine in experimental asthma in conscious guinea pigs, *Journal of Applied Physiology*, J Appl Physiol, 40, 6, 889–894. doi: 10.1152/jappl.1976.40.6.889.
Miner, J. R., Lewis, L. M., Mosnaim, G. S., Varon, J., Theodoro, D., Hoffmann, T. J., 2012. Feasibility of percutaneous vagus nerve stimulation for the treatment of acute asthma exacerbations, *Academic Emergency Medicine*, 19, 4, 421–429. doi: 10.1111/j.1553-2712.2012.01329.x.
Minette, P. A., Lammers, J. W., Dixon, C. M., McCusker, M. T., Barnes, P. J., 1989. A muscarinic agonist inhibits reflex bronchoconstriction in normal but not in asthmatic subjects., *Journal of applied physiology (Bethesda, Md.: 1985)*, 67, 6, 2461–5. doi: 10.1152/jappl.1989.67.6.2461.
Mitchell, R. A., Herbert, D. A., Baker, D. G., Basbaum, C. B., 1987. In vivo activity of tracheal parasympathetic ganglion cells innervating tracheal smooth muscle, *Brain Research*, Elsevier, 437, 1, 157–160. doi: 10.1016/0006-8993(87)91537-X.

Miura, M., Yamauchi, H., Ichinose, M., Ohuchi, Y., Kageyama, N., Tomaki, M., Endoh, N., Shirato, K., 1997. Impairment of neural nitric oxide-mediated relaxation after antigen exposure in guinea pig airways in vitro, *American Journal of Respiratory and Critical Care Medicine*, American Thoracic Society, 156, 1, 217–222. doi: 10.1164/ajrccm.156.1.9606040.

Morice, A. H., Kitt, M. M., Ford, A. P., Tershakovec, A. M., Wu, W.-C., Brindle, K., Thompson, R., Thackray-Nocera, S., Wright, C., 2019. The effect of gefapixant, a P2X3 antagonist, on cough reflex sensitivity: a randomised placebo-controlled study, *European Respiratory Journal*, 54, 1, 1900439–1900439. doi: 10.1183/13993003.00439-2019.

Morten, M., Collison, A., Murphy, V. E., Barker, D., Oldmeadow, C., Attia, J., Meredith, J., Powell, H., Robinson, P. D., Sly, P. D., Gibson, P. G., Mattes, J., 2018. Managing Asthma in Pregnancy (MAP) trial: FENO levels and childhood asthma., *The Journal of allergy and clinical immunology*, Elsevier, 142, 6, 1765-1772.e4. doi: 10.1016/j.jaci.2018.02.039.

Myers, A. C., Kajekar, R., Undem, B. J., 2002. Allergic inflammation-induced neuropeptide production in rapidly adapting afferent nerves in guinea pig airways, *American Journal of Physiology - Lung Cellular and Molecular Physiology*, 282, 4 26-4, L775-81. doi: 10.1152/ajplung.00353.2001.

Myers, A. C., Undem, B. J., Weinreich, D., 1990. Electrophysiological properties of neurons in guinea pig bronchial parasympathetic ganglia, *American Journal of Physiology - Lung Cellular and Molecular Physiology*, Am J Physiol, 259, 6 3–3. doi: 10.1152/ajplung.1990.259.6.l403.

Myers, A., Undem, B., 1991. Functional interactions between capsaicin-sensitive and cholinergic nerves in the guinea pig bronchus, *Journal of Pharmacology and Experimental Therapeutics*, 259, 1, 104–109.

Nachmansohn, D., Machado, A. L., 1943. THE FORMATION OF ACETYLCHOLINE. A NEW ENZYME:" CHOLINE ACETYLASE", *Journal of neurophysiology*, 6, 5, 397–403.

Nadel, J. A., Barnes, P. J., 1984. Autonomic regulation of the airways., *Annual review of medicine*, 35, 451–67. doi: 10.1146/annurev.me.35.020184.002315.

Nadel, J. A., Davis, B., 1980. Parasympathetic and sympathetic regulation of secretion from submucosal glands in airways., *Federation proceedings*, 39, 13, 3075–9.

Nagel, G., 2002. Channelrhodopsin-1: A Light-Gated Proton Channel in Green Algae, *Science*, 296, 5577. doi: 10.1126/science.1072068.

Nair, P., Pizzichini, M. M. M., Kjarsgaard, M., Inman, M. D., Efthimiadis, A., Pizzichini, E., Hargreave, F. E., O'Byrne, P. M., 2009. Mepolizumab for Prednisone-Dependent Asthma with Sputum Eosinophilia, *New England Journal of Medicine*, 360, 10. doi: 10.1056/NEJMoa0805435.

Nair, P., Wenzel, S., Rabe, K. F., Bourdin, A., Lugogo, N. L., Kuna, P., Barker, P., Sproule, S., Ponnarambil, S., Goldman, M., 2017. Oral Glucocorticoid–Sparing Effect of Benralizumab in Severe Asthma, *New England Journal of Medicine*, 376, 25. doi: 10.1056/NEJMoa1703501.

Nakajima, K., Tooyama, I., Yasuhara, O., Aimi, Y., Kimura, H., 2000. Immunohistochemical demonstration of choline acetyltransferase of a peripheral type (pChAT) in the enteric nervous system of rats, *Journal of Chemical Neuroanatomy*, 18, 1–2, 31–40. doi: 10.1016/s0891-0618(99)00058-7.

Nandiwada, P. A., Hyman, A. L., Kadowitz, P. J., 1983. Pulmonary vasodilator responses to vagal stimulation and acetylcholine in the cat., *Circulation Research*, 53, 1. doi: 10.1161/01.RES.53.1.86.

Nassenstein, C., Taylor-Clark, T. E., Myers, A. C., Ru, F., Nandigama, R., Bettner, W., Undem, B. J., 2010. Phenotypic distinctions between neural crest and placodal derived vagal C-fibres in mouse lungs., *The Journal of physiology*, Wiley-Blackwell, 588, Pt 23, 4769–83. doi: 10.1113/jphysiol.2010.195339.

Nie, Z., Jacoby, D. B., Fryer, A. D., 2009. Etanercept prevents airway hyperresponsiveness by protecting neuronal M 2 muscarinic receptors in antigen-challenged guinea pigs, *British Journal of Pharmacology*, 156, 1, 201–210. doi: 10.1111/j.1476-5381.2008.00045.x.

Nie, Z., Jacoby, D. B., Fryer, A. D., 2014. Hyperinsulinemia potentiates airway responsiveness to parasympathetic nerve stimulation in obese rats., *American journal of respiratory cell and molecular biology*, 51, 2, 251–61. doi: 10.1165/rcmb.2013-0452OC.

North, M. L., Khanna, N., Marsden, P. A., Grasemann, H., Scott, J. A., 2009. Functionally important role for arginase 1 in the airway hyperresponsiveness of asthma, *American Journal of Physiology-Lung Cellular and Molecular Physiology*, 296, 6, L911–L920. doi: 10.1152/ajplung.00025.2009.

Ochkur, S. I., Jacobsen, E. A., Protheroe, C. A., Biechele, T. L., Pero, R. S., McGarry, M. P., Wang, H., O'Neill, K. R., Colbert, D. C., Colby, T. V., Shen, H., Blackburn, M. R., Irvin, C. C., Lee, J. J., Lee, N. A., 2007. Coexpression of IL-5 and Eotaxin-2 in Mice Creates an Eosinophil-Dependent Model of Respiratory Inflammation with Characteristics of Severe Asthma, *The Journal of Immunology*, The American Association of Immunologists, 178, 12, 7879–7889. doi: 10.4049/jimmunol.178.12.7879.

Ollerenshaw, S., Jarvis, D., Woolcock, A., Sullivan, C., Scheibner, T., 1989. Absence of Immunoreactive Vasoactive Intestinal Polypeptide in Tissue from the Lungs of Patients with Asthma, *New England Journal of Medicine*, 320, 19. doi: 10.1056/NEJM198905113201904.

Ollerenshaw, S. L., Jarvis, D., Sullivan, C. E., Woolcock, A. J., 1991. Substance P immunoreactive nerves in airways from asthmatics and nonasthmatics., *The European respiratory journal*, 4, 6, 673–82.

Ortega, H. G., Liu, M. C., Pavord, I. D., Brusselle, G. G., FitzGerald, J. M., Chetta, A., Humbert, M., Katz, L. E., Keene, O. N., Yancey, S. W., Chanez, P., 2014. Mepolizumab Treatment in Patients with Severe Eosinophilic Asthma, *New England Journal of Medicine*, New England Journal of Medicine (NEJM/MMS), 371, 13, 1198–1207. doi: 10.1056/nejmoa1403290.

Ortega, H. G., Yancey, S. W., Mayer, B., Gunsoy, N. B., Keene, O. N., Bleecker, E. R., Brightling, C. E., Pavord, I. D., 2016. Severe eosinophilic asthma treated with mepolizumab stratified by baseline eosinophil thresholds: a secondary analysis of the DREAM and MENSA studies, *The Lancet Respiratory Medicine*, 4, 7. doi: 10.1016/S2213-2600(16)30031-5.

Paintal, A. S., 1955. Impulses in vagal afferent fibres from specific pulmonary deflation receptors. The response of these receptors to phenyl diguanide, potato starch, 5-hydroxytryptamine and nicotine, and their role in respiratory and cardiovascular reflexes, *Quarterly Journal of Experimental Physiology and Cognate Medical Sciences: Translation and Integration*, Wiley Online Library, 40, 2, 89–111.

Palmer, J. B. D., Cuss, F. M. C., Barnes, P. J., 1986. VIP and PHM and their role in nonadrenergic inhibitory responses in isolated human airways, *Journal of Applied Physiology*, J Appl Physiol (1985), 61, 4, 1322–1328. doi: 10.1152/jappl.1986.61.4.1322.

Papi, A., Brightling, C., Pedersen, S. E., Reddel, H. K., 2017. Asthma, *www.thelancet.com*, 783, 783–800. doi: 10.1016/S0140-6736(17)33311-1.

Papka, R. E., McNeill, D. L., Thompson, D., Schmidt, H. H. H. W., 1995. Nitric oxide nerves in the uterus are parasympathetic, sensory, and contain neuropeptides, *Cell & Tissue Research*, 279, 2. doi: 10.1007/BF00318490.

Patil, M. J., Meeker, S., Bautista, D., Dong, X., Undem, B. J., 2019. Sphingosine-1-phosphate activates mouse vagal airway afferent C-fibres via S1PR3 receptors, *Journal of Physiology*, Blackwell Publishing Ltd, 597, 7, 2007–2019. doi: 10.1113/JP277521.

Pavord, I. D., Korn, S., Howarth, P., Bleecker, E. R., Buhl, R., Keene, O. N., Ortega, H., Chanez, P., 2012. Mepolizumab for severe eosinophilic asthma (DREAM): a multicentre, double-blind, placebo-controlled trial, *The Lancet*, 380, 9842. doi: 10.1016/S0140-6736(12)60988-X.

Peters, S. P., Kunselman, S. J., Icitovic, N., Moore, W. C., Pascual, R., Ameredes, B. T., Boushey, H. A., Calhoun, W. J., Castro, M., Cherniack, R. M., Craig, T., Denlinger, L., Engle, L. L., DiMango, E. A., Fahy, J. V., Israel, E., Jarjour, N., Kazani, S. D., Kraft, M., Lazarus, S. C., Lemanske, R. F., Lugogo, N., Martin, R. J., Meyers, D. A., Ramsdell, J., Sorkness, C. A., Sutherland, E. R., Szefler, S. J., Wasserman, S. I., Walter, M. J., Wechsler, M. E., Chinchilli, V. M., Bleecker, E. R., 2010. Tiotropium bromide step-up therapy for adults with uncontrolled asthma, *New England Journal of Medicine*, Massachussetts Medical Society, 363, 18, 1715–1726. doi: 10.1056/NEJMoa1008770.

Petreanu, L., Huber, D., Sobczyk, A., Svoboda, K., 2007. Channelrhodopsin-2–assisted circuit mapping of long-range callosal projections, *Nature Neuroscience*, 10, 5. doi: 10.1038/nn1891.

Pincus, A. B., Adhikary, S., Lebold, K. M., Fryer, A. D., Jacoby, D. B., 2020. Optogenetic control of airway cholinergic neurons in vivo, *American Journal of Respiratory Cell and Molecular Biology*, American Thoracic Society, 62, 4, 423–429. doi: 10.1165/rcmb.2019-0378MA.

Proskocil, B. J., Bruun, D. A., Garg, J. A., Villagomez, C. C., Jacoby, D. B., Lein, P. J., Fryer, A. D., 2015. The influence of sensitization on mechanisms of organophosphorus pesticide-induced airway hyperreactivity, *American Journal of Respiratory Cell and Molecular Biology*, American Thoracic Society, 53, 5, 738–747. doi: 10.1165/rcmb.2014-0444OC.

Proskocil, B. J., Bruun, D. A., Jacoby, D. B., van Rooijen, N., Lein, P. J., Fryer, A. D., 2013. Macrophage TNF-α mediates parathion-induced airway hyperreactivity in guinea pigs, *American Journal of Physiology - Lung Cellular and Molecular Physiology*, Am J Physiol Lung Cell Mol Physiol, 304, 8. doi: 10.1152/ajplung.00381.2012.

Proskocil, B. J., Bruun, D. A., Lorton, J. K., Blensly, K. C., Jacoby, D. B., Lein, P. J., Fryer, A. D., 2008. Antigen sensitization influences organophosphorus pesticide-induced airway hyperreactivity, *Environmental Health Perspectives*, 116, 3, 381–388. doi: 10.1289/ehp.10694.

Rajendran, P. S., Challis, R. C., Fowlkes, C. C., Hanna, P., Tompkins, J. D., Jordan, M. C., Hiyari, S., Gabris-Weber, B. A., Greenbaum, A., Chan, K. Y., Deverman, B. E., Münzberg, H., Ardell, J. L., Salama, G., Gradinaru, V., Shivkumar, K., 2019. Identification of peripheral neural circuits that regulate heart rate using optogenetic and viral vector strategies, *Nature Communications*, Nature Publishing Group, 10, 1. doi: 10.1038/s41467-019-09770-1.

Ricciardolo, F. L. M., 2003. Multiple roles of nitric oxide in the airways, *Thorax*, 58, 2, 175–182. doi: 10.1136/thorax.58.2.175.

Ricciardolo, F. L. M., Timmers, M. C., Brahim, J. J., de Gouw, H. W. F. M., Hiemstra, P. S., Sterk, P. J., Geppetti, P., van Schadewijk, A., van Krieken, J. H. J. M., Sont, J. K., 2001. Allergen-induced impairment of bronchoprotective nitric oxide synthesis in asthma, *Journal of Allergy and Clinical Immunology*, Mosby Inc., 108, 2, 198–204. doi: 10.1067/mai.2001.116572.

Riccio, M. M., Myers, A. C., Undem, B. J., 1996. Immunomodulation of afferent neurons in guinea-pig isolated airway, *Journal of Physiology*, Cambridge University Press, 491, 2, 499–509. doi: 10.1113/jphysiol.1996.sp021234.

Richardson, R. J., Grkovic, I., Anderson, C. R., 2003. Immunohistochemical analysis of intracardiac ganglia of the rat heart, *Cell and Tissue Research*, 314, 3. doi: 10.1007/s00441-003-0805-2.

Roffel, A. F., Elzinga, C. R. S., Zaagsma, J., 1990. Muscarinic M3 receptors mediate contraction of human central and peripheral airway smooth muscle, *Pulmonary Pharmacology*, Pulm Pharmacol, 3, 1, 47–51. doi: 10.1016/0952-0600(90)90009-8.

Roossien, D. H., Sadis, B. V., Yan, Y., Webb, J. M., Min, L. Y., Dizaji, A. S., Bogart, L. J., Mazuski, C., Huth, R. S., Stecher, J. S., Akula, S., Shen, F., Li, Y., Xiao, T., Vandenbrink, M., Lichtman, J. W., Hensch, T. K., Herzog, E. D., Cai, D., 2019. Multispectral tracing in densely labeled mouse brain with nTracer, *Bioinformatics*, Oxford University Press, 35, 18, 3544–3546. doi: 10.1093/bioinformatics/btz084.

Rynko, A. E., 2013. *The role of TNF- [alpha] and IL-1[beta] in virus-induced M2 receptor dysfunction*, Oregon Health & Science University.

Rynko, A. E., Fryer, A. D., Jacoby, D. B., 2014. Interleukin-1β mediates virus-induced M2 muscarinic receptor dysfunction and airway hyperreactivity, *American Journal of Respiratory Cell and Molecular Biology*, American Thoracic Society, 51, 4, 494–501. doi: 10.1165/rcmb.2014-0009OC.

Samarasinghe, A. E., Hoselton, S. A., Schuh, J. M., 2010. Spatio-temporal localization of vasoactive intestinal peptide and neutral endopeptidase in allergic murine lungs, *Regulatory Peptides*, 164, 2–3, 151–157. doi: 10.1016/j.regpep.2010.05.017.

Sawatzky, D. A., Kingham, P. J., Court, E., Kumaravel, B., Fryer, A. D., Jacoby, D. B., Graham McLean, W., Costello, R. W., 2002. Eosinophil adhesion to cholinergic nerves via ICAM-1 and VCAM-1 and associated eosinophil degranulation, *American Journal of Physiology - Lung Cellular and Molecular*

Physiology, American Physiological Society, 282, 6 26-6. doi: 10.1152/ajplung.00279.2001.
Schultheis, A. H., Bassett, D. J. P., Fryer, A. D., 1994. Ozone-induced airway hyperresponsiveness and loss of neuronal M2 muscarinic receptor function, *Journal of Applied Physiology*, American Physiological Society, 76, 3, 1088–1097. doi: 10.1152/jappl.1994.76.3.1088.
Schuster, D. J., Dykstra, J. A., Riedl, M. S., Kitto, K. F., Belur, L. R., McIvor, R. S., Elde, R. P., Fairbanks, C. A., Vulchanova, L., 2014. Biodistribution of adeno-associated virus serotype 9 (AAV9) vector after intrathecal and intravenous delivery in mouse, *Frontiers in Neuroanatomy*, Frontiers Research Foundation, 8, JUN, 42–42. doi: 10.3389/fnana.2014.00042.
Scott, G. D., 2012. *Sensory neuroplasticity in asthma*.
Scott, G. D., Blum, E. D., Fryer, A. D., Jacoby, D. B., 2014. Tissue optical clearing, three-dimensional imaging, and computer morphometry in whole mouse lungs and human airways., *American journal of respiratory cell and molecular biology*, American Thoracic Society, 51, 1, 43–55. doi: 10.1165/rcmb.2013-0284OC.
Scott, G. D., Fryer, A. D., Jacoby, D. B., 2013. Quantifying Nerve Architecture in Murine and Human Airways Using Three-Dimensional Computational Mapping, *American Journal of Respiratory Cell and Molecular Biology*, American Thoracic Society, 48, 1, 10–16. doi: 10.1165/rcmb.2012-0290MA.
Sekizawa, S., Bechtold, A. G., Tham, R. C., Kott, K. S., Hyde, D. M., Joad, J. P., Bonham, A. C., 2010. House-dust mite allergen and ozone exposure decreases histamine H3 receptors in the brainstem respiratory nuclei, *Toxicology and Applied Pharmacology*, 247, 3. doi: 10.1016/j.taap.2010.06.014.
Sekizawa, S.-I., Chen, C.-Y., Bechtold, A. G., Tabor, J. M., Bric, J. M., Pinkerton, K. E., Joad, J. P., Bonham, A. C., 2008. Extended secondhand tobacco smoke exposure induces plasticity in nucleus tractus solitarius second-order lung afferent neurons in young guinea pigs, *European Journal of Neuroscience*, 28, 4. doi: 10.1111/j.1460-9568.2008.06378.x.
Shapiro, C. O., Proskocil, B. J., Oppegard, L. J., Blum, E. D., Kappel, N. L., Chang, C. H., Fryer, A. D., Jacoby, D. B., Costello, R. W., Drake, M. G., 2020. Airway Sensory Nerve Density is Increased in Chronic Cough, *American Journal of Respiratory and Critical Care Medicine*, American Thoracic Society. doi: 10.1164/rccm.201912-2347oc.
Sheppard, D., Thompson, J. E., Scypinski, L., Dusser, D., Nadel, J. A., Borson, D. B., 1988. Toluene diisocyanate increases airway responsiveness to substance P and decreases airway neutral endopeptidase., *Journal of Clinical Investigation*, 81, 4, 1111–1115. doi: 10.1172/JCI113424.
Sont, J. K., van Krieken, J. H., van Klink, H. C., Roldaan, A. C., Apap, C. R., Willems, L. N., Sterk, P. J., 1997. Enhanced expression of neutral endopeptidase (NEP) in airway epithelium in biopsies from steroid- versus nonsteroid-treated patients with atopic asthma., *American Journal of Respiratory Cell and Molecular Biology*, 16, 5, 549–556. doi: 10.1165/ajrcmb.16.5.9160837.
Sparrow, M. P., Weichselbaum, M., Mccray, P. B., 1999. *Development of the Innervation and Airway Smooth Muscle in Human Fetal Lung*, *Am. J. Respir. Cell Mol. Biol*, pp. 550–560. (online: www.atsjournals.org).
Spaziano, G., Luongo, L., Guida, F., Petrosino, S., Matteis, M., Palazzo, E., Sullo, N., De Novellis, V., Di Marzo, V., Rossi, F., Maione, S., D'Agostino, B., 2015. Exposure to allergen causes changes in nts neural activities after intratracheal capsaicin application, in endocannabinoid levels and in the glia morphology of nts, *BioMed Research International*, Hindawi Limited, 2015. doi: 10.1155/2015/980983.
Springall, D. R., Polak, J. M., Howard, L., Power, R. F., Krausz, T., Manickam, S., Banner, N. R., Khagani, A., Rose, M., Yacoub, M. H., 1990. Persistence of intrinsic neurones and possible phenotypic changes after extrinsic denervation of human respiratory tract by heart-lung transplantation, *The American Review of Respiratory Disease*, 141, 6, 1538–1546. doi: 10.1164/ajrccm/141.6.1538.
Steyn, E., Mohamed, Z., Husselman, C., 2013. Non-invasive vagus nerve stimulation for the treatment of acute asthma exacerbations - Results from an initial case series, *International Journal of Emergency Medicine*, 6, 1. doi: 10.1186/1865-1380-6-7.

Sui, P., Wiesner, D. L., Xu, J., Zhang, Y., Lee, J., Van Dyken, S., Lashua, A., Yu, C., Klein, B. S., Locksley, R. M., Deutsch, G., Sun, X., 2018. Pulmonary neuroendocrine cells amplify allergic asthma responses, *Science*, American Association for the Advancement of Science, 360, 6393. doi: 10.1126/science.aan8546.

Tränkner, D., Hahne, N., Sugino, K., Hoon, M. A., Zuker, C., 2014. Population of sensory neurons essential for asthmatic hyperreactivity of inflamed airways, *Proceedings of the National Academy of Sciences of the United States of America*, National Academy of Sciences, 111, 31, 11515–11520. doi: 10.1073/pnas.1411032111.

Tsai, H.-C., Zhang, F., Adamantidis, A., Stuber, G. D., Bonci, A., de Lecea, L., Deisseroth, K., 2009. Phasic Firing in Dopaminergic Neurons Is Sufficient for Behavioral Conditioning, *Science*, 324, 5930. doi: 10.1126/science.1168878.

Tsuriel, S., Gudes, S., Draft, R. W., Binshtok, A. M., Lichtman, J. W., 2015. Multispectral labeling technique to map many neighboring axonal projections in the same tissue, *Nature Methods*, 12, 6, 547–552. doi: 10.1038/nmeth.3367.

Turlo, K. A., Gallaher, S. D., Vora, R., Laski, F. A., Iruela-Arispe, M. L., 2010. When Cre-mediated recombination in mice does not result in protein loss, *Genetics*, 186, 3, 959–967. doi: 10.1534/genetics.110.121608.

Undem, B., Adams, G., Buckner, C., 1989. Influence of electrical field stimulation on antigen-induced contraction and mediator release in the guinea pig isolated superfused trachea and bronchus, *Journal of Pharmacology and Experimental Therapautics*, 249, 1, 23–30.

Undem, B. J., Carr, M. J., 2002. The role of nerves in asthma., *Current allergy and asthma reports*, 2, 2, 159–165. doi: 10.1007/s11882-002-0011-4.

Undem, B. J., Hunter, D. D., Liu, M., Haak-Frendscho, M., Oakragly, A., Fischer, A., 1999. Allergen-induced sensory neuroplasticity in airways, in, *International Archives of Allergy and Immunology*, S. Karger AG, pp. 150–153. doi: 10.1159/000024053.

Undem, B. J., Myers, A. C., Barthlow, H., Weinreich, D., 1990. Vagal innervation of guinea pig bronchial smooth muscle, *Journal of Applied Physiology*, J Appl Physiol (1985), 69, 4, 1336–1346. doi: 10.1152/jappl.1990.69.4.1336.

Undem, B. J., Weinreich, D., 1993. Electrophysiological properties and chemosensitivity of guinea pig nodose ganglion neurons in vitro, *Journal of the Autonomic Nervous System*, 44, 1, 17–33. doi: 10.1016/0165-1838(93)90375-5.

Verhein, K. C., Salituro, F. G., Ledeboer, M. W., Fryer, A. D., Jacoby, D. B., 2013. Dual p38/JNK mitogen activated protein kinase inhibitors prevent ozone-induced airway hyperreactivity in guinea pigs., *PloS one*, 8, 9, e75351–e75351. doi: 10.1371/journal.pone.0075351.

Vieira Braga, F. A., Kar, G., Berg, M., Carpaij, O. A., Polanski, K., Simon, L. M., Brouwer, S., Gomes, T., Hesse, L., Jiang, J., Fasouli, E. S., Efremova, M., Vento-Tormo, R., Talavera-López, C., Jonker, M. R., Affleck, K., Palit, S., Strzelecka, P. M., Firth, H. V., Mahbubani, K. T., Cvejic, A., Meyer, K. B., Saeb-Parsy, K., Luinge, M., Brandsma, C. A., Timens, W., Angelidis, I., Strunz, M., Koppelman, G. H., van Oosterhout, A. J., Schiller, H. B., Theis, F. J., van den Berge, M., Nawijn, M. C., Teichmann, S. A., 2019. A cellular census of human lungs identifies novel cell states in health and in asthma, *Nature Medicine*, Nature Publishing Group, 25, 7, 1153–1163. doi: 10.1038/s41591-019-0468-5.

Voorhorst, R., Spieksma, F. Th. M., Varekamp, H., Leupen, M. J., Lyklema, A. W., 1967. The house-dust mite (Dermatophagoides pteronyssinus) and the allergens it produces. Identity with the house-dust allergen, *Journal of Allergy*, 39, 6, 325–339. doi: 10.1016/0021-8707(67)90045-7.

Vos, T., Abajobir, A. A., Abate, K. H., Abbafati, C., Abbas, K. M., Abd-Allah, F., Abdulkader, R. S., Abdulle, A. M., Abebo, T. A., Abera, S. F., Aboyans, V., Abu-Raddad, L. J., Ackerman, I. N., Adamu, A. A., Adetokunboh, O., Afarideh, M., Afshin, A., Agarwal, S. K., Aggarwal, R., Agrawal, A., Agrawal, S., Ahmadieh, H., Ahmed, M. B., Aichour, M. T. E., Aichour, A. N., Aichour, I., Aiyar, S., Akinyemi, R. O., Akseer, N., Al Lami, F. H., Alahdab, F., Al-Aly, Z., Alam, K., Alam, N., Alam, T., Alasfoor, D.,

Alene, K. A., Ali, R., Alizadeh-Navaei, R., Alkerwi, A., Alla, F., Allebeck, P., Allen, C., Al-Maskari, F., Al-Raddadi, R., Alsharif, U., Alsowaidi, S., Altirkawi, K. A., Amare, A. T., Amini, E., Ammar, W., Amoako, Y. A., Andersen, H. H., Antonio, C. A. T., Anwari, P., Ärnlöv, J., Artaman, A., Aryal, K. K., Asayesh, H., Asgedom, S. W., Assadi, R., Atey, T. M., Atnafu, N. T., Atre, S. R., Avila-Burgos, L., Avokphako, E. F. G. A., Awasthi, A., Bacha, U., Badawi, A., Balakrishnan, K., Banerjee, A., Bannick, M. S., Barac, A., Barber, R. M., Barker-Collo, S. L., Bärnighausen, T., Barquera, S., Barregard, L., Barrero, L. H., Basu, S., Battista, B., Battle, K. E., Baune, B. T., Bazargan-Hejazi, S., Beardsley, J., Bedi, N., Beghi, E., Béjot, Y., Bekele, B. B., Bell, M. L., Bennett, D. A., Bensenor, I. M., Benson, J., Berhane, A., Berhe, D. F., Bernabé, E., Betsu, B. D., Beuran, M., Beyene, A. S., Bhala, N., Bhansali, A., Bhatt, S., Bhutta, Z. A., Biadgilign, S., Bicer, B. K., Bienhoff, K., Bikbov, B., Birungi, C., Biryukov, S., Bisanzio, D., Bizuayehu, H. M., Boneya, D. J., Boufous, S., Bourne, R. R. A., Brazinova, A., Brugha, T. S., Buchbinder, R., Bulto, L. N. B., Bumgarner, B. R., Butt, Z. A., Cahuana-Hurtado, L., Cameron, E., Car, M., Carabin, H., Carapetis, J. R., Cárdenas, R., Carpenter, D. O., Carrero, J. J., Carter, A., Carvalho, F., Casey, D. C., Caso, V., Castañeda-Orjuela, C. A., Castle, C. D., Catalá-López, F., Chang, H.-Y., Chang, J.-C., Charlson, F. J., Chen, H., Chibalabala, M., Chibueze, C. E., Chisumpa, V. H., Chitheer, A. A., Christopher, D. J., Ciobanu, L. G., Cirillo, M., Colombara, D., Cooper, C., Cortesi, P. A., Criqui, M. H., Crump, J. A., Dadi, A. F., Dalal, K., Dandona, L., Dandona, R., das Neves, J., Davitoiu, D. V., de Courten, B., De Leo, D. D., Defo, B. K., Degenhardt, L., Deiparine, S., Dellavalle, R. P., Deribe, K., Des Jarlais, D. C., Dey, S., Dharmaratne, S. D., Dhillon, P. K., Dicker, D., Ding, E. L., Djalalinia, S., Do, H. P., Dorsey, E. R., dos Santos, K. P. B., Douwes-Schultz, D., Doyle, K. E., Driscoll, T. R., Dubey, M., Duncan, B. B., El-Khatib, Z. Z., Ellerstrand, J., Enayati, A., Endries, A. Y., Ermakov, S. P., Erskine, H. E., Eshrati, B., Eskandarieh, S., Esteghamati, A., Estep, K., Fanuel, F. B. B., Farinha, C. S. E. S., Faro, A., Farzadfar, F., Fazeli, M. S., Feigin, V. L., Fereshtehnejad, S.-M., Fernandes, J. C., Ferrari, A. J., Feyissa, T. R., Filip, I., Fischer, F., Fitzmaurice, C., Flaxman, A. D., Flor, L. S., Foigt, N., Foreman, K. J., Franklin, R. C., Fullman, N., Fürst, T., Furtado, J. M., Futran, N. D., Gakidou, E., Ganji, M., Garcia-Basteiro, A. L., Gebre, T., Gebrehiwot, T. T., Geleto, A., Gemechu, B. L., Gesesew, H. A., Gething, P. W., Ghajar, A., Gibney, K. B., Gill, P. S., Gillum, R. F., Ginawi, I. A. M., Giref, A. Z., Gishu, M. D., Giussani, G., Godwin, W. W., Gold, A. L., Goldberg, E. M., Gona, P. N., Goodridge, A., Gopalani, S. V., Goto, A., Goulart, A. C., Griswold, M., Gugnani, H. C., Gupta, Rahul, Gupta, Rajeev, Gupta, T., Gupta, V., Hafezi-Nejad, N., Hailu, G. B., Hailu, A. D., Hamadeh, R. R., Hamidi, S., Handal, A. J., Hankey, G. J., Hanson, S. W., Hao, Y., Harb, H. L., Hareri, H. A., Haro, J. M., Harvey, J., Hassanvand, M. S., Havmoeller, R., Hawley, C., Hay, S. I., Hay, R. J., Henry, N. J., Heredia-Pi, I. B., Hernandez, J. M., Heydarpour, P., Hoek, H. W., Hoffman, H. J., Horita, N., Hosgood, H. D., Hostiuc, S., Hotez, P. J., Hoy, D. G., Htet, A. S., Hu, G., Huang, H., Huynh, C., Iburg, K. M., Igumbor, E. U., Ikeda, C., Irvine, C. M. S., Jacobsen, K. H., Jahanmehr, N., Jakovljevic, M. B., Jassal, S. K., Javanbakht, M., Jayaraman, S. P., Jeemon, P., Jensen, P. N., Jha, V., Jiang, G., John, D., Johnson, S. C., Johnson, C. O., Jonas, J. B., Jürisson, M., Kabir, Z., Kadel, R., Kahsay, A., Kamal, R., Kan, H., Karam, N. E., Karch, A., Karema, C. K., Kasaeian, A., Kassa, G. M., Kassaw, N. A., Kassebaum, N. J., Kastor, A., Katikireddi, S. V., Kaul, A., Kawakami, N., Keiyoro, P. N., Kengne, A. P., Keren, A., Khader, Y. S., Khalil, I. A., Khan, E. A., Khang, Y.-H., Khosravi, A., Khubchandani, J., Kiadaliri, A. A., Kieling, C., Kim, Y. J., Kim, D., Kim, P., Kimokoti, R. W., Kinfu, Y., Kisa, A., Kissimova-Skarbek, K. A., Kivimaki, M., Knudsen, A. K., Kokubo, Y., Kolte, D., Kopec, J. A., Kosen, S., Koul, P. A., Koyanagi, A., Kravchenko, M., Krishnaswami, S., Krohn, K. J., Kumar, G. A., Kumar, P., Kumar, S., Kyu, H. H., Lal, D. K., Lalloo, R., Lambert, N., Lan, Q., Larsson, A., Lavados, P. M., Leasher, J. L., Lee, P. H., Lee, J.-T., Leigh, J., Leshargie, C. T., Leung, J., Leung, R., Levi, M., Li, Yichong, Li, Yongmei, Li Kappe, D., Liang, X., Liben, M. L., Lim, S. S., Linn, S., Liu, P. Y., Liu, A., Liu, S., Liu, Y., Lodha, R., Logroscino, G., London, S. J., Looker, K. J., Lopez, A. D., Lorkowski, S., Lotufo, P. A., Low, N., Lozano, R., Lucas, T. C. D., Macarayan, E. R. K., Magdy Abd El Razek, H., Magdy Abd El

Razek, M., Mahdavi, M., Majdan, M., Majdzadeh, R., Majeed, A., Malekzadeh, R., Malhotra, R., Malta, D. C., Mamun, A. A., Manguerra, H., Manhertz, T., Mantilla, A., Mantovani, L. G., Mapoma, C. C., Marczak, L. B., Martinez-Raga, J., Martins-Melo, F. R., Martopullo, I., März, W., Mathur, M. R., Mazidi, M., McAlinden, C., McGaughey, M., McGrath, J. J., McKee, M., McNellan, C., Mehata, S., Mehndiratta, M. M., Mekonnen, T. C., Memiah, P., Memish, Z. A., Mendoza, W., Mengistie, M. A., Mengistu, D. T., Mensah, G. A., Meretoja, T. J., Meretoja, A., Mezgebe, H. B., Micha, R., Millear, A., Miller, T. R., Mills, E. J., Mirarefin, M., Mirrakhimov, E. M., Misganaw, A., Mishra, S. R., Mitchell, P. B., Mohammad, K. A., Mohammadi, A., Mohammed, K. E., Mohammed, S., Mohanty, S. K., Mokdad, A. H., Mollenkopf, S. K., Monasta, L., Montico, M., Moradi-Lakeh, M., Moraga, P., Mori, R., Morozoff, C., Morrison, S. D., Moses, M., Mountjoy-Venning, C., Mruts, K. B., Mueller, U. O., Muller, K., Murdoch, M. E., Murthy, G. V. S., Musa, K. I., Nachega, J. B., Nagel, G., Naghavi, M., Naheed, A., Naidoo, K. S., Naldi, L., Nangia, V., Natarajan, G., Negasa, D. E., Negoi, R. I., Negoi, I., Newton, C. R., Ngunjiri, J. W., Nguyen, T. H., Nguyen, Q. L., Nguyen, C. T., Nguyen, G., Nguyen, M., Nichols, E., Ningrum, D. N. A., Nolte, S., Nong, V. M., Norrving, B., Noubiap, J. J. N., O'Donnell, M. J., Ogbo, F. A., Oh, I.-H., Okoro, A., Oladimeji, O., Olagunju, T. O., Olagunju, A. T., Olsen, H. E., Olusanya, B. O., Olusanya, J. O., Ong, K., Opio, J. N., Oren, E., Ortiz, A., Osgood-Zimmerman, A., Osman, M., Owolabi, M. O., PA, M., Pacella, R. E., Pana, A., Panda, B. K., Papachristou, C., Park, E.-K., Parry, C. D., Parsaeian, M., Patten, S. B., Patton, G. C., Paulson, K., Pearce, N., Pereira, D. M., Perico, N., Pesudovs, K., Peterson, C. B., Petzold, M., Phillips, M. R., Pigott, D. M., Pillay, J. D., Pinho, C., Plass, D., Pletcher, M. A., Popova, S., Poulton, R. G., Pourmalek, F., Prabhakaran, D., Prasad, N. M., Prasad, N., Purcell, C., Qorbani, M., Quansah, R., Quintanilla, B. P. A., Rabiee, R. H. S., Radfar, A., Rafay, A., Rahimi, K., Rahimi-Movaghar, A., Rahimi-Movaghar, V., Rahman, M. H. U., Rahman, M., Rai, R. K., Rajsic, S., Ram, U., Ranabhat, C. L., Rankin, Z., Rao, P. C., Rao, P. V., Rawaf, S., Ray, S. E., Reiner, R. C., Reinig, N., Reitsma, M. B., Remuzzi, G., Renzaho, A. M. N., Resnikoff, S., Rezaei, S., Ribeiro, A. L., Ronfani, L., Roshandel, G., Roth, G. A., Roy, A., Rubagotti, E., Ruhago, G. M., Saadat, S., Sadat, N., Safdarian, M., Safi, S., Safiri, S., Sagar, R., Sahathevan, R., Salama, J., Saleem, H. O. B., Salomon, J. A., Salvi, S. S., Samy, A. M., Sanabria, J. R., Santomauro, D., Santos, I. S., Santos, J. V., Santric Milicevic, M. M., Sartorius, B., Satpathy, M., Sawhney, M., Saxena, S., Schmidt, M. I., Schneider, I. J. C., Schöttker, B., Schwebel, D. C., Schwendicke, F., Seedat, S., Sepanlou, S. G., Servan-Mori, E. E., Setegn, T., Shackelford, K. A., Shaheen, A., Shaikh, M. A., Shamsipour, M., Shariful Islam, S. M., Sharma, J., Sharma, R., She, J., Shi, P., Shields, C., Shifa, G. T., Shigematsu, M., Shinohara, Y., Shiri, R., Shirkoohi, R., Shirude, S., Shishani, K., Shrime, M. G., Sibai, A. M., Sigfusdottir, I. D., Silva, D. A. S., Silva, J. P., Silveira, D. G. A., Singh, J. A., Singh, N. P., Sinha, D. N., Skiadaresi, E., Skirbekk, V., Slepak, E. L., Sligar, A., Smith, D. L., Smith, M., Sobaih, B. H. A., Sobngwi, E., Sorensen, R. J. D., Sousa, T. C. M., Sposato, L. A., Sreeramareddy, C. T., Srinivasan, V., Stanaway, J. D., Stathopoulou, V., Steel, N., Stein, M. B., Stein, D. J., Steiner, T. J., Steiner, C., Steinke, S., Stokes, M. A., Stovner, L. J., Strub, B., Subart, M., Sufiyan, M. B., Sunguya, B. F., Sur, P. J., Swaminathan, S., Sykes, B. L., Sylte, D. O., Tabarés-Seisdedos, R., Taffere, G. R., Takala, J. S., Tandon, N., Tavakkoli, M., Taveira, N., Taylor, H. R., Tehrani-Banihashemi, A., Tekelab, T., Terkawi, A. S., Tesfaye, D. J., Tesssema, B., Thamsuwan, O., Thomas, K. E., Thrift, A. G., Tiruye, T. Y., Tobe-Gai, R., Tollanes, M. C., Tonelli, M., Topor-Madry, R., Tortajada, M., Touvier, M., Tran, B. X., Tripathi, S., Troeger, C., Truelsen, T., Tsoi, D., Tuem, K. B., Tuzcu, E. M., Tyrovolas, S., Ukwaja, K. N., Undurraga, E. A., Uneke, C. J., Updike, R., Uthman, O. A., Uzochukwu, B. S. C., van Boven, J. F. M., Varughese, S., Vasankari, T., Venkatesh, S., Venketasubramanian, N., Vidavalur, R., Violante, F. S., Vladimirov, S. K., Vlassov, V. V., Vollset, S. E., Wadilo, F., Wakayo, T., Wang, Y.-P., Weaver, M., Weichenthal, S., Weiderpass, E., Weintraub, R. G., Werdecker, A., Westerman, R., Whiteford, H. A., Wijeratne, T., Wiysonge, C. S., Wolfe, C. D. A., Woodbrook, R., Woolf, A. D., Workicho, A., Xavier, D., Xu, G., Yadgir, S., Yaghoubi, M., Yakob, B., Yan, L. L., Yano, Y., Ye, P., Yimam, H. H., Yip, P.,

Yonemoto, N., Yoon, S.-J., Yotebieng, M., Younis, M. Z., Zaidi, Z., Zaki, M. E. S., Zegeye, E. A., Zenebe, Z. M., Zhang, X., Zhou, M., Zipkin, B., Zodpey, S., Zuhlke, L. J., Murray, C. J. L., 2017. Global, regional, and national incidence, prevalence, and years lived with disability for 328 diseases and injuries for 195 countries, 1990–2016: a systematic analysis for the Global Burden of Disease Study 2016, *The Lancet*, 390, 10100. doi: 10.1016/S0140-6736(17)32154-2.

de Vries, A., Engels, F., Henricks, P. A. J., Leusink-Muis, T., McGregor, G. P., Braun, A., Groneberg, D. A., Dessing, M. C., Nijkamp, F. P., Fischer, A., 2006. Airway hyper-responsiveness in allergic asthma in guinea-pigs is mediated by nerve growth factor via the induction of substance P: a potential role for trkA., *Clinical and experimental allergy : journal of the British Society for Allergy and Clinical Immunology*, 36, 9, 1192–200. doi: 10.1111/j.1365-2222.2006.02549.x.

Ward, J. K., Belvisi, M. G., Fox, A. J., Miura, M., Tadjkarimi, S., Yacoub, M. H., Barnes, P. J., 1993. Modulation of cholinergic neural bronchoconstriction by endogenous nitric oxide and vasoactive intestinal peptide in human airways in vitro, *Journal of Clinical Investigation*, The American Society for Clinical Investigation, 92, 2, 736–742. doi: 10.1172/JCI116644.

Watson, J. H., Brinkman, G. L., 1964. Electron microscopy of the epithelial cells of normal and bronchitic human bronchus., *The American review of respiratory disease*, 90, 851–66. doi: 10.1164/arrd.1964.90.6.851.

Weichselbaum, M., Everett, A. W., Sparrow, M. P., 1996. Mapping the innervation of the bronchial tree in fetal and postnatal pig lung using antibodies to PGP 9.5 and SV2., *American Journal of Respiratory Cell and Molecular Biology*, 15, 6, 703–710. doi: 10.1165/ajrcmb.15.6.8969263.

Weigand, L. A., Myers, A. C., 2010. Synaptic and membrane properties of parasympathetic ganglionic neurons innervating mouse trachea and bronchi, *American Journal of Physiology-Lung Cellular and Molecular Physiology*, 298, 4. doi: 10.1152/ajplung.00386.2009.

Weller, P. F., Spencer, L. A., 2017. Functions of tissue-resident eosinophils, *Nature Reviews Immunology*, Nature Publishing Group, 17, 12, 746–760. doi: 10.1038/nri.2017.95.

Wenzel, S., Castro, M., Corren, J., Maspero, J., Wang, L., Zhang, B., Pirozzi, G., Sutherland, E. R., Evans, R. R., Joish, V. N., Eckert, L., Graham, N. M. H., Stahl, N., Yancopoulos, G. D., Louis-Tisserand, M., Teper, A., 2016. Dupilumab efficacy and safety in adults with uncontrolled persistent asthma despite use of medium-to-high-dose inhaled corticosteroids plus a long-acting β2 agonist: a randomised double-blind placebo-controlled pivotal phase 2b dose-ranging trial, *The Lancet*, 388, 10039. doi: 10.1016/S0140-6736(16)30307-5.

Wenzel, S. E., 2012. Asthma phenotypes: the evolution from clinical to molecular approaches, *Nature Medicine*, 18, 5, 716–725. doi: 10.1038/nm.2678.

West, J. B., 1974. *Respiratory Physiology: The Essentials*. 1st edn, Williams & Wilkins. (online: https://www.google.com/books/edition/Respiratory_physiology/Nl1UAAAAYAAJ?hl=en&gbpv=0).

West, P. W., Canning, B. J., Merlo-Pich, E., Woodcock, A. A., Smith, J. A., 2015. Morphologic characterization of nerves in whole-mount airway biopsies, *American Journal of Respiratory and Critical Care Medicine*, American Thoracic Society, 192, 1, 30–39. doi: 10.1164/rccm.201412-2293OC.

Whimster, W. F., 1986. Number and mean volume of individual submucous glands in the human tracheobronchial tree., *Applied pathology*, 4, 1–2, 24–32.

Widdicombe, J., 2001. Airway receptors, *Respiration Physiology*, 125, 1, 3–15. doi: 10.1016/S0034-5687(00)00201-2.

Widdicombe, J. G., 1981. Respiratory Pharmacology, in Widdicombe, J. G. (Ed.), *International Encyclopedia of Pharmacology and Therapeutics: Section 104*. 1st edn, Oxford, England, Pergamon Press Ltd.

Widdicombe, J. H., Chen, L. L.-K., Sporer, H., Choi, H. K., Pecson, I. S., Bastacky, S. J., 2001. Distribution of tracheal and laryngeal mucous glands in some rodents and the rabbit, *Journal of Anatomy*, Wiley-Blackwell, 198, 2, 207–221. doi: 10.1046/j.1469-7580.2001.19820207.x.

Wilson, C. G., Akhter, S., Mayer, C. A., Kc, P., Balan, K. V., Ernsberger, P., Haxhiu, M. A., 2007. Allergic lung

inflammation affects central noradrenergic control of cholinergic outflow to the airways in ferrets, *Journal of Applied Physiology*, 103, 6. doi: 10.1152/japplphysiol.01182.2006.

Woodcock, A., Forster, L., Matthews, E., Martin, J., Letley, L., Vickers, M., Britton, J., Strachan, D., Howarth, P., Altmann, D., Frost, C., Custovic, A., 2003. Control of Exposure to Mite Allergen and Allergen-Impermeable Bed Covers for Adults with Asthma, *New England Journal of Medicine*, Massachusetts Medical Society, 349, 3, 225–236. doi: 10.1056/NEJMoa023175.

Woolcock, A., Macklem, P., Hogg, J., Wilson, N., Nadal, J., Frank, N., Brain, J., 1967. The response of central and peripheral airways to vagal stimulation in dogs, *Aspen Emphysema Conf.*, 10, 275–85.

Wu, Z.-X., Satterfield, B. E., Dey, R. D., 2003. Substance P released from intrinsic airway neurons contributes to ozone-enhanced airway hyperresponsiveness in ferret trachea, *Journal of Applied Physiology*, 95, 2. doi: 10.1152/japplphysiol.00109.2003.

van Wyk, M., Pielecka-Fortuna, J., Löwel, S., Kleinlogel, S., 2015. Restoring the ON Switch in Blind Retinas: Opto-mGluR6, a Next-Generation, Cell-Tailored Optogenetic Tool, *PLOS Biology*, 13, 5. doi: 10.1371/journal.pbio.1002143.

Yim, P. D., Gallos, G., Perez-Zoghbi, J. F., Zhang, Y., Xu, D., Wu, A., Berkowitz, D. E., Emala, C. W., 2019. Airway smooth muscle photorelaxation via opsin receptor activation, *American Journal of Physiology - Lung Cellular and Molecular Physiology*, American Physiological Society, 316, 1, L82–L93. doi: 10.1152/ajplung.00135.2018.

Yost, B. L., Gleich, G. J., Fryer, A. D., 1999. Ozone-induced hyperresponsiveness and blockade of M2 muscarinic receptors by eosinophil major basic protein, *Journal of Applied Physiology*, American Physiological Society, 87, 4, 1272–1278. doi: 10.1152/jappl.1999.87.4.1272.

Yu, C.-K., Shieh, C.-M., Lei, H.-Y., 1999. Repeated intratracheal inoculation of house dust mite (Dermatophagoides farinae) induces pulmonary eosinophilic inflammation and IgE antibody production in mice☆☆☆★, *Journal of Allergy and Clinical Immunology*, 104, 1. doi: 10.1016/S0091-6749(99)70140-5.

Yu, L., Zhou, L., Cao, G., Po, S. S., Huang, B., Zhou, X., Wang, M., Yuan, S., Wang, Z., Wang, S., Jiang, H., 2017. Optogenetic Modulation of Cardiac Sympathetic Nerve Activity to Prevent Ventricular Arrhythmias, *Journal of the American College of Cardiology*, 70, 22, 2778–2790. doi: 10.1016/j.jacc.2017.09.1107.

Zhang, F., Prigge, M., Beyrière, F., Tsunoda, S. P., Mattis, J., Yizhar, O., Hegemann, P., Deisseroth, K., 2008. Red-shifted optogenetic excitation: A tool for fast neural control derived from Volvox carteri, *Nature Neuroscience*, 11, 6, 631–633. doi: 10.1038/nn.2120.

Zhang, F., Wang, L. P., Brauner, M., Liewald, J. F., Kay, K., Watzke, N., Wood, P. G., Bamberg, E., Nagel, G., Gottschalk, A., Deisseroth, K., 2007. Multimodal fast optical interrogation of neural circuitry, *Nature*, Nature Publishing Group, 446, 7136, 633–639. doi: 10.1038/nature05744.

Zhou, Y., Ling, E.-A., 1998. Colocalization of nitric oxide synthase and some neurotransmitters in the intramural ganglia of the guinea pig urinary bladder, *The Journal of Comparative Neurology*, 394, 4. doi: 10.1002/(SICI)1096-9861(19980518)394:4<496::AID-CNE7>3.0.CO;2-X.

Zhu, Y., Romero, M. I., Ghosh, P., Ye, Z., Charnay, P., Rushing, E. J., Marth, J. D., Parada, L. F., 2001. Ablation of NF1 function in neurons induces abnormal development of cerebral cortex and reactive gliosis in the brain, *Genes & Development*, 15, 7, 859–876. doi: 10.1101/gad.862101.

Appendix

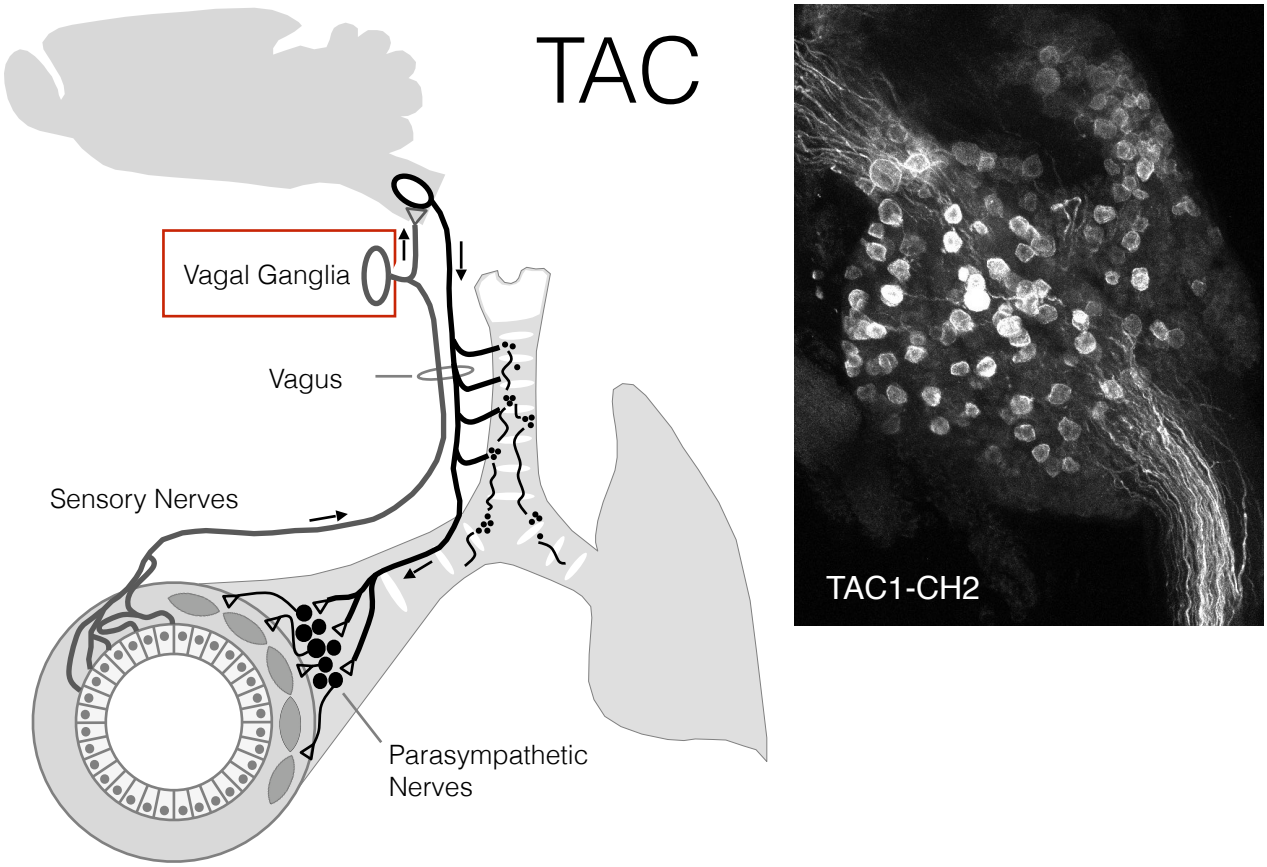

Figure A.1. TAC1-CH2 mice (see Chapter 2: Mouse Models) were used for preliminary optogenetics experiments. As expected, staining for EYFP showed a subset of nerves in the vagal ganglia expressing CH2 - these are expected to be the same nerves that express substance P.

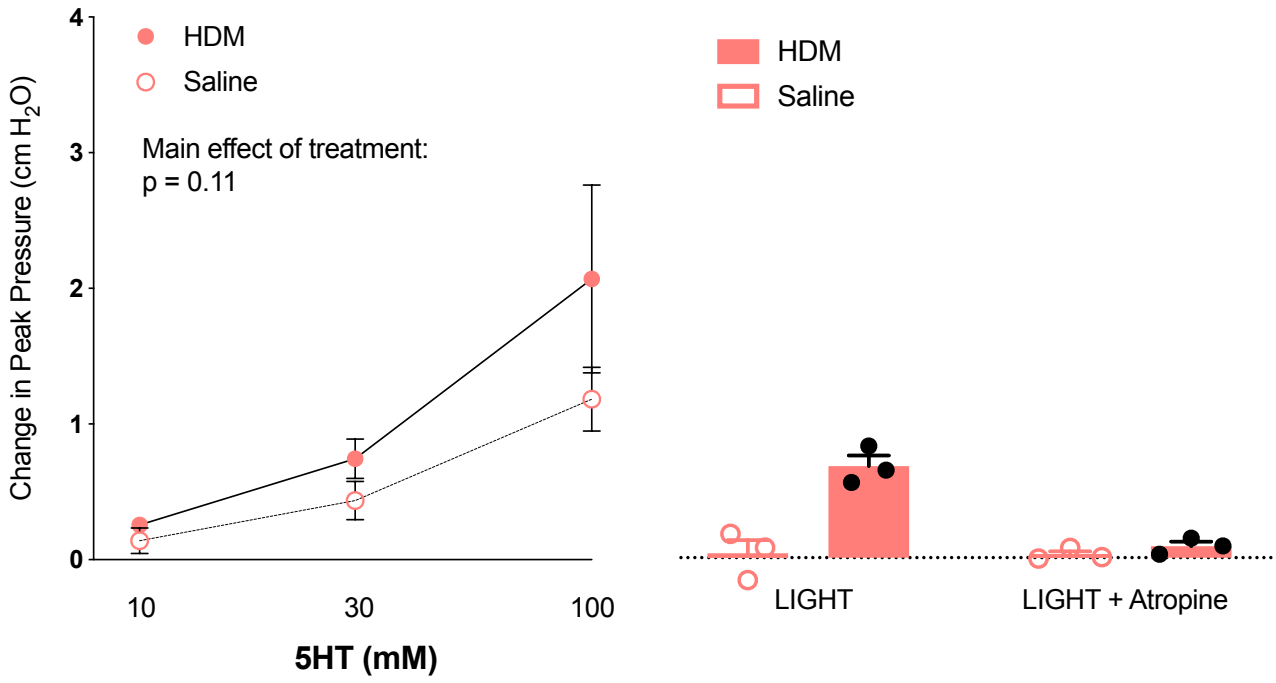

Figure A.2. Preliminary data from mice in which a subset of tachykinin-expressing sensory nerves are activated by light. Further experiments with these animals displayed high variability in response (data not shown).

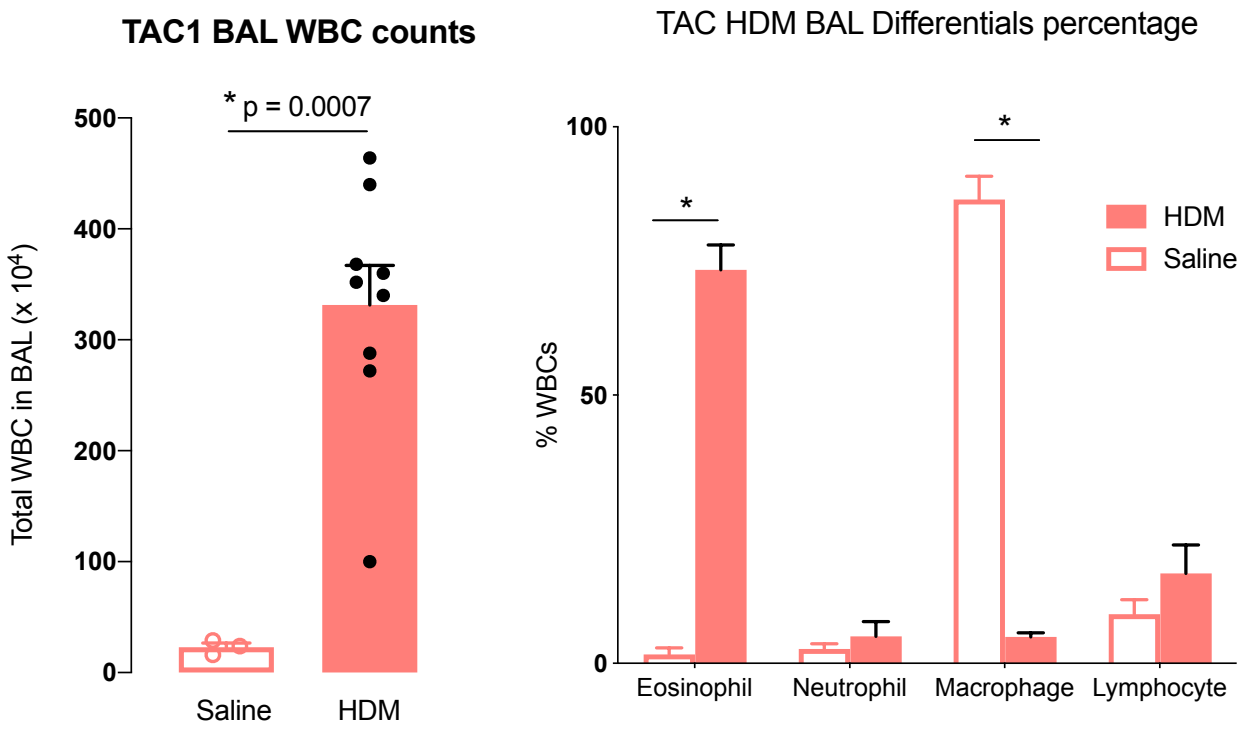

Figure A.3. TAC1-CH2 mice. Immune response in house dust mite treated (HDM) mice compared to saline treated controls. Total white blood cell (WBC) count in HDM vs Saline mice were analyzed by unpaired t test. WBC differential was analyzed using multiple t tests. *$p<0.05$.

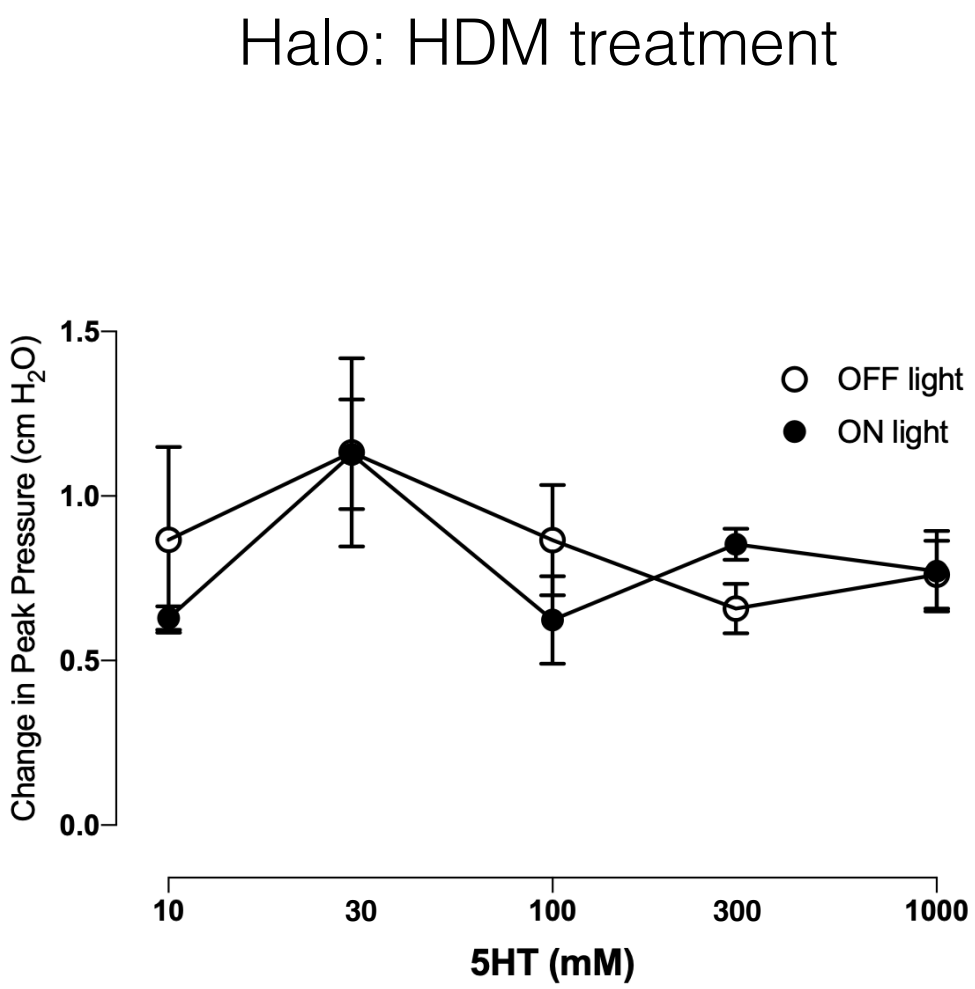

Figure A.4. CHAT-HALO mice (see Chapter 2: Mouse Models) were used for preliminary optogenetics experiments. All mice were treated with house dust mite, and surgery was performed on the mouse ventilator to expose tracheas to light. During a 5HT dose response curve, lime green light (activating halorhodopsin) was given at 20Hz for 60 seconds to one group of mice. No differences were seen between groups, however there was also an unusually small response to 5HT in both. Troubleshooting remains to be done to validate this technique and interpretation of data.

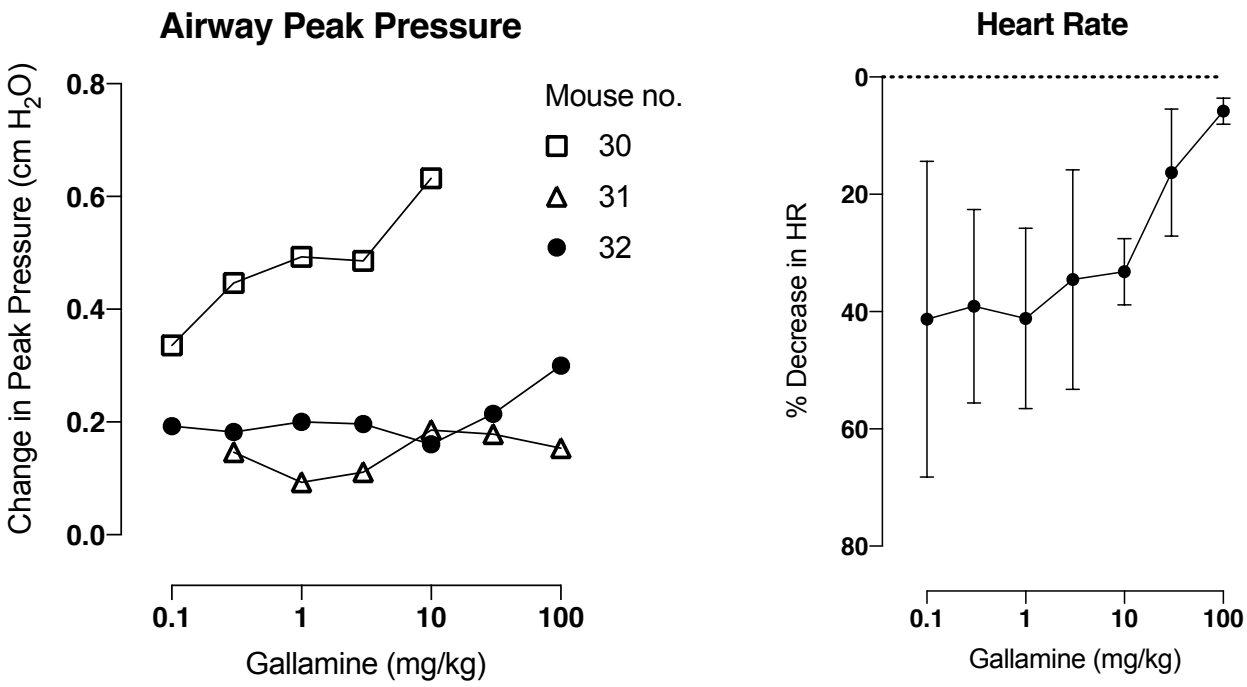

Figure A.5. CHAT-CH2 mice. Pilot study investigating gallamine administration. Collaboration with Jane Niw. Increasing doses of gallamine resulted in an attenuation of the heart rate response to blue light stimulation at 20Hz, but the bronchoconstriction response was less clear.

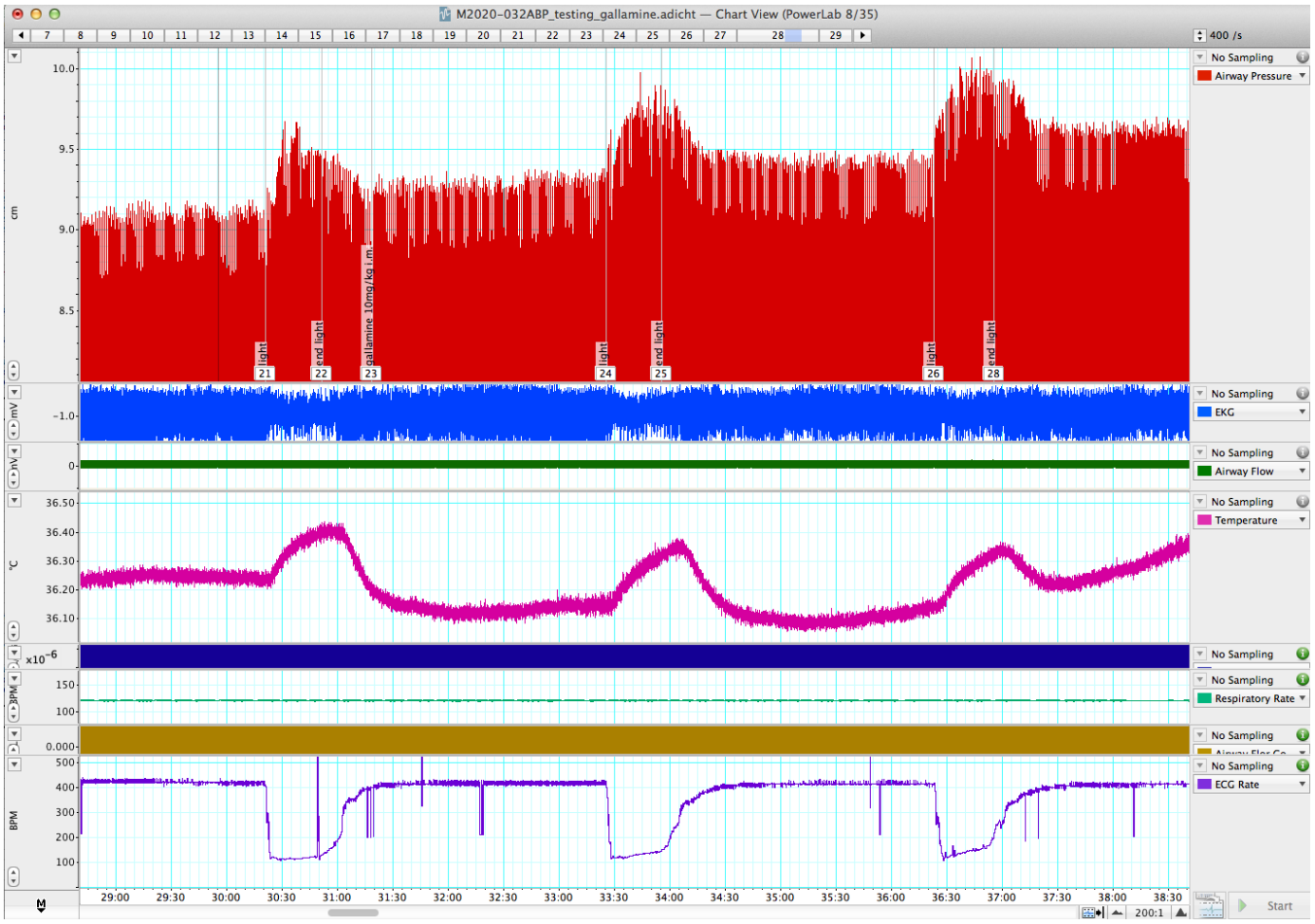

Figure A.6. CHAT-CH2 mice. Example trace showing that in addition to a decrease in heart rate and increase in airway peak pressure, a transient increase in measured mouse internal temperature was also noted during the period of light. This response was seen in less than half of all mice. I speculate that it may have been caused by some brief contraction of the rectum, rather than representing a true whole-animal spike in temperature, but I cannot be certain.

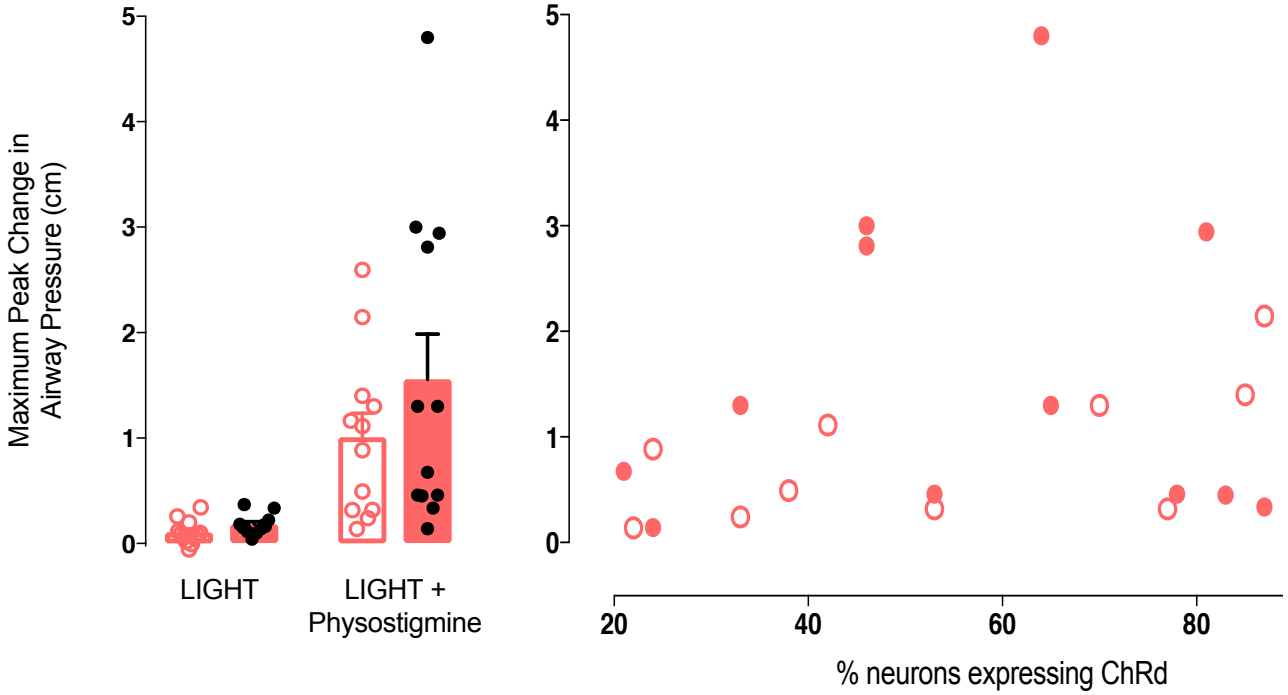

Figure A.7. CHAT-CH2 mice. In addition to light response after 5HT (see Chapter 4), light response after physostigmine was also investigated in saline and HDM treated animals. Although there was a trend toward higher airway pressure changes in the HDM animals, any statistical difference was prevented by the HDM treated low-responders. This data is complicated by variable anesthesia given to these animals (see Figure 3.13).

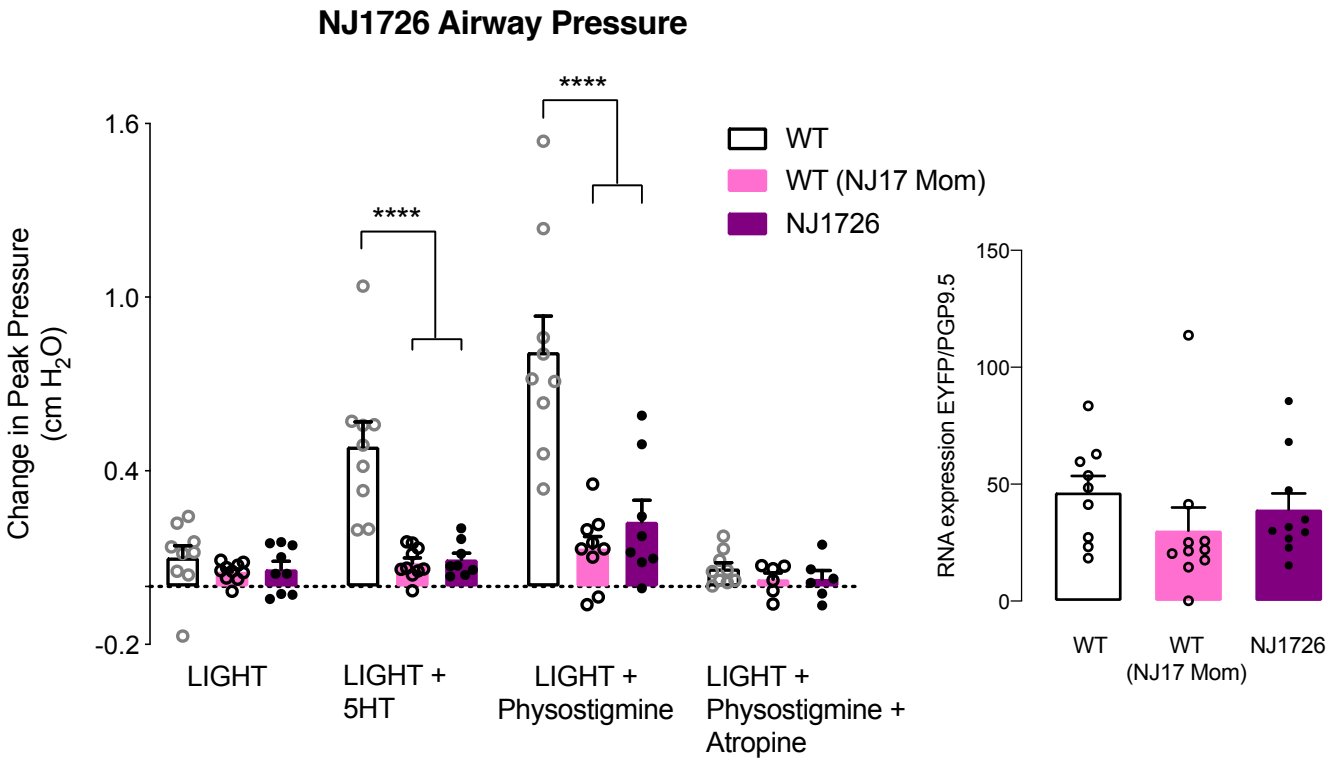

Figure A.8. CHAT-CH2 mice. Preliminary data showing that WT mice from NJ1726 mothers also have low airway pressure responses to blue light, more similar to their NJ1726 siblings than to true WT mice.

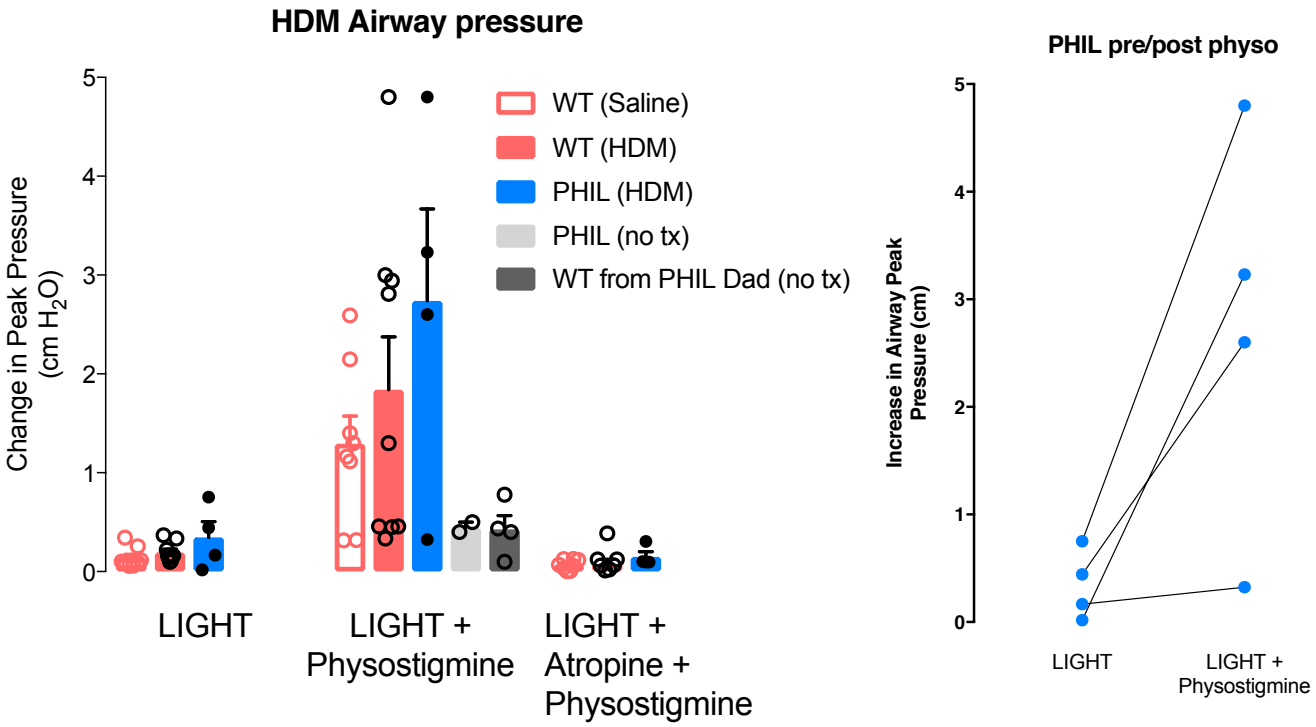

Figure A.9. CHAT-CH2 mice. Preliminary data showing that PHIL-CH2 mice (see Chapter 2: Mouse Models) treated with HDM responded similarly to optogenetic activation of parasympathetic nerves as WT HDM-treated mice after physostigmine. The response of PHIL-CH2 mice to light after 5HT has not yet been investigated.

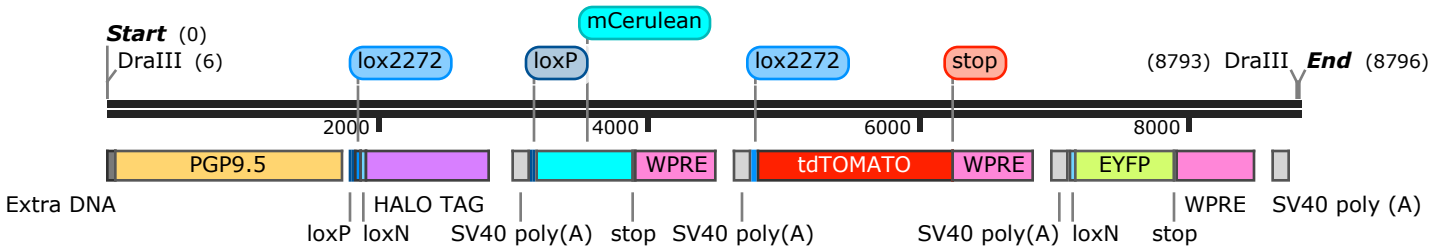

PGP-Panbow
8796 bp

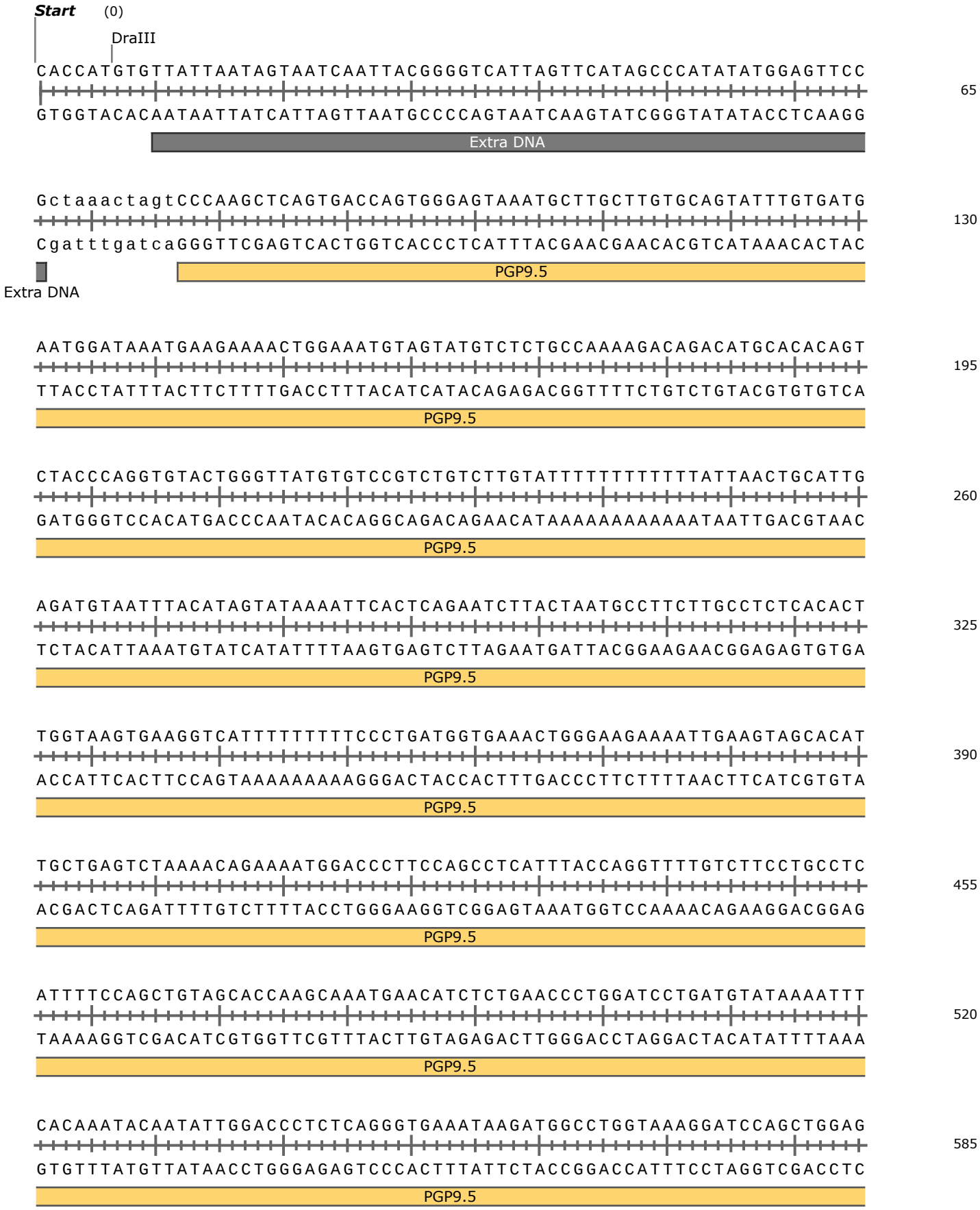
Start (0)
DraIII
5′ CACCATGTGTTATTAATAGTAATCAATTACGGGGTCATTAGTTCATAGCCCATATATGGAGTTCC
3′ GTGGTACACAATAATTATCATTAGTTAATGCCCCAGTAATCAAGTATCGGGTATATACCTCAAGG
65
Extra DNA
GctaaactagtCCCAAGCTCAGTGACCAGTGGGAGTAAATGCTTGCTTGTGCAGTATTTGTGATG
CgatttgatcaGGGTTCGAGTCACTGGTCACCCTCATTTACGAACGAACACGTCATAAACACTAC
130
PGP9.5
Extra DNA
AATGGATAAATGAAGAAAACTGGAAATGTAGTATGTCTCTGCCAAAAGACAGACATGCACACAGT
TTACCTATTTACTTCTTTTGACCTTTACATCATACAGAGACGGTTTTCTGTCTGTACGTGTGTCA
195
PGP9.5
CTACCCAGGTGTACTGGGTTATGTGTCCGTCTGTCTTGTATTTTTTTTTTTTTATTAACTGCATTG
GATGGGTCCACATGACCCAATACACAGGCAGACAGAACATAAAAAAAAAAAAATAATTGACGTAAC
260
PGP9.5
AGATGTAATTTACATAGTATAAAATTCACTCAGAATCTTACTAATGCCTTCTTGCCTCTCACACT
TCTACATTAAATGTATCATATTTTAAGTGAGTCTTAGAATGATTACGGAAGAACGGAGAGTGTGA
325
PGP9.5
TGGTAAGTGAAGGTCATTTTTTTTTCCCTGATGGTGAAACTGGGAAGAAAATTGAAGTAGCACAT
ACCATTCACTTCCAGTAAAAAAAAAGGGACTACCACTTTGACCCTTCTTTTAACTTCATCGTGTA
390
PGP9.5
TGCTGAGTCTAAAACAGAAAATGGACCCTTCCAGCCTCATTTACCAGGTTTTGTCTTCCTGCCTC
ACGACTCAGATTTTGTCTTTTACCTGGGAAGGTCGGAGTAAATGGTCCAAAACAGAAGGACGGAG
455
PGP9.5
ATTTTCCAGCTGTAGCACCAAGCAAATGAACATCTCTGAACCCTGGATCCTGATGTATAAAATTT
TAAAAGGTCGACATCGTGGTTCGTTTACTTGTAGAGACTTGGGACCTAGGACTACATATTTTAAA
520
PGP9.5
CACAAATACAATATTGGACCCTCTCAGGGTGAAATAAGATGGCCTGGTAAAGGATCCAGCTGGAG
GTGTTTATGTTATAACCTGGGAGAGTCCCACTTTATTCTACCGGACCATTTCCTAGGTCGACCTC
585
PGP9.5

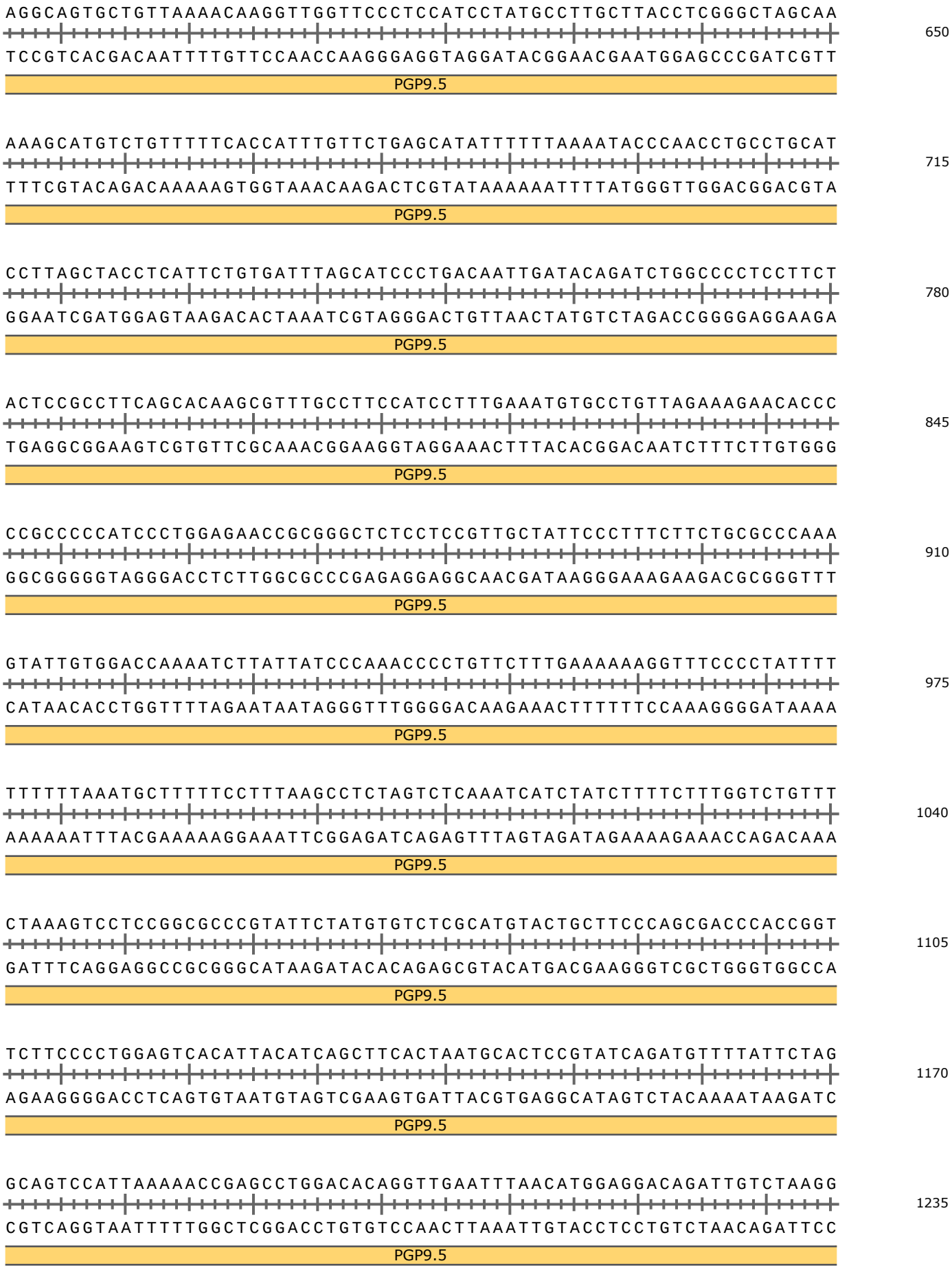
AGGCAGTGCTGTTAAAACAAGGTTGGTTCCCTCCATCCTATGCCTTGCTTACCTCGGGCTAGCAA
650
TCCGTCACGACAATTTTGTTCCAACCAAGGGAGGTAGGATACGGAACGAATGGAGCCCGATCGTT
PGP9.5
AAAGCATGTCTGTTTTTCACCATTTGTTCTGAGCATATTTTTTAAAATACCCAACCTGCCTGCAT
715
TTTCGTACAGACAAAAAGTGGTAAACAAGACTCGTATAAAAAATTTTATGGGTTGGACGGACGTA
PGP9.5
CCTTAGCTACCTCATTCTGTGATTTAGCATCCCTGACAATTGATACAGATCTGGCCCCTCCTTCT
780
GGAATCGATGGAGTAAGACACTAAATCGTAGGGACTGTTAACTATGTCTAGACCGGGGAGGAAGA
PGP9.5
ACTCCGCCTTCAGCACAAGCGTTTGCCTTCCATCCTTTGAAATGTGCCTGTTAGAAAGAACACCC
845
TGAGGCGGAAGTCGTGTTCGCAAACGGAAGGTAGGAAACTTTACACGGACAATCTTTCTTGTGGG
PGP9.5
CCGCCCCCATCCCTGGAGAACCGCGGGCTCTCCTCCGTTGCTATTCCCTTTCTTCTGCGCCCAAA
910
GGCGGGGGTAGGGACCTCTTGGCGCCCGAGAGGAGGCAACGATAAGGGAAAGAAGACGCGGGTTT
PGP9.5
GTATTGTGGACCAAAATCTTATTATCCCAAACCCCTGTTCTTTGAAAAAAGGTTTCCCCTATTTT
975
CATAACACCTGGTTTTAGAATAATAGGGTTTGGGGACAAGAAACTTTTTTCCAAAGGGGATAAAA
PGP9.5
TTTTTTAAATGCTTTTTCCTTTAAGCCTCTAGTCTCAAATCATCTATCTTTTCTTTGGTCTGTTT
1040
AAAAAATTTACGAAAAAGGAAATTCGGAGATCAGAGTTTAGTAGATAGAAAAGAAACCAGACAAA
PGP9.5
CTAAAGTCCTCCGGCGCCCGTATTCTATGTGTCTCGCATGTACTGCTTCCCAGCGACCCACCGGT
1105
GATTTCAGGAGGCCGCGGGCATAAGATACACAGAGCGTACATGACGAAGGGTCGCTGGGTGGCCA
PGP9.5
TCTTCCCCTGGAGTCACATTACATCAGCTTCACTAATGCACTCCGTATCAGATGTTTTATTCTAG
1170
AGAAGGGGACCTCAGTGTAATGTAGTCGAAGTGATTACGTGAGGCATAGTCTACAAAATAAGATC
PGP9.5
GCAGTCCATTAAAAACCGAGCCTGGACACAGGTTGAATTTAACATGGAGGACAGATTGTCTAAGG
1235
CGTCAGGTAATTTTTGGCTCGGACCTGTGTCCAACTTAAATTGTACCTCCTGTCTAACAGATTCC
PGP9.5

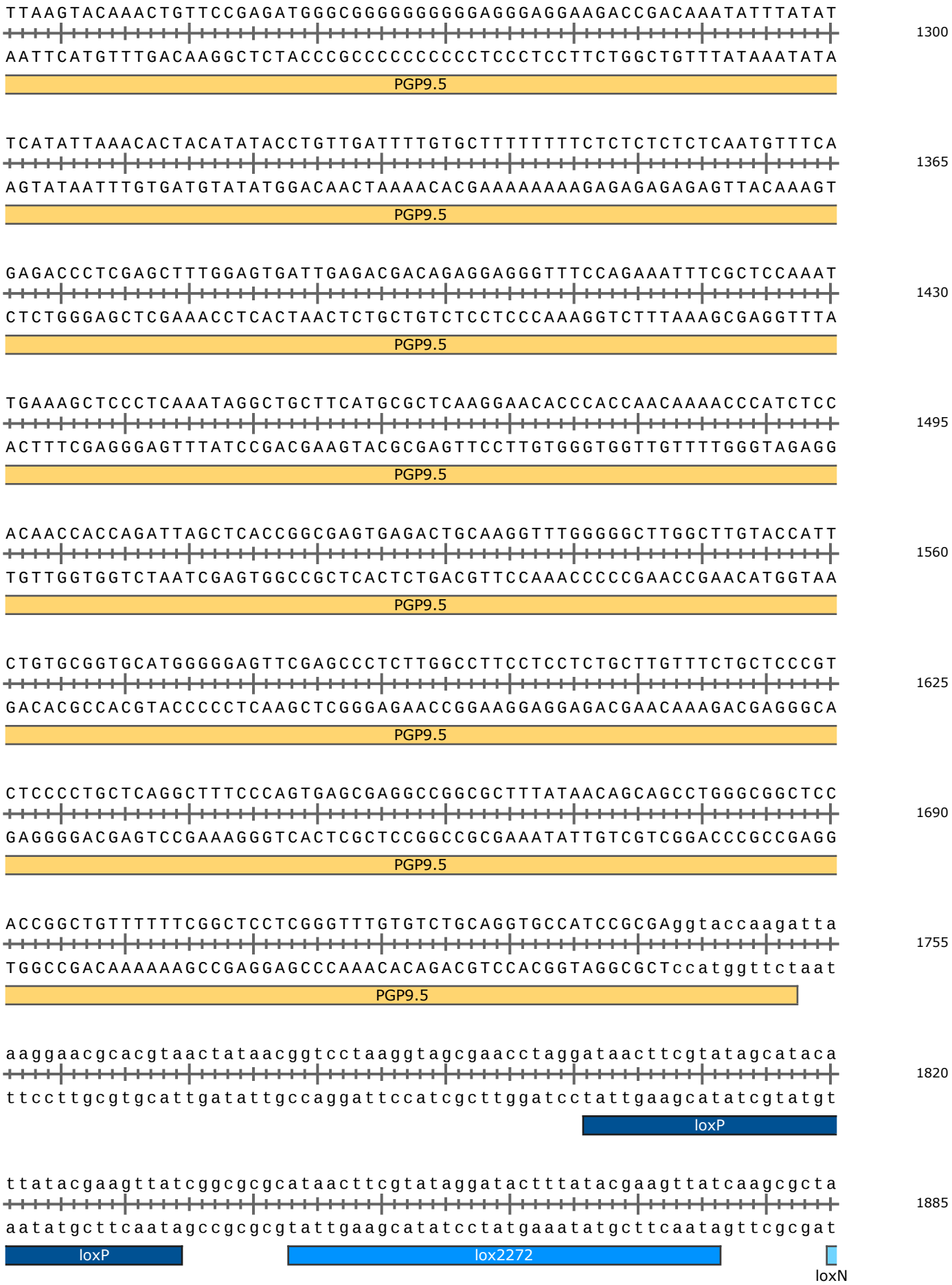
TTAAGTACAAACTGTTCCGAGATGGGCGGGGGGGGGGAGGGAGGAAGACCGACAAATATTTATAT
1300
AATTCATGTTTGACAAGGCTCTACCCGCCCCCCCCCTCCCTCCTTCTGGCTGTTTATAAATATA
PGP9.5
TCATATTAAACACTACATATACCTGTTGATTTTGTGCTTTTTTTTCTCTCTCTCTCAATGTTTCA
1365
AGTATAATTTGTGATGTATATGGACAACTAAAACACGAAAAAAAAGAGAGAGAGAGTTACAAAGT
PGP9.5
GAGACCCTCGAGCTTTGGAGTGATTGAGACGACAGAGGAGGGTTTCCAGAAATTTCGCTCCAAAT
1430
CTCTGGGAGCTCGAAACCTCACTAACTCTGCTGTCTCCTCCCAAAGGTCTTTAAAGCGAGGTTTA
PGP9.5
TGAAAGCTCCCTCAAATAGGCTGCTTCATGCGCTCAAGGAACACCCACCAACAAAACCCATCTCC
1495
ACTTTCGAGGGAGTTTATCCGACGAAGTACGCGAGTTCCTTGTGGGTGGTTGTTTTGGGTAGAGG
PGP9.5
ACAACCACCAGATTAGCTCACCGGCGAGTGAGACTGCAAGGTTTGGGGGCTTGGCTTGTACCATT
1560
TGTTGGTGGTCTAATCGAGTGGCCGCTCACTCTGACGTTCCAAACCCCCGAACCGAACATGGTAA
PGP9.5
CTGTGCGGTGCATGGGGGAGTTCGAGCCCTCTTGGCCTTCCTCCTCTGCTTGTTTCTGCTCCCGT
1625
GACACGCCACGTACCCCCTCAAGCTCGGGAGAACCGGAAGGAGGAGACGAACAAAGACGAGGGCA
PGP9.5
CTCCCCTGCTCAGGCTTTCCCAGTGAGCGAGGCCGGCGCTTTATAACAGCAGCCTGGGCGGCTCC
1690
GAGGGGACGAGTCCGAAAGGGTCACTCGCTCCGGCCGCGAAATATTGTCGTCGGACCCGCCGAGG
PGP9.5
ACCGGCTGTTTTTTCGGCTCCTCGGGTTTGTGTCTGCAGGTGCCATCCGCGAggtaccaagatta
1755
TGGCCGACAAAAAAGCCGAGGAGCCCAAACACAGACGTCCACGGTAGGCGCTccatggttctaat
PGP9.5
aaggaacgcacgtaactataacggtcctaaggtagcgaacctaggataacttcgtatagcataca
1820
ttccttgcgtgcattgatattgccaggattccatcgcttggatcctattgaagcatatcgtatgt
loxP
ttatacgaagttatcggcgcgcataacttcgtataggatactttatacgaagttatcaagcgcta
1885
aatatgcttcaatagccgcgcgtattgaagcatatcctatgaaatatgcttcaatagttcgcgat
loxP
lox2272
loxN

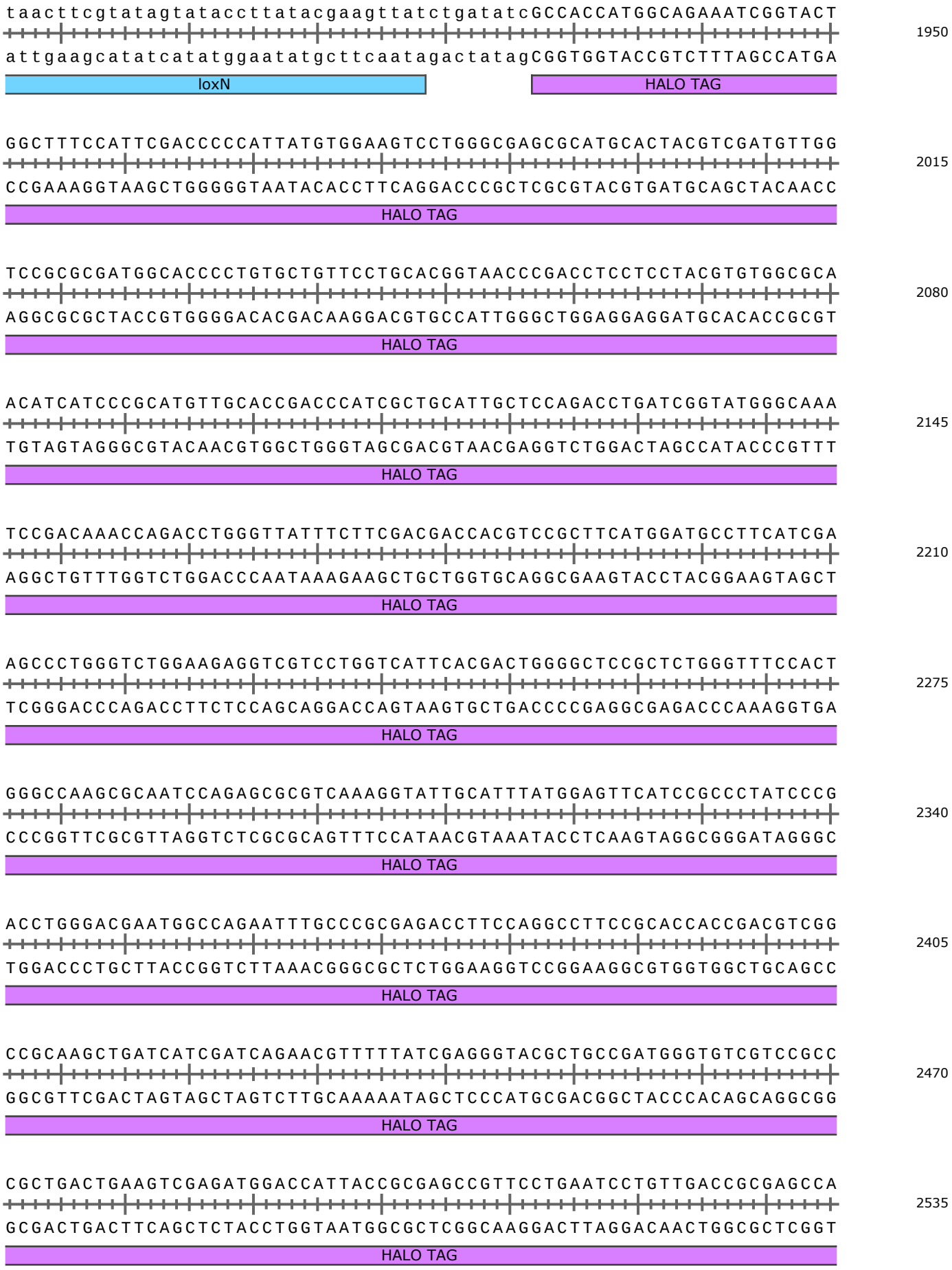
taacttcgtatagtatacctttatacgaagttatctgatatcGCCACCATGGCAGAAATCGGTACT
1950
attgaagcatatcatatggaatatgcttcaatagactatagCGGTGGTACCGTCTTTAGCCATGA
loxN
HALO TAG
GGCTTTCCATTCGACCCCCATTATGTGGAAGTCCTGGGCGAGCGCATGCACTACGTCGATGTTGG
2015
CCGAAAGGTAAGCTGGGGGTAATACACCTTCAGGACCCGCTCGCGTACGTGATGCAGCTACAACC
HALO TAG
TCCGCGCGATGGCACCCCTGTGCTGTTCCTGCACGGTAACCCGACCTCCTCCTACGTGTGGCGCA
2080
AGGCGCGCTACCGTGGGGACACGACAAGGACGTGCCATTGGGCTGGAGGAGGATGCACACCGCGT
HALO TAG
ACATCATCCCGCATGTTGCACCGACCCATCGCTGCATTGCTCCAGACCTGATCGGTATGGGCAAA
2145
TGTAGTAGGGCGTACAACGTGGCTGGGTAGCGACGTAACGAGGTCTGGACTAGCCATACCCGTTT
HALO TAG
TCCGACAAACCAGACCTGGGTTATTTCTTCGACGACCACGTCCGCTTCATGGATGCCTTCATCGA
2210
AGGCTGTTTGGTCTGGACCCAATAAAGAAGCTGCTGGTGCAGGCGAAGTACCTACGGAAGTAGCT
HALO TAG
AGCCCTGGGTCTGGAAGAGGTCGTCCTGGTCATTCACGACTGGGGCTCCGCTCTGGGTTTCCACT
2275
TCGGGACCCAGACCTTCTCCAGCAGGACCAGTAAGTGCTGACCCCGAGGCGAGACCCAAAGGTGA
HALO TAG
GGGCCAAGCGCAATCCAGAGCGCGTCAAAGGTATTGCATTTATGGAGTTCATCCGCCCTATCCCG
2340
CCCGGTTCGCGTTAGGTCTCGCGCAGTTTCCATAACGTAAATACCTCAAGTAGGCGGGATAGGGC
HALO TAG
ACCTGGGACGAATGGCCAGAATTTGCCCGCGAGACCTTCCAGGCCTTCCGCACCACCGACGTCGG
2405
TGGACCCTGCTTACCGGTCTTAAACGGGCGCTCTGGAAGGTCCGGAAGGCGTGGTGGCTGCAGCC
HALO TAG
CCGCAAGCTGATCATCGATCAGAACGTTTTTATCGAGGGTACGCTGCCGATGGGTGTCGTCCGCC
2470
GGCGTTCGACTAGTAGCTAGTCTTGCAAAAATAGCTCCCATGCGACGGCTACCCACAGCAGGCGG
HALO TAG
CGCTGACTGAAGTCGAGATGGACCATTACCGCGAGCCGTTCCTGAATCCTGTTGACCGCGAGCCA
2535
GCGACTGACTTCAGCTCTACCTGGTAATGGCGCTCGGCAAGGACTTAGGACAACTGGCGCTCGGT
HALO TAG

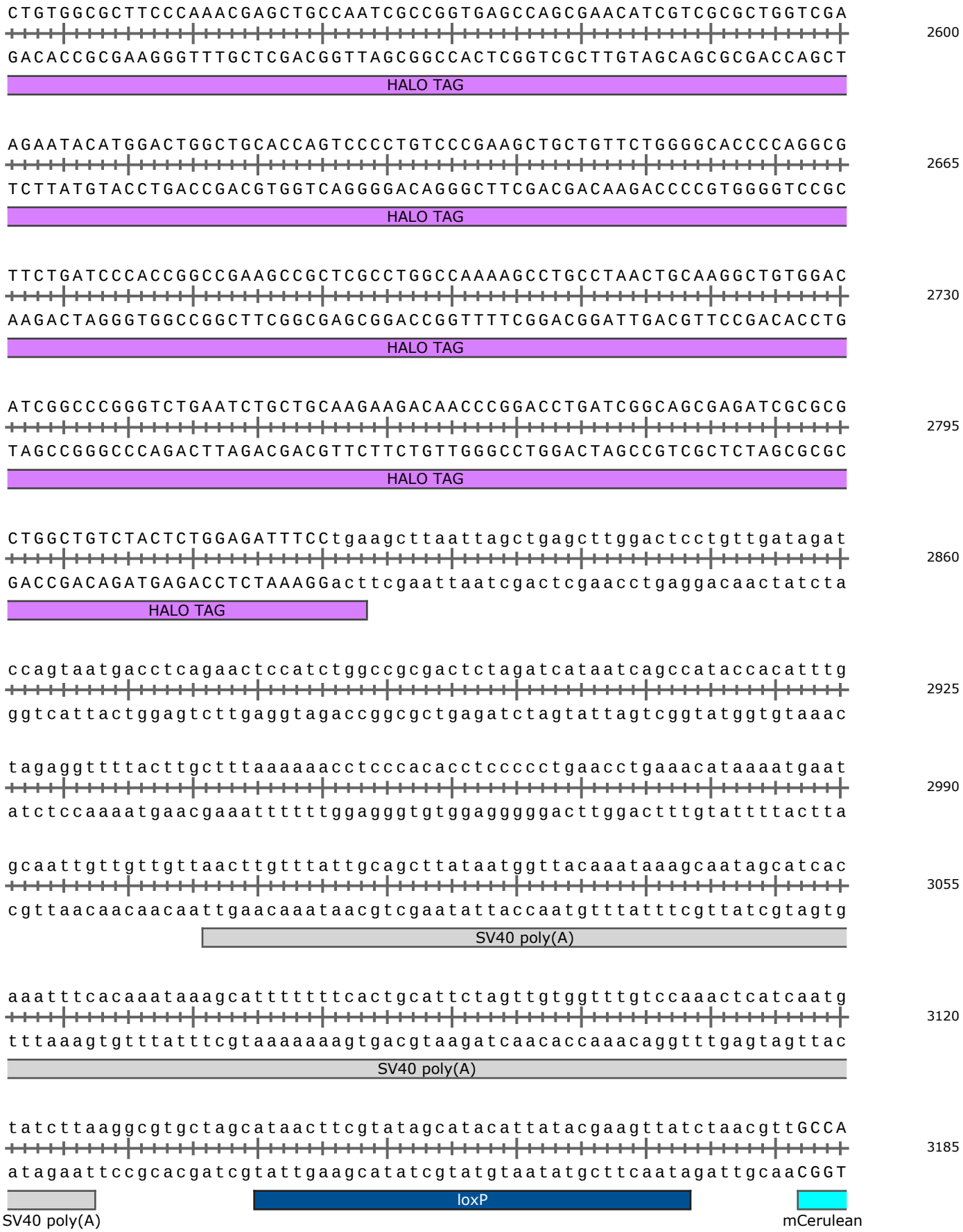
CTGTGGCGCTTCCCAAACGAGCTGCCAATCGCCGGTGAGCCAGCGAACATCGTCGCGCTGGTCGA
2600
GACACCGCGAAGGGTTTGCTCGACGGTTAGCGGCCACTCGGTCGCTTGTAGCAGCGCGACCAGCT
HALO TAG
AGAATACATGGACTGGCTGCACCAGTCCCCTGTCCCGAAGCTGCTGTTCTGGGGCACCCCAGGCG
2665
TCTTATGTACCTGACCGACGTGGTCAGGGGACAGGGCTTCGACGACAAGACCCCGTGGGGTCCGC
HALO TAG
TTCTGATCCCACCGGCCGAAGCCGCTCGCCTGGCCAAAAGCCTGCCTAACTGCAAGGCTGTGGAC
2730
AAGACTAGGGTGGCCGGCTTCGGCGAGCGGACCGGTTTTCGGACGGATTGACGTTCCGACACCTG
HALO TAG
ATCGGCCCGGGTCTGAATCTGCTGCAAGAAGACAACCCGGACCTGATCGGCAGCGAGATCGCGCG
2795
TAGCCGGGCCCAGACTTAGACGACGTTCTTCTGTTGGGCCTGGACTAGCCGTCGCTCTAGCGCGC
HALO TAG
CTGGCTGTCTACTCTGGAGATTTCCtgaagcttaattagctgagcttggactcctgttgatagat
2860
GACCGACAGATGAGACCTCTAAAGGacttcgaattaatcgactcgaacctgaggacaactatcta
HALO TAG
ccagtaatgacctcagaactccatctggccgcgactctagatcataatcagccataccacatttg
2925
ggtcattactggagtcttgaggtagaccggcgctgagatctagtattagtcggtatggtgtaaac
tagaggttttacttgctttaaaaaacctcccacacctcccccctgaacctgaaacataaaatgaat
2990
atctccaaaatgaacgaaatttttttggagggtgtggaggggacttggactttgtattttactta
gcaattgttgttgttaacttgtttattgcagcttataatggttacaaataaagcaatagcatcac
3055
cgttaacaacaacaattgaacaaataacgtcgaatattaccaatgtttatttcgttatcgtagtg
SV40 poly(A)
aaatttcacaaataaagcatttttttcactgcattctagttgtggtttgtccaaactcatcaatg
3120
tttaaagtgtttatttcgtaaaaaaagtgacgtaagatcaacaccaaacaggtttgagtagttac
SV40 poly(A)
tatcttaaggcgtgctagcataacttcgtatagcatacattatacgaagttatctaacgttGCCA
3185
atagaattccgcacgatcgtattgaagcatatcgtatgtaatatgcttcaatagattgcaaCGGT
SV40 poly(A)
loxP
mCerulean


CCATGGTGAGCAAGGGCGAGGAGCTGTTCACCGGGGTGGTGCCCATCCTGGTCGAGCTGGACGGC
3250
GGTACCACTCGTTCCCGCTCCTCGACAAGTGGCCCCACCACGGGTAGGACCAGCTCGACCTGCCG
mCerulean
GACGTAAACGGCCACAAGTTCAGCGTGTCCGGCGAGGGCGAGGGCGATGCCACCTACGGCAAGCT
3315
CTGCATTTGCCGGTGTTCAAGTCGCACAGGCCGCTCCCGCTCCCGCTACGGTGGATGCCGTTCGA
mCerulean
GACCCTGAAGTTCATCTGCACCACCGGCAAGCTGCCCGTGCCCTGGCCCACCCTCGTGACCACCC
3380
CTGGGACTTCAAGTAGACGTGGTGGCCGTTCGACGGGCACGGGACCGGGTGGGAGCACTGGTGGG
mCerulean
TGACCTGGGGCGTGCAGTGCTTCGCCCGCTACCCCGACCACATGAAGCAGCACGACTTCTTCAAG
3445
ACTGGACCCCGCACGTCACGAAGCGGGCGATGGGGCTGGTGTACTTCGTCGTGCTGAAGAAGTTC
mCerulean
TCCGCCATGCCCGAAGGCTACGTCCAGGAGCGCACCATCTTCTTCAAGGACGACGGCAACTACAA
3510
AGGCGGTACGGGCTTCCGATGCAGGTCCTCGCGTGGTAGAAGAAGTTCCTGCTGCCGTTGATGTT
mCerulean
GACCCGCGCCGAGGTGAAGTTCGAGGGCGACACCCTGGTGAACCGCATCGAGCTGAAGGGCATCG
3575
CTGGGCGCGGCTCCACTTCAAGCTCCCGCTGTGGGACCACTTGGCGTAGCTCGACTTCCCGTAGC
mCerulean
ACTTCAAGGAGGACGGCAACATCCTGGGGCACAAGCTGGAGTACAACGCCATCAGCGACAACGTC
3640
TGAAGTTCCTCCTGCCGTTGTAGGACCCCGTGTTCGACCTCATGTTGCGGTAGTCGCTGTTGCAG
mCerulean
TATATCACCGCCGACAAGCAGAAGAACGGCATCAAGGCCAACTTCAAGATCCGCCACAACATCGA
3705
ATATAGTGGCGGCTGTTCGTCTTCTTGCCGTAGTTCCGGTTGAAGTTCTAGGCGGTGTTGTAGCT
mCerulean
GGACGGCAGCGTGCAGCTCGCCGACCACTACCAGCAGAACACCCCCATCGGCGACGGCCCCGTGC
3770
CCTGCCGTCGCACGTCGAGCGGCTGGTGATGGTCGTCTTGTGGGGGTAGCCGCTGCCGGGGCACG
mCerulean
TGCTGCCCGACAACCACTACCTGAGCACCCAGTCCAAGCTGAGCAAAGACCCCAACGAGAAGCGC
3835
ACGACGGGCTGTTGGTGATGGACTCGTGGGTCAGGTTCGACTCGTTTCTGGGGTTGCTCTTCGCG
mCerulean


GATCACATGGTCCTGCTGGAGTTCGTGACCGCCGCCGGGATCACTCTCGGCATGGACGAGCTGTA
3900
CTAGTGTACCAGGACGACCTCAAGCACTGGCGGCGGCCCTAGTGAGAGCCGTACCTGCTCGACAT
mCerulean
CAAGTGAgcggccgctaatcaacctctggattacaaaatttgtgaaagattgactggtattctta
3965
GTTCACTcgccggcgattagttggagacctaatgttttaaacactttctaactgaccataagaat
WPRE
mCerulean mCerulean
actatgttgctccttttacgctatgtggatacgctgctttaatgcctttgtatcatgctattgct
4030
tgatacaacgaggaaaatgcgatacacctatgcgacgaaattacggaaacatagtacgataacga
WPRE
tcccgtatggctttcattttctcctccttgtataaatcctggttgctgtctctttatgaggagtt
4095
agggcataccgaaagtaaaagaggaggaacatatttaggaccaacgacagagaaatactcctcaa
WPRE
gtggcccgttgtcaggcaacgtggcgtggtgtgcactgtgtttgctgacgcaaccccactggtt
4160
caccgggcaacagtccgttgcaccgcaccacacgtgacacaaacgactgcgttgggggtgaccaa
WPRE
ggggcattgccaccacctgtcagctcctttccgggactttcgctttcccctccctattgccacg
4225
ccccgtaacggtggtggacagtcgaggaaaggccctgaaagcgaaaggggggagggataacggtgc
WPRE
gcggaactcatcgccgcctgccttgcccgctgctggacaggggctcggctgttgggcactgacaa
4290
cgccttgagtagcggcggacggaacgggcgacgacctgtccccgagccgacaacccgtgactgtt
WPRE
ttccgtggtgttgtcggggaaatcatcgtcctttccttggctgctcgcctgtgttgccacctgga
4355
aaggcaccacaacagcccctttagtagcaggaaaggaaccgacgagcggacacaacggtggacct
WPRE
ttctgcgcgggacgtccttctgctacgtcccttcggccctcaatccagcggaccttccttcccgc
4420
aagacgcgccctgcaggaagacgatgcagggaagccgggagttaggtcgcctggaaggaagggcg
WPRE
ggcctgctgccggctctgcggcctcttccgcgtcttcgccttcgccctcagacgagtcggatctc
4485
ccggacgacggccgagacgccggagaaggcgcagaagcggaagcgggagtctgctcagcctagag
WPRE

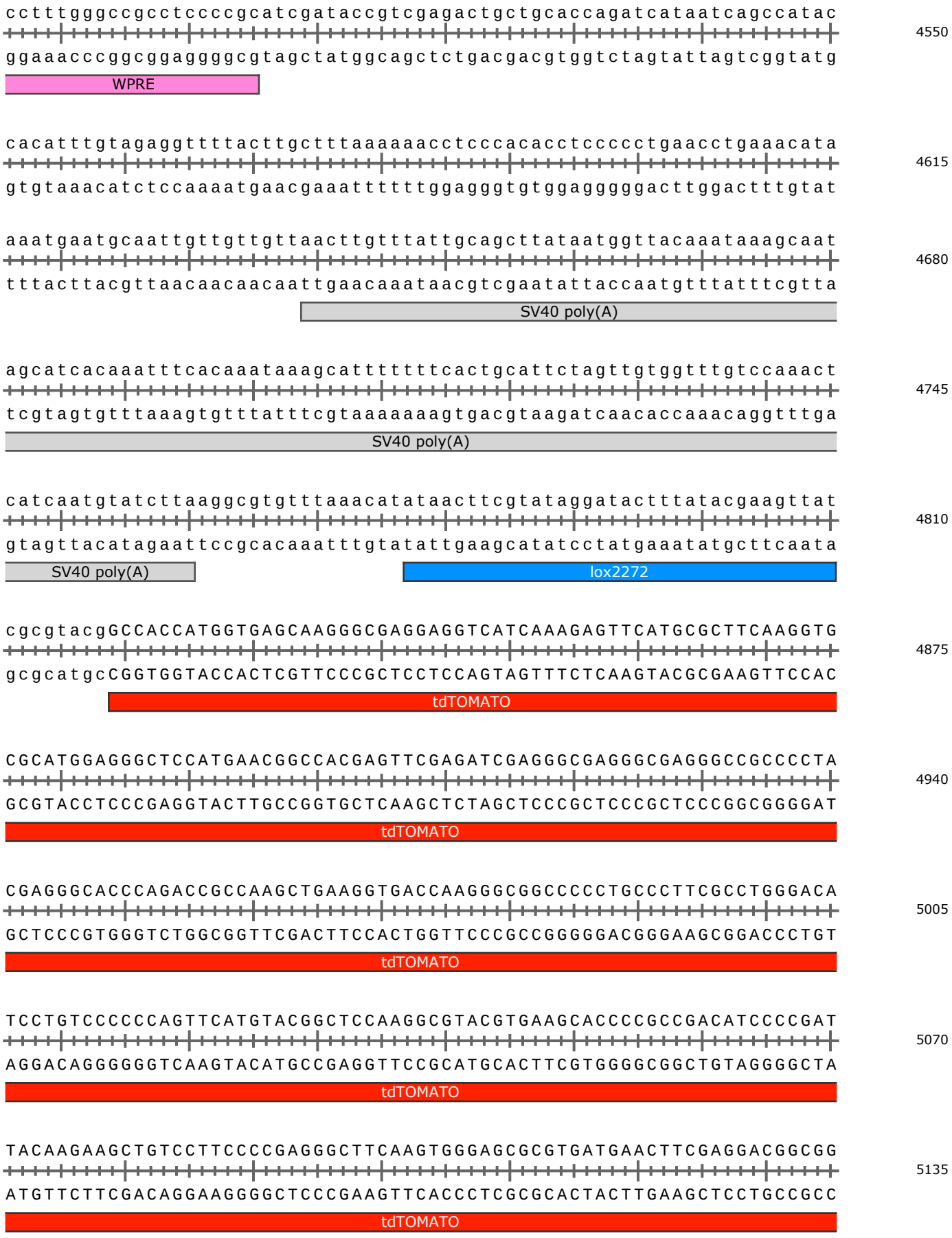
cctttgggccgcctccccgcatcgataccgtcgagactgctgcaccagatcataatcagccatac
4550
ggaaacccggcggaggggcgtagctatggcagctctgacgacgtggtctagtattagtcggtatg
WPRE
cacatttgtagaggttttacttgctttaaaaaacctcccacacctcccccctgaacctgaaacata
4615
gtgtaaacatctccaaaatgaacgaaatttttttggagggtgtggaggggggacttggactttgtat
aaatgaatgcaattgttgttgttaacttgtttattgcagcttataatggttacaaataaagcaat
4680
tttacttacgttaacaacaacaattgaacaaataacgtcgaatattaccaatgtttatttcgtta
SV40 poly(A)
agcatcacaaatttcacaaataaagcatttttttcactgcattctagttgtggtttgtccaaact
4745
tcgtagtgtttaaagtgtttatttcgtaaaaaaagtgacgtaagatcaacaccaaacaggtttga
SV40 poly(A)
catcaatgtatcttaaggcgtgtttaaacatataacttcgtataggatactttatacgaagttat
4810
gtagttacatagaattccgcacaaatttgtatattgaagcatatcctatgaaatatgcttcaata
SV40 poly(A)
lox2272
cgcgtacgGCCACCATGGTGAGCAAGGGCGAGGAGGTCATCAAAGAGTTCATGCGCTTCAAGGTG
4875
gcgcatgcCGGTGGTACCACTCGTTCCCGCTCCTCCAGTAGTTTCTCAAGTACGCGAAGTTCCAC
tdTOMATO
CGCATGGAGGGCTCCATGAACGGCCACGAGTTCGAGATCGAGGGCGAGGGCGAGGGCCGCCCCTA
4940
GCGTACCTCCCGAGGTACTTGCCGGTGCTCAAGCTCTAGCTCCCGCTCCCGCTCCCGGCGGGGAT
tdTOMATO
CGAGGGCACCCAGACCGCCAAGCTGAAGGTGACCAAGGGCGGCCCCCTGCCCTTCGCCTGGGACA
5005
GCTCCCGTGGGTCTGGCGGTTCGACTTCCACTGGTTCCCGCCGGGGGACGGGAAGCGGACCCTGT
tdTOMATO
TCCTGTCCCCCCAGTTCATGTACGGCTCCAAGGCGTACGTGAAGCACCCCGCCGACATCCCCGAT
5070
AGGACAGGGGGGTCAAGTACATGCCGAGGTTCCGCATGCACTTCGTGGGGCGGCTGTAGGGGCTA
tdTOMATO
TACAAGAAGCTGTCCTTCCCCGAGGGCTTCAAGTGGGAGCGCGTGATGAACTTCGAGGACGGCGG
5135
ATGTTCTTCGACAGGAAGGGGCTCCCGAAGTTCACCCTCGCGCACTACTTGAAGCTCCTGCCGCC
tdTOMATO

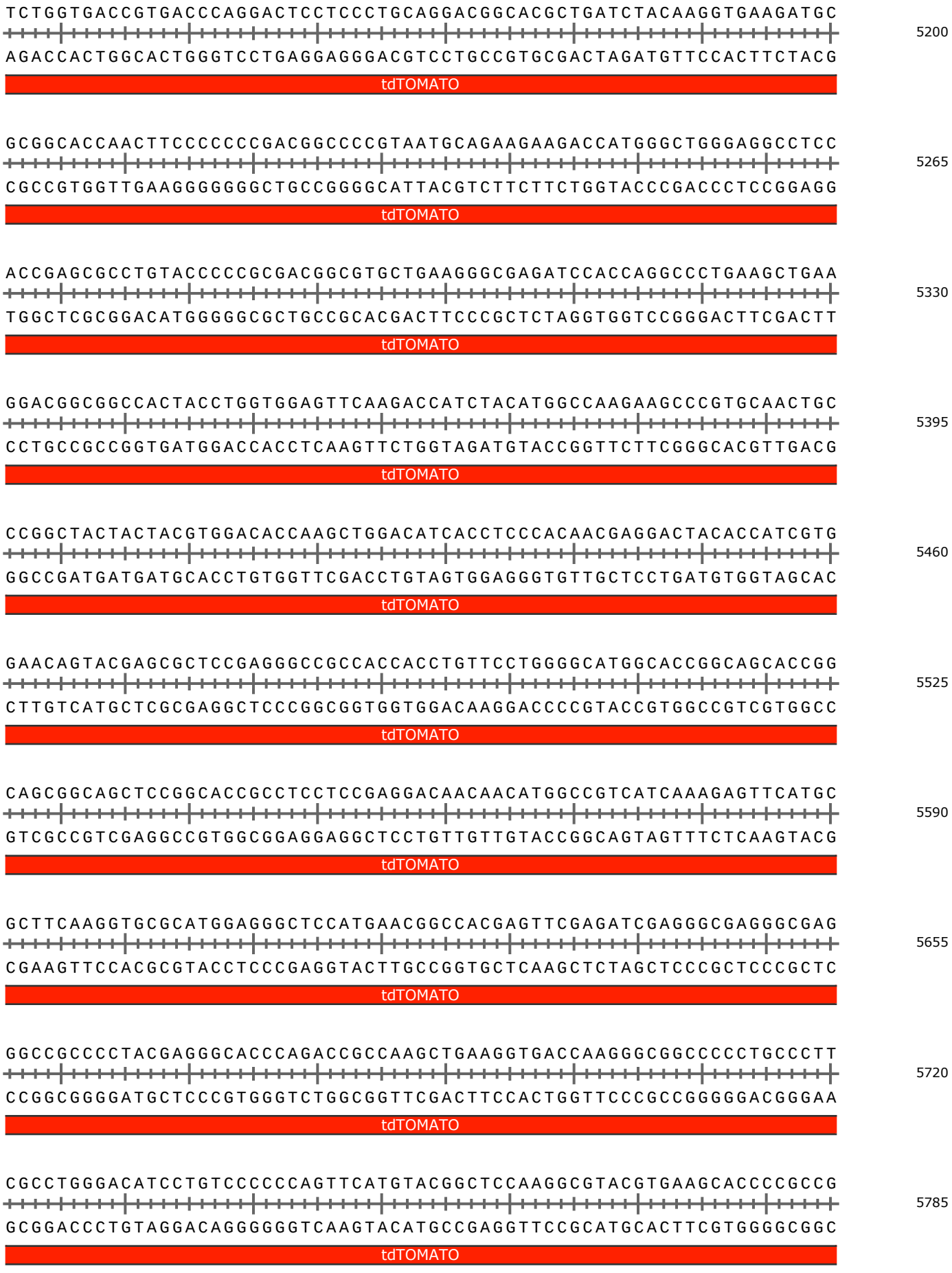
TCTGGTGACCGTGACCCAGGACTCCTCCCTGCAGGACGGCACGCTGATCTACAAGGTGAAGATGC
5200
AGACCACTGGCACTGGGTCCTGAGGAGGGACGTCCTGCCGTGCGACTAGATGTTCCACTTCTACG
tdTOMATO
GCGGCACCAACTTCCCCCCCGACGGCCCCGTAATGCAGAAGAAGACCATGGGCTGGGAGGCCTCC
5265
CGCCGTGGTTGAAGGGGGGGCTGCCGGGGCATTACGTCTTCTTCTGGTACCCGACCCTCCGGAGG
tdTOMATO
ACCGAGCGCCTGTACCCCCGCGACGGCGTGCTGAAGGGCGAGATCCACCAGGCCCTGAAGCTGAA
5330
TGGCTCGCGGACATGGGGGCGCTGCCGCACGACTTCCCGCTCTAGGTGGTCCGGGACTTCGACTT
tdTOMATO
GGACGGCGGCCACTACCTGGTGGAGTTCAAGACCATCTACATGGCCAAGAAGCCCGTGCAACTGC
5395
CCTGCCGCCGGTGATGGACCACCTCAAGTTCTGGTAGATGTACCGGTTCTTCGGGCACGTTGACG
tdTOMATO
CCGGCTACTACTACGTGGACACCAAGCTGGACATCACCTCCCACAACGAGGACTACACCATCGTG
5460
GGCCGATGATGATGCACCTGTGGTTCGACCTGTAGTGGAGGGTGTTGCTCCTGATGTGGTAGCAC
tdTOMATO
GAACAGTACGAGCGCTCCGAGGGCCGCCACCACCTGTTCCTGGGGCATGGCACCGGCAGCACCGG
5525
CTTGTCATGCTCGCGAGGCTCCCGGCGGTGGTGGACAAGGACCCCGTACCGTGGCCGTCGTGGCC
tdTOMATO
CAGCGGCAGCTCCGGCACCGCCTCCTCCGAGGACAACAACATGGCCGTCATCAAAGAGTTCATGC
5590
GTCGCCGTCGAGGCCGTGGCGGAGGAGGCTCCTGTTGTTGTACCGGCAGTAGTTTCTCAAGTACG
tdTOMATO
GCTTCAAGGTGCGCATGGAGGGCTCCATGAACGGCCACGAGTTCGAGATCGAGGGCGAGGGCGAG
5655
CGAAGTTCCACGCGTACCTCCCGAGGTACTTGCCGGTGCTCAAGCTCTAGCTCCCGCTCCCGCTC
tdTOMATO
GGCCGCCCCTACGAGGGCACCCAGACCGCCAAGCTGAAGGTGACCAAGGGCGGCCCCCTGCCCTT
5720
CCGGCGGGGATGCTCCCGTGGGTCTGGCGGTTCGACTTCCACTGGTTCCCGCCGGGGGACGGGAA
tdTOMATO
CGCCTGGGACATCCTGTCCCCCCAGTTCATGTACGGCTCCAAGGCGTACGTGAAGCACCCCGCCG
5785
GCGGACCCTGTAGGACAGGGGGGTCAAGTACATGCCGAGGTTCCGCATGCACTTCGTGGGGCGGC
tdTOMATO

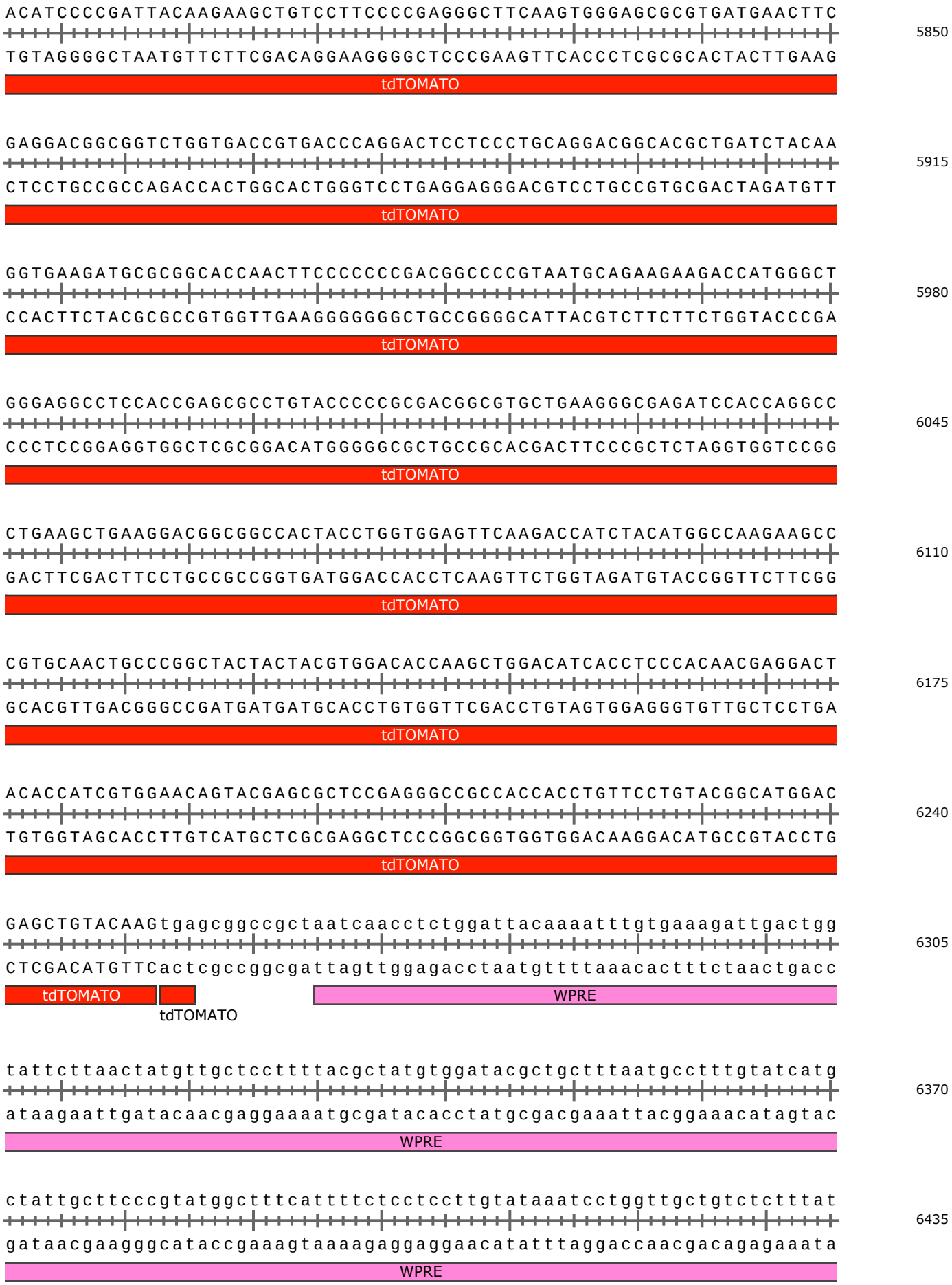
ACATCCCCGATTACAAGAAGCTGTCCTTCCCCGAGGGCTTCAAGTGGGAGCGCGTGATGAACTTC
5850
TGTAGGGGCTAATGTTCTTCGACAGGAAGGGGCTCCCGAAGTTCACCCTCGCGCACTACTTGAAG
tdTOMATO
GAGGACGGCGGTCTGGTGACCGTGACCCAGGACTCCTCCCTGCAGGACGGCACGCTGATCTACAA
5915
CTCCTGCCGCCAGACCACTGGCACTGGGTCCTGAGGAGGGACGTCCTGCCGTGCGACTAGATGTT
tdTOMATO
GGTGAAGATGCGCGGCACCAACTTCCCCCCCGACGGCCCCGTAATGCAGAAGAAGACCATGGGCT
5980
CCACTTCTACGCGCCGTGGTTGAAGGGGGGGCTGCCGGGGCATTACGTCTTCTTCTGGTACCCGA
tdTOMATO
GGGAGGCCTCCACCGAGCGCCTGTACCCCCGCGACGGCGTGCTGAAGGGCGAGATCCACCAGGCC
6045
CCCTCCGGAGGTGGCTCGCGGACATGGGGGCGCTGCCGCACGACTTCCCGCTCTAGGTGGTCCGG
tdTOMATO
CTGAAGCTGAAGGACGGCGGCCACTACCTGGTGGAGTTCAAGACCATCTACATGGCCAAGAAGCC
6110
GACTTCGACTTCCTGCCGCCGGTGATGGACCACCTCAAGTTCTGGTAGATGTACCGGTTCTTCGG
tdTOMATO
CGTGCAACTGCCCGGCTACTACTACGTGGACACCAAGCTGGACATCACCTCCCACAACGAGGACT
6175
GCACGTTGACGGGCCGATGATGATGCACCTGTGGTTCGACCTGTAGTGGAGGGTGTTGCTCCTGA
tdTOMATO
ACACCATCGTGGAACAGTACGAGCGCTCCGAGGGCCGCCACCACCTGTTCCTGTACGGCATGGAC
6240
TGTGGTAGCACCTTGTCATGCTCGCGAGGCTCCCGGCGGTGGTGGACAAGGACATGCCGTACCTG
tdTOMATO
GAGCTGTACAAGtgagcggccgctaatcaacctctggattacaaaatttgtgaaagattgactgg
6305
CTCGACATGTTCactcgccggcgattagttggagacctaatgttttaaacactttctaactgacc
tdTOMATO
tdTOMATO
WPRE
tattcttaactatgttgctccttttacgctatgtggatacgctgctttaatgcctttgtatcatg
6370
ataagaattgatacaacgaggaaaatgcgatacacctatgcgacgaaattacggaaacatagtac
WPRE
ctattgcttcccgtatggctttcattttctcctccttgtataaatcctggttgctgtctctttat
6435
gataacgaagggcataccgaaagtaaaagaggaggaacatatttaggaccaacgacagagaaata
WPRE

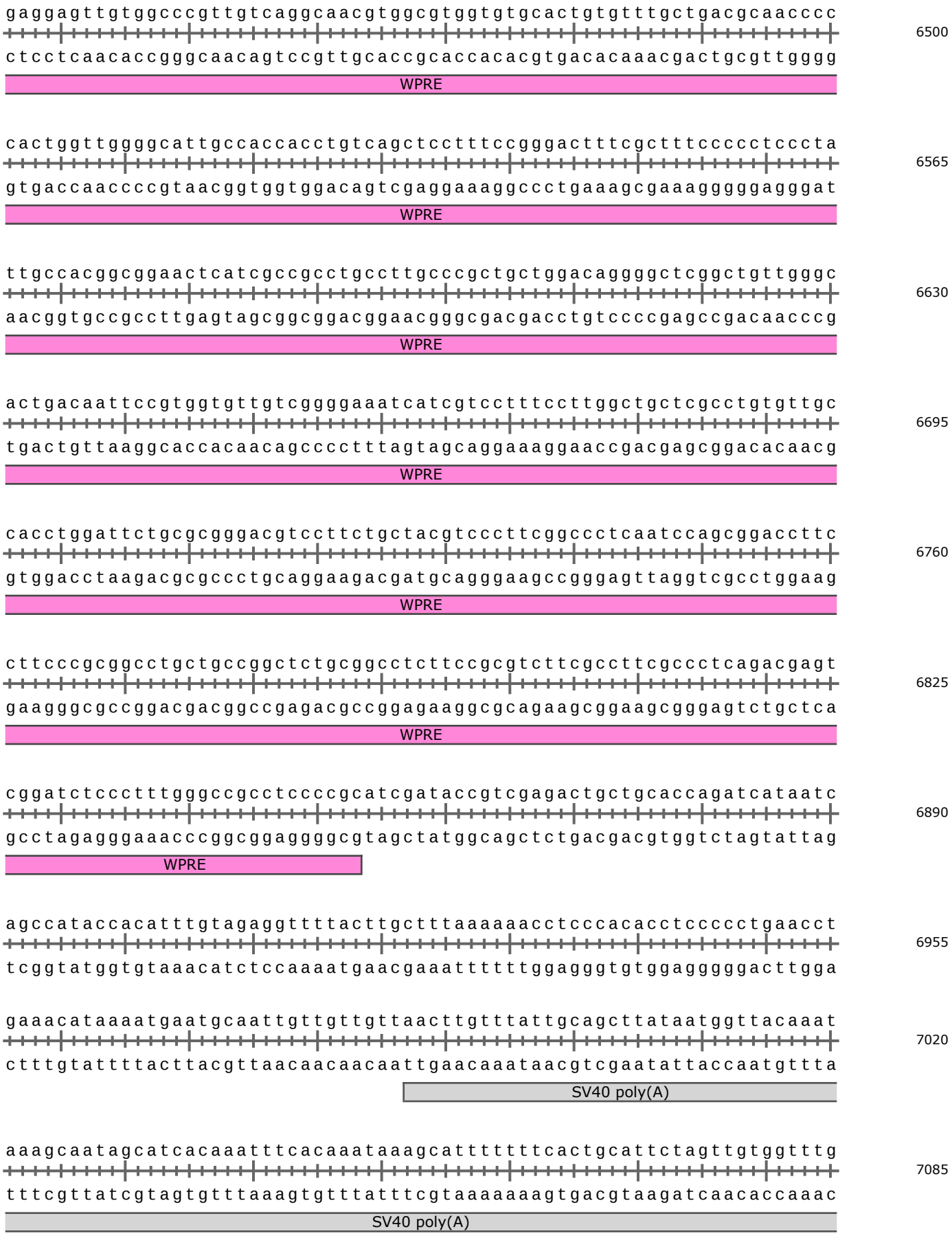
gaggagttgtggcccgttgtcaggcaacgtggcgtggtgtgcactgtgtttgctgacgcaacccc
6500
ctcctcaacaccgggcaacagtccgttgcaccgcaccacacgtgacacaaacgactgcgttgggg
WPRE
cactggttggggcattgccaccacctgtcagctcctttccgggactttcgctttcccctcccta
6565
gtgaccaaccccgtaacggtggtggacagtcgaggaaaggccctgaaagcgaaaggggggagggat
WPRE
ttgccacggcggaactcatcgccgcctgccttgcccgctgctggacaggggctcggctgttgggc
6630
aacggtgccgccttgagtagcggcggacggaacgggcgacgacctgtccccgagccgacaacccg
WPRE
actgacaattccgtggtgttgtcggggaaatcatcgtcctttccttggctgctcgcctgtgttgc
6695
tgactgttaaggcaccacaacagccccttttagtagcaggaaaggaaccgacgagcggacacaacg
WPRE
cacctggattctgcgcgggacgtccttctgctacgtcccttcggccctcaatccagcggaccttc
6760
gtggacctaagacgcgccctgcaggaagacgatgcagggaagccgggagttaggtcgcctggaag
WPRE
cttcccgcggcctgctgccggctctgcggcctcttccgcgtcttcgccttcgccctcagacgagt
6825
gaagggcgccggacgacggccgagacgccggagaaggcgcagaagcggaagcgggagtctgctca
WPRE
cggatctccctttgggccgcctccccgcatcgataccgtcgagactgctgcaccagatcataatc
6890
gcctagagggaaacccggcggaggggcgtagctatggcagctctgacgacgtggtctagtattag
WPRE
agccataccacatttgtagaggttttacttgctttaaaaaacctcccacacctcccccctgaacct
6955
tcggtatggtgtaaacatctccaaaatgaacgaaatttttggagggtgtggaggggacttgga
gaaacataaaatgaatgcaattgttgttgttaacttgtttattgcagcttataatggttacaaat
7020
ctttgtattttacttacgttaacaacaacaattgaacaaataacgtcgaatattaccaatgttta
SV40 poly(A)
aaagcaatagcatcacaaatttcacaaataaagcatttttttcactgcattctagttgtggtttg
7085
tttcgttatcgtagtgtttaaagtgtttatttcgtaaaaaaagtgacgtaagatcaacaccaaac
SV40 poly(A)

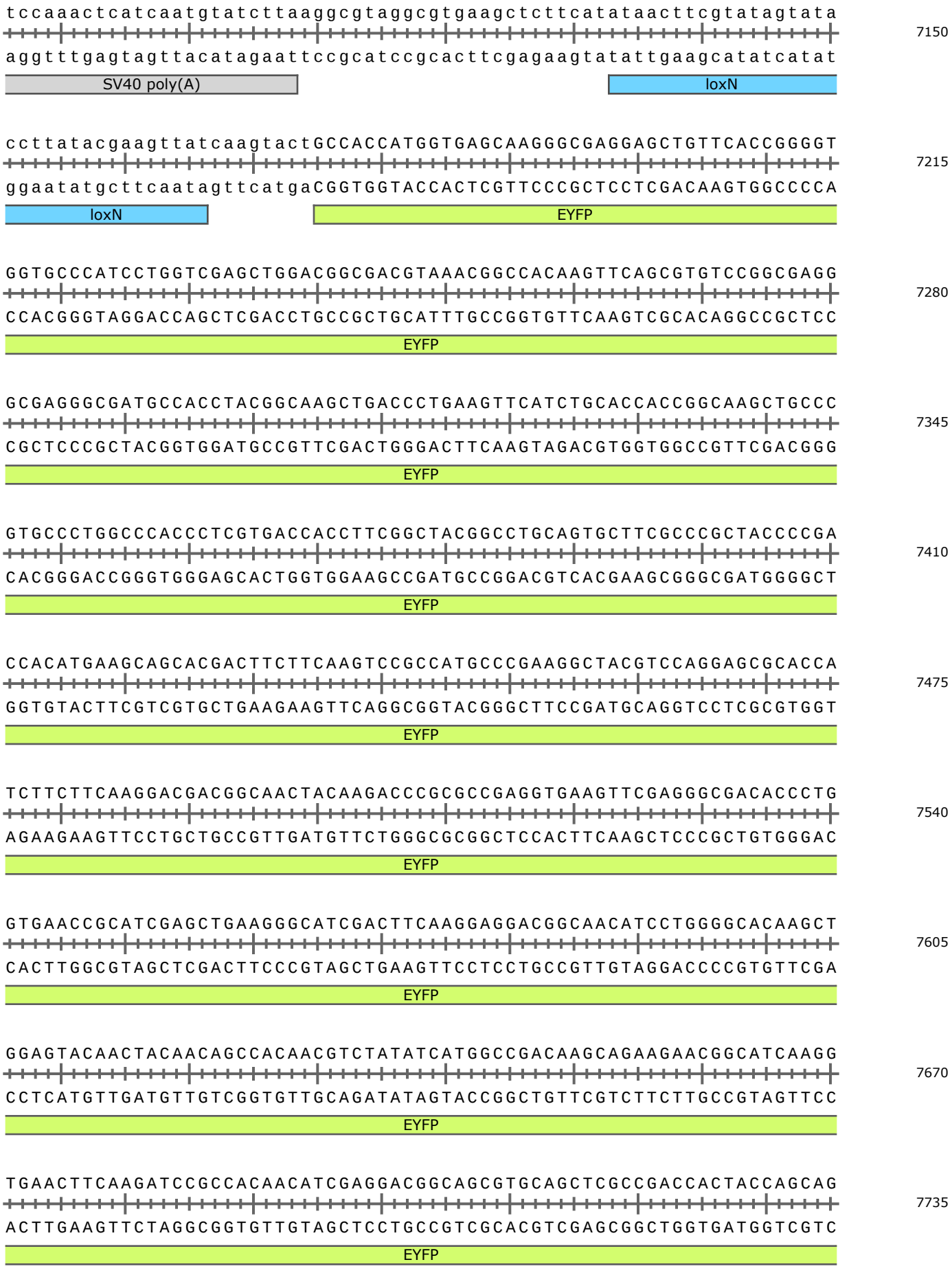
tccaaactcatcaatgtatcttaaggcgtaggcgtgaagctcttcatataacttcgtatagtata
7150
aggtttgagtagttacatagaattccgcatccgcacttcgagaagtatattgaagcatatcatat
SV40 poly(A)
loxN
ccttatacgaagttatcaagtactGCCACCATGGTGAGCAAGGGCGAGGAGCTGTTCACCGGGGT
7215
ggaatatgcttcaatagttcatgaCGGTGGTACCACTCGTTCCCGCTCCTCGACAAGTGGCCCCA
loxN
EYFP
GGTGCCCATCCTGGTCGAGCTGGACGGCGACGTAAACGGCCACAAGTTCAGCGTGTCCGGCGAGG
7280
CCACGGGTAGGACCAGCTCGACCTGCCGCTGCATTTGCCGGTGTTCAAGTCGCACAGGCCGCTCC
EYFP
GCGAGGGCGATGCCACCTACGGCAAGCTGACCCTGAAGTTCATCTGCACCACCGGCAAGCTGCCC
7345
CGCTCCCGCTACGGTGGATGCCGTTCGACTGGGACTTCAAGTAGACGTGGTGGCCGTTCGACGGG
EYFP
GTGCCCTGGCCCACCCTCGTGACCACCTTCGGCTACGGCCTGCAGTGCTTCGCCCGCTACCCCGA
7410
CACGGGACCGGGTGGGAGCACTGGTGGAAGCCGATGCCGGACGTCACGAAGCGGGCGATGGGGCT
EYFP
CCACATGAAGCAGCACGACTTCTTCAAGTCCGCCATGCCCGAAGGCTACGTCCAGGAGCGCACCA
7475
GGTGTACTTCGTCGTGCTGAAGAAGTTCAGGCGGTACGGGCTTCCGATGCAGGTCCTCGCGTGGT
EYFP
TCTTCTTCAAGGACGACGGCAACTACAAGACCCGCGCCGAGGTGAAGTTCGAGGGCGACACCCTG
7540
AGAAGAAGTTCCTGCTGCCGTTGATGTTCTGGGCGCGGCTCCACTTCAAGCTCCCGCTGTGGGAC
EYFP
GTGAACCGCATCGAGCTGAAGGGCATCGACTTCAAGGAGGACGGCAACATCCTGGGGCACAAGCT
7605
CACTTGGCGTAGCTCGACTTCCCGTAGCTGAAGTTCCTCCTGCCGTTGTAGGACCCCGTGTTCGA
EYFP
GGAGTACAACTACAACAGCCACAACGTCTATATCATGGCCGACAAGCAGAAGAACGGCATCAAGG
7670
CCTCATGTTGATGTTGTCGGTGTTGCAGATATAGTACCGGCTGTTCGTCTTCTTGCCGTAGTTCC
EYFP
TGAACTTCAAGATCCGCCACAACATCGAGGACGGCAGCGTGCAGCTCGCCGACCACTACCAGCAG
7735
ACTTGAAGTTCTAGGCGGTGTTGTAGCTCCTGCCGTCGCACGTCGAGCGGCTGGTGATGGTCGTC
EYFP


AACACCCCCATCGGCGACGGCCCCGTGCTGCTGCCCGACAACCACTACCTGAGCTACCAGTCCGC
7800
TTGTGGGGGTAGCCGCTGCCGGGGCACGACGACGGGCTGTTGGTGATGGACTCGATGGTCAGGCG
EYFP
CCTGAGCAAAGACCCCAACGAGAAGCGCGATCACATGGTCCTGCTGGAGTTCGTGACCGCCGCCG
7865
GGACTCGTTTCTGGGGTTGCTCTTCGCGCTAGTGTACCAGGACGACCTCAAGCACTGGCGGCGGC
EYFP
GGATCACTCTCGGCATGGACGAGCTGTACAAGTGAgcggccgctaatcaacctctggattacaaa
7930
CCTAGTGAGAGCCGTACCTGCTCGACATGTTCACTcgccggcgattagttggagacctaatgttt
EYFP
EYFP
WPRE
atttgtgaaagattgactggtattcttaactatgttgctccttttacgctatgtggatacgctgc
7995
taaacactttctaactgaccataagaattgatacaacgaggaaaatgcgatacacctatgcgacg
WPRE
tttaatgcctttgtatcatgctattgcttcccgtatggctttcattttctcctccttgtataaat
8060
aaattacggaaacatagtacgataacgaagggcataccgaaagtaaaagaggaggaacatattta
WPRE
cctggttgctgtctctttatgaggagttgtggcccgttgtcaggcaacgtggcgtggtgtgcact
8125
ggaccaacgacagagaaatactcctcaacaccgggcaacagtccgttgcaccgcaccacacgtga
WPRE
gtgtttgctgacgcaacccccactggttggggcattgccaccacctgtcagctcctttccgggac
8190
cacaaacgactgcgttgggggtgaccaaccccgtaacggtggtggacagtcgaggaaaggccctg
WPRE
tttcgctttcccccctccctattgccacggcggaactcatcgccgcctgccttgcccgctgctgga
8255
aaagcgaaaggggagggataacggtgccgccttgagtagcggcggacggaacgggcgacgacct
WPRE
caggggctcggctgttgggcactgacaattccgtggtgttgtcggggaaatcatcgtcctttcct
8320
gtccccgagccgacaacccgtgactgttaaggcaccacaacagccccttagtagcaggaaagga
WPRE
tggctgctcgcctgtgttgccacctggattctgcgcgggacgtccttctgctacgtcccttcggc
8385
accgacgagcggacacaacggtggacctaagacgcgccctgcaggaagacgatgcagggaagccg
WPRE


cctcaatccagcggaccttccttcccgcggcctgctgccggctctgcggcctcttccgcgtcttc
8450
ggagttaggtcgcctggaaggaagggcgccggacgacggccgagacgccggagaaggcgcagaag
WPRE
gccttcgccctcagacgagtcggatctccctttgggccgcctccccgcatcgataccgtcgagac
8515
cggaagcgggagtctgctcagcctagagggaaacccggcggaggggcgtagctatggcagctctg
WPRE
tgctgcaccagatcataatcagccataccacatttgtagaggttttacttgctttaaaaaacctc
8580
acgacgtggtctagtattagtcggtatggtgtaaacatctccaaaatgaacgaaatttttggag
ccacacctccccctgaacctgaaacataaaatgaatgcaattgttgttgttaacttgtttattgc
8645
ggtgtggaggggacttggactttgtattttacttacgttaacaacaacaattgaacaaataacg
SV40 poly (A)
agcttataatggttacaaataaagcaatagcatcacaaatttcacaaataaagcatttttttcac
8710
tcgaatattaccaatgtttatttcgttatcgtagtgtttaaagtgtttatttcgtaaaaaaagtg
SV40 poly (A)
tgcattctagttgtggtttgtccaaactcatcaatgtatcttaaggcgtaggcgtactagctcga
8775
acgtaagatcaacaccaaacaggtttgagtagttacatagaattccgcatccgcatgatcgagct
SV40 poly (A)
DraIII
End
(8796)
ggtccttcctctCACTAGGTG
3′
8796
ccaggaaggagaGTGATCCAC
5′

	Feature			Location			Size			Type
✓	**Extra DNA**			10	..	66	57 bp			misc_feature
	/locus_tag	=	Extra DNA							
	/label	=	Extra DNA							
✓	**PGP9.5**			77	..	1752	1676 bp			misc_feature
	/locus_tag	=	PGP9.5							
	/label	=	PGP9.5							
✓	**loxP**			1801	..	1834	34 bp			misc_feature
	/locus_tag	=	loxP							
	/label	=	loxP							
✓	**lox2272**			1843	..	1876	34 bp			misc_feature
	/locus_tag	=	lox2272(1)							
	/label	=	lox2272(1)							
✓	**loxN**			1885	..	1918	34 bp			misc_feature
	/locus_tag	=	loxN							
	/label	=	loxN							
✓	**HALO TAG**			1927	..	2823	897 bp			misc_feature
	/locus_tag	=	HALO TAG							
	/label	=	HALO TAG							
✓	**SV40 poly(A)**			3006	..	3127	122 bp			misc_feature
	/locus_tag	=	SV40 poly(A)							
	/label	=	SV40 poly(A)							
✓	**loxP**			3140	..	3173	34 bp			misc_feature
	/locus_tag	=	loxP(1)							
	/label	=	loxP(1)							
✓	**mCerulean**			3182	..	3904	723 bp			misc_feature
	/locus_tag	=	mCerulean							
	/label	=	mCerulean							
✓	**mCerulean**			3905	..	3907	3 bp			misc_feature
	/locus_tag	=	mCerulean(1)							
	/label	=	mCerulean(1)							
✓	**WPRE**			3917	..	4505	589 bp			misc_feature
	/locus_tag	=	WPRE							
	/label	=	WPRE							
✓	**SV40 poly(A)**			4639	..	4760	122 bp			misc_feature
	/locus_tag	=	SV40 poly(A)(1)							
	/label	=	SV40 poly(A)(1)							
✓	**lox2272**			4777	..	4810	34 bp			misc_feature
	/locus_tag	=	lox2272							
	/label	=	lox2272							

	Feature			Location			Size			Type
✓	**tdTOMATO**			4819	..	6252	1434 bp			misc_feature
	/locus_tag	=	tdTOMATO							
	/label	=	tdTOMATO							
✓	**tdTOMATO**			6253	..	6255	3 bp			misc_feature
	/locus_tag	=	tdTOMATO(1)							
	/label	=	tdTOMATO(1)							
✓	**WPRE**			6265	..	6853	589 bp			misc_feature
	/locus_tag	=	WPRE(1)							
	/label	=	WPRE(1)							
✓	**SV40 poly(A)**			6987	..	7108	122 bp			misc_feature
	/locus_tag	=	SV40 poly(A)(2)							
	/label	=	SV40 poly(A)(2)							
✓	**loxN**			7133	..	7166	34 bp			misc_feature
	/locus_tag	=	loxN(1)							
	/label	=	loxN(1)							
✓	**EYFP**			7175	..	7897	723 bp			misc_feature
	/locus_tag	=	EYFP							
	/label	=	EYFP							
✓	**EYFP**			7898	..	7900	3 bp			misc_feature
	/locus_tag	=	EYFP(1)							
	/label	=	EYFP(1)							
✓	**WPRE**			7910	..	8498	589 bp			misc_feature
	/locus_tag	=	WPRE(2)							
	/label	=	WPRE(2)							
✓	**SV40 poly (A)**			8632	..	8753	122 bp			misc_feature
	/locus_tag	=	SV40 poly (A)							
	/label	=	SV40 poly (A)							

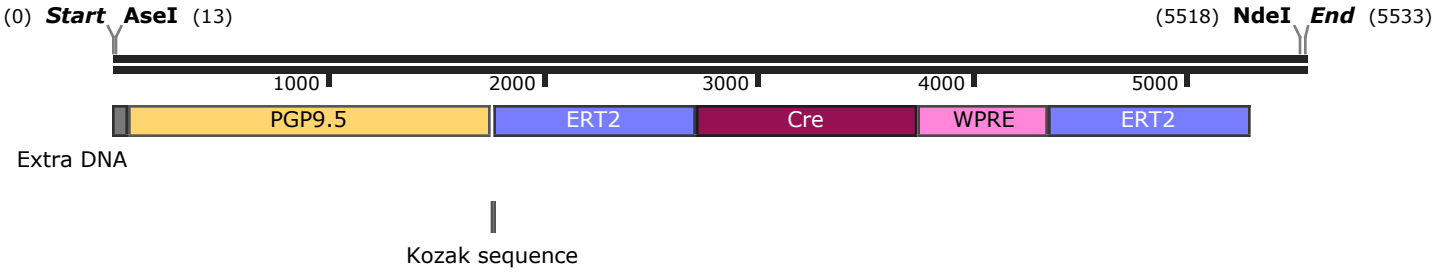

PGP_iCre_sequence
5533 bp

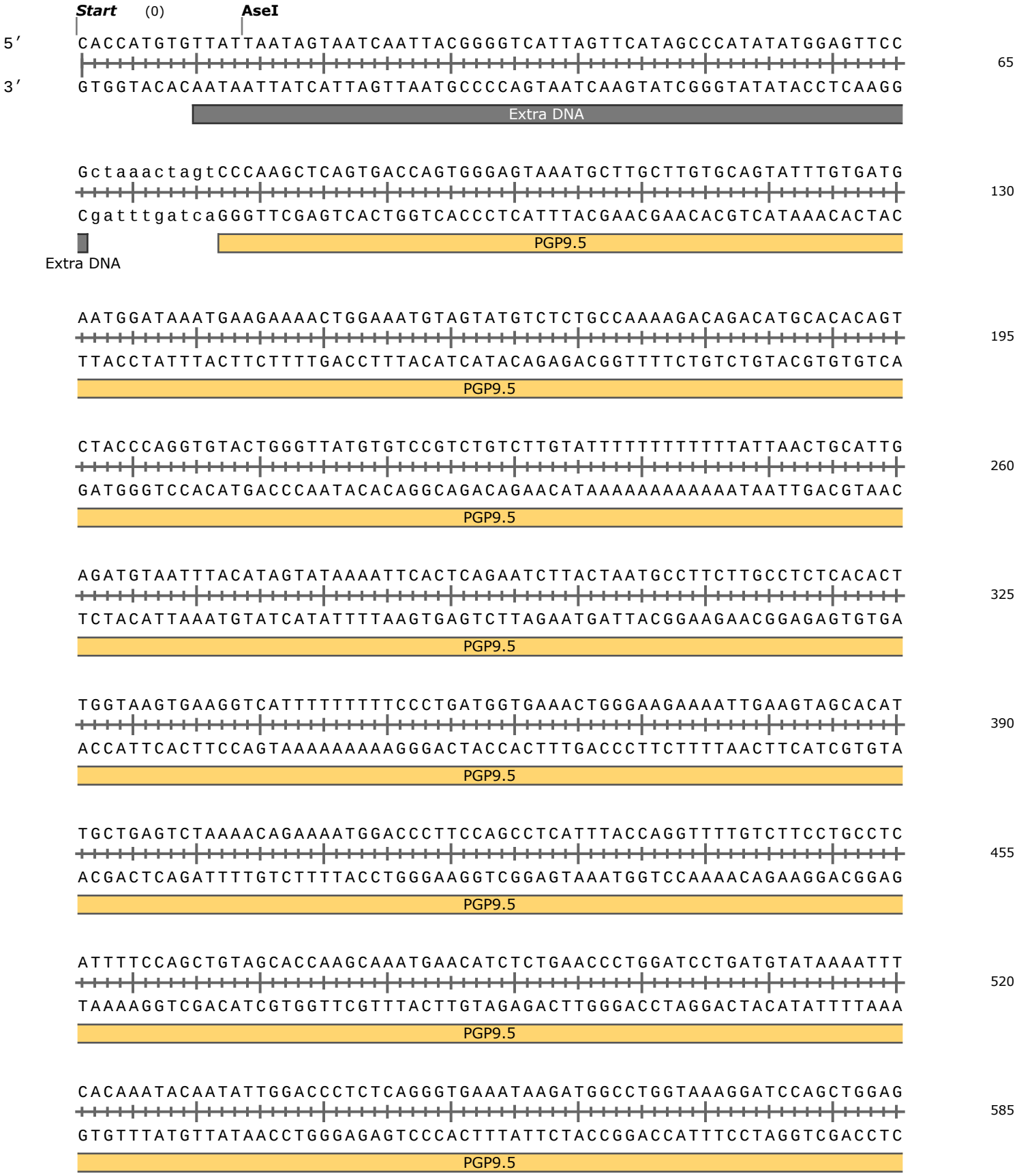
Start (0)
AseI
5′ CACCATGTGTTATTAATAGTAATCAATTACGGGGTCATTAGTTCATAGCCCATATATGGAGTTCC
3′ GTGGTACACAATAATTATCATTAGTTAATGCCCCAGTAATCAAGTATCGGGTATATACCTCAAGG
65
Extra DNA
GctaaactagtCCCAAGCTCAGTGACCAGTGGGAGTAAATGCTTGCTTGTGCAGTATTTGTGATG
CgatttgatcaGGGTTCGAGTCACTGGTCACCCTCATTTACGAACGAACACGTCATAAACACTAC
130
PGP9.5
Extra DNA
AATGGATAAATGAAGAAAACTGGAAATGTAGTATGTCTCTGCCAAAAGACAGACATGCACACAGT
TTACCTATTTACTTCTTTTGACCTTTACATCATACAGAGACGGTTTTCTGTCTGTACGTGTGTCA
195
PGP9.5
CTACCCAGGTGTACTGGGTTATGTGTCCGTCTGTCTTGTATTTTTTTTTTTTTATTAACTGCATTG
GATGGGTCCACATGACCCAATACACAGGCAGACAGAACATAAAAAAAAAAAAATAATTGACGTAAC
260
PGP9.5
AGATGTAATTTACATAGTATAAAATTCACTCAGAATCTTACTAATGCCTTCTTGCCTCTCACACT
TCTACATTAAATGTATCATATTTTAAGTGAGTCTTAGAATGATTACGGAAGAACGGAGAGTGTGA
325
PGP9.5
TGGTAAGTGAAGGTCATTTTTTTTTCCCTGATGGTGAAACTGGGAAGAAAATTGAAGTAGCACAT
ACCATTCACTTCCAGTAAAAAAAAAGGGACTACCACTTTGACCCTTCTTTTAACTTCATCGTGTA
390
PGP9.5
TGCTGAGTCTAAAACAGAAAATGGACCCTTCCAGCCTCATTTACCAGGTTTTGTCTTCCTGCCTC
ACGACTCAGATTTTGTCTTTTACCTGGGAAGGTCGGAGTAAATGGTCCAAAACAGAAGGACGGAG
455
PGP9.5
ATTTTCCAGCTGTAGCACCAAGCAAATGAACATCTCTGAACCCTGGATCCTGATGTATAAAATTT
TAAAAGGTCGACATCGTGGTTCGTTTACTTGTAGAGACTTGGGACCTAGGACTACATATTTTAAA
520
PGP9.5
CACAAATACAATATTGGACCCTCTCAGGGTGAAATAAGATGGCCTGGTAAAGGATCCAGCTGGAG
GTGTTTATGTTATAACCTGGGAGAGTCCCACTTTATTCTACCGGACCATTTCCTAGGTCGACCTC
585
PGP9.5

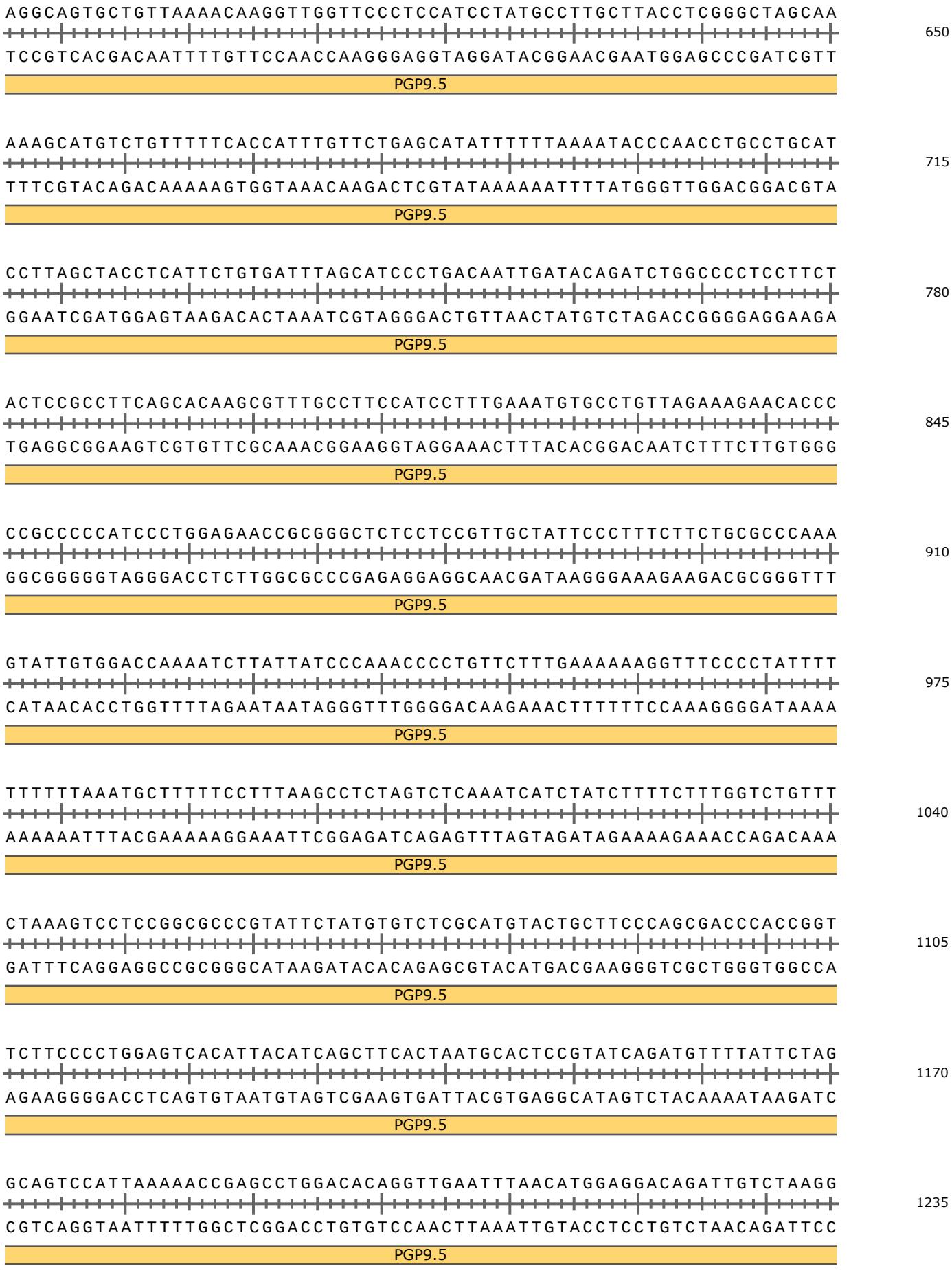
AGGCAGTGCTGTTAAAACAAGGTTGGTTCCCTCCATCCTATGCCTTGCTTACCTCGGGCTAGCAA
650
TCCGTCACGACAATTTTGTTCCAACCAAGGGAGGTAGGATACGGAACGAATGGAGCCCGATCGTT
PGP9.5
AAAGCATGTCTGTTTTTCACCATTTGTTCTGAGCATATTTTTTAAAATACCCAACCTGCCTGCAT
715
TTTCGTACAGACAAAAAGTGGTAAACAAGACTCGTATAAAAAATTTTATGGGTTGGACGGACGTA
PGP9.5
CCTTAGCTACCTCATTCTGTGATTTAGCATCCCTGACAATTGATACAGATCTGGCCCCTCCTTCT
780
GGAATCGATGGAGTAAGACACTAAATCGTAGGGACTGTTAACTATGTCTAGACCGGGGAGGAAGA
PGP9.5
ACTCCGCCTTCAGCACAAGCGTTTGCCTTCCATCCTTTGAAATGTGCCTGTTAGAAAGAACACCC
845
TGAGGCGGAAGTCGTGTTCGCAAACGGAAGGTAGGAAACTTTACACGGACAATCTTTCTTGTGGG
PGP9.5
CCGCCCCCATCCCTGGAGAACCGCGGGCTCTCCTCCGTTGCTATTCCCTTTCTTCTGCGCCCAAA
910
GGCGGGGGTAGGGACCTCTTGGCGCCCGAGAGGAGGCAACGATAAGGGAAAGAAGACGCGGGTTT
PGP9.5
GTATTGTGGACCAAAATCTTATTATCCCAAACCCCTGTTCTTTGAAAAAAGGTTTCCCCTATTTT
975
CATAACACCTGGTTTTAGAATAATAGGGTTTGGGGACAAGAAACTTTTTTCCAAAGGGGATAAAA
PGP9.5
TTTTTTAAATGCTTTTTCCTTTAAGCCTCTAGTCTCAAATCATCTATCTTTTCTTTGGTCTGTTT
1040
AAAAAATTTACGAAAAAGGAAATTCGGAGATCAGAGTTTAGTAGATAGAAAAGAAACCAGACAAA
PGP9.5
CTAAAGTCCTCCGGCGCCCGTATTCTATGTGTCTCGCATGTACTGCTTCCCAGCGACCCACCGGT
1105
GATTTCAGGAGGCCGCGGGCATAAGATACACAGAGCGTACATGACGAAGGGTCGCTGGGTGGCCA
PGP9.5
TCTTCCCCTGGAGTCACATTACATCAGCTTCACTAATGCACTCCGTATCAGATGTTTTATTCTAG
1170
AGAAGGGGACCTCAGTGTAATGTAGTCGAAGTGATTACGTGAGGCATAGTCTACAAAATAAGATC
PGP9.5
GCAGTCCATTAAAAACCGAGCCTGGACACAGGTTGAATTTAACATGGAGGACAGATTGTCTAAGG
1235
CGTCAGGTAATTTTTGGCTCGGACCTGTGTCCAACTTAAATTGTACCTCCTGTCTAACAGATTCC
PGP9.5

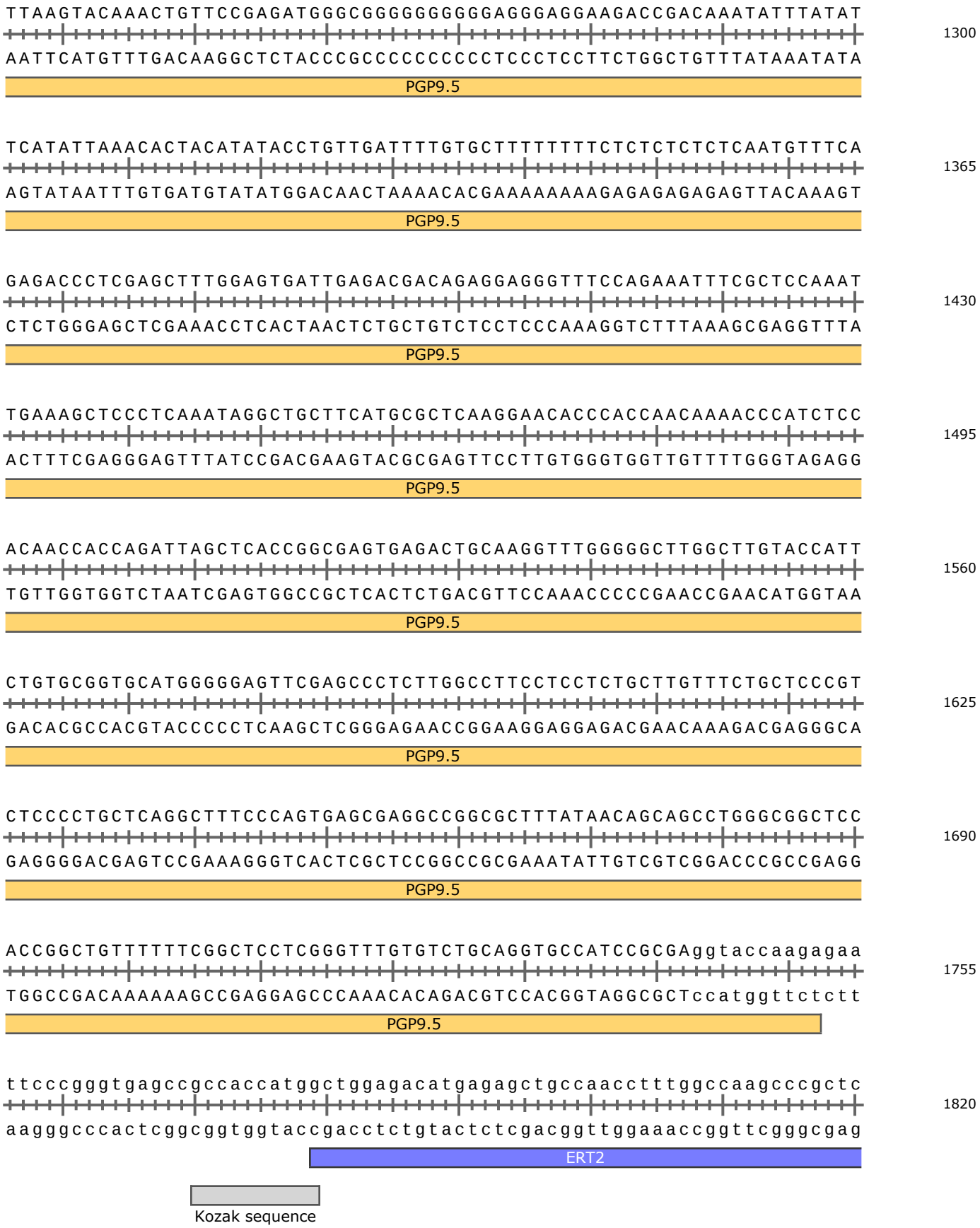
TTAAGTACAAACTGTTCCGAGATGGGCGGGGGGGGGGAGGGAGGAAGACCGACAAATATTTATAT
1300
AATTCATGTTTGACAAGGCTCTACCCGCCCCCCCCCTCCCTCCTTCTGGCTGTTTATAAATATA
PGP9.5
TCATATTAAACACTACATATACCTGTTGATTTTGTGCTTTTTTTTCTCTCTCTCTCAATGTTTCA
1365
AGTATAATTTGTGATGTATATGGACAACTAAAACACGAAAAAAAAGAGAGAGAGAGTTACAAAGT
PGP9.5
GAGACCCTCGAGCTTTGGAGTGATTGAGACGACAGAGGAGGGTTTCCAGAAATTTCGCTCCAAAT
1430
CTCTGGGAGCTCGAAACCTCACTAACTCTGCTGTCTCCTCCCAAAGGTCTTTAAAGCGAGGTTTA
PGP9.5
TGAAAGCTCCCTCAAATAGGCTGCTTCATGCGCTCAAGGAACACCCACCAACAAAACCCATCTCC
1495
ACTTTCGAGGGAGTTTATCCGACGAAGTACGCGAGTTCCTTGTGGGTGGTTGTTTTGGGTAGAGG
PGP9.5
ACAACCACCAGATTAGCTCACCGGCGAGTGAGACTGCAAGGTTTGGGGGCTTGGCTTGTACCATT
1560
TGTTGGTGGTCTAATCGAGTGGCCGCTCACTCTGACGTTCCAAACCCCCGAACCGAACATGGTAA
PGP9.5
CTGTGCGGTGCATGGGGGAGTTCGAGCCCTCTTGGCCTTCCTCCTCTGCTTGTTTCTGCTCCCGT
1625
GACACGCCACGTACCCCCTCAAGCTCGGGAGAACCGGAAGGAGGAGACGAACAAAGACGAGGGCA
PGP9.5
CTCCCCTGCTCAGGCTTTCCCAGTGAGCGAGGCCGGCGCTTTATAACAGCAGCCTGGGCGGCTCC
1690
GAGGGGACGAGTCCGAAAGGGTCACTCGCTCCGGCCGCGAAATATTGTCGTCGGACCCGCCGAGG
PGP9.5
ACCGGCTGTTTTTTCGGCTCCTCGGGTTTGTGTCTGCAGGTGCCATCCGCGAggtaccaagagaa
1755
TGGCCGACAAAAAAGCCGAGGAGCCCAAACACAGACGTCCACGGTAGGCGCTccatggttctctt
PGP9.5
ttcccgggtgagccgccaccatggctggagacatgagagctgccaacctttggccaagcccgctc
1820
aagggcccactcggcggtggtaccgacctctgtactctcgacggttggaaaccggttcgggcgag
ERT2
Kozak sequence

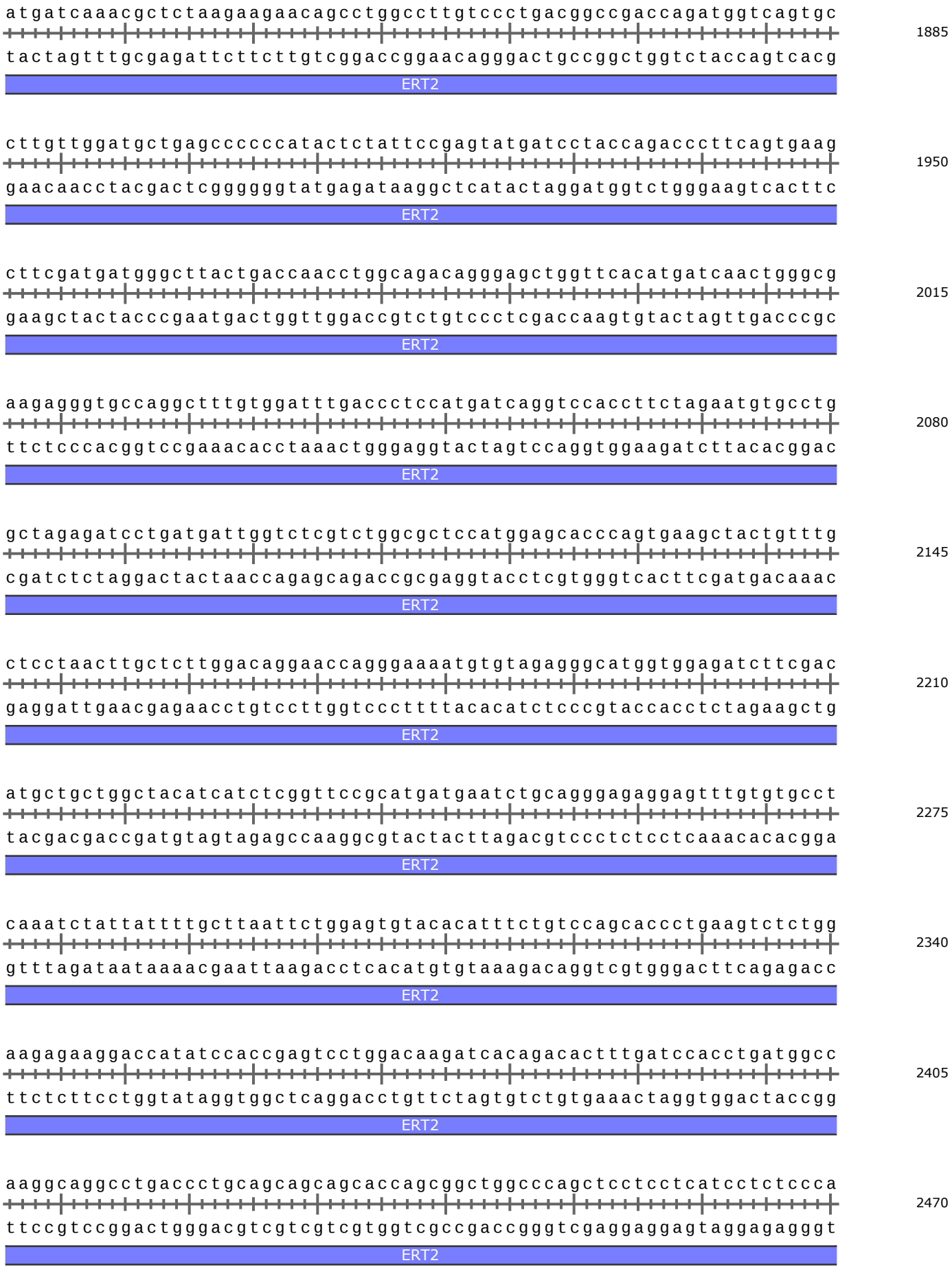
atgatcaaacgctctaagaagaacagcctggccttgtccctgacggccgaccagatggtcagtgc
1885
tactagtttgcgagattcttcttgtcggaccggaacagggactgccggctggtctaccagtcacg
ERT2
cttgttggatgctgagccccccatactctattccgagtatgatcctaccagacccttcagtgaag
1950
gaacaacctacgactcgggggggtatgagataaggctcatactaggatggtctgggaagtcacttc
ERT2
cttcgatgatgggcttactgaccaacctggcagacagggagctggttcacatgatcaactgggcg
2015
gaagctactacccgaatgactggttggaccgtctgtccctcgaccaagtgtactagttgacccgc
ERT2
aagagggtgccaggctttgtggatttgaccctccatgatcaggtccaccttctagaatgtgcctg
2080
ttctcccacggtccgaaacacctaaactgggaggtactagtccaggtggaagatcttacacggac
ERT2
gctagagatcctgatgattggtctcgtctggcgctccatggagcacccagtgaagctactgtttg
2145
cgatctctaggactactaaccagagcagaccgcgaggtacctcgtgggtcacttcgatgacaaac
ERT2
ctcctaacttgctcttggacaggaaccagggaaaatgtgtagagggcatggtggagatcttcgac
2210
gaggattgaacgagaacctgtccttggtccctttacacatctcccgtaccacctctagaagctg
ERT2
atgctgctggctacatcatctcggttccgcatgatgaatctgcagggagaggagtttgtgtgcct
2275
tacgacgaccgatgtagtagagccaaggcgtactacttagacgtccctctcctcaaacacacgga
ERT2
caaatctattattttgcttaattctggagtgtacacatttctgtccagcaccctgaagtctctgg
2340
gtttagataataaaacgaattaagacctcacatgtgtaaagacaggtcgtgggacttcagagacc
ERT2
aagagaaggaccatatccaccgagtcctggacaagatcacagacactttgatccacctgatggcc
2405
ttctcttcctggtataggtggctcaggacctgttctagtgtctgtgaaactaggtggactaccgg
ERT2
aaggcaggcctgaccctgcagcagcagcaccagcggctggcccagctcctcctcatcctctccca
2470
ttccgtccggactgggacgtcgtcgtcgtggtcgccgaccgggtcgaggaggagtaggagagggt
ERT2

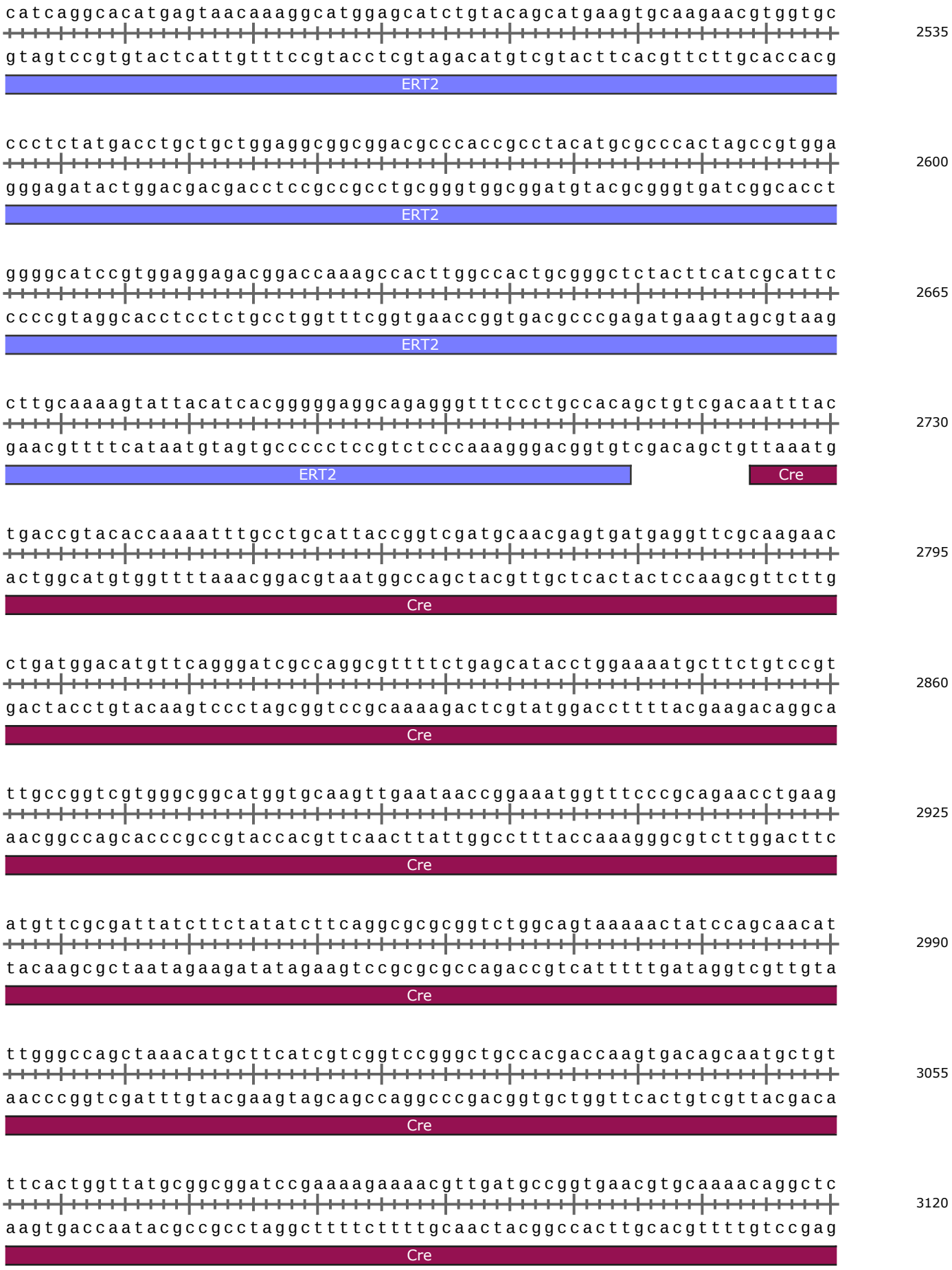
catcaggcacatgagtaacaaaggcatggagcatctgtacagcatgaagtgcaagaacgtggtgc
2535
gtagtccgtgtactcattgtttccgtacctcgtagacatgtcgtacttcacgttcttgcaccacg
ERT2
ccctctatgacctgctgctggaggcggcggacgcccaccgcctacatgcgcccactagccgtgga
2600
gggagatactggacgacgacctccgccgcctgcgggtggcggatgtacgcgggtgatcggcacct
ERT2
ggggcatccgtggaggagacggaccaaagccacttggccactgcgggctctacttcatcgcattc
2665
ccccgtaggcacctcctctgcctggtttcggtgaaccggtgacgcccgagatgaagtagcgtaag
ERT2
cttgcaaaagtattacatcacgggggaggcagagggtttccctgccacagctgtcgacaatttac
2730
gaacgttttcataatgtagtgcccccctccgtctcccaaagggacggtgtcgacagctgttaaatg
ERT2
Cre
tgaccgtacaccaaaatttgcctgcattaccggtcgatgcaacgagtgatgaggttcgcaagaac
2795
actggcatgtggttttaaacggacgtaatggccagctacgttgctcactactccaagcgttcttg
Cre
ctgatggacatgttcagggatcgccaggcgttttctgagcatacctggaaaatgcttctgtccgt
2860
gactacctgtacaagtccctagcggtccgcaaaagactcgtatggacctttacgaagacaggca
Cre
ttgccggtcgtgggcggcatggtgcaagttgaataaccggaaatggtttcccgcagaacctgaag
2925
aacggccagcacccgccgtaccacgttcaacttattggcctttaccaaagggcgtcttggacttc
Cre
atgttcgcgattatcttctatatcttcaggcgcgcggtctggcagtaaaaactatccagcaacat
2990
tacaagcgctaatagaagatatagaagtccgcgcgccagaccgtcatttttgataggtcgttgta
Cre
ttgggccagctaaacatgcttcatcgtcggtccgggctgccacgaccaagtgacagcaatgctgt
3055
aacccggtcgatttgtacgaagtagcagccaggcccgacggtgctggttcactgtcgttacgaca
Cre
ttcactggttatgcggcggatccgaaaagaaaacgttgatgccggtgaacgtgcaaaacaggctc
3120
aagtgaccaatacgccgcctaggcttttcttttgcaactacggccacttgcacgttttgtccgag
Cre


tagcgttcgaacgcactgatttcgaccaggttcgttcactcatggaaaatagcgatcgctgccag
3185
atcgcaagcttgcgtgactaaagctggtccaagcaagtgagtacctttttatcgctagcgacggtc
Cre
gatatacgtaatctggcatttctggggattgcttataacaccctgttacgtatagccgaaattgc
3250
ctatatgcattagaccgtaaagacccctaacgaatattgtgggacaatgcatatcggctttaacg
Cre
caggatcagggttaaagatatctcacgtactgacggtgggagaatgttaatccatattggcagaa
3315
gtcctagtcccaatttctatagagtgcatgactgccaccctcttacaattaggtataaccgtctt
Cre
cgaaaacgctggttagcaccgcaggtgtagagaaggcacttagcctgggggtaactaaactggtc
3380
gcttttgcgaccaatcgtggcgtccacatctcttccgtgaatcggacccccattgatttgaccag
Cre
gagcgatggatttccgtctctggtgtagctgatgatccgaataactacctgttttgccgggtcag
3445
ctcgctacctaaaggcagagaccacatcgactactaggcttattgatggacaaaacggcccagtc
Cre
aaaaaatggtgttgccgcgccatctgccaccagccagctatcaactcgcgccctggaagggattt
3510
ttttttaccacaacggcgcggtagacggtggtcggtcgatagttgagcgcgggaccttccctaaa
Cre
ttgaagcaactcatcgattgatttacggcgctaaggatgactctggtcagagatacctggcctgg
3575
aacttcgttgagtagctaactaaatgccgcgattcctactgagaccagtctctatggaccggacc
Cre
tctggacacagtgcccgtgtcggagccgcgcgagatatggcccgcgctggagtttcaataccgga
3640
agacctgtgtcacgggcacagcctcggcgcgctctataccgggcgcgacctcaaagttatggcct
Cre
gatcatgcaagctggtggctggaccaatgtaaatattgtcatgaactatatccgtaacctggata
3705
ctagtacgttcgaccaccgacctggttacatttataacagtacttgatataggcattggacctat
Cre
gtgaaacaggggcaatggtgcgcctgctggaagatggcgatgcggccgctaatcaacctctggat
3770
cactttgtccccgttaccacgcggacgaccttctaccgctacgccggcgattagttggagaccta
Cre
WPRE


tacaaaatttgtgaaagattgactggtattcttaactatgttgctccttttacgctatgtggata
3835
atgttttaaacactttctaactgaccataagaattgatacaacgaggaaaatgcgatacacctat
WPRE
cgctgctttaatgcctttgtatcatgctattgcttcccgtatggctttcattttctcctccttgt
3900
gcgacgaaattacggaaacatagtacgataacgaagggcataccgaaagtaaaagaggaggaaca
WPRE
ataaatcctggttgctgtctctttatgaggagttgtggcccgttgtcaggcaacgtggcgtggtg
3965
tatttaggaccaacgacagagaaatactcctcaacaccgggcaacagtccgttgcaccgcaccac
WPRE
tgcactgtgtttgctgacgcaacccccactggttggggcattgccaccacctgtcagctccttcc
4030
acgtgacacaaacgactgcgttgggggtgaccaaccccgtaacggtggtggacagtcgaggaaag
WPRE
cgggactttcgctttcccctccctattgccacggcggaactcatcgccgcctgccttgcccgct
4095
gccctgaaagcgaaaggggagggataacggtgccgccttgagtagcggcggacggaacgggcga
WPRE
gctggacaggggctcggctgttgggcactgacaattccgtggtgttgtcggggaaatcatcgtcc
4160
cgacctgtccccgagccgacaacccgtgactgttaaggcaccacaacagccccttagtagcagg
WPRE
tttccttggctgctcgcctgtgttgccacctggattctgcgcgggacgtccttctgctacgtccc
4225
aaaggaaccgacgagcggacacaacggtggacctaagacgcgccctgcaggaagacgatgcaggg
WPRE
ttcggccctcaatccagcggaccttccttcccgcggcctgctgccggctctgcggcctcttccgc
4290
aagccgggagttaggtcgcctggaaggaagggcgccggacgacggccgagacgccggagaaggcg
WPRE
gtcttcgccttcgccctcagacgagtcggatctccctttgggccgcctccccgcctcgagccatc
4355
cagaagcggaagcgggagtctgctcagcctagagggaaacccggcggaggggcggagctcggtag
WPRE
tgctggagacatgagagctgccaacctttggccaagcccgctcatgatcaaacgctctaagaaga
4420
acgacctctgtactctcgacggttggaaaccggttcgggcgagtactagtttgcgagattcttct
ERT2

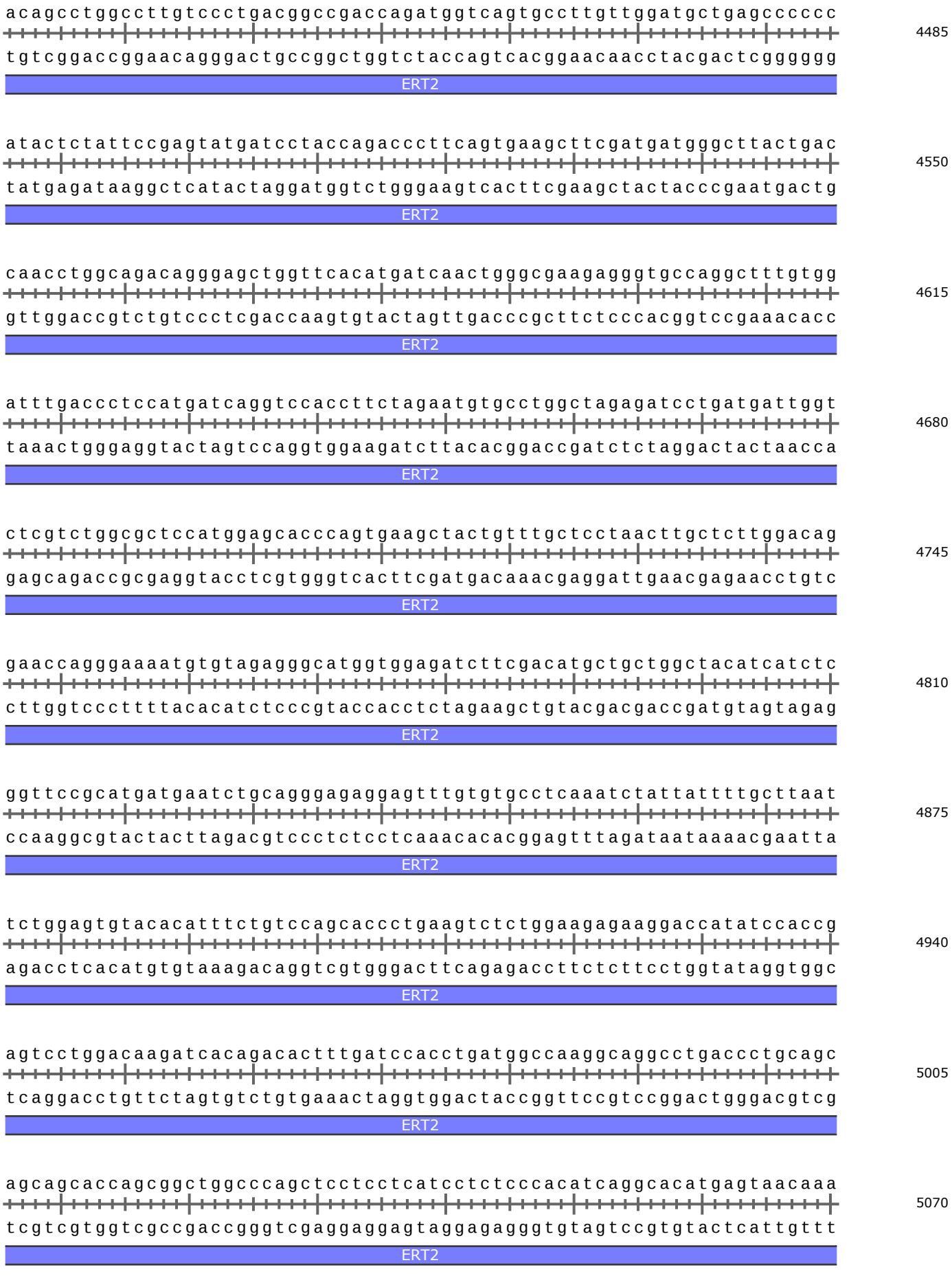
acagcctggccttgtccctgacggccgaccagatggtcagtgccttgttggatgctgagccccccc
4485
tgtcggaccggaacagggactgccggctggtctaccagtcacggaacaacctacgactcgggggg
ERT2
atactctattccgagtatgatcctaccagacccttcagtgaagcttcgatgatgggcttactgac
4550
tatgagataaggctcatactaggatggtctgggaagtcacttcgaagctactacccgaatgactg
ERT2
caacctggcagacagggagctggttcacatgatcaactgggcgaagagggtgccaggctttgtgg
4615
gttggaccgtctgtccctcgaccaagtgtactagttgacccgcttctcccacggtccgaaacacc
ERT2
atttgaccctccatgatcaggtccaccttctagaatgtgcctggctagagatcctgatgattggt
4680
taaactgggaggtactagtccaggtggaagatcttacacggaccgatctctaggactactaacca
ERT2
ctcgtctggcgctccatggagcacccagtgaagctactgtttgctcctaacttgctcttggacag
4745
gagcagaccgcgaggtacctcgtgggtcacttcgatgacaaacgaggattgaacgagaacctgtc
ERT2
gaaccagggaaaatgtgtagagggcatggtggagatcttcgacatgctgctggctacatcatctc
4810
cttggtccctttttacacatctcccgtaccacctctagaagctgtacgacgaccgatgtagtagag
ERT2
ggttccgcatgatgaatctgcagggagaggagtttgtgtgcctcaaatctattattttgcttaat
4875
ccaaggcgtactacttagacgtccctctcctcaaacacacggagtttagataataaaacgaatta
ERT2
tctggagtgtacacatttctgtccagcaccctgaagtctctggaagagaaggaccatatccaccg
4940
agacctcacatgtgtaaagacaggtcgtgggacttcagagaccttctcttcctggtataggtggc
ERT2
agtcctggacaagatcacagacactttgatccacctgatggccaaggcaggcctgaccctgcagc
5005
tcaggacctgttctagtgtctgtgaaactaggtggactaccggttccgtccggactgggacgtcg
ERT2
agcagcaccagcggctggcccagctcctcctcatcctctcccacatcaggcacatgagtaacaaa
5070
tcgtcgtggtcgccgaccgggtcgaggaggagtaggagagggtgtagtccgtgtactcattgttt
ERT2

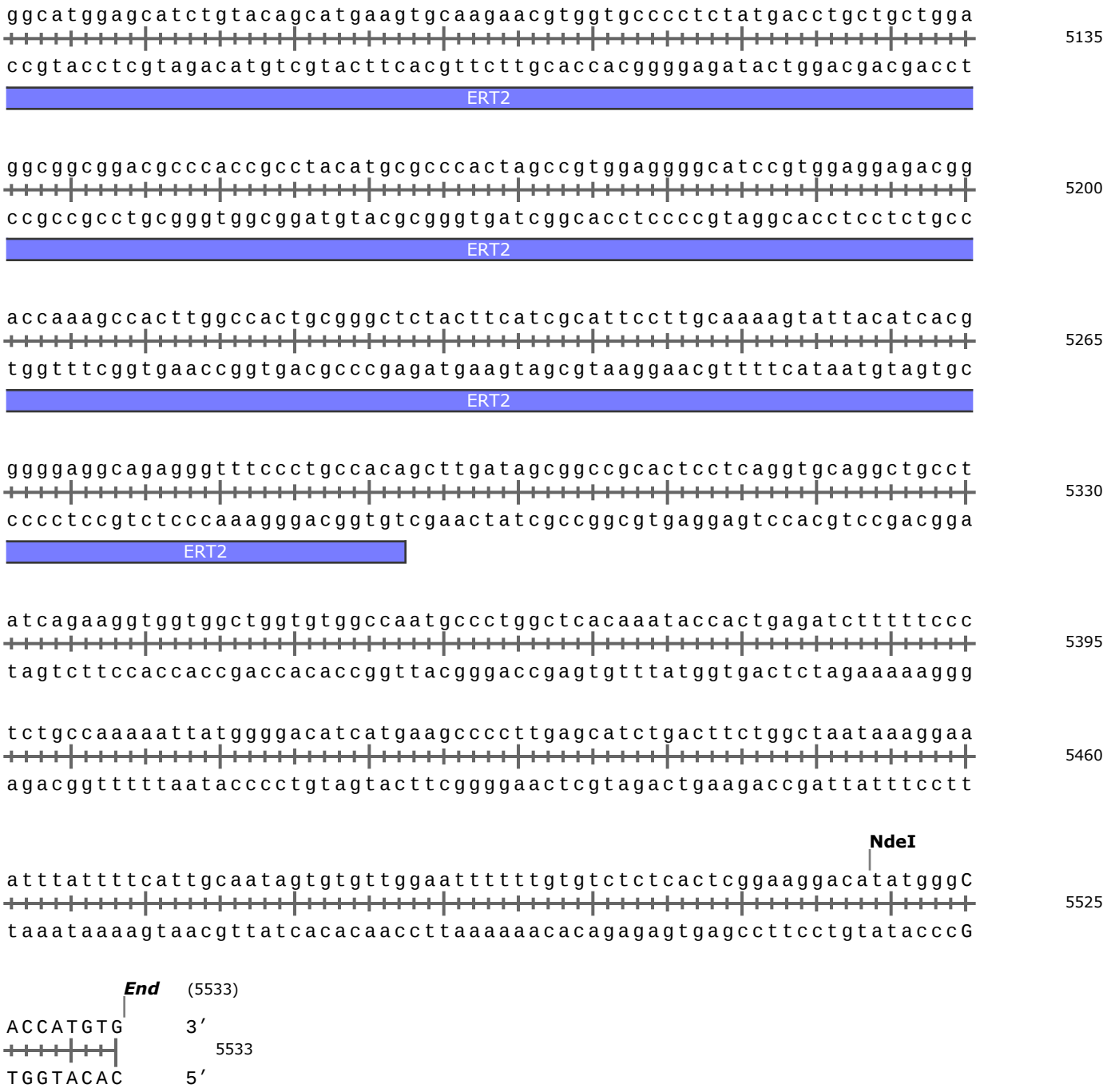
ggcatggagcatctgtacagcatgaagtgcaagaacgtggtgccctctatgacctgctgctgga
5135
ccgtacctcgtagacatgtcgtacttcacgttcttgcaccacggggagatactggacgacgacct
ERT2
ggcggcggacgcccaccgcctacatgcgcccactagccgtggaggggcatccgtggaggagacgg
5200
ccgccgcctgcgggtggcggatgtacgcgggtgatcggcacctccccgtaggcacctcctctgcc
ERT2
accaaagccacttggccactgcgggctctacttcatcgcattccttgcaaaagtattacatcacg
5265
tggtttcggtgaaccggtgacgcccgagatgaagtagcgtaaggaacgttttcataatgtagtgc
ERT2
ggggaggcagagggtttccctgccacagcttgatagcggccgcactcctcaggtgcaggctgcct
5330
ccccctccgtctcccaaagggacggtgtcgaactatcgccggcgtgaggagtccacgtccgacgga
ERT2
atcagaaggtggtggctggtgtggccaatgccctggctcacaaataccactgagatcttttccc
5395
tagtcttccaccaccgaccacaccggttacgggaccgagtgtttatggtgactctagaaaaaggg
tctgccaaaaattatggggacatcatgaagccccttgagcatctgacttctggctaataaaggaa
5460
agacggttttaatacccctgtagtacttcggggaactcgtagactgaagaccgattatttcctt
NdeI
atttattttcattgcaatagtgtgttggaatttttgtgtctctcactcggaaggacatatgggC
5525
taaataaaagtaacgttatcacacaaccttaaaaaacacagagagtgagccttcctgtatacccG
End (5533)
ACCATGTG 3′
5533
TGGTACAC 5′

	Feature	Location	Size	Type
✓	**Extra DNA**	10 .. 66	57 bp	misc_feature
	/locus_tag = Extra DNA			
	/label = Extra DNA			
✓	**PGP9.5**	77 .. 1752	1676 bp	misc_feature
	/locus_tag = PGP9.5			
	/label = PGP9.5			
✓	**Kozak sequence**	1770 .. 1779	10 bp	misc_feature
	/locus_tag = Kozak sequence			
	/label = Kozak sequence			
✓	**ERT2**	1779 .. 2714	936 bp	misc_feature
	/locus_tag = ERT2			
	/label = ERT2			
✓	**Cre**	2724 .. 3746	1023 bp	misc_feature
	/locus_tag = Cre			
	/label = Cre			
✓	**WPRE**	3756 .. 4344	589 bp	misc_feature
	/locus_tag = WPRE			
	/label = WPRE			
✓	**ERT2**	4357 .. 5292	936 bp	misc_feature
	/locus_tag = ERT2(1)			
	/label = ERT2(1)			